On dynamics beyond time-dependent mean-field theories

Lionel Lacombe

THÈSE

En vue de l'obtention du

DOCTORAT DE L'UNIVERSITÉ DE TOULOUSE

Délivré par : *l'Université Toulouse 3 Paul Sabatier (UT3 Paul Sabatier)*

Présentée et soutenue le *27/09/2016* **par :**

Lionel LACOMBE

On dynamics beyond time-dependent mean-field theories

JURY

SEVE DINH P. M.	Professeur des universités	Directeur de thèse
MORAWETZ K.	Professeur des universités	Rapporteur
GATTI F.	Directeur de recherche	Rapporteur
LACROIX D.	Directeur de recherche	Examinateur
MEIER C.	Professeur des universités	Membre du Jury
SURAUD E.	Professeur des universités	Membre du Jury
REINHARD P.-G.	Professeur émérite	Membre du Jury

École doctorale et spécialité :
SDM : Physique de la matière - CO090
Unité de Recherche :
Laboratoire de Physique Théorique Toulouse (UMR 5152)
Directeur de Thèse :
SEVE DINH Phuong Mai
Rapporteurs :
MORAWETZ Klaus et GATTI Fabien

Contents

Chapter 1

Introduction

The many-body problem in quantum physics is a large and tough subject that never ceased to interest the scientific community. The Schrödinger's equation found in 1925 contains formally everything needed to describe any kind of microscopic behaviour in the non-relativistic limit. Actually, the many-body wave function $|\Psi\rangle$ turns out to be a very complicated object of $3N$ variables if one consider a 3D system of N electrons. To handle this kind of object many theories with various levels of approximation have been developed, allowing the treatment of a broad range of system sizes and excitations energies. These approximations are even more needed when describing dynamics of these systems which is our aim here. Examples of methods used to treat a microscopic system of a given size N and a given excitation energy are sketched in Fig. 1.1. Of course, this is not an exhaustive view and serves only to give orders of magnitude.

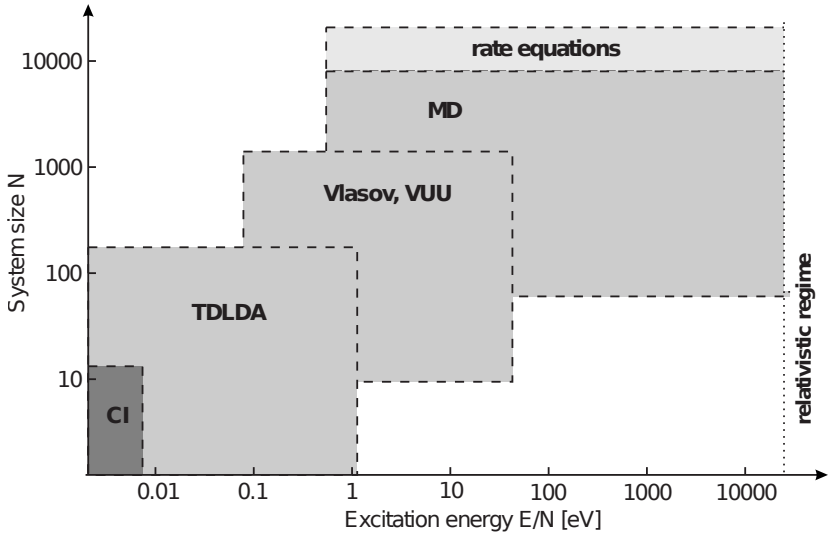

Figure 1.1: Schematic view showing the (rough) domains of applicability of various theories considering the system size and excitation energies of the microscopic systems described (see text for details). From [1].

Let us introduce the acronyms appearing in this figure. The true solution of the Schrödinger equation is tractable only in the case of very few particles. The next class of approximations are the configuration interaction (CI) methods together with the

multiconfigurational time-dependent Hartree-Fock (MCTDHF) approach [2] [3]. They consider the real Hamiltonian of the system, the only approximation being the size of the considered Hilbert space. Though these methods are formally valid for any system, the basis used to describe the Hilbert space drastically increases with the number of particles or the excitation energy, making these approaches numerically affordable only for small energies and limited sizes.

The (time-dependent) density functional theory or (TD)DFT is a reformulation of the quantum many-body problem in terms of the electronic density alone. It stems from a variational principle that maps a problem of interacting particles onto non-interacting particles with an effective potential. This mapping has been proved to be exact [4, 5, 6, 7] and would generate the solution of any problem provided that one has access to the exact functional, which is currently out of reach. There is a large range of available approximated functionals, (adiabatic) time-dependent local density approximation (TDLDA) being the less numerically demanding and thus encompassing the others in Fig. 1.1 [8].

For higher energies or number of electrons, we leave the realm of *ab initio* methods and semi-classical approaches are considered. They are based on the description of the phase-space density $f(\mathbf{r}, \mathbf{p})$. The Vlasov-Uehling-Uhlenbeck (VUU) [9] or Boltzmann-Uehling-Uhlenbeck (BUU) equation read as:

$$\partial_t f + \frac{\mathbf{p}}{m}.\nabla_{\mathbf{r}} f - \nabla_{\mathbf{p}} f \nabla_{\mathbf{r}} V(\mathbf{r}, t) = I(\mathbf{r}, \mathbf{p}) \tag{1.1}$$

$$\begin{aligned} I(\mathbf{r}, \mathbf{p}) = \int d\Omega d^3\mathbf{p}_1 \frac{|\mathbf{p} - \mathbf{p}_1|}{m} \frac{d\sigma(\theta, |\mathbf{p} - \mathbf{p}_1|)}{d\omega} \\ \times [f_{\mathbf{p}'} f_{\mathbf{p}'_1} (1 - \tilde{f}_{\mathbf{p}})(1 - \tilde{f}_{\mathbf{p}_1}) - f_{\mathbf{p}} f_{\mathbf{p}_1} (1 - \tilde{f}_{\mathbf{p}'})(1 - \tilde{f}_{\mathbf{p}'_1})] \end{aligned} . \tag{1.2}$$

It contains a collision term of the Boltzmann type modified with a Pauli blocking factors for fermions where $\tilde{f}_{\mathbf{p}} = (2\pi\hbar)^3 f_{\mathbf{p}}/2$ is the occupation of an element of volume of phase-space for a fermion of same spin. This kind of equation, though losing most of the quantum effects such as tunneling, interferences and shell closures, contains binary collisions between electrons and the resulting dissipative features. Such features become increasingly important with excitation energies [1].

Molecular dynamics methods and fully classical treatment of the electrons allow to treat higher energies where various trajectories have to be treated statistically. Contrary to the Vlasov equation, classical electrons allow one to plug back an electron-electron correlation that was lost in the mean-field phase-space treatment. This is still limited to a few thousands of atoms. Beyond that only macroscopic quantities related with rate equations are usable [10].

The aim of this thesis is to address the areas at the frontiers of VUU and TDLDA. At this point, we here draw a brief history of what will be presented. It has started with an issue faced in the first time-dependent Hartree-Fock (TDHF) approaches in nuclear physics. When describing fusion between heavy ions these calculations predicted a lower limit for the angular momentum for fusion. Below this limit, i.e. when the impact parameter was close to zero, there was no fusion occuring at all. However, this behavior has never been observed experimentally. It has been concluded that the amount of dissipation that was not accounted for in TDHF calculations was responsible of this "fusion window" problem. This has been part of the motivation for a huge

amount of work on the inclusion of dissipation in the TDHF theory. The handling of two-body correlations were performed by adding a VUU-like collision term in the evolution of the quantum density matrix. These theories are referred to as extended time-dependent Hartree-Fock (ETDHF). This kind of term has been derived using many approaches like time-dependent Green's functions [11, 12, 13]. A review of the methods discussed to include correlations can be found for example in [14]. As Green's functions are complicated objects to compute numerically, perturbative assumptions were made to obtain usable equations or to obtain off-diagonal terms and short memory effects [15]. The BBGKY hierarchy (after Bogolioubov, Born, Green, Kirkwood and Yvon) is another approach that allows to deal directly with simpler density matrices [16]. We give here as an example the first two terms of the hierarchy that will be detailed in Sec. 2.4:

$$\begin{aligned} \mathrm{i}\partial_t \rho_1 &= [h_1^0, \rho_1] + \mathrm{Tr}_2[v_{12}, \rho_{12}] \\ \mathrm{i}\partial_t \rho_{12} &= [h_1^0 + h_2^0 + v_{12}, \rho_{12}] + \mathrm{Tr}_3[v_{13} + v_{23}, \rho_{123}] \quad . \end{aligned}$$

The hierarchy links the 1-body density matrix ρ_1 to the 2-body matrix ρ_{12}, the 2-body to the 3-body ρ_{123} and so on until the full N-body density matrix with the help of the 1-body Hamiltonian h_1^0 of a non-interacting system, and v_{ij} the 2-body interaction.

In [16], starting from the BBGKY hierarchy, a cluster expansion of the reduced density matrices is introduced and a truncation scheme is proposed that yields a collision term similar to those previously obtained (see Sec. 2.5). This time, full memory effects and non-diagonal terms are naturally included. This approach is non perturbative in the sense that it is not based on small perturbation near an equilibrium state as the aim is to obtain a theory for highly non-linear behavior to describe a collision. However it truncates at a certain level of correlation. This approach serves as the basis for the calculation of observables in heavy-ion collisions [17, 18] and more scattering-theory oriented derivations can be found in [19, 20]. Actually a paper by Umar et al. [21] showed in 1986 that the "fusion window" issue could be solved by including the spin-orbit coupling. But ETDHF was still an improvement over a mere TDHF propagation and a way to retrieve the spreading width of one particle operators that is underestimated in TDHF. A truncation at the level of the Born term as done in ETDHF theories still yields a complicated memory term. To deal with this kind of terms stochastic approaches have been developped such as stochastic TDHF (STDHF) [22]. This kind of theory adds a fluctuation term to the previous Boltzmann-like collision term and can be reduced to a quantum Boltzmann-Langevin equation [23]. Reviews of the stochastic methods in nuclear dynamics can be found in [24] or more recently in [25].

In parallel of the development of ETDHF, the Runge-Gross theorem [7] lays the foundations of the TDDFT that is now mostly used in its Kohn-Sham (KS) form [26]. The KS scheme uses N orbitals of non-interacting KS particles that reproduce the exact electronic density $\varrho(\mathbf{r}, t)$ of the N interacting electrons at any time t. These KS particles evolve in an effective potential which is a functional of the initial state and all the previous densities $\varrho(\mathbf{r}, t')$ with $t' \leq t$. The TDDFT theory brings the promise of implicitly accounting for all exchange and correlation effects in a dynamical calculation. TDDFT has been mostly used in the linear response regime [27] with reliable results for a low calculation cost. Formally, the TDDFT approach is exact and also applies

for ionization processes of clusters in strong laser fields which is our field of interest [28, 1].

But TDDFT has many drawbacks. First of all, the exact exchange correlation functional of ϱ is unknown. Many approximations have been proposed from basic local density approximation (LDA) to generalized gradient approximation (GGA) [29, 30]. The latest approximations contains hybrid functionals that are composed as the linear commbination of functionals and exact exchange term computed as in Hartree-Fock theory [31, 32]. How to obtain the observables is another encountered problem. The Runge-Gross theorem ensures that all observables can be calculated from KS orbitals in theory, as they are functionals of $\varrho(\mathbf{r})$, but the way to obtain such functionals is unclear. The only case where it is obvious is if the observable is directly dependent on $\varrho(\mathbf{r})$ as for example the dipole moment $\mathbf{d} = \int \varrho(\mathbf{r}, t)\mathbf{r}d^3\mathbf{r}$. In other cases, one can choose as a first approximation to interpret the KS orbitals as actual electronic orbitals. This approach fails to deal with dynamical problems that are basically based on two electrons behaviour such as non-sequential double-ionization of a system as simple as the He atom [33, 34]. In this precise case actually, classical calculations with two fully correlated, but classically, electrons give much better results than any TDDFT calculation. It is actually easy to understand: the time-dependent KS system deals with effective uncorrelated particles. It can be represented by a single Slater determinant or by a 1-body density matrix which eigenvalues (occupation numbers) are either 0 or 1. On the other hand, the actual density matrix of the system possesses time-dependent occupation numbers that are fractional due to the correlation. The physical orbitals and the KS orbitals are very far from each other in such a case. Moreover, the exact exchange-correlation potential exhibit very complicated structures to account for this two-electron dynamics that are hardly reproduced in an approximation as those used in TDDFT.

Electron thermalization of a system is another effect that is hard to capture with standard TDDFT as it stems from collisions between electrons. This kind of feature can be seen experimentally in properties of photoelectrons. More precisely, one shines a cluster with a laser field and records the kinetic energy of the emitted electrons (producing a photoelectron spectrum or PES) and/or the angle of the direction of emission (giving a photoangular distribution or PAD). If a bound electron of given energy ε absorbs either one photon of high energy or several photons with energy lower than the ionization potential (IP) so that it reaches the continuum, then the electron is emitted with the following kinetic energy

$$E_{\text{kin}} = \varepsilon + \nu\hbar\omega_{\text{laser}} \tag{1.3}$$

where ν is the number of absorbed photons and ω_{laser} the laser frequency. For processes involving one electron of energy higher than the IP, rearrangement and correlation effects can be neglected in such a direct excitation, and the PES is usually interpreted as the density of states shifted by the photon energy (even if dynamical features do appear in a PES as the width of the peaks for instance).

At high photon density (i.e. high intensity of the laser), the electron can be excited by several photons simultaneously and be emitted even when energy of one photon is lower than the IP. The spectrum then exhibits the same peak structure but repeated many times, each peak separated from the previous one by the energy of one photon.

Such a structure is presented in panels a) [35] and b) [36] of Fig. 1.2 for C_{60} irradiated by an intense infrared laser pulse. Panel b) compares the experimental measurements

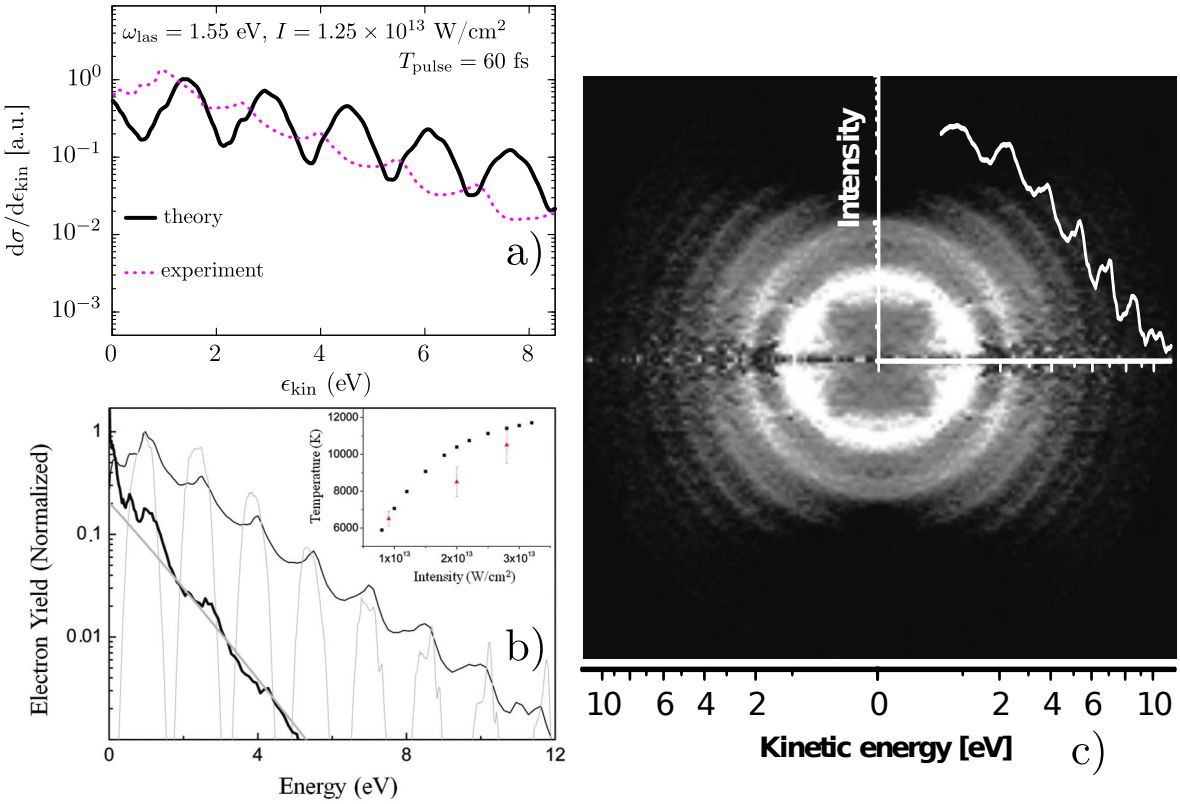

Figure 1.2: Experimental and theoretical results obtained on C_{60} excited by a laser with $\lambda = 800$ nm ($\omega_{laser} = 1.55$ eV), pulse width of 60 fs. More precisely: a) Theoretical photoelectron spectrum (full line) obtained in TDDFT with a laser of intensity 1.25×10^{13} W/cm^2 compared to the experimental results in b). b) Experimental results (black curves) with a laser intensity of 2×10^{13} W/cm^2 perpendicular (solid black) or parallel to the the polarization axis (thin black) compared with single-active-electron calculations (grey curves). c) Experimental PAD obtained with a laser with an intensity of 10^{13} W/cm^2, a 60 fs duration and a 800 nm wavelength.

(thin black curve) with a theoretical single-active-electron calculation coupled to a jellium model (thin grey curve) where only the HOMO electron is considered. Even if the peak positions are well reproduced, this calculation produces much too large a contrast of the peaks, probably resulting from the lack of either collisions with a real ionic structure or dynamical electron collisions. When ions are explicitly taken into account, as done in the calculation presented in panel a) and performed in our group, the contrast of the peaks is dramatically reduced, even it remains too large when compared to the experimental one (dotted curve).

A more decisive observable for electron thermalization is the PAD. Indeed, electrons that evaporate by thermalization generate an isotropic emission. An isotropic emission is visible in panel c) of the figure representing an experimental PAD from C_{60} irradiated by a laser with $\lambda = 800$ nm, pulse width of 60 fs and intensity of 10^{13} W/cm^2 [1]. The thermal emission is stronger at low energies and electrons with kinetic energy close

to zero take more time to leave the system and then interact more with the other electrons. This question of characteristic time of the interaction can be studied also by varying the duration of the laser pulse. For the effect of intensity and laser pulse duration on thermalization emission, see e.g. [37].

We have presented here two examples of situations where including an efficient 2-body correlation is crucial. The first example has motivated the development of time-dependent (reduced) density matrix functional theory or TD(R)DMFT. Instead of expressing everything as a functional of the electronic density $\varrho(\mathbf{r}, t)$, the functionals are now dependent on the density matrix $\rho(\mathbf{r}, \mathbf{r}', t)$. The most obvious asset is that 1-body observables are now directly accessible and the single-particle wave functions have a direct physical meaning. A lot of work has been focused on the static version of the theory, the (R)DMFT, or the linear response approach [38, 39]. The adiabatic functionals developed for the static calculation cannot lead to the time evolution of the occupation numbers [40] which is basically the wanted feature. For real-time time-dependent calculations, semiclassical methods are developed [41, 42] to include correlation and the truncation of BBGKY hierarchy is adressed again [43] almost two decades after the development in nuclear physics but this time in electronic systems.

In this thesis, we will focus on the inclusion of 2-body correlations in a mean-field framework. The far end would be to obtain the thermalization features in PES and PAD presented in the second example. The work presented here is the first steps in that direction and is more in the continuity of what have been developed in nuclear physics, though being applied in electronic systems. The thesis is organized as follows: first we present in Chapter 2 the formalism of the approaches that have been mentioned in this introduction. Three approaches, namely ETDHF, STDHF and collisional TDHF (CTDHF) are introduced. Then a first study on a ansatz of a collision term on top of TDDFT calculation to compute a rare reaction channel is presented in Chapter 3. The last two chapters study the range of validity of the schemes introduced in Chapter 2: that is the validity of STDHF in detail on a schematic two-band model (see Chapter 4) and a quantitative comparison of ETDHF, STDHF and CTDHF in a 1D continuous model closer to a realistic molecular model (see Chapter 5). We finally draw some conclusion and give some perspectives in Chapter 6.

Chapter 2

Theoretical framework

Contents

2.1 Introduction

Mean field theories are widely used as a first approach to describe a complex system. The mean field approach is often the lightest theory in terms of computation time. But most of such theories do not include correlation and provide only the main trajectories among all possible ones (e.g.in a dissociation process). The only mean field theory that would possess these features is the time-dependent density functional theory (TDDFT) with the exact functional for both the wave functions of electrons and nuclei. For the time being, such a theory is out of reach and functionals are approximated. On the other hand a configuration interaction (CI) calculation or multiconfiguration time-dependent Hartree-Fock (MCTDHF) contain all the needed correlation but are highly limited in terms of propagated time, excitation energy and number of particles.

As we want to describe non-linear problems with medium to high excitation energy, we need the computational efficiency of the mean field approach as well as effects beyond mean field. The main effect beyond a mean field approach is the dissipation induced by correlation. This can be interpreted as the effect of collisions between electrons. We can include this effect with a heuristic approach on top of a density functional theory, using an ansatz for a collision potential or derive more formally a theory that contains a dissipative term.

In this chapter, we will first present mean field theories, namely TDDFT and Hartree-Fock (HF). From HF, the residual interaction is introduced. Then, a density matrix functional is derived by truncating the BBGKY hierarchy. A collision integral and a stochastic force are derived to yield a quantum Boltzmann-Langevin equation. This equation being hard to numerically deal with, some approximations are introduced and three different algorithms, namely extended, stochastic and collisional time dependent HF (ETDHF, STDHF and CTDHF) are developed. Each of these algorithms has its own range of applicability. We will discuss the reliability of each scheme, compare the various levels of approximations involved and present how they are actually implemented.

2.2 Density Functional Theory and its Time-Dependent version

The time evolution of a quantum system is described by time-dependent Schrödinger equation (TDSE). However, it is generally not possible to find solutions of TDSE for realistic systems of more than a few particles. Density functional theory (DFT) and its time-dependent counterpart (TDDFT) simplify the calculations by mapping an exact interacting system of fermions on a non-interacting system in an effective potential that only depends on $\varrho(\mathbf{r})$ (or $\varrho(\mathbf{r},t)$ and the initial-time N-body wave function $|\Psi(t=0)\rangle$ for TDDFT). This mapping is exact as long as the exact functional of ϱ is known [7] which is not actually the case. We do not enter into the details of the derivation of DFT and TDDFT that can be found in [26, 44, 45, 46, 7, 8] and only provide here the practical equations and approximations.

We first consider the static case for the sake of simplicity. The non-interacting system of electrons can be treated directly with ϱ or in the Kohn-Sham (KS) scheme.

In this scheme, a set of N non-interacting KS orbitals φ_i replace N interacting electrons with the same total electronic density computed the following way:

$$\varrho(\mathbf{r}) = \sum_{i=1}^{N} \left|\varphi_i(\mathbf{r})\right|^2 \quad . \tag{2.1}$$

From this density, one can compute the energy using a functional of the form:

$$E_{\text{total,el}}[\varrho] = E_{\text{kin}}(\{\varphi_i\}' + E_{\text{H}}[\varrho] + E_{\text{xc}}[\varrho] + E_{\text{ions}} + E_{\text{ext}} \ , \tag{2.2a}$$

$$E_{\text{kin}}\left(\{\varphi_i\}\right) = -\int \mathrm{d}^3\mathbf{r} \sum_{i=1}^{N} \varphi_i^*(\mathbf{r})\ \nabla^2\ \varphi_i(\mathbf{r}) \ , \tag{2.2b}$$

$$E_{\text{H}}[\varrho] = \frac{e^2}{2} \iint \mathrm{d}^3\mathbf{r}\ \mathrm{d}^3\mathbf{r}'\ \frac{\varrho(\mathbf{r})\varrho(\mathbf{r}')}{|\mathbf{r}-\mathbf{r}'|} = \frac{1}{2}\int \mathrm{d}^3\mathbf{r}\ \varrho(\mathbf{r})\ U_{\text{H}}[\varrho] \ , \tag{2.2c}$$

$$E_{\text{ions}} = \int \mathrm{d}^3\mathbf{r} \sum_{i=1}^{N} \varphi_i^*(\mathbf{r})\ \hat{V}_{\text{ions}}\ \varphi_i(\mathbf{r}) \ , \tag{2.2d}$$

$$E_{\text{ext}} = \int \mathrm{d}^3\mathbf{r}\ \varrho(\mathbf{r})\ U_{\text{ext}}(\mathbf{r}) \quad . \tag{2.2e}$$

Here the spin degree of freedom has not been noted for simplicity. Each of the terms entering (2.2a) stands for:

- E_{kin} is the kinetic energy for non-interacting particles.
- $E_{\text{H}}[\varrho]$ is the Hartree term associated with the Hartree potential U_{H}. It represents the direct charge repulsion of an electronic density.
- E_{ion} is the energy from the coupling with the ions (nuclei + core electrons) gathered in one term $\hat{V}_{\text{ion}}$. Explicit expressions of E_{ion} will be given in Chapters 3 and 5.
- E_{ext} is an external potential (for example an electric field).
- E_{xc} is the exchange-correlation potential of the DFT that basically contains everything not accounted for in the other terms.

A simple and robust approximation consists in the Local Density Approximation (LDA). It assumes that the exchange-correlation potential can be treated locally in space:

$$E_{\text{xc}}^{\text{LDA}} = \int e_{\text{xc}}[\varrho(\mathbf{r})]\varrho(\mathbf{r})d\mathbf{r} \quad . \tag{2.3}$$

where e_{xc} is a local density of exchange-correlation energy. LDA is however plagued with a self-interaction issue. This means that each electron interacts with its own density participating to the total $\varrho(\mathbf{r})$. It leads to an exponentially decreasing tail of the LDA potential for a charged system instead of being proportional to $1/r$. Many strategies have been developed to solve this issue and provide a self-interaction correction (SIC). They go from the most refined (e.g. 2setSIC [47]) to the simplest ones (e.g. ADSIC [48]). In chapter 3 we will discuss more in details the SIC problem on an example. Over the past decades, many functionals more advanced than LDA have

been proposed. As the electron gas is not uniform (case where LDA is most suited), the next step has been to introduce the gradient of the electronic in the functionals, yielding the generalized gradient approximation (GGA). The most widely used functional nowadays belongs to the class of hybrid functionals and is called B3LYP [49, 50]. Hybrid functionals are linear combination of other functionals and generally incorporate a certain amount of exact exchange. In this work, we use LDA mostly because of its numerical efficiency, and occasionally ADSIC in Chapter 3.

For the time-dependent DFT, one can also consider LDA to be local in time, leading to adiabatic LDA (ALDA) and replace $\varrho(\mathbf{r})$ by $\varrho(\mathbf{r},t)$. In the following, we will just use the generic notation LDA for ALDA. (TD)LDA has been widely used in many calculations of electronic structure and dynamics, see e.g. [51, 52, 46, 1].

Once this energy functional obtained, variation of the total energy with respect to the single particle (s.p.) wave functions provides the KS equations:

$$\hat{h}_{\mathrm{KS}}[\varrho]\ |\varphi_i\rangle = \varepsilon_i\ |\varphi_i\rangle\ , \tag{2.4a}$$

$$\hat{h}_{\mathrm{KS}}[\varrho] = -\frac{\nabla^2}{2m} + U_{\mathrm{KS}}[\varrho] + \hat{V}_{\mathrm{ions}} + U_{\mathrm{ext}}\ , \tag{2.4b}$$

$$U_{\mathrm{KS}}[\varrho] = U_{\mathrm{H}}[\varrho] + U_{\mathrm{xc}}[\varrho] \quad . \tag{2.4c}$$

The local and density-dependent Kohn-Sham potential U_{KS} consists in the direct Coulomb term U_{H} and the exchange-correlation potential, $U_{\mathrm{xc}} = \delta E_{\mathrm{xc}}/\delta\varrho$. Coupling potentials to ions and to the external field are trivially given. The static problem is self-consistent as the potential depends on $\varrho(\mathbf{r})$.

The time-dependent KS equations analogously read:

$$\mathrm{i}\ \partial_t \varphi_i(\mathbf{r},t) = \hat{h}_{\mathrm{KS}}[\varrho]\,\varphi_i(\mathbf{r},t)\ , \tag{2.5}$$

where $\hat{h}_{\mathrm{KS}}$ is composed in the same manner as above, provided that one replaces $\varrho(\mathbf{r})$ by $\varrho(\mathbf{r},t)$[1]. This assumes an instantaneous adjustment of the total electronic density, although memory effects can play in some cases an important role, especially in E_{xc} [53].

2.3 Hartree Fock and collision term

Simpler than DFT, the famous HF approximation provides a first approximation of the exact Hamiltonian. We derive here the HF Hamiltonian in order to introduce the notations and the notion of residual interaction. We consider the non-relativistic Hamiltonian for a system of interacting electrons that reads in second quantization

$$\hat{H} = \int dx\, h^0(x,t)\hat{\Psi}^\dagger(x,t)\hat{\Psi}(x,t) + \frac{1}{2}\int dx dx'\, v(x,x')\hat{\Psi}^\dagger(x,t)\hat{\Psi}^\dagger(x',t)\hat{\Psi}(x',t)\hat{\Psi}(x,t)$$
$$h^0(x,t) = -\Delta_x/2 + u_{\mathrm{ext}}(x,t) \quad . \tag{2.6}$$

We use here a general coordinate x and spinless particles for simpler notations but it can be easily generalized. This Hamiltonian can also be written in any s.p. basis,

[1] Throughout this thesis, we have adopted the atomic units $e = \hbar = 1$).

leading to the general form:

$$\hat{H} = \underbrace{\sum_{i,j} h^0_{ij} \hat{a}^\dagger_i \hat{a}_j}_{\hat{h}^0} + \underbrace{\frac{1}{2} \sum_{i,j,k,l} v_{ijkl} \hat{a}^\dagger_i \hat{a}^+_j \hat{a}_l \hat{a}_k}_{\hat{V}} = \sum_{i,j} h^0_{ij} \hat{a}^\dagger_i \hat{a}_j + \frac{1}{4} \sum_{i,j,k,l} \tilde{v}_{ijkl} \hat{a}^\dagger_i \hat{a}^\dagger_j \hat{a}_l \hat{a}_k \tag{2.7}$$

where $\tilde{v}_{ijkl}$ is the antisymmetrized interaction

$$\tilde{v}_{ijkl} = v_{ijkl} - v_{ijlk} \quad . \tag{2.8}$$

2.3.1 HF: factorization

A way to obtain the HF Hamiltonian is to factorize directly the interaction term $\hat{V}$:

$$\hat{V} = \frac{1}{2} \sum_{i,j,k,l} v_{ijkl} \hat{a}^\dagger_i \hat{a}^\dagger_j \hat{a}_l \hat{a}_k \quad . \tag{2.9}$$

Wick's theorem with respect to the Fermi sea allows us to rewrite the product of the four operators as

$$\begin{aligned} \hat{a}^\dagger_i \hat{a}^\dagger_j \hat{a}_l \hat{a}_k = & \langle \hat{a}^\dagger_i \hat{a}_k \rangle \langle \hat{a}^\dagger_j \hat{a}_l \rangle - \langle \hat{a}^\dagger_i \hat{a}_l \rangle \langle \hat{a}^\dagger_j \hat{a}_k \rangle \\ & - \langle \hat{a}^\dagger_i \hat{a}_l \rangle \, : \hat{a}^\dagger_j \hat{a}_k : \\ & + \langle \hat{a}^\dagger_i \hat{a}_k \rangle \, : \hat{a}^\dagger_j \hat{a}_l : \\ & + \langle \hat{a}^\dagger_j \hat{a}_l \rangle \, : \hat{a}^\dagger_i \hat{a}_k : \\ & - \langle \hat{a}^\dagger_j \hat{a}_k \rangle \, : \hat{a}^\dagger_i \hat{a}_l : \\ & + : \hat{a}^\dagger_i \hat{a}^\dagger_j \hat{a}_l \hat{a}_k : \quad . \end{aligned} \tag{2.10}$$

The first term of Eq. (2.10) is a constant term leading to the HF energy of the interaction. It is the only remaining term when taking the mean value of $\hat{V}$ with respect to the HF determinant. All other terms cancel out because of the ordered products. The mean value of the last term equals zero: this is what we call residual interaction in HF theory and it can be considered as quantum fluctuations. The HF approximation consists in neglecting this term. The 1-body operators can be rewritten making use of $: \hat{a}^\dagger_i \hat{a}_l := \hat{a}^\dagger_i \hat{a}_l - \langle \hat{a}^\dagger_i \hat{a}_l \rangle$. The constant terms are dropped and the only remaining terms are the following:

$$\begin{aligned} \hat{a}^\dagger_i \hat{a}^\dagger_j \hat{a}_l \hat{a}_k \approx & - \langle \hat{a}^\dagger_i \hat{a}_l \rangle \hat{a}^\dagger_j \hat{a}_k \\ & + \langle \hat{a}^\dagger_i \hat{a}_k \rangle \hat{a}^\dagger_j \hat{a}_l \\ & + \langle \hat{a}^\dagger_j \hat{a}_l \rangle \hat{a}^\dagger_i \hat{a}_k \\ & - \langle \hat{a}^\dagger_j \hat{a}_k \rangle \hat{a}^\dagger_i \hat{a}_l \quad . \end{aligned} \tag{2.11}$$

This approximation enables to define the HF interaction term $\hat{w}$ using $\langle \hat{a}^\dagger_i \hat{a}_l \rangle = \delta_{il}$ if i belongs to the occupied states (also called hole states) and zero otherwise:

$$\hat{w} = \frac{1}{2} \left[- \sum_{\substack{ijk \\ i \in \text{occ}}} v_{ijki} \hat{a}^\dagger_j \hat{a}_k + \sum_{\substack{ijl \\ i \in \text{occ}}} v_{ijil} \hat{a}^\dagger_j \hat{a}_l + \sum_{\substack{ijk \\ j \in \text{occ}}} v_{ijkj} \hat{a}^\dagger_i \hat{a}_k - \sum_{\substack{ijl \\ j \in \text{occ}}} v_{ijjl} \hat{a}^\dagger_i \hat{a}_l \right] \quad . \tag{2.12}$$

Using that $v_{ijkl} = v_{jilk}$ it simplifies into

$$\hat{w} = \sum_{kl} \left(\sum_{j \in \text{occ}} \tilde{v}_{kjlj} \right) \hat{a}_k^\dagger \hat{a}_l \quad . \tag{2.13}$$

The HF Hamiltonian is then

$$\hat{h} = \hat{h}^0 + \hat{w} \tag{2.14}$$

with the matrix elements read as

$$h_{kl} = h_{kl}^0 + \sum_{j \in \text{occ}} \tilde{v}_{kjlj} \quad . \tag{2.15}$$

We recall the expression of the HF energy and the mean value of $\hat{h}$:

$$E_{\text{HF}} = \langle \Psi_{\text{HF}} | \hat{H} | \Psi_{\text{HF}} \rangle = \sum_{m \in \text{occ}} t_{mm} + \frac{1}{2} \sum_{m,n \in \text{occ}} \tilde{v}_{mnmn} \tag{2.16}$$

$$\langle \Psi_{\text{HF}} | \hat{h} | \Psi_{\text{HF}} \rangle = \sum_{m \in \text{occ}} t_{mm} + \sum_{m,n \in \text{occ}} \tilde{v}_{mnmn} \tag{2.17}$$

2.3.2 Residual interaction

The residual interaction can be derived using Wick's theorem. This is the neglected fluctuation term in Eq. (2.10):

$$\hat{V}_{\text{res}} = \frac{1}{2} \sum_{i,j,k,l} v_{ijkl} :\hat{a}_i^\dagger \hat{a}_j^\dagger \hat{a}_l \hat{a}_k: \quad . \tag{2.18}$$

By definition, this term has a vanishing mean value. Applied to a determinant in the same basis, this term is non zero only if l, k are hole (= occupied) states and i, j are particle (= unoccupied) states respectively. In all other cases, there exists a creation or an annihilation operator that cancels the determinant, and the normal ordering applies them first to the determinant. The residual interaction generates only 2-particle-2-hole ($2p2h$) excitations.

2.4 Basic derivation of BBGKY hierarchy

On top of this mean field approximation, particles develop n-body correlations which must be taken care of, otherwise physical behaviors are lost. Reduced density matrix theory is a useful formalism that allows one to have a direct access to a physical interpretation and observable. The equations of motion of reduced density matrices form a hierarchy of equations. This hierarchy is called BBGKY hierarchy after its classical statistical counterpart developed by Born, Bogoliubov, Green, Kirkwood and Yvon [54, 55, 56, 57]. From Green's function formalism, it can also be refered as a Martin-Schwinger hierarchy for density matrices. This hierarchy is totally equivalent to TDSE but it enables a deeper understanding of the possible level of approximations and truncations. We give here as an example the derivation of the first two terms

of the hierarchy. The equations of motion for creation and annihilation operators in Heisenberg picture are

$$\Big(\mathrm{i}\partial_t - h^0(x,t)\Big)\hat{\Psi}(x,t) = \int d\bar{x}\, v(x,\bar{x})\hat{\Psi}^\dagger(\bar{x},t)\hat{\Psi}(\bar{x},t)\hat{\Psi}(x,t) \tag{2.19}$$

$$\Big(-\mathrm{i}\partial_t - h^0(x,t)\Big)\hat{\Psi}^\dagger(x,t) = \hat{\Psi}^\dagger(x,t)\int d\bar{x}\, v(x,\bar{x})\hat{\Psi}^\dagger(\bar{x},t)\hat{\Psi}(\bar{x},t) \quad . \tag{2.20}$$

The reduced density matrices are defined as follow

$$\rho^{(n)}(x_1\dots x_n; x_{1'}\dots x_{n'}; t) = \langle\hat{\Psi}^\dagger(x_{1'},t)\dots\hat{\Psi}^\dagger(x_{n'},t)\hat{\Psi}(x_n,t)\dots\hat{\Psi}(x_1,t)\rangle \quad . \tag{2.21}$$

In the following the 1-body density matrix $\rho^{(1)}$ is simply noted ρ and its diagonal elements $\varrho(x,t) = \rho(x;x;t)$. The time index will be omitted most of the time for the sake of simplicity. The equation of motion of ρ is straightforward:

$$\begin{aligned}\mathrm{i}\partial_t\rho(x_1;x_{1'}) &= \Big(h^0(x_1) - h^0(x_{1'})\Big)\rho(x_1;x_{1'}) \\ &+ \int dx_2\Big(v(x_1,x_2) - v(x_{1'},x_{2'})\Big)\rho^{(2)}(x_1,x_2;x_{1'},x_{2'}) \quad .\end{aligned} \tag{2.22}$$

The equation of $\rho^{(2)}$ gives more details about what occurs in the general case:

$$\begin{aligned}\mathrm{i}\partial_t\rho^{(2)}(x_1,x_2;x_{2'},x_{1'}) &= \Big(h^0(x_1) - h^0(x_{1'}) + h^0(x_2) - h^0(x_{2'})\Big)\rho^{(2)}(x_1,x_2;x_{1'},x_{2'}) \\ &+ \int dx_3\Big(v(x_2,x_3) - v(x_{2'},x_3)\Big)\rho^{(3)}(x_1,x_2,x_3;x_{1'},x_{2'},x_3) \\ &+ \int dx_3\Big(v(x_1,x_3)\langle\hat{\Psi}^\dagger(x_{1'},t)\hat{\Psi}^\dagger(x_{2'},t)\hat{\Psi}(x_2,t)\hat{\Psi}^\dagger(x_3,t)\hat{\Psi}(x_3,t)\hat{\Psi}(x_1,t)\rangle \\ &\quad - v(x_{1'},x_3)\langle\hat{\Psi}^\dagger(x_{1'},t)\hat{\Psi}^\dagger(x_3,t)\hat{\Psi}(x_3,t)\hat{\Psi}^\dagger(x_{2'},t)\hat{\Psi}(x_2,t)\hat{\Psi}(x_1,t)\rangle\Big)\end{aligned} \tag{2.23}$$

A few commutations are necessary in the last term to write everything in terms of the 3-body density matrix:

$$\begin{aligned}&\mathrm{i}\partial_t\rho^{(2)}(x_1,x_2;x_{2'},x_{1'}) = \\ &\quad\Big(h^0(x_1) - h^0(x_{1'}) + h^0(x_2) - h^0(x_{2'}) + v(x_1,x_2) - v(x_{1'},x_{2'})\Big)\rho^{(2)}(x_1,x_2;x_{1'},x_{2'}) \\ &\quad + \int dx_3\Big(v(x_2,x_3) - v(x_{2'},x_3) + v(x_1,x_3) - v(x_{1'},x_3)\Big)\rho^{(3)}(x_1,x_2,x_3;x_{1'},x_{2'},x_{3'})\end{aligned} \tag{2.24}$$

Here we derived only the first two equations of the hierarchy but one can easily generalize the procedure to obtain the equations for $\rho^{(n)}$.

2.5 Truncation of BBGKY hierarchy

2.5.1 Cluster expansion

The general form of these equations reads as:

$$\begin{aligned}&\Big(\mathrm{i}\partial_t - k(x_1..x_n) + k(x_{1'}..x_{n'})\Big)\rho^{(n)}(x_1..x_n;x_{1'}..x_{n'}) \\ &\quad = \sum_{j=1}^{n}\int dx_{n+1}\Big(v(x_j,x_{n+1}) - v(x_{j'},x_{n+1})\Big)\rho^{(n+1)}(x_1..x_n,x_{n+1};x_{1'}..x_{n'},x_{n+1})\end{aligned} \tag{2.25}$$

where

$$k(x_1..x_n;t) = \sum_{i=1}^{n} h^0(x_i;t) + \frac{1}{2}\sum_{i\neq j}^{n} v(x_i,x_j) \quad . \tag{2.26}$$

Time indices are implicit in Eq. (2.25). In the following i will stand for x_i. The first two equations of this hierarchy are written again explicitly:

$$\Big(\mathrm{i}\partial_t - h^0(1) + h^0(1')\Big)\rho(1;1') = \int d2\Big(v(1,2) - v(1',2)\Big)\rho^{(2)}(1,2;1',2) \;, \tag{2.27}$$

$$\begin{aligned}\Big(\mathrm{i}\partial_t - h^0(1) + h^0(1') - h^0(2) + h^0(2') - v(1,2) + v(1',2')\Big)\rho^{(2)}(1,2;1',2') \\ = \int d3\Big(v(1,3) - v(1',3) + v(2,3) - v(2',3)\Big)\rho^{(3)}(1,2,3;1',2',3) \quad .\end{aligned} \tag{2.28}$$

The BBGKY hierarchy is not solvable as it is. It has to be truncated for instance at level $n-1$ and the n-body density matrix has to be approximated as an antisymmetrized product of p-body matrices, $p < n$. One way to truncate has been proposed by Wang and Cassing [16]. It begins with a cluster expansion of the various reduced density matrices. For example the 2-body density matrix reads

$$\rho^{(2)}(1,2;1',2') = \rho(1;1')\rho(2;2') - \rho(1;2')\rho(2;1') + c^{(2)}(1,2;1',2') \quad . \tag{2.29}$$

The advantage of this expression is to separate the various levels of correlation. For the 2-body density matrix in Eq. (2.29), $c^{(2)}$ is the two-particle correlation term once the mean field is substracted. In a more general way, the n-body density matrix can be written in a compact form as:

$$\rho^{(n)} = AS\{\sum_{p=1}^{n-1} \rho^{(n-p)}\rho^{(p)}\} + c^{(n)} \quad , \tag{2.30}$$

where S symmetrizes with respect to pair indices (i,i') and A antisymmetrizes the i' indices with the corresponding sign. Another rule is that every term appears only once. For example, we have:

$$\begin{aligned}AS\{\rho\rho^{(2)}\} &= A\Big\{\rho(1;1')\rho^{(2)}(2,3;2',3') + \rho(2;2')\rho^{(2)}(1,3;1',3') + \rho(3;3')\rho^{(2)}(1,2;1',2')\Big\} \\ &= \rho(1;1')\rho^{(2)}(2,3;2',3') - \rho(1;2')\rho^{(2)}(2,3;1',3') - \rho(1;3')\rho^{(2)}(2,3;2',1') \\ &+ \rho(2;2')\rho^{(2)}(1,3;1',3') - \rho(2;1')\rho^{(2)}(1,3;2',3') - \rho(2;3')\rho^{(2)}(1,3;1',2') \\ &+ \rho(3;3')\rho^{(2)}(1,2;1',2') + \rho(3;1')\rho^{(2)}(1,2;3',2') + \rho(3;2')\rho^{(2)}(1,2;1',3') \quad .\end{aligned} \tag{2.31}$$

This is quite a lengthy expression for just one term.

We introduce some compact notations here: superscripts correspond to the number of particles of the element, subscripts enable to know which coordinates are coupled. They are not directly related to the x_i of the operator as we can write for example

$$c^{(2)}(1,2;1',2') = c_{12}(1,2;1',2') = c_{23}(1,2;1',2') \quad . \tag{2.32}$$

The number of indices giving the number of particles, superscripts are omitted when subscripts are used. We will switch between both notations and omit the coordinates when there is no ambiguity, leading sometimes to identify abusively a matrix element

with the matrix itself. The notation $\mathrm{Tr}_2(F_{12})$ corresponds to $\int d2\Big(F(1,2;1',2')_{2=2'}\Big)$ for a given function F. Permutation operators P_{ij} will be used if convenient. They are defined as

$$P_{ij}|ij\rangle = |ji\rangle \tag{2.33}$$
$$\text{or } P_{12}(1,2;1',2') = \delta(1-2')\delta(2-1') \quad . \tag{2.34}$$

For example, we have:

$$\begin{aligned}(P_{12}\rho_1\rho_2)(1,2;1',2') &= \rho(2,1')\rho(1,2')\ ,\\ (\rho_1\rho_2P_{12})(1,2;1',2') &= \rho(1,2')\rho(2,1') = (P_{12}\rho_1\rho_2)(1,2;1',2') \quad .\end{aligned} \tag{2.35}$$

Therefore P_{12} commutes with $\rho_1\rho_2$ and $AS\{\rho\rho\} = \rho_1\rho_2(1-P_{12})$. For instance, if $\rho^{(2)}$ is replaced by $AS\{\rho\rho\} = \rho_1\rho_2(1-P_{12}) + c_{12}$ in Eq. (2.27), it reads

$$\mathrm{i}\partial_t\rho_1 - [h_1,\rho_1] = \mathrm{Tr}_2[v_{12},c_{12}] \tag{2.36}$$

where

$$h_1\rho_1 = h_1^0\rho_1 + \mathrm{Tr}_2\{v_{12}\rho_2\}\rho_1 - \mathrm{Tr}_2\{v_{12}\rho_2\rho_1P_{12}\} \tag{2.37}$$

which is simply the HF Hamiltonian.

2.5.2 Deriving the Boltzmann-Langevin equation

The idea behind deriving a Boltzmann-Langevin equation from the BBGKY hierarchy is the following: first the hierarchy is truncated at the 2-body level ($c^{(3)} = 0$), then the equation of evolution for the 2-body correlation is formally solved and then inserted in the 1-body density matrix evolution. In the truncation, one can assume that

$$\rho^{(3)} \approx AS\{\rho^{(2)}\rho\} \tag{2.38}$$

since $c^{(3)}$ has been neglected. It is exactly the terms explicitly written in Eq. (2.31). One can expand $\rho^{(3)}$ using $\rho^{(2)} = AS\{\rho\rho\} + c^{(2)}$. This yields

$$\begin{aligned}\rho^{(3)} &\approx AS\{\rho\rho\rho + \rho c^{(2)}\}\\ &= \rho_1c_{23}(1-P_{12}-P_{13}) + \rho_2c_{13}(1-P_{21}-P_{23}) + \rho_3c_{12}(1-P_{31}-P_{32})\\ &+ \rho_1\rho_2\rho_3(1-P_{12})(1-P_{12}-P_{23}) \quad .\end{aligned} \tag{2.39}$$

Thus only the equation of evolution for $c^{(2)}$ is needed. First of all, we need the evolution of the term $AS\{\rho\rho\}$:

$$\begin{aligned}\mathrm{i}\partial_t\rho_1\rho_1(1-P_{12}) &= [h_1^0,\rho_1]\rho_2(1-P_{12}) + [h_2^0,\rho_2]\rho_1(1-P_{12})\\ &+ \mathrm{Tr}_3[v_{13},\rho_{13}]\rho_2(1-P_{12}) + \mathrm{Tr}_3[v_{23},\rho_{23}]\rho_1(1-P_{12}) \quad .\end{aligned} \tag{2.40}$$

It can be seen that it generates all unlinked terms. We give an example of unlinked terms as $v(2,3)\rho^{(2)}(2,3;2',3')\rho(1;1')$ where v_{12} does not couple the two density matrices. A more general result has been proved in [16], but here it is only needed to prove it for the first two equations. Therefore the evolution of $c^{(2)}$ only takes into account

the linked terms. After some cumbersome but straightforward calculations, one can obtain

$$\begin{aligned} \mathrm{i}\partial_t c_{12} - [h_1 + h_2, c_{12}] = \\ \frac{1}{2}\Big(\bar{\rho_1}\bar{\rho_2}(1-P_{12})v_{12}\rho_1\rho_2(1-P_{12}) - \rho_1\rho_2(1-P_{12})v_{12}\bar{\rho_1}\bar{\rho_2}(1-P_{12})\Big) \\ + O(c_{12}v_{12}) \end{aligned} \quad (2.41)$$

where $\bar{\rho_1} = 1 - \rho_1$. Most of the terms proportional to $c_{12}v_{12}$ are neglected here. For a complete derivation, see [18]. These results can also be found in [58] with examples of application on physical systems. The right hand side is the collision term or Born term B_{12} that leads to the dissipative term in ETDHF theory (see Sec. 2.5.3). This term stems entirely from $AS\{\rho\rho\rho\}$. The expression of two terms of Eq. (2.41) are given here as examples to make the notations really clear:

$$\begin{aligned} \rho_1\rho_2 P_{12}v_{12}\rho_2 &= \int d3v(1';3)\rho(1;3)\rho(2;1')\rho(3;2') \ , \\ -\rho_2 v_{12}\rho_1\rho_2 P_{12} &= -\int d3v(1;3)\rho(1;2')\rho(2;3)\rho(3;1') \quad . \end{aligned} \quad (2.42)$$

We remind the reader that $v(i;j) \leftrightarrow v(i,j;i',j')\delta(i-i')\delta(j-j')$ so the right hand side is consistent with the 2-body operator notation. It has to be noticed that this term is not derived by replacing $\rho^{(3)}$ directly by $AS\{\rho\rho\rho\}$ but also by taking into account the unlinked terms of Eq. (2.40) and some terms of $\rho_3 c_{12}(1 - P_{13} - P_{23})$ that turn $h_1^0 + h_2^0$ into $h_1 + h_2$. Now it is possible to solve formally Eq. (2.41) to get

$$c_{12}(t) = -\mathrm{i}\int_{t_0}^{t} ds U_{12}(t,s)B_{12}(s)U_{12}(s,t) + \delta c_{12}(t) \quad (2.43)$$

where $U_{12} = U_1 U_2$ with $U_i = \mathcal{T}\exp\Big(-i\int_{t_0}^{t} h_i(s)ds\Big)$ and $\mathcal{T}$ the time ordering operator. The second term $\delta c_{12}(t) = U_{12}(t,t_0)c_{12}(t_0)U_{12}(t_0,t)$ is the mean field propagation of the initial correlation. It is now possible to insert c_{12} in Eq. (2.36):

$$\mathrm{i}\partial_t \rho = [h,\rho] + K[\rho] + \delta K(t) \ , \quad (2.44)$$

$$K[\rho] = -\mathrm{i}\int_{t_0}^{t} ds \, \mathrm{Tr}_2[v_{12}, U_{12}(t,s)B_{12}(s)U_{12}(s,t)] \ , \quad (2.45)$$

$$\delta K(t) = \mathrm{Tr}_2[v_{12}, \delta c_{12}(t)] \quad . \quad (2.46)$$

In this equation $K[\rho]$ is interpreted as a collision term and $\delta K(t)$ as a stochastic force, see [22] for more details.

We write again explicitly the collision integral:

$$\begin{aligned} K[\rho] = \frac{\mathrm{i}}{2}\int_{t_0}^{t} ds \, \mathrm{Tr}_2 \Big\{ \Big[v, U(t,s)AS\{\rho\rho\}vAS\{\bar{\rho}\bar{\rho}\}U^\dagger(t,s)\Big] \\ - \Big[v, U(t,s)AS\{\bar{\rho}\bar{\rho}\}vAS\{\rho\rho\}U^\dagger(t,s)\Big]\Big\} \quad . \end{aligned} \quad (2.47)$$

Here we have omitted the subscripts (12). When a thermal equilibrium with respect to the mean field Hamiltonian is reached the term c_{12} vanishes. Then $\mathrm{Tr}_2[v_{12}, c_{12}]$ in Eq. (2.36) cancels out and only the mean field drives the propagation of ρ. We can expect a Fermi-Dirac distribution to remain stable over time. The relation between the stochastic force and the collision term has been studied in details in [23].

2.5.3 Extended TDHF

Extended TDHF has been introduced as a way to include dissipation due to collisions between hadron in nuclei [14]. At the beginning, it has been introduced in a more semiclassical approach based on VUU equations. What is presented here reduces to the "historical" ETDHF in the Markovian limit (see Eq. 2.62).

To obtain ETDHF, the stochastic force term δK is set to zero. This amounts to assume that there is no initial correlation in our system. Eq. (2.44) then reduces to:

$$\mathrm{i}\partial_t \rho = [h, \rho] + K[\rho] \quad . \tag{2.48}$$

It leads to the version of ETDHF with a non-Markovian collision term. Indeed the collision term (2.47) includes an integral over the full past of the system. We introduce the instantaneous natural basis, i.e. the basis that diagonalizes the 1-body density matrix $\rho(t)$:

$$\rho(t) = \sum_i |i(t)\rangle \, n_i(t) \, \langle i(t)| \tag{2.49}$$

By defining

$$\langle kj|\tilde{v}|lm\rangle_s = \langle kj|v|lm\rangle_s - \langle kj|v|ml\rangle_s \tag{2.50}$$

we can write the matrix element of the collision integral (2.47) in this basis:

$$\begin{aligned}\langle j|K|i\rangle = \frac{\mathrm{i}}{2}\int_{t_0}^{t} ds \sum_{klm} \Big[&\langle jk|\tilde{v}|lm\rangle_t \langle lm|\tilde{v}|ik\rangle_s \Big(n_l n_m (1-n_i)(1-n_k) - n_i n_k (1-n_l)(1-n_m) \Big)_s \\ &+ \langle jk|\tilde{v}|lm\rangle_s \langle lm|\tilde{v}|ik\rangle_t \Big(n_l n_m (1-n_j)(1-n_k) - n_j n_k (1-n_l)(1-n_m) \Big)_s \Big] \quad .\end{aligned} \tag{2.51}$$

where the subscript indicates that we used the natural basis at time s [2].

Note that the propagator U in the collision integral K in Eq. (2.47) corresponds to the mean field propagation of the density matrix and not the full propagation taking into account K. Therefore the terms at time s are to be used with caution. Actually $|lm\rangle_t = U(t,s)|lm\rangle_s$ where $|lm\rangle_s$ is really in the instantaneous natural basis at time s whereas $|lm\rangle_t$ is *not* as the mean field propagation does not equal the full one. More details on the numerical implementation of this equation are given for example in [59].

2.5.4 Markovian approximation

The mean field propagator

$$U_i(t,s) = \mathcal{T} \exp\Big(-\mathrm{i}\int_s^t h_i(t')dt' \Big) \tag{2.52}$$

is a complicated term because the mean field Hamiltonian depends on $\rho(t)$ and t and there is an integration over time. We assume that the terms of the form $\langle jk|\tilde{v}|lm\rangle_t \langle lm|\tilde{v}|ik\rangle_s$ vanish for s far from t. Therefore we can replace in the time interval $[s,t]$:

$$h(t') \approx h(t) \text{ for } t' \text{ in } [s,t] \, , \tag{2.53}$$

$$\rho(t') \approx \rho(t) \text{ for } t' \text{ in } [s,t] \, . \tag{2.54}$$

[2] The closure relation $\mathbb{I} = \frac{1}{2}\sum_{lm} |lm\rangle\langle lm| + |ml\rangle\langle ml|$ is used to make $\tilde{v}$ appear.

The 2-body mean field propagator becomes:

$$U = e^{-\mathrm{i}(t-s)(h_1(t)+h_2(t))} \tag{2.55}$$

We now consider the instantaneous eigenbasis of the mean field Hamiltonian i.e. the basis such as:

$$h(t)|i\rangle = \varepsilon_i|i\rangle \tag{2.56}$$

at a given t. In this basis, the propagator is diagonal:

$$U_{ijkl} = \delta_{ik}\delta_{jl}e^{-\mathrm{i}(t-s)(\varepsilon_i+\varepsilon_j)} \quad . \tag{2.57}$$

We keep on assuming that the collision integral has a short memory. Therefore it makes no difference to extend the lower integration limit t_0 to $-\infty$. We also make the following approximation:

$$\int_{-\infty}^{t} ds\, e^{-\mathrm{i}(t-s)(\varepsilon_i+\varepsilon_j-\varepsilon_k-\varepsilon_l)} \approx \pi\delta(\varepsilon_i+\varepsilon_j-\varepsilon_k-\varepsilon_l) \quad . \tag{2.58}$$

Here, the principal value has been dropped as it would generate only off-diagonal elements. These elements add up to the mean field but we assume that the mean field mainly prevales in the non-dissipative evolution. More formally it can be written with the help of the mean field Liouvillian $\mathcal{L}_0$:

$$\int_{-\infty}^{t} ds\, e^{-\mathrm{i}(t-s)\mathcal{L}_0} = \pi\delta(\mathcal{L}_0) \tag{2.59}$$

where $\mathcal{L}_0$ fulfills $\mathcal{L}_0 A_{12} = [h_1 + h_2, A_{12}]$. Therefore in the Markovian approximation, the collision integral is

$$K = \mathrm{i}\frac{\pi}{2}\,\mathrm{Tr}_2\{[v, \delta(\mathcal{L}_0)AS\{\rho\rho\}vAS\{\bar{\rho}\bar{\rho}\}] - [v, \delta(\mathcal{L}_0)AS\{\bar{\rho}\bar{\rho}\}vAS\{\rho\rho\}]\} \quad . \tag{2.60}$$

Now we consider again the ETDHF collision integral of Eq. (2.51). In addition to the Markovian approximation, we assume that there exists a basis in which ρ is diagonal, and h close to diagonal, i.e.

$$\Delta h = \sqrt{\mathrm{Tr}\{h\rho\}^2 - \mathrm{Tr}\{h^2\rho\}} \tag{2.61}$$

is small enough to be neglected. We also consider only the diagonal elements:

$$\begin{aligned}\langle i|K|i\rangle = \mathrm{i}\pi \sum_{klm} &|\langle ik|\tilde{v}|lm\rangle|^2 \delta(\varepsilon_k+\varepsilon_i-\varepsilon_l-\varepsilon_m) \\ &\times \Big(n_l n_m(1-n_i)(1-n_k) - n_i n_k(1-n_l)(1-n_m)\Big) \quad .\end{aligned} \tag{2.62}$$

This term is actually the only diagonal term in the right hand side of Eq. (2.48). It directly acts on the occupation numbers of the density matrix. The assumption of a small Δh is expected to be fulfilled in the case of low energy excitations. In the following, ETDHF will always refer to this Markovian version restricted to diagonal elements. In practice, the delta function that appears in Eq. (2.62) is replaced by a door function with a certain width. This idea will be discussed more in details for STDHF and CTDHF.

2.5.5 Relation to the (Time-Dependent) Reduced Density Matrix Functional Theory

In this work, we only deal with time-dependent theories. For any dynamical calculation one could use as a starting point a density matrix obtained from a static calculation in the Reduced Density Matrix Functional Theory (RDMFT) framework (see [38] and references therein). Moreover, TD-RDMFT is also based on BBGKY hierarchy assuming the 2-body density matrix is a functional of the 1-body density matrix. Runge-Gross theorem [7, 44, 45] ensures that this is true for a local external potential. Actually, Eq. (2.44) contains such a functional. The term $K[\rho]$ as expressed in Eq. (2.47) only depends on the 1-body density matrix ρ and δK is the dependence on the initial state. This initial dependence is limited to the 2-body correlation as this is our level of truncation of the BBGKY hierarchy. With this initial dependence it fulfills the criterium derived in [60] on the compatibility between the memory and the initial state dependence.

2.6 Stochastic TDHF

We now turn to the core of this thesis based on the seminal work of Reinhard, Suraud and Ayik [23]. Stochastic TDHF (STDHF) is a theory that approximates the exact propagation of a quantum state by an ensemble of Slater determinants which density matrices are propagated in time in a mean field framework and incoherently added up. This scheme has been presented and studied in [23, 24, 61, 62]. For the sake of completeness, most of the demonstrations are done in this part.

2.6.1 Ensemble of trajectories

We first assume that our starting point at time t' is a N-body density matrix of the form

$$\mathcal{D}(t') = \sum_{\alpha} x^{(\alpha)}(t') D^{(\alpha)}(t') \quad . \tag{2.63}$$

Here $D^{(\alpha)}(t') = |\Phi^{(\alpha)}(t')\rangle\langle\Phi^{(\alpha)}(t')|$, $|\Phi^{(\alpha)}(t')\rangle$ being a Slater determinant, and α the index in the ensemble of density matrices that are incoherently added up to form $\mathcal{D}(t')$. We now look at the evolution of the system over the time interval $[t', t]$ and define $\tau = t - t'$. To do so, only one uncorrelated density matrix $D^{(\alpha)}$ will be considered first. With no loss of generality, the initial time is taken as $t' = 0$. Each $D^{(\gamma)}$ is propagated in its own mean field, and this is what we call a "trajectory".

2.6.2 Propagation of one trajectory

Let us first consider one trajectory, labeled by α, and starting from $|\Phi^{(\alpha)}(0)\rangle$. The corresponding mean field at any time s is denoted $h(s)$ and can be complemented by a residual interaction $V(s)$ to get the exact Hamiltonian $H(s) = h(s) + V(s)$. The time

evolution operators are the following ones:

$$\begin{aligned} U(\tau,\epsilon) &= \mathcal{T} e^{-\mathrm{i}\int_\epsilon^\tau H(s)ds} \\ U_0(\tau,\epsilon) &= \mathcal{T} e^{-\mathrm{i}\int_\epsilon^\tau h(s)ds} \end{aligned} \tag{2.64}$$

with $\tau > \epsilon$. In the same way as done in the interaction picture, one can obtain:

$$\mathrm{i}\partial_\epsilon\Big(U(\tau,\epsilon)U_0(\epsilon,\tau)\Big) = -U(\tau,\epsilon)U_0(\epsilon,\tau)\widetilde{V}(\epsilon) \tag{2.65}$$

where

$$\widetilde{V}(\epsilon) = U_0(\tau,\epsilon)V(\epsilon)U_0(\epsilon,\tau) \quad . \tag{2.66}$$

The formal expression of the product $U(\tau,\epsilon)U_0(\epsilon,\tau)$ is:

$$U(\tau,\epsilon)U_0(\epsilon,\tau) = \mathcal{T} e^{-\mathrm{i}\int_\epsilon^\tau \widetilde{V}(s)ds} \tag{2.67}$$

Now let $\epsilon \to 0$. The operator $\Omega_+ = U(\tau,0)U_0(0,\tau)$ allows to go back and forth between the exact evolution $|\Psi^{(\alpha)}(\tau)\rangle$ and the mean field one $|\Phi^{(\alpha)}(\tau)\rangle$ of the initial state $|\Phi^{(\alpha)}(0)\rangle$:

$$|\Psi^{(\alpha)}(\tau)\rangle = \Omega_+|\Phi^{(\alpha)}(\tau)\rangle \quad . \tag{2.68}$$

It can be approximated up to the second order in $\widetilde{V}$ as:

$$|\Psi^{(\alpha)}(\tau)\rangle \approx |\Phi^{(\alpha)}(\tau)\rangle - \mathrm{i}\int \widetilde{V}|\Phi^{(\alpha)}(\tau)\rangle - \frac{1}{2}\mathcal{T}\Big\{\int \widetilde{V}\int \widetilde{V}\Big\}|\Phi^{(\alpha)}(\tau)\rangle \tag{2.69}$$

where $\int \widetilde{V} = \int_0^\tau \widetilde{V}(s)ds$. The corresponding time-dependent N-body density matrix $\mathcal{D}^{(\alpha)}(\tau)$ reads:

$$\begin{aligned} \mathcal{D}^{(\alpha)}(\tau) &= |\Phi^{(\alpha)}(\tau)\rangle\langle\Phi^{(\alpha)}(\tau)| + \Big(-\mathrm{i}\int \widetilde{V}|\Phi^{(\alpha)}(\tau)\rangle\langle\Phi^{(\alpha)}(\tau)| + \mathrm{h.c.}\Big) \\ &+ \int \widetilde{V}|\Phi^{(\alpha)}(\tau)\rangle\langle\Phi^{(\alpha)}(\tau)|\int \widetilde{V} - \Big(\frac{1}{2}\mathcal{T}\Big\{\int \widetilde{V}\int \widetilde{V}\Big\}|\Phi^{(\alpha)}(\tau)\rangle\langle\Phi^{(\alpha)}(\tau)| + \mathrm{h.c.}\Big) \end{aligned} \tag{2.70}$$

Let us now consider an instantaneous orthonormal basis at time τ, denoted by $|\kappa\rangle = |\Phi^{(\alpha)}_\kappa(\tau)\rangle$. We also write $|0\rangle = |\Phi^{(\alpha)}(\tau)\rangle$ to simplify the notations. Keeping only the diagonal terms, the N-body density matrix simplifies as

$$\begin{aligned} \mathcal{D}^{(\alpha)}(\tau) \approx\ & |0\rangle\langle 0| + \sum_\kappa |\kappa\rangle\langle\kappa|\int \widetilde{V}|0\rangle\langle 0|\int \widetilde{V}|\kappa\rangle\langle\kappa| \\ & - \frac{1}{2}|0\rangle\langle 0|\mathcal{T}\Big\{\int \widetilde{V}\int \widetilde{V}\Big\}|0\rangle\langle 0| - \frac{1}{2}|0\rangle\langle 0|\bar{\mathcal{T}}\Big\{\int \widetilde{V}\int \widetilde{V}\Big\}|0\rangle\langle 0| \end{aligned} \tag{2.71}$$

where $\bar{\mathcal{T}}$ is the reverse time ordering. It is possible to get rid of the two time ordering operators using $\mathcal{T}\Big\{\int \widetilde{V}\int \widetilde{V}\Big\} + \bar{\mathcal{T}}\Big\{\int \widetilde{V}\int \widetilde{V}\Big\} = 2\int \widetilde{V}\int \widetilde{V}$. As h and V depend a priori on the initial Slater determinant, we use in the following a superscript $H = h^{(\alpha)} + V^{(\alpha)}$. Finally, we get

$$\mathcal{D}^{(\alpha)}(\tau) \approx |0\rangle\langle 0|\Big(1 - \sum_{\kappa\neq 0}\Big|\langle\kappa|\int \widetilde{V}^{(\alpha)}|0\rangle\Big|^2\Big) + \sum_{\kappa\neq 0}|0\rangle\Big|\langle\kappa|\int \widetilde{V}^{(\alpha)}|0\rangle\Big|^2\langle 0| \quad . \tag{2.72}$$

Before we proceed, we discuss a bit the physical validity of what is done here. We aim at describing high energy situations where many transitions occur. The off-diagonal matrix elements are then expected to have fast oscillations with random phases and to average out to zero. The considered main process is dissipation that arises from the diagonal terms when neglecting quantum fluctuations. To this point the scheme can be interpreted as follows: the initial statistical and non-coherent state is our "molecular chaos" hypothesis and, with the use of Ω_+, we consider a collision mediated by V. We then assume that τ is long enough so that the system has forgotten the correlations and we can again consider only an incoherent sum, i.e. we are back to molecular chaos.

The transition matrix element $\left|\langle\kappa|\int\widetilde{V}^{(\alpha)}|0\rangle\right|^2$ can be approximated by a Fermi's golden rule:

$$\begin{aligned}\left|\langle\kappa|\int\widetilde{V}^{(\alpha)}|0\rangle\right|^2 &= \left|\langle\Phi_\kappa^{(\alpha)}(\tau)|\int\widetilde{V}^{(\alpha)}|\Phi^{(\alpha)}(\tau)\rangle\right|^2 \\ &\approx 2\pi\left|\langle\Phi_\kappa^{(\alpha)}(0)|V^{(\alpha)}(0)|\Phi^{(\alpha)}(0)\rangle\right|^2\delta(E_\kappa^{(\alpha)}-E^{(\alpha)})\tau = P_\kappa^{(\alpha)}\tau = P_{\alpha\to\kappa[\alpha]}\tau\end{aligned} \tag{2.73}$$

where $E_\kappa^{(\alpha)}$ and $E^{(\alpha)}$ are the HF energies of $|\Phi_\kappa^{(\alpha)}(\tau)\rangle$ and $|\Phi^{(\alpha)}(\tau)\rangle$ respectively. This is an acceptable approximation if:

- $\sum_\kappa P_\kappa^{(\alpha)}\tau \ll 1$, to justify the perturbative treatment.
- $E^{(\alpha)}$ is large compared to the fluctuations $\Delta h^{(\alpha)}$ (as defined in Eq. (2.61)). In an equivalent way, we can assume that the mean field is almost constant over τ, i.e. $\tau \ll t_{\mathrm{MF}}$ where $t_{\mathrm{MF}} \propto 1/\Delta h$. This also implies that $V^{(\alpha)}$ does not vary too much over $[0,\tau]$.
- $[0,\tau]$ is long enough so that there is a fully developed transition between $|\Phi^{(\alpha)}\rangle$ and $|\Phi_\kappa^{(\alpha)}\rangle$. This means that the delta function is a relevant approximation. "Long enough" can thus be interpreted as $\tau \gg 1/\Delta E$ where ΔE is the typical energy separation in a discrete spectrum.

As the residual interaction $V^{(\alpha)}$ is of $2p2h$ nature, the only terms taken into account in the transition are $2p2h$ excitations from the ket $|\Phi^{(\alpha)}\rangle$. Therefore κ is the index for this kind of excitations i.e. $\kappa \equiv pp'hh'$. To be more precise, we have

$$V^{(\alpha)}|\Phi^{(\alpha)}\rangle = \sum_{pp'hh'} V_{pp'hh'}\underbrace{a_p^\dagger a_{p'}^\dagger a_{h'}a_h|\Phi^{(\alpha)}\rangle}_{|\Phi_\kappa^{(\alpha)}(\tau)\rangle} \tag{2.74}$$

where p, p' are particle states and h, h' are hole states with respect to $|\Phi^{(\alpha)}\rangle$. In terms of density matrices it yields:

$$V^{(\alpha)}D^{(\alpha)} = \sum_{\kappa[\alpha]\neq\alpha} D^{(\kappa[\alpha])}V^{(\alpha)}D^{(\alpha)} \tag{2.75}$$

where we have used the notations $|0\rangle\langle 0| = D^{(\alpha)}(\tau)$ and $|\kappa\rangle\langle\kappa| = D^{(\kappa[\alpha])}(\tau)$. The index $\kappa[\alpha] \neq \alpha$ means that there is no diagonal term. The final equation for the density matrix is

$$\mathcal{D}^{(\alpha)}(\tau) \approx D^{(\alpha)}(\tau) + \sum_{\kappa[\alpha]\neq\alpha}[D^{(\kappa[\alpha])}(\tau) - D^{(\alpha)}(\tau)]P_{\alpha\to\kappa[\alpha]}\tau \quad . \tag{2.76}$$

This gives the evolution of the exact matrix in the form of a master equation with a gain and loss term from the initial state $|\Phi^{(\alpha)}\rangle$.

2.6.3 General equation of motion for STDHF

Each trajectory α generates its own set of $2p2h$ density matrices $D_\kappa^{(\alpha)}$ and the total correlated N-body density matrix at time τ is taken as:

$$\begin{aligned}\mathcal{D}(\tau) &= \sum_\alpha x^{(\alpha)}(0)\mathcal{D}^{(\alpha)}(\tau) \\ &\approx \sum_\gamma x^{(\gamma)}(\tau)D^{(\gamma)}(\tau) \quad .\end{aligned} \tag{2.77}$$

This equation has to be read carefully: the first line is a sum over correlated N-body density matrices, while the second line contains only uncorrelated matrices incoherently added up at time τ. In Sec. 2.6.2, we perform the scheme from $t = 0$ to $t = \tau$. It is possible to do the same step again m times. The time can be discretized along those steps and we write $t_m = m\tau$. Using Eq. (2.76), we rewrite $\mathcal{D}(t_m)$ as

$$\mathcal{D}(t_m) = \sum_\alpha x^{(\alpha)}(t_{m-1})\mathcal{D}^{(\alpha)}(t_m)$$

$$\approx \sum_\alpha x^{(\alpha)}(t_{m-1})\Big(D^{(\alpha)}(t_m) + \sum_{\kappa\neq\alpha}[D^{(\kappa[\alpha])}(t_m) - D^{(\alpha)}(t_m)]P_{\alpha\to\kappa[\alpha]}\tau\Big) \tag{2.78}$$

$$\approx \sum_\gamma x^{(\gamma)}(t_{m-1})D^{(\gamma)}(t_m) + \sum_{\substack{\gamma,\beta\\ \gamma\neq\beta}}(x^{(\beta)}(t_{m-1})P_{\beta\to\gamma} - x^{(\gamma)}(t_{m-1})P_{\gamma\to\beta})D^{(\gamma)}(t_m)\tau \tag{2.79}$$

where γ is a general index gathering both α and $\kappa[\alpha]$. From Eq. (2.73) we have $P_{\beta\to\gamma} = P_{\gamma\to\beta}$ but we keep the most general form at this point. Now we define the coarse time derivative of any function f as:

$$\partial_t f \approx \frac{f(t_m) - f(t_{m-1})}{\tau} \quad . \tag{2.80}$$

This definition, together with $\mathcal{D}(t_{m-1}) \approx \sum_\gamma x^{(\gamma)}(t_{m-1})D^{(\gamma)}(t_{m-1})$, allows us to write the equation of motion for $\mathcal{D}$:

$$\mathrm{i}\partial_t\mathcal{D} = \sum_\gamma x^{(\gamma)}[h^{(\gamma)}, D^{(\gamma)}] + \mathrm{i}\sum_{\substack{\gamma,\beta\\ \gamma\neq\beta}}(x^{(\beta)}P_{\beta\to\gamma} - x^{(\gamma)}P_{\gamma\to\beta})D^{(\gamma)} \tag{2.81}$$

The second term can be interpreted as:

$$\partial_t x^{(\gamma)} = \sum_{\substack{\beta\\ \gamma\neq\beta}}(x^{(\beta)}P_{\beta\to\gamma} - x^{(\gamma)}P_{\gamma\to\beta}) \quad . \tag{2.82}$$

From Eq. (2.78) we can also write Eq. (2.81) the following way:

$$\mathrm{i}\partial_t\mathcal{D} = \sum_\gamma x^{(\gamma)}[h^{(\gamma)}, D^{(\gamma)}] + \mathrm{i}\sum_{\substack{\gamma,\beta\\ \gamma\neq\beta}} x^{(\beta)}P_{\beta\to\gamma}(D^{(\gamma)} - D^{(\beta)}) \quad . \tag{2.83}$$

In the following, we need to introduce the 1-body projection operator e which definition in an arbitrary s.p. basis is

$$\mathrm{Tr}\{eO\} = \sum_{ij}\mathrm{Tr}\{a_j^\dagger a_i O\}a_i^\dagger a_j \tag{2.84}$$

where O is a N-body operator. Mind that this is an abusive notation as $\mathrm{Tr}\{eO\}$ is not a number but a 1-body operator. The 1-body density matrices are then easy to obtain:

$$\begin{aligned} \rho &= \mathrm{Tr}\{e\mathcal{D}\} \ , \\ \rho^{(\gamma)} &= \mathrm{Tr}\{eD^{(\gamma)}\} \quad . \end{aligned} \tag{2.85}$$

Note that $\rho^{(\gamma)}$ is the density matrix of a pure state (with 0 and 1 as occupation numbers) whereas ρ is a mixed state density matrix (with partial occupation numbers). For any 1-body operator T, e has also the property

$$\mathrm{Tr}\{e[T,\mathcal{D}]\} = [T,\rho] \tag{2.86}$$

and conserves the freedom to do circular permutations under the trace. We define $\bar{h}$ as the mean field corresponding to $\rho = \mathrm{Tr}\{e\mathcal{D}\}$ and $\bar{V}$ so that $H = \bar{h} + \bar{V} = h^{(\gamma)} + V^{(\gamma)}$.

We now derive the equation of motion of the 1-body density matrix. First, we make use of

$$[h^{(\gamma)}, D^{(\gamma)}] = [\bar{h}, D^{(\gamma)}] + [\bar{V}, D^{(\gamma)}] - [V^{(\gamma)}, D^{(\gamma)}] \tag{2.87}$$

to make $\bar{h}$ appear in the first term of Eq. (2.83) and then we project this equation using $\mathrm{Tr}\{e...\}$. Note that the last term of (2.87) then vanishes:

$$\begin{aligned} V^{(\gamma)}D^{(\gamma)} &= \sum_{\kappa[\gamma]\neq\gamma} D^{(\kappa[\gamma])}V^{(\gamma)}D^{(\gamma)} \\ \mathrm{Tr}\{eD^{(\kappa[\gamma])}V^{(\gamma)}D^{(\gamma)}\}_{ji} &= \underbrace{\langle\Phi^{(\gamma)}|a_i^\dagger a_j|\Phi_\kappa^{(\gamma)}\rangle}_{0}\langle\Phi_\kappa^{(\gamma)}|V^{(\gamma)}|\Phi^{(\gamma)}\rangle = 0 \quad . \end{aligned} \tag{2.88}$$

Altogether it yields

$$\mathrm{i}\partial_t\rho = [\bar{h},\rho] + K + \delta K \tag{2.89}$$

$$K = \mathrm{i}\sum_{\substack{\gamma,\beta \\ \gamma\neq\beta}} x^{(\beta)}P_{\beta\to\gamma}(\rho^{(\gamma)} - \rho^{(\beta)}) \tag{2.90}$$

$$\delta K = \sum_\gamma x^{(\gamma)}\,\mathrm{Tr}\{[e,\bar{V}]D^{(\gamma)}\} \quad . \tag{2.91}$$

It can be shown [23] that the collision integral K and the stochastic force δK are to some extent equivalent to those found in Eq. (2.44) in the Markovian approximation.

2.6.4 On the residual interaction in STDHF with DFT

The scheme presented so far used a residual interaction $V(t)$. If one uses the simple HF Hamiltonian h_{HF} as mean-field Hamiltonian h then $V(t)$ is equal to V_{res} defined in Eq. (2.18). In the case one uses a KS Hamiltonian h_{KS} for the mean field, the formal justification of the choice of V_{res} can become a bit more tricky. One can write the very formal equation:

$$\mathrm{i}\partial_t\rho_{\mathrm{exact}} = [h_{\mathrm{KS}}[\varrho],\rho_{\mathrm{exact}}] + C[\varrho] \tag{2.92}$$

where C is a functional that corrects the difference between the KS propagation and the exact one. Of course we still have $\rho_{\mathrm{exact}}(\mathbf{r},\mathbf{r}) = \varrho(\mathbf{r}) = \rho_{\mathrm{KS}}(\mathbf{r},\mathbf{r})$. C acts on the

occupation numbers that the KS Hamiltonian kept untouched, and also on the natural basis. Therefore one can assume it is possible to write C as an effective collision integral $K_{\text{eff}}[\rho_{\text{exact}}]$, defined for example in Eq. (2.47), with an effective v_{eff} instead of the interaction v. This v_{eff} is highly nontrivial and one can use an ansatz as for example a screened Coulomb term. Because of the structure of K, one can expect to reproduce qualitatively the dissipative features, provided that v_{eff} is not too unphysical. This v_{eff} can be plugged for example into STDHF with a LDA functional to obtain a Stochastic TDLDA. A quantitative reproduction of the exact solution may need further development in the calculation of v_{eff} or a bit of tuning of the ansatz chosen.

2.6.5 STDHF in practice

The numerical implementation of STDHF is straightforward once the derivation has been done. Every τ, this state generates as many density matrices $D^{(\kappa[\gamma])}$ as allowed $2p2h$ transitions according to Eq. (2.73). This ensemble is however too huge to be dealt with numerically. The idea of STDHF is to replace the ensemble of trajectories weighted by $P_{\beta\to\gamma}\tau$ by a fixed number $\mathcal{N}$ of trajectories chosen in a stochastic manner with the probability $P_{\beta\to\gamma}\tau$ defined in Eq. (2.73). The correlated density matrix $\mathcal{D}$ is thus

$$\mathcal{D} = \frac{1}{\mathcal{N}} \sum_{\gamma=1}^{\mathcal{N}} D^{(\gamma)}(t) \tag{2.93}$$

where the same matrix $D^{(\gamma)}$ can appear several times in the sum. Let us denote by $\mathcal{N}^{(\gamma)}$ this number. We have:

$$\frac{\mathcal{N}^{(\gamma)}}{\mathcal{N}} \xrightarrow[\mathcal{N}\to\infty]{} x^{(\gamma)} \quad . \tag{2.94}$$

$\mathcal{N}$ is of the order of some hundreds in our calculations to allow enough statistics. As each trajectory has to be propagated using its own mean field, the calculation is still numerically heavy. Since in a finite system the energy spectrum is discrete, the delta function in $P_{\beta\to\gamma}$ is replaced by a door function with a finite width Γ, as:

$$\delta_\Gamma(x) = \begin{cases} \dfrac{1}{2\Gamma} & \text{if } |x| \leq \Gamma \\ \\ 0 & \text{otherwise} \end{cases} \quad . \tag{2.95}$$

We have observed that, for the sake of numerical efficiency, we need to preselect the transition states with another delta function of width $\Gamma_\varepsilon > \Gamma$. We typically take $\Gamma_\varepsilon \approx 5\Gamma$. This preselection is done on the s.p. energies, i.e. for a state $D^{(\alpha)}$ that jumps to a state $D^{(\kappa[\alpha])}$. More precisely the preselection condition reads:

$$|\varepsilon_p + \varepsilon_{p'} - \varepsilon_h - \varepsilon_{h'}| \leq \Gamma_\varepsilon \quad . \tag{2.96}$$

This whole process is sketched in Fig. 2.1 where the trajectories are represented in purple and every τ an instantaneous jump occurs (in red), choosing one transition $D^{(\kappa[\gamma])}$ (full red) amongst all the possible transitions (dashed red) with a certain probability. There is also a certain degree of freedom in the transition itself. Indeed all unitary

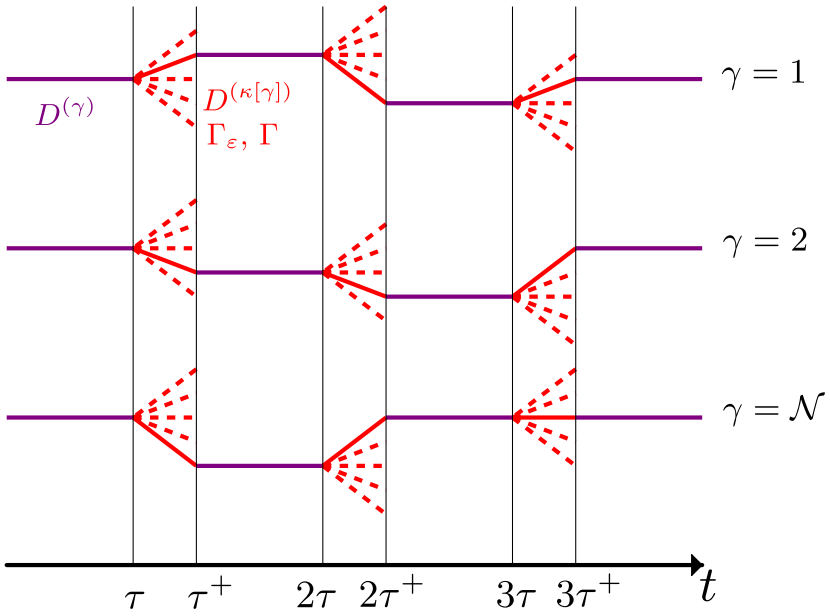

Figure 2.1: Schematic view of the time propagation of Stochastic TDHF ensemble. See text for more details.

transformations that conserve the subspaces of occupied (h-space) and empty states (p-space) in one trajectory leave $D^{(\gamma)}$ unchanged but it does change the possible $2p2h$ transitions. Before each transition we choose the s.p. wave functions $|\varphi_\nu^{(\gamma)}\rangle$ that diagonalize the mean field Hamiltonian $h^{(\gamma)}$ in the h-space and p-space separately. The aim of this process is to reduce the uncertainty on the s.p. energies and on the total energy $E_\kappa^{(\alpha)}$ of the $2p2h$ transition.

2.6.6 Limitations of STDHF

The STDHF scheme presented here has difficulties to deal with low excitation energies (see Chapter 4). Indeed, when the excitation energy is low, the probability of transition decreases and the number of trajectories has to be increased accordingly to capture the right dynamics. The difference between the mean-field Hamiltonian of the ensemble of trajectories become much smaller. In a numerical point of view, the cost of propagating hundreds of trajectories even in a mean field manner can become prohibitive. This motivated the choice to use only a unique mean field $\bar{h}$ for the propagation. From Eq. (2.89), we deduce this is equivalent to run a Markovian ETDHF calculation (where the fluctuations are neglected) without the low-energy assumption that assumed there is a common eigenbasis of $\bar{h}$ and ρ. Therefore, as we kept only the collisional integral, we call this method Collisional TDHF.

2.7 CTDHF

As just explained previously, the mean field Hamiltonian of each trajectory is replaced in the CTDHF scheme by the common mean field $\bar{h}$ which corresponds to neglecting the term $[\bar{V}, D^{(\gamma)}]$ in Eq. (2.87). Therefore the stochastic force δK does not appear

and we obtain only

$$i\partial_t \rho = [\bar{h}, \rho] + K \tag{2.97}$$

as an equation of motion for ρ. With Eqs. (2.90) and (2.97) we note that CTDHF does not actually need trajectories of $D^{(\gamma)}$ to be propagated. It only needs the "mixed state" density matrix $\rho(t)$ and the ensemble of pure state density matrices $\rho^{(\gamma)}$ to make transitions every τ. This ensemble is reconstructed in an approximate way that will be explained more in details in the following. In CTDHF the possible transitions are not sampled as in STDHF but added up with their weight $P_{\beta\to\gamma}$. The scheme is then more robust for small transitions probabilities. In STDHF the majority of the calculation time is used to propagate the ensemble of trajectories. In CTDHF there is only one trajectory and we have a calculation time that can be two orders of magnitude smaller than that in STDHF.

2.7.1 Representation of the mixed states

The CTDHF scheme treats the state of a N-particle system in parallel by two equivalent representations: a (mixed) 1-body density matrix ρ and an ensemble $\mathcal{E}$ of pure Slater states,

$$\rho = \sum_{\nu=1}^{\Omega} |\varphi_\nu\rangle w_\nu \langle\varphi_\nu| \;\longleftrightarrow\; \mathcal{E} = \{|\Phi^{(\alpha)}\rangle, x^{(\alpha)}, \alpha = 1, ..., \mathcal{N}\} = \{D^{(\alpha)}, x^{(\alpha)}\} \tag{2.98}$$

where the $x^{(\alpha)}$ are the weights with which the Slater state $|\Phi^{(\alpha)}\rangle$ does contribute. The latter reads in occupation number representation

$$|\Phi^{(\alpha)}\rangle = |n_1^{(\alpha)}, n_2^{(\alpha)}, ..., n_\Omega^{(\alpha)}\rangle \;,\; n_\nu^{(\alpha)} \in \{0, 1\} \;,\; \sum_\nu n_\nu^{(\alpha)} = N \;, \tag{2.99}$$

where N is the total number of physical particles and Ω the total number of s.p. wave functions considered. All $|\Phi^{(\alpha)}\rangle$ are formed from the same basis of s.p. states $\mathcal{B} = \{|\varphi_\nu\rangle, \nu = 1, ..., \Omega\}$ which is also the basis that builds ρ. One $|\Phi^{(\alpha)}\rangle$ (or the corresponding D^α) is thus uniquely characterized by the vectors $\mathbf{n}^{(\alpha)}$ and the ensemble by the matrix $A \equiv n_\nu^{(\alpha)}$ of size $\Omega \times \mathcal{N}$ where $\mathbf{n}^{(\alpha)}$ represents the columns. We will sometimes write

$$\{\mathcal{B}, A\} = \{|\Phi^{(\alpha)}\rangle\} = \{D^{(\alpha)}\} \quad . \tag{2.100}$$

In a same way we can define the vector $X \equiv x^{(\alpha)}$ of size $\mathcal{N}$. The ensemble defined in (2.98) can then be written as

$$\mathcal{E} = \{\mathcal{B}, A, X\} = \{|\Phi^{(\alpha)}\rangle, X\} = \{D^{(\alpha)}, X\} \quad . \tag{2.101}$$

How to read $\{\mathcal{B}, A, X\}$ is sketched in Fig. 2.2. Each $|\Phi^{(\alpha)}\rangle$ corresponds a 1-body density matrix $\rho^{(\alpha)}$:

$$|\Phi^{(\alpha)}\rangle \;\longleftrightarrow\; \rho^{(\alpha)} = \sum_{\nu=1}^{\Omega} |\varphi_\nu\rangle n_\nu^{(\alpha)} \langle\varphi_\nu| \;. \tag{2.102}$$

$$
\begin{array}{c}
\\
n_1 \\ n_2 \\ n_3 \\ n_4 \\ \vdots \\ n_{\Omega-1} \\ n_\Omega \\
|\Phi^{(1)}\rangle|\Phi^{(2)}\rangle
\end{array}
\overset{A}{\begin{pmatrix} 0 & 1 & \dots & 0 \\ 1 & 0 & \dots & 0 \\ 0 & 0 & \dots & 0 \\ 1 & 0 & \dots & 1 \\ \vdots & \vdots & \dots & \vdots \\ 0 & 1 & \dots & 1 \\ 1 & 1 & \dots & 1 \end{pmatrix}}
\overset{\mathcal{B}}{\begin{matrix} |\varphi_1\rangle \\ |\varphi_2\rangle \\ |\varphi_3\rangle \\ |\varphi_4\rangle \\ \vdots \\ |\varphi_{\Omega-1}\rangle \\ |\varphi_\Omega\rangle \end{matrix}}
\times
\overset{X}{\begin{pmatrix} x^{(1)} \\ x^{(2)} \\ x^{(3)} \\ \vdots \\ \vdots \\ x^{(\mathcal{N})} \end{pmatrix}}
=
\begin{pmatrix} w_1 \\ w_2 \\ w_3 \\ w_4 \\ \vdots \\ w_{\Omega-1} \\ w_\Omega \end{pmatrix}
$$

Figure 2.2: The $\mathcal{E}$ ensemble is represented by the triplet $\{\mathcal{B}, A, X\}$. The matrix product of A with X gives the diagonal terms of ρ that have to be read in the natural basis $\mathcal{B}$.

And the connection from $\mathcal{E}$ to ρ is done by using

$$\rho = \sum_{\alpha=1}^{\mathcal{N}} x^{(\alpha)} \rho^{(\alpha)} = \sum_{\nu=1}^{\Omega} |\varphi_\nu\rangle \underbrace{\sum_{\alpha=1}^{\mathcal{N}} x^\alpha n_\nu^{(\alpha)}}_{=w_\nu} \langle\varphi_\nu| \; . \tag{2.103}$$

The variety of Slater states (2.99) with arbitrary distribution of $n_\nu^{(\alpha)}$ is huge. We restrict, in fact, the ensemble $\mathcal{E}$ to those $|\Phi^{(\alpha)}\rangle$ which remain close to the energy of the state ρ. This will be detailed in Sec. 2.7.4 in connection with the stepping scheme.

2.7.2 From a mixed state to a sum of pure states

The mapping from $\mathcal{E}$ to ρ is straightforward as seen from Eq. (2.103). The reverse mapping

$$w_\nu \longrightarrow x^{(\alpha)} \tag{2.104}$$

is ambiguous and has only approximate solutions. We determine the vector X by a least squares fit minimizing

$$\chi^2 = ||W - AX||^2 + \eta||X||^2 = \sum_\nu \left(w_\nu - \sum_\alpha n_\nu^{(\alpha)} x^{(\alpha)} \right)^2 + \eta \sum_\alpha \left(x^{(\alpha)} \right)^2 = \text{minimal} \; , \tag{2.105}$$

where $W \equiv w_\nu$ and η is some small positive numerical parameter. The minimization is done with the constraint $1 \geq x^{(\alpha)} \geq 0$. The second term weighted by η serves to prefer the solution with the most evenly distributed coefficients $x^{(\alpha)}$. Finding X corresponds to solving the non-negative least square (NNLS) problem. There are many algorithms available to do that. We have modified the sequential coordinate-wise algorithm based on an article of Franc et al. [63] for the NNLS problem to include the $\eta||X||^2$ term. This algorithm has been chosen because it is easy to modify and to implement. It is also expected to be efficient when the dimension of X is a much larger than the dimension of W which is precisely the case we are facing. Since this algorithm is gradient-descent-based, it allows us to use a previous calculation as a starting point. This property is used in our calculations.

One option to find $X(\lambda_n)$ consists in minimizing the following expression:

$$\chi^2(\eta_n) = ||W - AX||^2 + \eta_n||X||^2 \tag{2.106}$$

and using $X(\eta_n)$ as a starting point to find $X(\eta_{n+1})$ with $\eta_n \to 0$. However this would be numerically too demanding. Therefore this solution has been avoided.

Instead, during the gradient descent steps solving the NNLS problem, η is reduced rapidly. Even if it does not ensure that X is a minimum of χ^2, X remains a minimum of $||W - AX||^2$ and we then expect X to be close to the optimal solution. However, this solution may sometimes lead to a ρ_{sampled} too far from the original ρ, yielding discontinuities in observables such as the energy. To solve this, we have introduced the remaining density matrix ρ_{rem} defined as

$$\rho_{\text{rem}} = \rho - \rho_{\text{sampled}} = \sum_\nu (w_\nu - \sum_\alpha n_\nu^{(\alpha)} x^{(\alpha)}) |\varphi_\nu\rangle\langle\varphi_\nu| \quad . \tag{2.107}$$

We will always assume $\rho = \rho_{\text{sampled}}$ in the following and use only ρ. In practice, all the transformations of CTDHF in the dissipative step will be done on ρ_{sampled}. ρ_{rem} is computed and stored after the sampling and finally added up at the end of the CTDHF step to preserve the continuity of ρ. This matrix ρ_{rem} remains untouched during this process. The effect of ρ_{rem} is illustrated in Fig. 2.3 on a typical exemple which will be presented and discussed at length in Chapter 4.

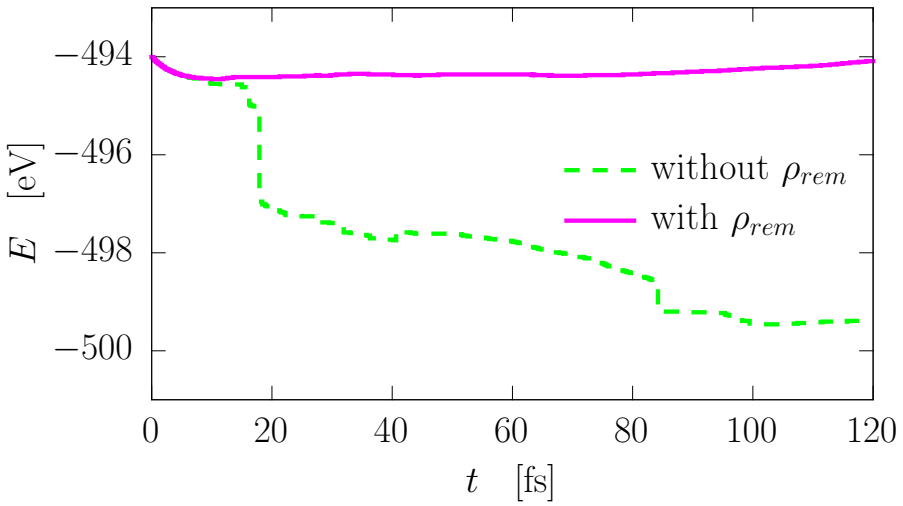

Figure 2.3: Example of discontinuities in the total energy E in a time evolution of a system (presented in chapter 5) propagated in the Collisional TDHF scheme, with ρ_{rem} (solid magenta curve) and without it (green dashes).

2.7.3 Energy conservation

Before proceeding to the practical realization of CTDHF, we here give more words about energy conservation. In STDHF, each Slater state $|\Phi^{(\alpha)}\rangle$ is propagated during

the TDHF part with its own mean field Hamiltonian $h^{(\alpha)}$. Indeed CTDHF uses a unique mean field deduced from the mixed state density matrix

$$\rho \longrightarrow \varrho(\mathbf{r},t) = \sum_\nu w_\nu \left|\varphi_\nu(\mathbf{r},t)\right|^2 \longrightarrow h[\varrho] \tag{2.108}$$

where $\varrho(\mathbf{r},t)$ is the local density according to ρ and $h[\varrho]$ the KS mean field according to this density (see Eq. (2.4)). This mean field is then used to generate the 1-body propagator $U(t_2,t_1)$ where the time dependence of h comes through the time dependence of ϱ.

There are actually different energies in the game. The total energy

$$E_{\rm tot} = E[\rho] \equiv E \tag{2.109}$$

is computed from the total 1-body density matrix ρ. It is the single relevant energy for the final result. As we will see later, the energy of state $|\Phi^{(\alpha)}\rangle$ is nevertheless important for the selection of the ensemble, namely

$$E^{(\alpha)} = E^{(\alpha)}[\rho^{(\alpha)}] \ , \tag{2.110}$$

which is computed with the local density $\varrho^{(\alpha)}$ according to $\rho^{(\alpha)}$ (or $|\Phi^{(\alpha)}\rangle$). Mind that $E^{(\alpha)}$ has to be taken with care. The s.p. states $|\varphi_\nu\rangle$, and with it the $|\Phi^{(\alpha)}\rangle$, are propagated with the common mean field $h[\varrho]$. For then, the energy $E^{(\alpha)}$ of each $|\Phi^{(\alpha)}\rangle$ is not necessarily conserved during TDHF propagation. In other words, we have

$$\partial_t E^{(\alpha)}[\rho^{(\alpha)}] \neq 0 \quad \text{with} \quad \rho^{(\alpha)}(t) = U(t,t_0)\rho^{(\alpha)}(t_0)U(t_0,t) \quad . \tag{2.111}$$

This raises, however, no principle problem. What counts here is to conserve the total energy $E[\rho]$. This energy conservation will be discussed on typical examples in Chapter 5.

2.7.4 From one dissipative step to the next one

The propagation proceeds at two time scales: at a coarse time step τ for the evaluation the 2-body jumps and a fine time step $\delta t (< \tau)$ for TDHF propagation. We consider here the CTDHF procedure from $t_{m-1} = (m-1)\tau$ to $t_m = m\tau$.

Mean field propagation

We start at t_{m-1} with a given state $\rho(t_{m-1})$ and the ensemble $\mathcal{E}(t_{m-1})$ corresponding to Eq. (2.98). We propagate the s.p. wave functions by TDHF

$$\varphi_\nu(t_{m-1}) \ \longrightarrow \ \widetilde{\varphi_\nu} = U\varphi_\nu(t_{m-1}) \ . \tag{2.112}$$

where $U = U(t_m, t_{m-1})$. This defines the set $\widetilde{\mathcal{B}}$ from $\mathcal{B}(t_{m-1})$. We also need the matrix A which is constant as occupations $n_\nu^{(\alpha)}$ remain unchanged during the time propagation. These occupation numbers are now read in the propagated basis $\widetilde{\varphi_\nu}$. This is equivalent to propagate the following set

$$\{|\Phi^{(\alpha)}(t_{m-1})\rangle\} \rightarrow \{|\widetilde{\Phi}^{(\alpha)}\rangle\} \ , \ |\widetilde{\Phi}^{(\alpha)}\rangle = U|\Phi^{(\alpha)}(t_{m-1})\rangle \ . \tag{2.113}$$

The propagated mixed state reads:

$$\widetilde{\rho} = \sum_{\nu=1}^{\Omega} |\widetilde{\varphi}_\nu\rangle w_\nu \langle\widetilde{\varphi}_\nu| \tag{2.114}$$

with unchanged occupations $w_\nu = w_\nu(t_{m-1})$. Note that $\widetilde{\varphi}_\nu$, $\widetilde{\Phi}^{(\alpha)}$, and $\widetilde{\rho}$ are preliminary objects. The final quantities at t_m are determined after the dissipative step is performed.

Selecting an energy-matching ensemble

The $|\widetilde{\Phi}^{(\alpha)}\rangle$ may have developed during propagation a broad distribution of energies $\widetilde{E}^{(\alpha)}$. We want to confine the sampling states to a narrow energy band again. Thus we need first to extend the ensemble to produce enough choices of states in a narrow energy band about the total energy $E[\rho]$. To this end we start from the $|\widetilde{\Phi}^{(\alpha)}\rangle$ and consider for such each state all corresponding $2p2h$ states $|\widetilde{\Phi}^{(\alpha)}_\kappa\rangle$ with $\kappa \equiv pp'hh'$. This generates a temporary super ensemble

$$\{\widetilde{\mathcal{B}}, \tilde{A}^{(\mathrm{S})}\} = \left\{|\widetilde{\Phi}^{(\alpha)}_\kappa\rangle\right\} \ , \ |\widetilde{\Phi}^{(\alpha)}_\kappa\rangle \equiv c^\dagger_{p'} c^\dagger_p c_h c_{h'} |\widetilde{\Phi}^{(\alpha)}\rangle \tag{2.115}$$

where $\kappa = 0$ stands for original $0p0h$ state. The creation-annihilation operators correspond to the basis $\widetilde{\mathcal{B}}$. From this huge ensemble, we collect $\mathcal{N}$ states $|\widetilde{\Phi}^{(\gamma)}\rangle$ amongst those which verify

$$\delta E^{(\gamma)} = E[\widetilde{\rho}^{(\gamma)}] - E[\widetilde{\rho}] \leq \Gamma_{\mathcal{E}} \quad , \tag{2.116}$$

where $\Gamma_{\mathcal{E}}$ is a small numerical parameter, the allowed energy band for the ensemble (as indicated by the index $\mathcal{E}$). The choice of $|\widetilde{\Phi}^{(\gamma)}\rangle$ to keep in the new set $\widetilde{A}$ is not an easy task. We have tried two tactics.

(i) We only keep the first $\mathcal{N}$ states with the best energy matching. The procedure ensures a good energy conservation of the considered states. Thus the set $\widetilde{A}$ is constructed using only an energy criterium. χ^2 and X are computed only once at the end. Due to the non-negativity constraint, after the calculation of χ^2, see Eq. (2.106), it turns out that this choice results in most elements of the vector X to be equal to zero. This means that we actually deal with a lot of excitations that do not contribute at all in the calculation of ρ. Most of the ensemble is useless then.

(ii) We scan the $2p2h$ transitions and we reject immediatly those which are too far way in energy. And for the remaining ones, we look at $\min_\alpha \ x^{(\alpha)}$. Once the corresponding α_0 is found, we replace the column $[\mathbf{n}^{(\alpha_0)}]$ in A and compute χ^2 again (see Fig. 2.4). If the replacement lowers χ^2 then the $2p2h$ excitation is accepted. The calculation time is a bit increased comparing to the previous tactics but $\mathcal{N}$ can be taken smaller and we obtain better numerical stability.

Once $\widetilde{A} = \{|\widetilde{\Phi}^{(\gamma)}\rangle\}$ is obtained, the corresponding weights $\widetilde{x}^{(\gamma)}$ are computed by reverse engineering with respect to $\widetilde{\rho}$ as outlined in Sec. 2.7.2. The ensemble $\widetilde{\mathcal{E}} = \{|\widetilde{\Phi}^{(\gamma)}\rangle, \widetilde{x}^{(\gamma)}\}$ thus produced becomes the starting point for the following dissipative step. In figure 2.5, this ensemble of $\widetilde{\rho}^{(\gamma)}$ corresponds to the first branching in purple.

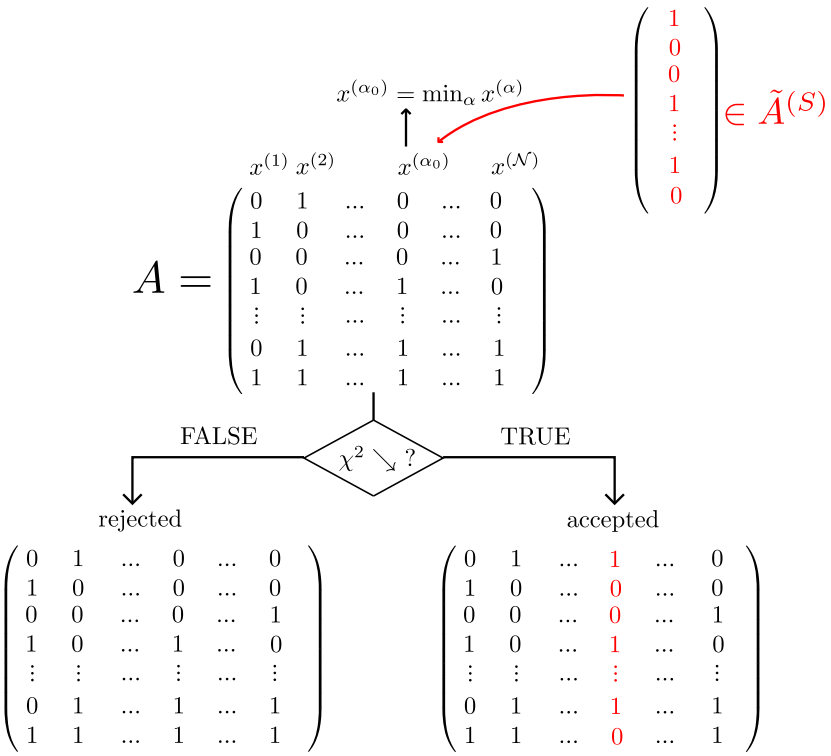

Figure 2.4: Schematic representation of the choice of the states $|\Phi^{(\alpha)}\rangle$ to create $\tilde{A}$ from A and $\tilde{A}^{(S)}$. This is repeated as many times as there are states in $\tilde{A}^{(S)}$.

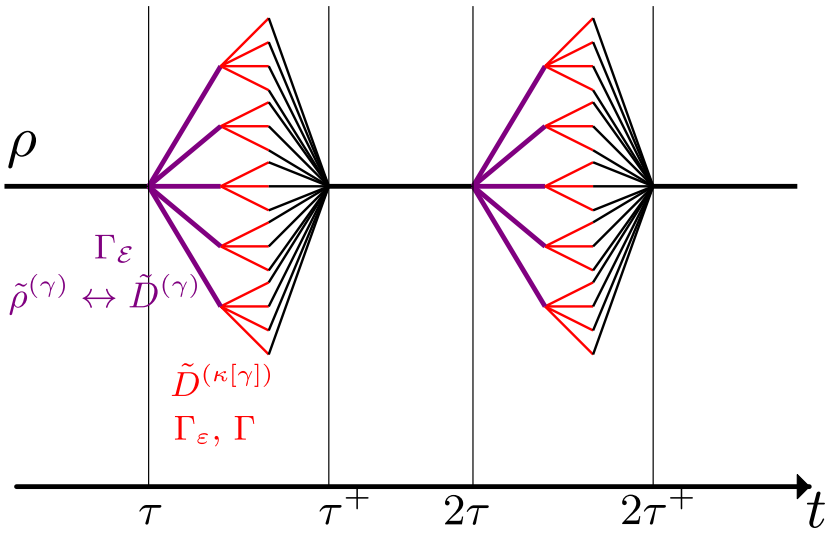

Figure 2.5: Schematic view of the time propagation of the Collisional TDHF scheme. See text for details.

Dissipative step

Starting from the $|\widetilde{\Phi}^{(\gamma)}\rangle$ and its 1-body density matrix $\widetilde{\rho}^{(\gamma)}$, all corresponding $2p2h$ states $|\widetilde{\Phi}^{(\gamma)}_{\kappa}\rangle$ (or the density matrices $\widetilde{D}^{(\kappa[\gamma])}$) are built by flipping two $\widetilde{n}^{(\gamma)}_{\nu} = 0 \nearrow 1$ and two other $\widetilde{n}^{(\gamma)}_{\nu} = 1 \searrow 0$. We remind that $|\widetilde{\Phi}^{(\gamma)}\rangle$ is a pure state represented by occupation numbers $\widetilde{n}^{(\gamma)}_{\nu}$ which are either 0 or 1. The considered $2p2h$ transitions are now the physical ones and shall not be confused with the previous ones that are only used to sample ρ. We focus here only on one specific γ. At that stage we have not modified yet the s.p. wave functions $\widetilde{\varphi}^{(\gamma)}_{\nu}$ which are thus strictly the original $\widetilde{\varphi}_{\nu}$ at the considered time step.

There are now 2 options: either we keep the $\widetilde{\varphi}_{\nu}$ or we diagonalize the mean-field Hamiltonian $h^{(\gamma)}$ within p-space and h-space as we do in STDHF, thus leading to a new basis $\widetilde{\varphi}^{(\gamma)}_{\nu}$. The first option is called "diagonal CTDHF" because it only acts on the diagonal elements of the density matrix and the second option is simply called "CTDHF". Without loss of generality we can consider the second option which actually reduces to the diagonal CTDHF when (although delivering different transition rates) when replacing $\widetilde{\varphi}^{(\gamma)}_{\nu}$ by $\widetilde{\varphi}_{\nu}$.

For our particular $|\widetilde{\Phi}^{(\gamma)}\rangle$ we evaluate the transition rates $P^{(\gamma)}_{pp'hh'} \equiv P^{(\gamma)}_{\kappa}$ defined in Eq. (2.73) and the complement $P^{(\gamma)}_{0} = 1 - \sum_{\kappa} P^{(\gamma)}_{\kappa}$. The delta function that appears in the transition rate $P^{(\gamma)}_{\kappa}$ is replaced by an energy selection of the accessible transitions split in two steps as in STDHF (see Sec. 2.6.5): Firstly, a fast energy preselector is applied using the s.p. energies:

$$|\varepsilon_p + \varepsilon_{p'} - \varepsilon_h - \varepsilon_{h'}| \leq \Gamma_{\varepsilon} \tag{2.117}$$

within a larger band $\Gamma_{\varepsilon} > \Gamma$. Secondly, the preselected states are chosen according to the conservation of total energies:

$$\left| E[\rho^{(\gamma)}_{\kappa}] - E[\rho^{(\gamma)}] \right| \leq \Gamma \ . \tag{2.118}$$

Having the set of allowed transition states $|\widetilde{\Phi}^{(\gamma)}_{\kappa}\rangle$, we compute $\rho^{(\gamma)}$:

$$\rho^{(\gamma)} = P^{(\gamma)}_{0} \sum_{\nu} \widetilde{n}^{(\gamma)}_{\nu} |\widetilde{\varphi}^{(\gamma)}_{\nu}\rangle\langle\widetilde{\varphi}^{(\gamma)}_{\nu}| + \sum_{\kappa} P^{(\gamma)}_{\kappa} \sum_{\nu} \widetilde{n}^{(\gamma)}_{\nu,\kappa} |\widetilde{\varphi}^{(\gamma)}_{\nu}\rangle\langle\widetilde{\varphi}^{(\gamma)}_{\nu}| \tag{2.119}$$

where $\widetilde{n}^{(\gamma)}_{\nu,\kappa} = \begin{cases} 1 & \text{if } \nu = p \text{ or } \nu = p' \\ 0 & \text{if } \nu = h \text{ or } \nu = h' \\ \widetilde{n}^{(\gamma)}_{\nu} & \text{otherwise} \end{cases}$.

This step is represented in Fig. 2.5 by the red branching from a purple line that represents one particular γ. Once this is done for each γ, we add up incoherently the various $\rho^{(\gamma)}$ as in Eq. (2.103) to obtain the final $\rho(t_m)$ with dissipation:

$$\rho = \sum_{\gamma=1}^{\mathcal{N}} \widetilde{x}^{(\gamma)} \rho^{(\gamma)} = \sum_{\nu=1}^{\Omega} |\varphi_{\nu}(t_m)\rangle w_{\nu}(t_m) \langle\varphi_{\nu}(t_m)| \ . \tag{2.120}$$

In the right hand side, $\mathcal{B}(t_m) = \{|\varphi_{\nu}(t_m)\rangle\}$ is obtained by diagonalization of the new ρ. Before going further, we need to define which matrix A of occupation numbers to use as a starting point for our ensemble for the next step. The simplest solution

is to recycle the ensemble of occupations $\widetilde{A} = \widetilde{n}_\nu^{(\gamma)}$ and combine it with $\mathcal{B}(t_n)$. This is possible because the changes $|\widetilde{\varphi}_\nu\rangle \longrightarrow |\varphi_\nu(t_n)\rangle$ induced by the dissipative step can be assumed to be small. This has to be taken with some care. Groups of states with (nearly) degenerated w_ν may be rotated arbitrarily by the diagonalization routine. But this is not harmful as these states have same weight and are thus exchangeable. We can eventually start a new cycle and propagate to the next dissipative step.

2.8 Conclusion

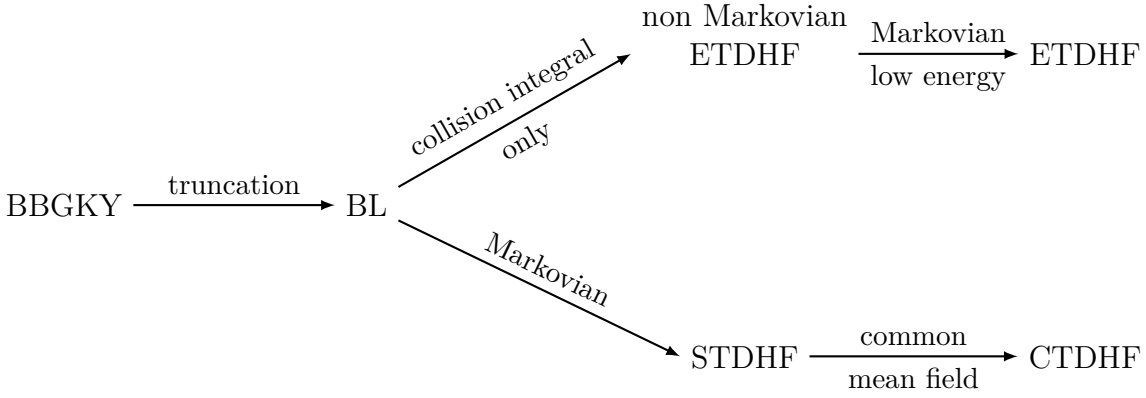

Figure 2.6: Relationship between the three approaches: Extended (ETDHF), Stochastic (STDHF) and Collisional TDHF.

In this chapter, we have derived three approaches for the inclusion of dissipative effects on top of a mean-field theory. They are summarized in Fig 2.6. The three of them are reducible to a Boltzmann (or Boltzmann-Langevin for STDHF) equation with different approximations. STDHF and ETDHF have already been studied in the past by several groups [62, 61, 59]. CTDHF constitutes a new scheme which allows to bridge the gap between STDHF and ETDHF. Indeed, CTDHF is expected to agree with STDHF (but without the fluctuations) at high excitation energy and to have the same behavior than ETDHF at low excitation energy. Numerically speaking, in the systems explored in Chapter 5, CTDHF exhibits more or less twice the cost of ETDHF, and at least two orders of magnitude less than STDHF. Therefore it should be numerically tractable in 3D realistic systems. In the next chapters, we are testing these schemes on physical systems. We begin with a perturbative approach on top of mean field, then we study STDHF in details, and eventually we compare CTDHF to STDHF and ETDHF.

Chapter 3

Electron attachment as a rare reaction channel

Contents

3.1 Introduction

In this chapter we follow the approach discussed in Sec. 2.6.4. One of the goals is to test an ansatz for v_{eff} (or $\hat{V}_{\text{res}}$ here) for the two-particle collision and use the basic elements of a STDHF treatment to obtain quantities that would not be accessible in the mean field. Therefore, the present study also serves as a way to illustrate the basic step in STDHF. This proof of concept is done on systems with a more general interest in biology and medicine.

Hadron therapies and radiation therapy are broadly used as cancer treatments. They act by transferring energy to the biological tissues and kill cells by provoking strand breaks in DNA. However, the underlying mechanisms of strand breaking in DNA are complex and still not fully understood. High energy radiations can lead to strand breaking either by interacting directly with DNA or with the surrounding environment producing radicals and secondary electrons of energy lower than 30 eV. These indirect effects are responsible for at least half the damages caused on DNA [64].

While most of the work has been focused on the effect of radicals, the seminal paper by the group of L. Sanche [65] showed that those low-energy electrons (LEE) can produce strand breaks in plasmid DNA. The use of metal clusters and molecules (as e.g. gold and platinum) has enable to produce LEE in critical areas and thus enhance the effect of radiation therapies [66]. Therefore the understanding of dynamics of irradiation in living cells at microscopic level is of great interest in medical research in strong connection with chemistry and physics.

LEE have a high probability to attach a molecule resonantly and produce a metastable ion. This ion can emit again the electron, leaving the molecule in a dissociative excited state or results in the production of anion radical and a highly reactive neutral. The latter process is called dissociative electron attachment (DEA). The theoretical treatment of this process is generally done with static calculations using for example R-matrix theory[67, 68] or perturbation theory [69, 70]. The few dynamical ones are interested mostly to the dissociation following the attachment, using for example local complex potential theory to describe the transient dissociative state [71].

We aim here at a microscopic picture of the attachment as such, which is a fast process running at electronic time scale. To do so, we use the real-space and real-time TDDFT briefly presented in Sec. 2.2. We here present a way to explore a rare reaction channel, as electron attachment, in a mean field approach. Indeed TDDFT, being a mean field theory, can only describe the leading reaction channel in an average manner and does not resolve rare channels (here the electron attachment) such as the dissociative channel we are interested in. In this study, we describe the electron attachment as a result of a two-particle collision from the leading TDLDA trajectory to the final state, a process often called "core-excited resonance". The idea is thus to estimate the attachment rates from time-dependent perturbation theory around the TDLDA trajectory. This is what we shall explore in the following. We focus on small water clusters as the simplest systems. In addition, in the quantum dynamical calculation, the computation time as we perform here becomes relatively heavy and we cannot afford bigger systems.

Part of the results presented here have already been published in [72] and will be in a forthcoming book published by Springer. In this chapter, we first present the theoretical and numerical framework and present some issues that must be tackled. Then we discuss at length the results obtained on H_2O on which most of the calculations have been run and finally we show the results obtained on $(H_2O)_2$ and H_3O^+.

3.2 Theory

3.2.1 TDDFT framework

Real-time and real-space TDDFT is used for the description of electron dynamics, for details see [51, 73] and Sec. 2.2. We summarize here briefly the main ingredients which are specific to the present test case.

The colliding system is either H_2O, $(H_2O)_2$ or H_3O^+. Only valence electrons (1 for H and 6 for O) are propagated. Core electrons and nuclei (=ions) are coupled to the valence electrons by Goedecker-like pseudopotentials [74] (see below). Ions are kept frozen in this study because the collision time, of the order of a few fs, is much

smaller than the typical time scale of ionic motion (several tens of fs). The N valence electrons of the water system plus the incoming electron are described by $N_{\rm el}(=N+1)$ single-electron wave functions φ_α. These, and all other spatial fields, are discretized on a 3-dimension cartesian grid of size 50×40^2 a_0^3 with a mesh size of 0.412 a_0. The time-dependent Kohn-Sham equations are solved by accelerated gradient iterations for the stationary solution [75], and by the time-splitting method [76] with a time step of 0.6 attosec for dynamical propagation. The Coulomb problem is solved on a double grid to reproduce correctly the long range asymptotics [77, 78]. The exchange-correlation functional is treated at the level of the adiabatic time-dependent local spin density approximation (TDLDA) [79] with the parametrization from Perdew and Wang [80]. The somewhat involved formal and numerical details will be discussed in Sec. 3.2.2.

In the present calculation we handle nuclei and core electrons(=ions) with pseudopotentials. They are inserted as $\hat{V}_{\rm ions}$ in Eq. (2.4b). These pseudopotentials have a separable form and can be local (for metallic clusters for example) or non-local (for covalent molecules). Pseudopotentials of the Goedecker form [74] have been adjusted to allow the use of a unique length scale $r_{\rm loc}$. Each ion is described by a pseudopotential $V_{\rm PsP}$ which reads:

$$V_{\rm PsP}(\vec{r})\,\varphi_j(\vec{r}) = V_{\rm loc}(r)\,\varphi_j(\vec{r}) + \int {\rm d}^3\vec{r}\,'\, V_{\rm nloc}(\vec{r},\vec{r}\,')\,\varphi_j(\vec{r}\,') \;, \tag{3.1}$$

$$V_{\rm loc}(r) = -\frac{Z}{r}\,{\rm erf}\left(x/\sqrt{2}\right) + \exp\left(-x^2/2\right)\left[C_1 + C_2\,x^2\right],\; x = \frac{r}{r_{\rm loc}} \;, \tag{3.2}$$

$$V_{\rm nloc}(\vec{r},\vec{r}\,') = p(r)\,h_0\,p(r\,') \;, \tag{3.3}$$

$$p(r) = \frac{\sqrt{2}}{{r_{\rm loc}}^{3/2}\sqrt{\Gamma\,(3/2)}}\exp\left(-\frac{r^2}{2{r_{\rm loc}}^2}\right) \tag{3.4}$$

where Z is the valence of the atom, φ_j is a s.p. wave function in $\vec{r}$ representation, erf the error function, Γ the Gamma function, and $x = r/r_{\rm loc}$. The parameters C_1, C_2, $r_{\rm loc}$, and h_0 are obtained by fitting to reproduce static properties like bond length and dissociation energy. For H and O atoms, the parameters are the following ones:

atom	C_1	C_2	$r_{\rm loc}$	h_0
H	0.5	0.0	0.35	−0.745
O	−0.409	−1.876	0.35	4.480

To describe electron emission, we use absorbing boundary conditions [51, 73, 81] which gently absorb all outgoing electron flow reaching the bounds of the grid and thus prevent artifacts from reflection back into the reaction zone. This allows us to define the total ionization, i.e. the number of escaped electrons $N_{\rm esc}$, as

$$N_{\rm esc}(t) = \sum_{\alpha=1}^{N_{\rm el}} \left(1 - \langle\varphi_\alpha(t)|\varphi_\alpha(t)\rangle\right) \quad . \tag{3.5}$$

The initial state of the incoming electron $\varphi_{\rm in}(\mathbf{r}, t=0)$ is a Gaussian wavepacket with an average incident energy $E_{\rm in}$. It is propagated by TDDFT like all other electron wave functions of the target molecule. As we use a Gaussian wavepacket, the wave function of the incoming electron carries some energy uncertainty given by

$$\Delta E_{\rm in} = \frac{3\hbar^2}{8m\Delta r^2} \quad , \tag{3.6}$$

where Δr^2 is the spatial variance of the electron density of the wavepacket. Note that, since we solve the time-dependent Kohn-Sham equations on a 3D spatial grid, one has to find a compromise between the initial widths of momentum and position. Too large a Δr^2 would quickly produce a non-physical absorption of the wavepacket at the boundaries of the numerical box. Similarly, if the wavepacket possesses too small an initial kinetic energy, due to Heisenberg inequality, the wavepacket would spread over the whole numerical box almost instantaneously. In practice, we used a spatial width of $5/\sqrt{2}$ a_0, producing an uncertainty of 0.82 eV on E_{in}. Note also that, because of this spatial width which is larger than the molecule, changing the impact parameter of the collision (as far as possible given the size of the numerical box) has basically no impact on the results. Moreover, due to the finite size of our numerical box, we place the incoming Gaussian at a finite distance $d_0 = 16$ a_0 from the center of mass of the target. We make a scan in E_{in} between 3 and 16 eV. We perform the simulations up to 9 fs, which is large enough since the incoming electron collides the target molecule in about 1 fs.

3.2.2 Calculation of attachment probability

Since the cross-section of electron attachment to H_2O is very small, that is less than 10^{-17} cm^2 [82] (see figure 3.1), we evaluate it perturbatively. To that end, we consider

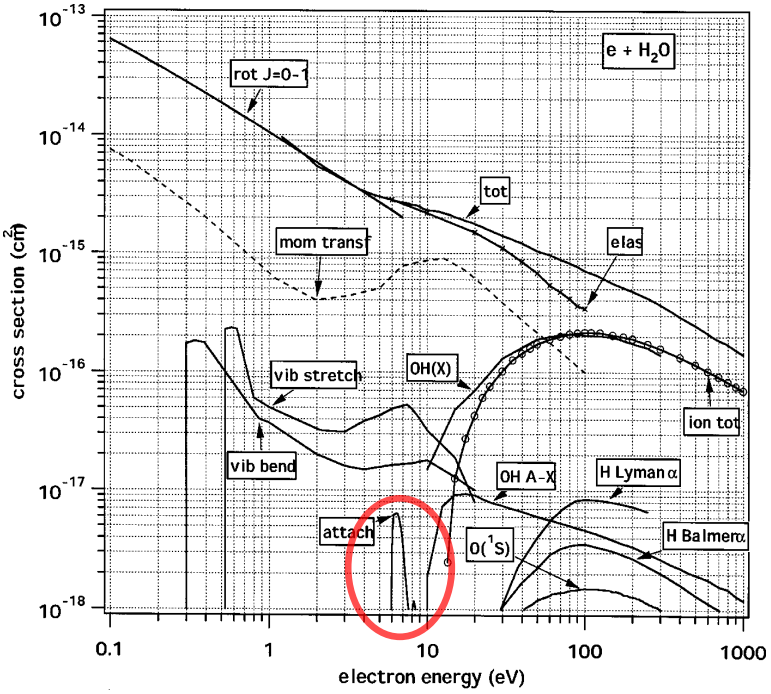

Figure 3.1: Cross section of various processes resulting from the collision of an electron to a water molecule plotted against the energy of incoming electron. The cross section of electron attachment is encircled in red. Adapted from [82].

all excited states of the target $|\Psi_n\rangle$ whose energy fulfills approximately $E_n = E_{\text{in}} + E_0$, where E_0 is the ground state energy of the target. One has now to choose these excited states which, in principle, should typically cover RPA excited states of the final system.

However, rearrangement effects are probably rather small in the small water clusters considered here, even if $E_{\rm in} \leq 15$ eV. We thus approximate the excitation spectrum by "1-particle-1-hole" ($1ph$) states. In addition, we have the projectile electron which, when captured, fills another particle (=unoccupied) state, thus leading to "2 particles-1 hole" ($2p1h$) excitations with a corresponding energy E_n approximated as follows :

$$|\Psi_n\rangle \approx |\Phi_{pp'h}\rangle \quad , \quad E_n \approx E_0 + \varepsilon_p + \varepsilon_{p'} - \varepsilon_h \quad , \tag{3.7}$$

where the excited states $|\Phi_{pp'h}\rangle$ are build from the Kohn-Sham wave functions of the target molecule in its ground state. This kind of transitions are also called "core-excited" resonances and constitute a candidate for the electron attachment process (the other one being the so-called "shape" resonance in which the incoming electron is temporarily trapped in an excited state of the target molecule).

The probability of attachment is computed by a Fermi's golden rule as :

$$\mathcal{P}_{\rm att}(t) = \frac{2\pi}{\hbar} \int_0^t {\rm d}\tau \sum_{n=1}^{N_{2p1h}} \left| \langle \Psi_n | \hat{V}_{\rm res} | \Phi_{\rm in}(\tau) \rangle \right|^2 \delta(E_n - E_{\rm in} - E_0) \tag{3.8}$$

where N_{2p1h} is the total number of $2p1h$ transitions matching the energy condition $E_n = E_{\rm in} + E_0$, and $\hat{V}_{\rm res}$ is the residual interaction for the collision channel.

The standard formula in scattering theory deals with a stationary continuum state for the incoming wave. The present recipe (3.8) uses a time-dependent wavepacket and employs simple time integration to accumulate the total capture probability. The simple time integration contains actually an approximation that has to be discussed. Let us assume that the time evolution is discretized in finite intervals Δt, each one appropriate for evaluating a transition. At time step t_ν, we have a transition probability

$$\begin{aligned} t_\nu \ : \quad \eta_\nu &= \frac{2\pi}{\hbar} \Delta t \sum_n \left| \langle \Psi_n | V_{\rm res} | \Phi_{\rm in}(t_\nu) \rangle \right|^2 \delta(E_n - E_{\rm in}) \\ &\Longrightarrow \begin{cases} |\Phi_{\rm in}(t)\rangle & \text{with probability} \quad (1-\eta_\nu) \\ |\Psi_n\rangle & \text{with probability} \quad \eta_\nu \end{cases} \end{aligned} \tag{3.9}$$

During the next step at $t_{\nu+1}$, we find the probability for capture as $\eta_\nu(1-\eta_\nu)$. This is continued along the whole path. We finally accumulate the probabilities for capture and employ the basic assumption that capture is a rare process, i.e. that $\eta_\nu \ll 1$. This yields

$$\mathcal{P}_{\rm att} = \sum_\nu \eta_\nu \prod_\mu (1-\eta_\mu) \approx \sum_\nu \eta_\nu \quad . \tag{3.10}$$

Inserting the η_ν from Eq. (3.9) yields precisely a discretized from of the integral (3.8) which proves the validity of Eq. (3.8).

There is also a spin conservation law which is implicitly accounted for in the calculation of $\mathcal{P}_{\rm att}$. As a convention, the incoming electron is given a spin up, while the target molecules considered here are always spin-saturated. For the electronic case, a reasonable choice for $\hat{V}_{\rm res}$ is the Coulomb potential screened according to the actual electron density of the system. For the sake of simplicity, we approximate it by a genuine contact potential as $\hat{V}_{\rm res}(\mathbf{r}_1, \mathbf{r}_2) = V_0\, \delta(\mathbf{r}_1 - \mathbf{r}_2)$ with an amplitude V_0 which

simulates roughly the in-medium cross section for electron-electron collisions (we chose here $V_0 = 13.6$ eV).

Once $\hat{V}_{\rm res}$ is chosen, there remains a question in Eq. (3.8) on the energy constraint : the resolution of the δ function cannot be better than the initial energy uncertainty. We therefore use a smoothed δ distribution as $\delta(E_n - E_{\rm in} - E_0) \longrightarrow \delta_{\Delta E_{\rm in}}(E_n - E_{\rm in} - E_0)$ with the initial width $\Delta E_{\rm in}$ as given in Eq. (3.6). In practice, we use a box function.

3.2.3 Detailed evaluation of Slater states

The two-body matrix element in Eq. (3.8) can be easily evaluated if the initial and the final states are Slater states like in our actual calculation. However, both states may be defined with respect to different single-particle sets. Let us assume that

$$|\Phi_{\rm in}(t)\rangle = \hat{a}^\dagger_{\alpha_N} ... \hat{a}^\dagger_{\alpha_1} |{\rm vac}\rangle \quad , \quad |\Psi_n\rangle = \hat{b}^\dagger_{\beta_N} ... \hat{b}^\dagger_{\beta_1} |{\rm vac}\rangle \tag{3.11}$$

where $|{\rm vac}\rangle$ is the vacuum state. The two-body interaction can be expanded as

$$\hat{V}_{\rm res} = \sum_{i_1<i_2, j_1<j_2} (\beta_{i_1}\beta_{i_2}|\widetilde{V_{\rm res}}|\alpha_{j_1}\alpha_{j_2}) \hat{b}^\dagger_{\beta_{i_1}} \hat{b}^\dagger_{\beta_{i_2}} \hat{a}_{\beta_{j_2}} \hat{a}_{\beta_{j_1}} \tag{3.12}$$

where

$$(\beta_{i_1}\beta_{i_2}|\widetilde{V_{\rm res}}|\alpha_{j_1}\alpha_{j_2}) = (\beta_{i_1}\beta_{i_2}|V_{\rm res}|\alpha_{j_1}\alpha_{j_2}) - (\beta_{i_1}\beta_{i_2}|V_{\rm res}|\alpha_{j_2}\alpha_{j_1}) \tag{3.13}$$

is the anti-symmetrized matrix element of $V_{\rm res}$. This then yields

$$\langle\Psi_n|\hat{V}_{\rm res}|\Phi_{\rm in}(t)\rangle = \sum_{i_1<i_2, j_1<j_2} (\beta_{i_1}\beta_{i_2}|\widetilde{V_{\rm res}}|\alpha_{j_1}\alpha_{j_2}) \langle\Psi_n|\hat{b}^\dagger_{\beta_{i_1}} \hat{b}^\dagger_{\beta_{i_2}} \hat{a}_{\beta_{j_2}} \hat{a}_{\beta_{j_1}}|\Phi_{\rm in}(t)\rangle \quad . \tag{3.14}$$

We introduce the matrix of single-particle overlaps

$$\mathcal{N}_{ij} = \langle\beta_i|\alpha_j\rangle \quad . \tag{3.15}$$

The basic overlap between "in" and "out" states then reads:

$$\langle\Psi_n|\Phi_{\rm in}(t)\rangle = \det{}_N \{\mathcal{N}_{ij}\} \tag{3.16}$$

where the index N indicates that this determinant is taken over a $N \times N$ matrix. For the two-body transition element, we have to introduce a sub-matrix of dimension $N-2$ where two lines and two columns are annihilated, i.e.

$$\mathcal{N}^{(i_1 i_2 j_1 j_2)}_{ij} = \begin{pmatrix} \mathcal{N}_{11} & \dots & \mathcal{N}_{1i_1} & \dots & \mathcal{N}_{1i_2} & \dots & \mathcal{N}_{1N} \\ \dots & \dots & \dots & \dots & \dots & \dots & \dots \\ \mathcal{N}_{j_1 1} & \dots & \mathcal{N}_{j_1 i_1} & \dots & \mathcal{N}_{j_1 i_2} & \dots & \mathcal{N}_{j_1 N} \\ \dots & \dots & \dots & \dots & \dots & \dots & \dots \\ \mathcal{N}_{j_2 1} & \dots & \mathcal{N}_{j_2 i_1} & \dots & \mathcal{N}_{j_2 i_2} & \dots & \mathcal{N}_{j_2 N} \\ \dots & \dots & \dots & \dots & \dots & \dots & \dots \\ \mathcal{N}_{N1} & \dots & \mathcal{N}_{N i_1} & \dots & \mathcal{N}_{N i_2} & \dots & \mathcal{N}_{NN} \end{pmatrix} \tag{3.17}$$

The transition matrix element then becomes

$$\langle\Psi_n|\hat{V}_{\rm res}|\Phi_{\rm in}(t)\rangle = \frac{1}{2} \sum_{i_1<i_2, j_1<j_2} (\beta_{i_1}\beta_{i_2}|\widetilde{V_{\rm res}}|\alpha_{j_1}\alpha_{j_2}) (-1)^{i_1+i_2+j_1+j_2} \det{}_{N-2} \left\{\mathcal{N}^{(i_1 i_2 j_1 j_2)}_{ij}\right\} \quad . \tag{3.18}$$

3.2.4 Problem of self-interaction correction

LDA is plagued by a self-interaction error which still constitutes a great hindrance in many applications, as typically a known underestimation of s.p. energies, and the ionization potential in particular [83]. In dynamical processes, the self-interaction error can thus significantly affect the dynamics of electron emission, especially close to threshold [1, 84, 85, 86]. In this study, we evaluate the probability of electron attachment via $2p1h$ transitions (see Sec. 3.2.2). This implies to work with correct s.p. energies on the one hand, and with a sufficient number of unoccupied states on the other hand. LDA not only provides too weakly bound states but it is not able to supply enough empty bound states. Therefore, a time-dependent self-interaction correction (TDSIC) turns out to be compulsory in this study. We use here the technically inexpensive and very robust average-density SIC (ADSIC). It has been proposed already in the 1930s [87] and has been revisited more recently [48]. The essence of ADSIC is to treat the self-interaction contribution of each electron on the same footing by averaging the SIC over all $N_{\rm el}$ electrons. More precisely, the SIC energy reads :

$$E_{\rm ADSIC} = E_{\rm kin} + E_{\rm LDA}[\varrho] - N_{\rm el}\, E_{\rm LDA}[\varrho/N_{\rm el}] \ . \tag{3.19}$$

For the sake of simplicity, we do not write explicitly the spin degree of freedom, although it is fully taken into account in our calculations. The first term in Eq. (3.19) is the kinetic energy, the second one stands for the LDA energy, considered as a functional of the total (time-dependent) electron density $\varrho = \sum_{\alpha=1}^{N_{\rm el}} \langle\varphi_\alpha|\varphi_\alpha\rangle$ (see Eq. 2.1), and the last (negative) one is the ADSIC term. The simplification consists in using the same reference density $\varrho/N_{\rm el}$ for all electrons. This automatically produces one common local SIC potential which allows to treat occupied and unoccupied states the same way. This SIC is by construction designed for metallic systems where the electron delocalization over the whole system justifies to treat the SIC in an average way. It has been recently demonstrated in a variety of atoms and molecules that ADSIC performs surprisingly well also for covalent systems [88]. The effect of this kind of SIC on s.p. levels is depicted in figure 3.2. This confirms that at the level of a mere LDA, we obtain only two degenerated bound empty states for H_2O, which is by far not sufficient to allow for any core-excited resonance.

One hindrance of ADSIC is that it explicitly depends on the number of electrons $N_{\rm el}$ in the system. This means that ADSIC is not suited for multi-centered electron systems as those considered in this study (the remote incoming electron and the target electrons of the molecule), where the wave functions by definition cover very different regions of space.

More quantitatively, in Eq. (3.7), the $2p1h$ excitation states and their related energies are constructed from the N occupied bound states plus all possible unoccupied bound states of the target alone, that is in the absence of the incoming electron. In other words, we perform a static calculation (say, at $t = 0^-$) on the target alone and the corresponding ADSIC uses $N_{\rm el}(t = 0^-) = N$. Therefore the potential seen by the electrons also exhibits a discontinuity and the s.p. energies are changed between $t = 0^-$ and $t = 0^+$. Now, for the dynamical calculation of the collision between the incoming electron and the target, we switch on at $t = 0^+$ the wave function of the remote electron. This thus produces a discontinuity of the number of electrons entering ADSIC, for we have $N_{\rm el}(t = 0^+) = N + 1$. In figure 3.3, we show the evolution of this shift

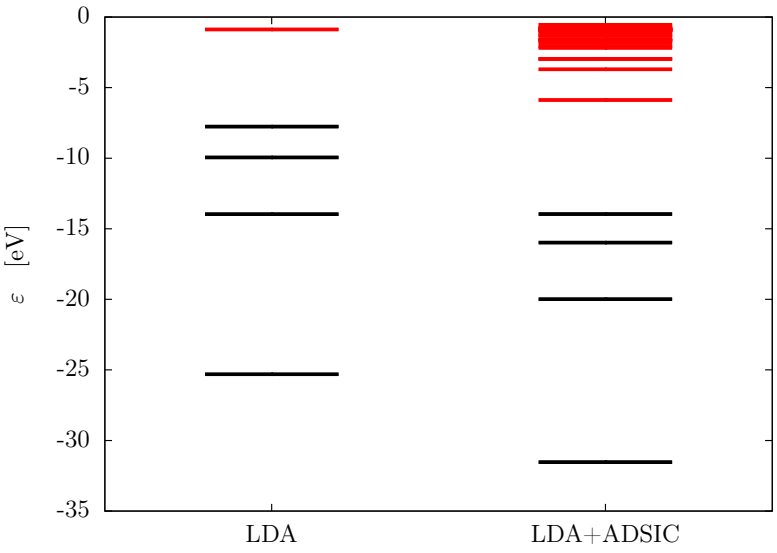

Figure 3.2: Comparison between the bound single particle levels for occupied (black) and empty (red) obtained with a static calculation using plain LDA (left) or LDA+ADSIC (right).

with d, the distance between the remote electron and H_2O. The energy $\varepsilon(0^-)$ for the electron stands for the simple kinetic energy of a Gaussian wavepacket with no potential and for the target s.p energies it corresponds to the s.p. energies obtained from a static calculation. Its counterpart $\varepsilon(0^+)$ is the actual s.p energies in the code at $t = 0$. In a perfect SIC, one expects the shift to tend to zero when $d \to \infty$ which is clearly not the case here. This effect is worsened while decreasing the width of the Gaussian wavepacket (not shown here). However, apart from this nonphysical limit, the general trend of the s.p. energies of the electron is not aberrant. ADSIC artificially tends to delocalize the $N + 1$ wave functions between the two subparts of the whole system which produces a large error when the two parts are far apart. For instance, with a Gaussian wavepacket initially at 16 a_0 from the center of mass of the target molecule and with a spatial width of $5/\sqrt{2}$ a_0, the remote electron with an initial kinetic energy of E_{in} possesses at $t = 0^+$ an "effective" kinetic energy reduced by 2.3, 4.1 and 0.7 eV in the presence of H_2O, H_3O^+ and $(H_2O)_2$ respectively. We should also mention that, as expected, the discontinuity of the s.p.e. of the target wave functions at $t = 0$ is smaller for those which have a spin down, since the incoming electron has a spin up.

From now on, we will upshift all theoretical E_{in} by the right deviation computed using the static calculation to account for this ADSIC artifact. Note that we have elaborated a TDSIC applicable in any case (system in one or several pieces) [47]. But it cannot be applied to our perturbative treatment of electron attachment because unoccupied states, which we need for the final states, are undefined in this scheme. For the present exploratory study, we thus live with the compromise offered by ADSIC.

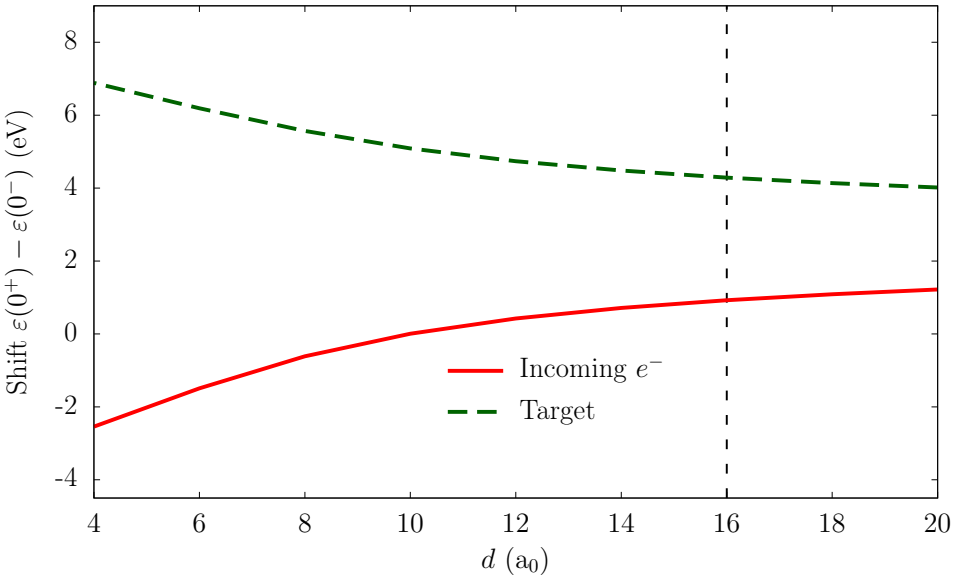

Figure 3.3: Shift in the single particle energies (s.p.e.) as a function of the distance d between the incoming electron and the target molecule. Dashed green line: difference between the static calculation of s.p.e. of the molecule $\varepsilon(t = 0^-)$ and its s.p.e. when adding the electron $\varepsilon(t = 0^+)$ just before starting the dynamic. Full red line: difference between the exact kinetic energy of a Gaussian wavepacket at infinite distance and the s.p.e. of the Gaussian wavepacket in the numerical box at $t = 0^+$. Dashed black line: value used in dynamical calculations.

3.3 Results

3.3.1 Electron attachment to H_2O

We start with the case of an electron colliding with H_2O, since many detailed experimental data of DEA exist for this combination, see e.g. [89, 90, 91, 92]. One identifies three resonances located in the following ranges of incoming energies : 6.4–6.9, 8.4–8.9, and 11.2–11.8 eV. There also exist detailed R-matrix calculations giving three resonances around 6.5–6.994, 8.6–10.2 and 11.8–12.97 eV (see e.g. [67] and references therein).

The leading physical process that TDDFT can describe is the following : the incoming electron colliding with the water molecule is diffracted and finally escapes the numerical box. Therefore, as a first observable, we record the number of emitted electrons N_{esc} defined in Eq. (3.5). In the case of an elastic collision, one expects to observe at the end of the day $N_{\text{esc}}(t_{\text{final}}) = 1$. On the contrary, if some electron attachment occurs, we should get $N_{\text{esc}}(t_{\text{final}}) < 1$. The lower panel of Fig. 3.4 shows the time evolution of N_{esc} for three slightly different E_{in} around 13 eV. The results show at drawing resolution $N_{\text{esc}} \longrightarrow 1$ for $t > 3$ fs in all three cases. This is not surprising as our mean-field calculations provide the most probable pathway and that the faint effects of electron attachment are not visible against the main stream. Remind that the absolute cross-section of electron attachment is very small [82]. To make it visible, we plot in the upper panel of Fig. 3.4 the time evolution of $\mathcal{P}_{\text{att}}$ as such. Even if

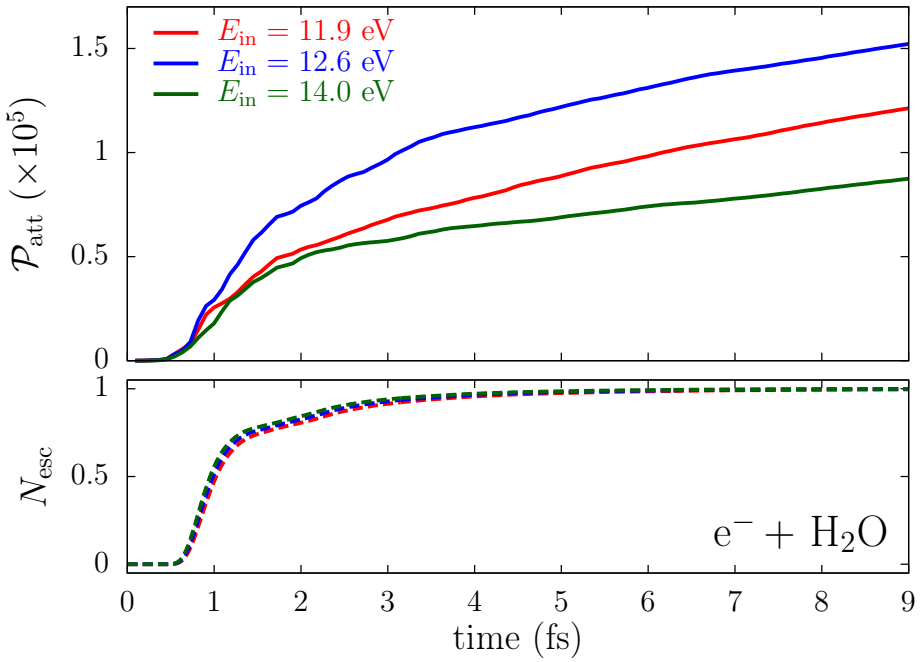

Figure 3.4: Probability of attachment $\mathcal{P}_{\rm att}$ (top) defined in Eq. (3.8) and total ionization $N_{\rm esc}$ (bottom) defined in Eq. (3.5), as functions of time, for an incoming electron of initial kinetic energy $E_{\rm in}$ colliding with a water molecule, at vanishing impact parameter, and for three values of $E_{\rm in}$ as indicated.

the values are small (of the order of 10^{-5}), we do observe a dependence on $E_{\rm in}$ and a non-monotonous behavior of the asymptotic value of the attachment probability : $\mathcal{P}_{\rm att}(14.0\text{ eV}) < \mathcal{P}_{\rm att}(11.9\text{ eV}) < \mathcal{P}_{\rm att}(12.6\text{ eV})$. We therefore observe a resonance around $E_{\rm in} = 12.6$ eV.

We now varied $E_{\rm in}$ in finer steps from 5.7 to 16 eV. Figure 3.5 shows $N_{\rm esc}$ as a function of $E_{\rm in}$ (dashed line). As already observed previously, the asymptotic value of $N_{\rm esc}$ is invariably equal to 1 except for very small $E_{\rm in}$ for which the incoming electron, with a very small initial velocity, has probably not completely escaped the numerical box.

We complement Fig. 3.5 by comparing $N_{\rm esc}$ to the number of $2p1h$ transitions N_{2p1h}, that is the number of excited states fulfilling the energy constraint $E_n \approx E_{\rm in}$. This number exhibits strong resonances at $E_{\rm in} = 9.8$, 11.8 eV (and possibly around 16 eV). This is a sign that the probability of attachment may exhibit strong resonances.

We now turn in figure 3.6 to the asymptotic value of $\mathcal{P}_{\rm att}$ as a function of $E_{\rm in}$. We obtain three clear resonances, located at 6.8, 9.2, and 12.6 eV (that was already deduced from Fig. 3.4), plus a faint one at 14.6 eV. We note that the position of these peaks differs to that observed in N_{2p1h}. This means that the matrix elements entering the calculation of $\mathcal{P}_{\rm att}$ in Eq. (3.8) significantly contribute, and that a mere combinatorial calculation of the number of possible $2p1h$ transitions is not sufficient to quantitatively determine the position of the resonances.

We also compare our results with experimental measurements of DEA [91] in Fig. 3.6. The experimental curves correspond to the measurement of negatively charged

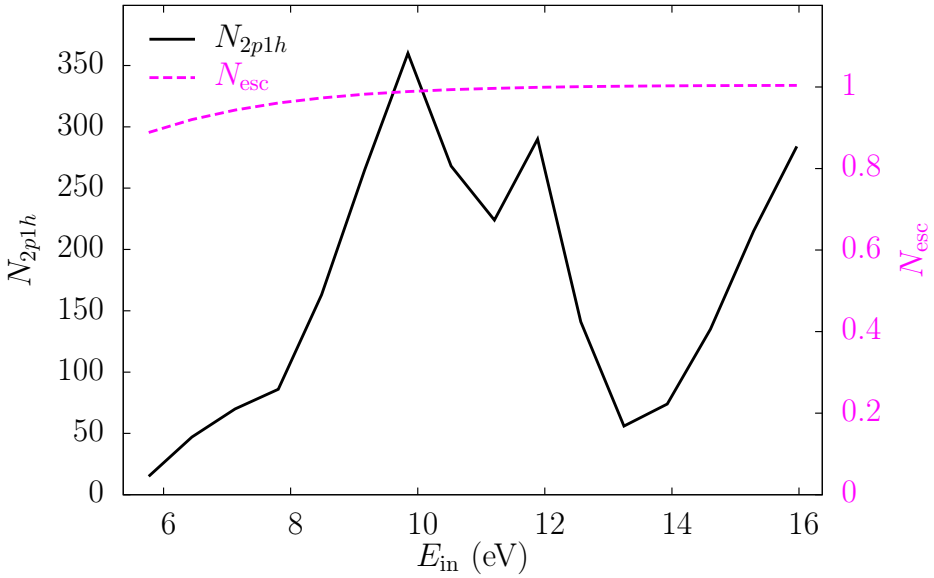

Figure 3.5: Electronic density $N_{\rm esc}$ absorbed after 9 fs at the boundaries of the box (dashes and vertical scale on the right) and number of $2p1h$ excitations N_{2p1h} fulfilling the energy criterion in Eq. (3.8) (full line and vertical scale on the left) plotted against the energy of incoming electron $E_{\rm in}$ on H_2O.

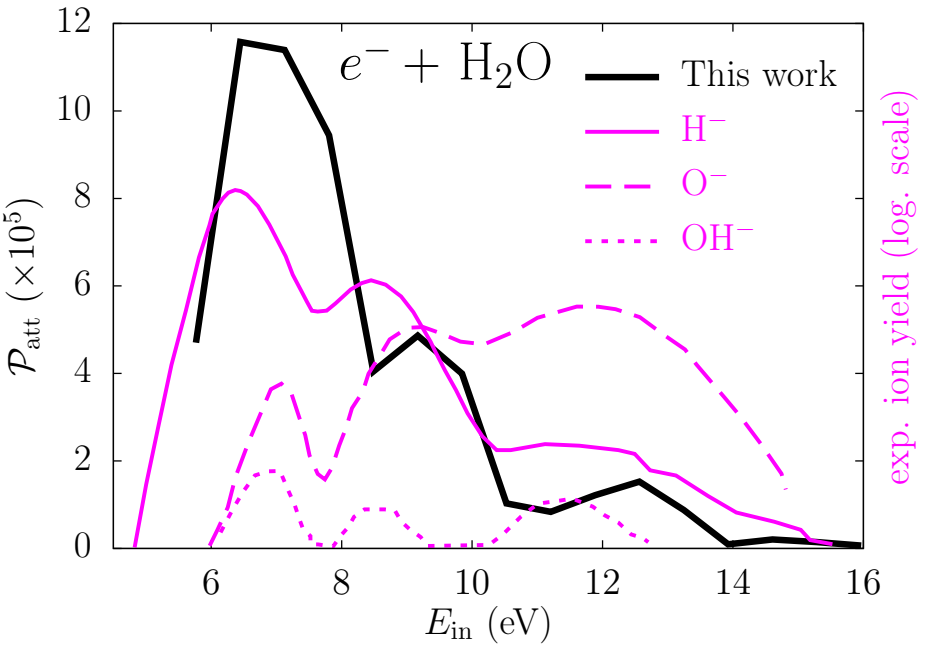

Figure 3.6: Electron attachment to H_2O as a function of energy of incoming electron $E_{\rm in}$. Black thick line and left (linear) vertical scale : asymptotic value of the calculated probability of electron attachment $\mathcal{P}_{\rm att}$. Light curves and right (logarithmic) vertical scale : experimental measurements of dissociative electron attachment yielding H^- (solid curve) O^- (dashes), and OH^- (dots) from [91].

fragments after DEA on H_2O, that is either H^- (full thin line), O^- (dashes) or OH^- (dots), exhibiting three resonances approximately located at the same incident energies. Our theoretical peaks compare very well with the experimental resonances. This is all the more true if we add an horizontal error of 0.82 eV corresponding to the uncertainty on $E_{\rm in}$ due to the finite size of the Gaussian wavepacket describing the incoming electron (see discussion related to Eq. (3.6)).

Note, however, that the absolute yield of our calculated resonances does not reproduce the experimental ones, for the latter ones are plotted in logarithmic scale. It should be reminded that we employ a very simple form of the residual interaction in the rates (3.8) and a rough choice of its strength V_0. We also tried the full Coulomb

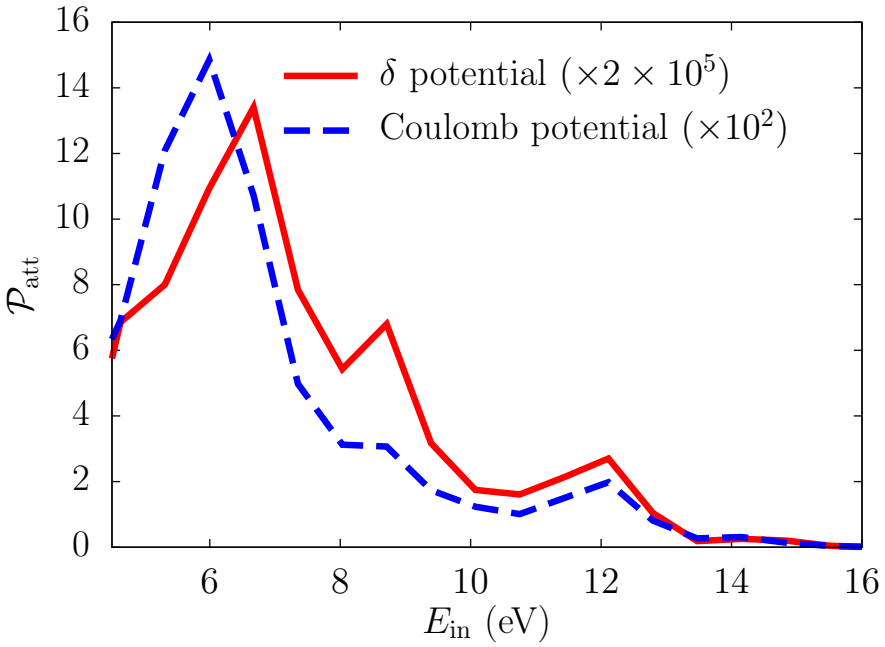

Figure 3.7: Asymptotic probability of attachment to H_2O as a function of energy of incoming electron $E_{\rm in}$ for two modeling of $V_{\rm res}$: (red full line) δ function or (blue dashed line) the Coulomb potential.

potential as an alternative. The size of the box has been reduced to 40^3 a_0^3 as the Coulomb potential is more numerically demanding. We also reduced a bit the width of the Gaussian wavepacket to $4/\sqrt{2}$ to ensure that not too much electronic density is absorbed at $t = 0^+$. The initial position of the electron is also closer to the molecule: 14 a_0 instead of 16 a_0. The results are displayed in Fig. 3.7. Qualitatively the results are almost the same but the second resonance peak at 9.2 eV (which is now at 8.4 eV) is less pronounced. The transition probability is three orders of magnitude higher for the Coulomb potential. The δ potential is therefore an approximation that saves a lot of computational effort and gives comparable results.

We now can check the effect of the width of the initial Gaussian wavepacket, the effect of distance to the molecule being well described in Sec. 3.2.4. We explored three different widths. The numerical box is also taken equal to 40^3 a_0^3 and the initial separation between the colliding electron and H_2O to 14 a_0. The corresponding results are plotted in figure 3.8. Firstly, we note that a larger wavepacket gives a lower

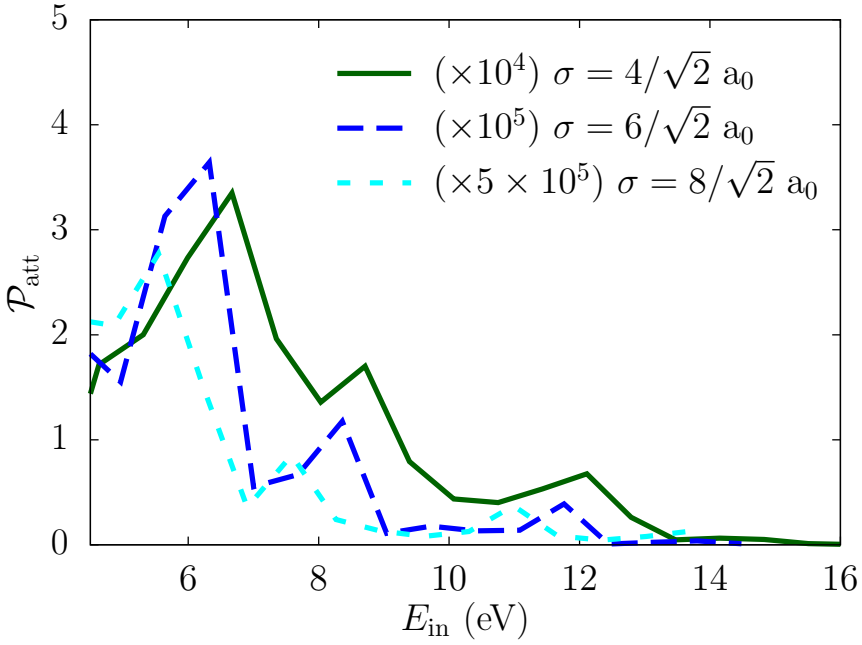

Figure 3.8: Asymptotic probability of attachment to H_2O as a function of energy of incoming electron $E_{\rm in}$ for three widths of the Gaussian wavepacket as indicated.

probability of attachment. This behavior is obvious as the density of the wavepacket is lower because it is more spread. Secondly, a larger width decreases the ADSIC artifact and seems to induce a general red shift on the curve. Therefore, the numerical results presented in figure 3.6 should be red-shifted a little to compensate again the ADSIC error if one varies the impact parameter. We however note that, regardless the impact parameter, the presence of three resonances is robust.

3.3.2 Exploration of other small water systems

We now extend the study to H_3O^+ and $(H_2O)_2$, and compare the results with those obtained in H_2O. Figure 3.9 summarizes the results on N_{2p1h} (top panel) and the asymptotic value of $\mathcal{P}_{\rm att}$ (bottom) as functions of incident kinetic energy $E_{\rm in}$, for H_3O^+ (long dashes), $(H_2O)_2$ (short dashes), and H_2O (solid line).

Even if the occupied states of H_3O^+ are more bound than those of H_2O, due to the positive charge (our theoretical ionization potentials are 24.9 eV for H_3O^+ and 14.0 eV for H_2O), the numbers of $2p1h$ transitions are comparable in both systems (they possess the same number of electrons). On the contrary, N_{2p1h} can be twice or three times larger for the water dimer. This renders the computation of the attachment probability in the latter case much more expensive, but still feasible. Results for $\mathcal{P}_{\rm att}$ are shown in the bottom panel : for the dimer $(H_2O)_2$, there are strong resonances at very low energies (2.7 and 4.1 eV), a smaller one at 5.4 eV, and a very faint one at 9.5 eV. There is unfortunately, to the best of our knowledge, no experimental measurements of DEA specifically for the water dimer for comparison. As for H_3O^+, even if the energy dependence of $\mathcal{P}_{\rm att}$ is more fuzzy than in the neutral systems, clear resonances are also observed in the ranges of 8.1–8.8, 12.1–13.6 and 15.6–16.3 eV. For the case of a

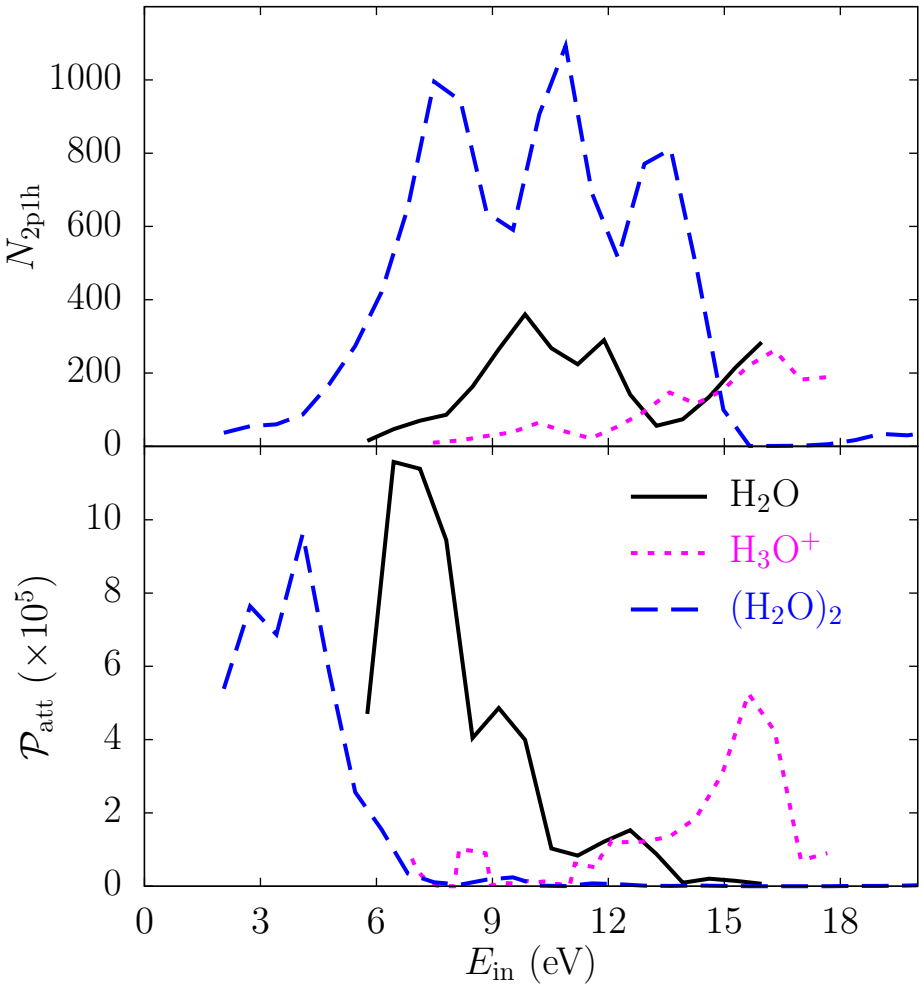

Figure 3.9: Number of $2p1h$ excitations N_{2p1h} (top) and asymptotic value of the electron attachment probability $\mathcal{P}_{att}$ (bottom) as functions of initial kinetic energy E_{in} of the incoming electron, on H_2O (full curves), $(H_2O)_2$ (long dashes) and H_3O^+ (short dashes). For the sake of clarity, the probability of attachment to H_3O^+ has been multiplied by 2.

cationic species, electron attachment leading to a break-up constitutes the dissociative recombination (DR) instead of the DEA. Experimentally, DR have been measured on H_3O^+ at 5.792 and 6.443 eV [93, 94], and also at 11 eV [95, 94], giving a less satisfactory agreement with our calculations. Nevertheless, despite the ADSIC artifact being larger in this case, clear resonances appear below 30 eV in electron attachment to the three targets investigated here.

3.4 Conclusion and perspectives

We have presented a microscopic and dynamical calculation of the probability of electron attachment occuring in water-based systems using TDLDA augmented by ADSIC. The physical described process is the collision of an electronic Gaussian wavepacket with a target molecule, and the evaluation of $2p1h$ transitions via a time-dependent perturbative treatment using a Fermi's golden rule. This method is well suited when the mean-field is a good approximation at the leading order of the propagation. It produces satisfying results for H_2O and predict the existence of resonances in $(H_2O)_2$ and H_3O^+. Because of the exponentially increasing number of $2p1h$ transitions involved, this method is still restricted to small systems and does not enable yet to model electron attachment in water clusters large enough to extract information for solvated DNA. A calculation with a base pair of DNA surrounded by water is thus out of reach. From a more technical point of view, we can improve our method by introducing rearrangements that have been neglected and project on actual RPA states instead of ground state states. We can also allow ions to move to see resonances due to interactions with molecular parameters but that would mean, once again, to project on the target states "on the fly" and this would be very numerically demanding. Finally the spurious ADSIC effects could be solved by using a SIC in optimized effective potential (OEP) formalism. However, regarding the number of empty states to deal with, a full TDOEP treatment might also be too heavy numerically speaking.

Still, a true dynamical electron attachment is not expected to be described at all in a mean-field calculation as rare events are screened by the most probable evolution of the system. Nevertheless this calculation, being the first microscopic calculation of this kind to the best of our knowledge, has also the advantage of introducing the philosophy behind the algorithms that appear in the next chapters. Our approaches proposed in chapter 2 to include dissipative features are probably not able to describe DEA as they are not suited for multiple fragmentation paths. One can argue that STDHF allows trajectories to diverge but its applicability for this kind of events will probably be hindered by too low probabilities.

Chapter 4

Test of STDHF in a schematic model

Contents

4.1 Introduction

In this part we compare STDHF with an exact calculation in a schematic model. This model is strongly inspired by a Lipkin-Meshkov-Glick model [96, 97, 98] of Ω particles distributed into two bands of energy. This model has been used in nuclear physics and produces many-body behaviors such as large-amplitude collective motion or spontaneous symmetry breaking [99]. It contains a non-local 2-body interaction that models in simple way collisions between two fermions. We use a slightly modified

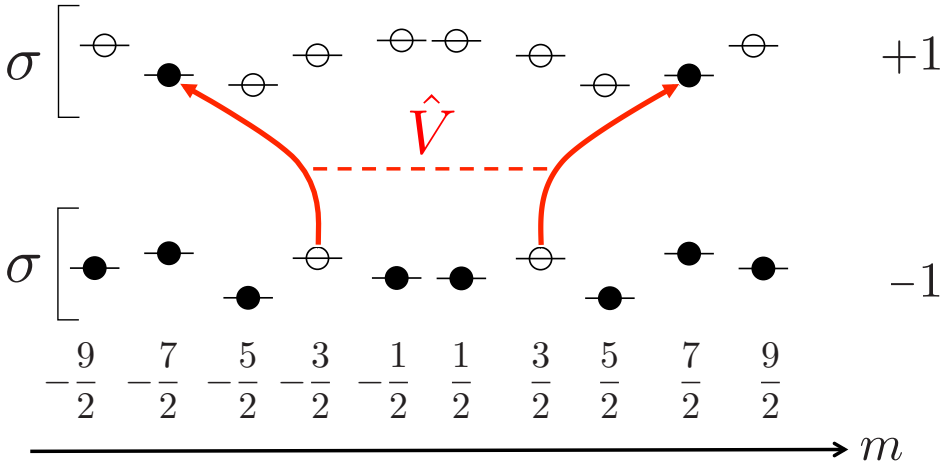

Figure 4.1: Illustration of the Stochastic Two-Band Model with the action of $\hat{V}$, defined in Eq. (4.3c), applied to the ground state of $\hat{H}_0$, defined in Eq. (4.3b), for $j = 9/2$.

version of the interaction in this work. Indeed the original model is too coherent to allow an efficient application of STDHF [100]. The advantage of such a model is the numerical determination of the exact solution for small Ω. It can be therefore used as a benchmark to test the performances of the STDHF scheme introduced in chapter 2.

This work is the subject of an article that will be published soon [1]. This chapter is organized as follows: we first introduce the modified model and how we compute the various schemes in this special case. Then some observables are defined and a first test case is discussed. We then discuss in more details the robustness of the scheme with respect to the parameters of the model, either the numerical or the physical ones, as excitation energies, bandwidth, system size. We finally conclude on the validity of the STDHF scheme and its improvement compared to TDHF.

4.2 Theoretical framework

4.2.1 A stochastic two-band model

The Stochastic Two-Band Model (STBM) is sketched in fig. 4.1. It consists in two bands of single-particle (s.p.) levels, the lower band denoted by the principle quantum number $s = -1$ and the upper one by $s = +1$. Each band contains an even number of Ω levels denoted by the secondary quantum number m running from $-j$ to $+j$ in steps of 1 such that $\Omega = 2j + 1$ (j is then half integer). In the example displayed in fig. 4.1, the case $j = 9/2$ yields 10 different m values from $-9/2$ to $+9/2$. S.p. states are thus represented by a combined quantum number :

$$\alpha = (s_\alpha, m_\alpha) \ , \ s_\alpha \in \{-1, +1\} \ , \ m_\alpha \in \{-j, -j+1, ..., j-1, j\} \ . \tag{4.1}$$

[1] L. Lacombe, P. M. Dinh, E. Suraud, P.-G. Reinhard, "Stochastic TDHF in an exactly solvable model", accepted in Annals of Physics (2016).

States are gathered into $\pm m_\alpha$ partners and we keep this symmetry to reduce the complexity. For a compact notation, we introduce the following abbreviations wherever convenient

$$\bar{m}_\alpha = -m_\alpha \ , \ \bar{\alpha} = (s_\alpha, \bar{m}_\alpha) = (s_\alpha, -m_\alpha) \equiv -\alpha \ . \tag{4.2}$$

The notation $\alpha > 0$ then means $m_\alpha > 0$.

The model Hamiltonian consists in a 1-body Hamiltonian $\hat{H}_0$ plus a 2-body interaction $\hat{V}$. It is constructed in a standard manner on the basis of annihilation (and creation) operators $\hat{a}^{(\dagger)}_{s_\alpha, m_\alpha} = \hat{a}^{(\dagger)}_\alpha$ for each s. p. state as :

$$\hat{H} = \hat{H}_0 + \hat{V} \quad , \tag{4.3a}$$

$$\hat{H}_0 = \sum_\alpha \frac{s_\alpha \varepsilon_\alpha}{2} \hat{a}^\dagger_\alpha \hat{a}_\alpha \quad , \tag{4.3b}$$

$$\hat{V} = v_0 \hat{S}_+ \hat{S}_- \quad , \tag{4.3c}$$

$$\hat{S}_+ = \sum_{\alpha>0} \hat{a}^\dagger_\alpha \hat{a}^\dagger_{\bar{\alpha}} = (\hat{S}_-)^\dagger \quad , \tag{4.3d}$$

$$\varepsilon_\alpha = \Delta + \delta\varepsilon_\alpha \quad , \tag{4.3e}$$

$$\delta\varepsilon_\alpha : \sum_{m_\alpha} \delta\varepsilon_\alpha \ \xrightarrow{\Omega\to+\infty} \ 0 \quad , \quad \frac{1}{\Omega}\sum_{m_\alpha} (\delta\varepsilon_\alpha)^2 \ \xrightarrow{\Omega\to+\infty} \ \sigma^2 \quad , \tag{4.3f}$$

where Δ stands for the average level spacing between the two shells $s = -1$ and $s = +1$ and the $\delta\varepsilon_\alpha$ are chosen randomly according to a Gaussian distribution with width σ and centroid zero. The gap Δ defines the energy unit and the time unit is accordingly $[\Delta^{-1}]$. We shall use these units all over this chapter. With $\sigma = 0$, the model reduces to the case with fully degenerated bands. Finally, v_0 describes the strength of the coupling $\hat{V}$.

The original LMG model [96, 97, 98, 101] is very similar to this one except that it allows only vertical jumps (from the lower band to the upper one) and there is no $m/\bar{m}$ pair involved: each particle interacts with all the others. The LMG model has been used in nuclear physics and has the advantage of being exactly solvable [102]. This interaction in the model presented here is in the form of a pairing interaction as used in the seniority model or BCS for the description of nuclei (see sections 6.2 and 6.3 of [102]). It models in most simple manner collisions between α-$\bar{\alpha}$ pairs of fermions. In the following, we always consider half-filled systems such that the particle number becomes $N = \Omega$. In addition, we only consider weak and repulsive interactions $v_0 > 0$. This minimizes the effect of $\hat{V}$ on the ground state such that $\hat{V}$ serves mainly to induce correlations. From a more physical perspective, it also lies in typical systems in which the mean-field provides a good description of ground state properties. This is also well suited for our purpose to study the treatment of dynamical correlations with STDHF. The ground state $|\Phi_0\rangle$ of the free Hamiltonian $\hat{H}_0$ possesses all electrons in the lower band $s = -1$. This feature is still approximately correct for the weak interactions $\hat{V}$ considered here and it remains even exact at Hartree-Fock (HF) level. More precisely, for the exact ground state the weight of the determinant having all electrons in the lower band is 0.990.

4.2.2 The Hartree-Fock approach

The operator $\hat{a}^\dagger_\alpha$ creates a s.p. basis state and $\hat{a}_\alpha$ annihilates it. The creation operator for any other s.p. state is obtained by the linear combination

$$\hat{b}^\dagger_\kappa = \sum_{\alpha>0} \hat{a}^\dagger_\alpha A_{\alpha\kappa} \quad , \quad \hat{b}^\dagger_{\bar{\kappa}} = \sum_{\alpha>0} \hat{a}^\dagger_{\bar{\alpha}} A_{\bar{\alpha}\bar{\kappa}} \quad , \tag{4.4}$$

where $\kappa > 0$ and $\bar{\kappa} = -\kappa$. The symmetry of $\hat{H}$ allows us to skip the cross couplings $\alpha \leftrightarrow \bar{\kappa}$ and $\bar{\alpha} \leftrightarrow \kappa$. A general independent-particle state (Slater state) for $N = \Omega$ particles is generated by applying $\hat{b}^\dagger_\kappa$:

$$|\Phi\rangle = \hat{b}^\dagger_{\kappa_1} \hat{b}^\dagger_{\kappa_2} \dots \hat{b}^\dagger_{\kappa_\Omega} |\mathrm{vac}\rangle \quad . \tag{4.5}$$

The energy expectation value of this state is the Hartree-Fock energy

$$\begin{aligned} E_{\mathrm{HF}} &= \langle\Phi|\hat{H}|\Phi\rangle \\ &= \frac{1}{2} \sum_{m_\alpha>0} \varepsilon_{m_\alpha} \left(\rho_{1m_\alpha,1m_\alpha} - \rho_{-1m_\alpha,-1m_\alpha}\right) + v_0 \sum_{\alpha,\alpha'>0} \rho_{\alpha'\alpha}\rho_{\bar{\alpha}'\bar{\alpha}} \quad , \end{aligned} \tag{4.6a}$$

$$\rho_{\alpha'\alpha} = \langle\Phi|\hat{a}^\dagger_\alpha \hat{a}_{\alpha'}|\Phi\rangle = \sum_{\kappa>0} n_\kappa A^*_{\alpha\kappa} A_{\alpha'\kappa} \quad , \tag{4.6b}$$

$$\rho_{\bar{\alpha}'\bar{\alpha}} = \langle\Phi|\hat{a}^\dagger_{\bar{\alpha}} \hat{a}_{\bar{\alpha}'}|\Phi\rangle = \sum_{\kappa>0} n_{\bar{\kappa}} A^*_{\bar{\alpha}\bar{\kappa}} A_{\bar{\alpha}'\bar{\kappa}} \quad , \tag{4.6c}$$

where $\rho_{\alpha'\alpha}$ is the 1-body density matrix and n_κ is the occupation number of state κ. The ground state of the mean-field approximation is obtained by minimizing E_{HF} with respect to the $\rho_{\alpha'\alpha}$ or to $A_{\alpha'\kappa}$. For the regime of weak $v_0 > 0$ which we are studying, the mean-field ground state $|\Phi_0\rangle$ of the interacting system is identical to the ground state of $\hat{H}_0$ which is given by the trivial non-transformation $A_{\alpha\kappa} = \delta_{\alpha\kappa}$. The time evolution of s.p. states $\hat{b}^\dagger_\kappa$ is given by the TDHF equations

$$\mathrm{i}\partial_t \hat{b}^\dagger_\kappa = -\left[\hat{h}, \hat{b}^\dagger_\kappa\right] \quad . \tag{4.7}$$

They are driven by the mean-field Hamiltonian $\hat{h}$ which is an effective 1-body operator obtained by contracting the 2-body interaction $\hat{V}$ over a particle-hole pair $\hat{a}^\dagger\hat{a}$. It reads

$$\hat{h} = \hat{H}_0 + v_0 \sum_{\alpha,\alpha'>0} \left(\rho_{\bar{\alpha}'\bar{\alpha}} \hat{a}^\dagger_\alpha \hat{a}_{\alpha'} + \rho_{\alpha'\alpha} \hat{a}^\dagger_{\bar{\alpha}} \hat{a}_{\bar{\alpha}'}\right) \quad , \tag{4.8}$$

Note that we exploit again the $\pm m$ symmetry to ignore the mixing terms $\alpha \leftrightarrow \bar{\alpha}'$ and $\bar{\alpha} \leftrightarrow \alpha'$ which correspond to the exchange terms. The same equations can be expressed also in terms of the amplitudes $A_{\alpha\kappa}(t)$, yielding

$$\mathrm{i}\partial_t A_{\alpha\kappa} = \sum_{\alpha'} h_{\alpha\alpha'} A_{\alpha'\kappa} \quad , \quad h_{\alpha\alpha'} = \frac{\varepsilon_{m_\alpha}}{2} s_\alpha \delta_{\alpha\alpha'} + \rho_{\bar{\alpha}'\bar{\alpha}} \quad . \tag{4.9}$$

The numerical solution is done using an implementation of the Crank-Nicolson scheme [103]

$$\hat{A}(t+dt) = \frac{1 - \frac{\mathrm{i}\mathrm{d}t}{2}\hat{h}(t + \mathrm{d}t/2)}{1 + \frac{\mathrm{i}\mathrm{d}t}{2}\hat{h}(t + \mathrm{d}t/2)} \hat{A}(t) \quad , \tag{4.10}$$

where $\hat{A}$ is a compact notation of the matrix $A_{\alpha\kappa}$ of expansion coefficients. $\hat{h}(t+\mathrm{d}t/2)$ is computed in a predictor step which looks like the full step (4.10) but propagating only by $\mathrm{d}t/2$ and using $\hat{h}(t)$. The Crank-Nicolson step maintains ortho-normality by construction. To obtain satisfying energy conservation, one has to choose the step size $\mathrm{d}t$ sufficiently small (see discussion in Sec. 4.2.7).

4.2.3 Stochastic Time-Dependent Hartree Fock (STDHF)

Mean-field propagation with TDHF, as outlined in Sec. 4.2.2, takes only part of the 2-body interaction $\hat{V}$ into account. There remains a residual interaction from $\hat{V}$ which generates correlations. This $\hat{V}_{\mathrm{res}}$ is used to compute the transition probability entering Eq. (2.73) in STDHF:

$$\mathcal{P}_{\kappa_1\kappa_2\kappa_3\kappa_4}\tau = 2\pi\ \delta_\Gamma(E^{\mathrm{HF}}_{\kappa_1\kappa_2\kappa_3\kappa_4} - E^{\mathrm{HF}}_0)\ \left|\langle\Phi^{(\alpha)}_{\kappa_1\kappa_2\kappa_3\kappa_4}|\hat{V}_{\mathrm{res}}|\Phi^{(\alpha)}\rangle\right|^2\ \tau \tag{4.11}$$

where δ_Γ is a δ function with finite width Γ and α is the index of the STDHF trajectory. It turns out that the sole matrix elements of the residual interaction which are non-vanishing for the STBM read :

$$\langle\Phi^{(\alpha)}_{\kappa_1\bar{\kappa}_2\bar{\kappa}_3\kappa_4}|\hat{V}_{\mathrm{res}}|\Phi^{(\alpha)}\rangle = v_0 \sum_{\alpha,\alpha'>0} A^{(\alpha)*}_{\alpha\kappa_1} A^{(\alpha)*}_{\bar{\alpha}\bar{\kappa}_2} A^{(\alpha)}_{\bar{\alpha}'\bar{\kappa}_3} A^{(\alpha)}_{\alpha'\kappa_4} \quad , \tag{4.12}$$

where all κ's entering the latter equation are now positive.

4.2.4 Exact propagation

The exact solution is conceptually the simplest but computationally the most expensive. The fully correlated state is expanded into a complete basis of mean-field states

$$|\Psi\rangle = \sum_{\alpha_n,\alpha'_n>0} c_{\alpha_1\ldots\alpha_{\Omega/2},\bar{\alpha}'_1\ldots\bar{\alpha}'_{\Omega/2}} \hat{a}^\dagger_{\alpha_1}\ldots\hat{a}^\dagger_{\alpha_{\Omega/2}}\hat{a}^\dagger_{\bar{\alpha}'_1}\ldots\hat{a}^\dagger_{\bar{\alpha}'_{\Omega/2}}|\mathrm{vac}\rangle\ . \tag{4.13}$$

The time-dependent Schrödinger equation

$$\mathrm{i}\partial_t|\Psi\rangle = \hat{H}|\Psi\rangle \tag{4.14}$$

is solved by mapping it into a matrix equation for the expansion coefficients $c_{\alpha_1\ldots\alpha_{\Omega/2},\bar{\alpha}'_1\ldots\bar{\alpha}'_{\Omega/2}}$. For the solution, we use again the Crank-Nicolson scheme (4.10) but now with the full Hamiltonian $\hat{H}$.

4.2.5 Initial excitation

As a first step, we have to prepare the ground state of the stationary problem. This is for TDHF and STDHF the Slater state with each $s_\alpha = -1$ s.p. state occupied and each $s_\alpha = +1$ unoccupied. For the exact solution, we have to solve the static Schrödinger equation with the full Hamiltonian $\hat{H}$.

The initial state for dynamical evolution is taken as follow: we apply an instantaneous boost excitation on the ground state.

$$|\Phi(t=0)\rangle = e^{\mathrm{i}\lambda(\hat{D}+\gamma\hat{W})}|\Phi_{\mathrm{gs}}\rangle \quad , \tag{4.15a}$$

$$\hat{D} = \sum_{m_\alpha}\left(\hat{a}^\dagger_{1\,m_\alpha}\hat{a}_{-1\,m_\alpha} + \hat{a}^\dagger_{-1\,m_\alpha}\hat{a}_{1\,m_\alpha}\right) \quad , \tag{4.15b}$$

$$\hat{W} = \frac{1}{2}\sum_{\alpha,\alpha'>0}\left(\hat{a}^\dagger_\alpha\hat{a}_{\alpha'} + \hat{a}^\dagger_{\bar{\alpha}}\hat{a}_{\bar{\alpha}'}\right) \quad . \tag{4.15c}$$

$\hat{D}$ simulates a dipole operator of a typical many-particle system and the excitation operator $e^{\mathrm{i}\lambda\hat{D}}$ induces initial $1p1h$ transitions within the same m_α. For example, one can consider the operator that couples a laser field to the electrons of an atom, and an instantaneous boost is the most generic excitation simulating a short pulse.

The parameter λ tunes the strength of the initial excitation. The $\hat{W}$ operator serves a different purpose. At the mean-field level, the interaction (4.3c) deals only with vertical transitions which maintain the m quantum number. This emphasizes coherence which, in turn, overlays dissipation with large memory effects as we will see. To explore the level of dissipation in a more flexible manner, we initiate the interaction with transition across different m's by applying the unitary transformation $e^{\mathrm{i}\lambda\gamma\hat{W}}\hat{V}e^{-\mathrm{i}\lambda\gamma\hat{W}}$ on the coupling $\hat{V}$ with the mixing operator $\hat{W}$. This transformation maintains the overall interaction strength without rescaling v_0. For simplicity, we applied the transformation to the initial state which turns out to be a good approximation to solving the dynamical equations with the modified interaction. The parameter γ quantifies the amount of mixing with respect to the dipole operator. We will detail the numerical values λ and γ in Sec. 4.2.7.

4.2.6 Observables

Our main aim here is to study the dynamics of thermalization after initial excitation. This is for instance quantified by the fermionic entropy

$$S = -k_{\mathrm{B}}\,\mathrm{Tr}\left[\hat{\rho}\ln\hat{\rho} + (1-\hat{\rho})\ln(1-\hat{\rho})\right] \ , \tag{4.16}$$

where $\hat{\rho}$ is the one-body density operator whose matrix elements are $\rho_{\alpha'\alpha} = \langle\hat{a}^\dagger_\alpha\hat{a}_{\alpha'}\rangle$. A pure mean field state has $S = 0$. The entropy thus stays zero at all time in any TDHF calculation, while STDHF and the exact solution are expected to exhibit a time-dependent S.

A further test observable is the difference between one-body matrices in all combinations between TDHF, STDHF and the exact solution, quantified as

$$\delta_\rho = 2\frac{||\rho-\rho_{\mathrm{ex}}||}{||\rho+\rho_{\mathrm{ex}}||} \quad , \tag{4.17}$$

where $||...||$ stands for the Frobenius matrix norm $||A|| = \sqrt{\mathrm{Tr}(\hat{A}^\dagger\hat{A})}$ and ρ_{ex} is the exact 1-body density matrix.

Because of the expression of the interacting term $\hat{V}$, see Eqs. (4.3) and fig. 4.1, and the resulting $\pm m$ symmetry of the ground state, it is also worth looking at the

time evolution of the total $M = \sum_\alpha m_\alpha$, i.e. the sum over all occupied m values. The corresponding observable $\hat{M}$ is given by

$$\hat{M} = \sum_\alpha m_\alpha \left(a^\dagger_{1m_\alpha} a_{1m_\alpha} + a^\dagger_{-1m_\alpha} a_{-1m_\alpha} \right) \quad . \tag{4.18}$$

The initial excitation conserves $\langle \hat{M} \rangle$ but not the $\pm m$ symmetry in each determinant of the expansion (4.13). Since the exact propagation conserves the M of each determinant, $\langle \hat{M} \rangle$ is obviously conserved. On the contrary, the mean field propagation only conserves the symmetry $\rho_{\alpha'\alpha} = \rho_{\bar{\alpha}'\bar{\alpha}}$. This is enough to guarantee the conservation of $\langle \hat{M} \rangle$. As for the STDHF scheme, nothing ensures that $\langle \hat{M} \rangle$ is conserved. However one expects a statistical conservation when averaging over all trajectories, because of the symmetries of $\mathcal{P}_{\kappa_1\bar{\kappa}_2\bar{\kappa}_3\kappa_4}$. We will explore the time evolution of $\langle \hat{M} \rangle$ in various schemes in more details in Sec. 4.3.2.

4.2.7 Numerical and model parameters

We complete this section with specifying numerical details. We propagate TDHF and the exact solution using the Crank-Nicolson scheme with a time step $\mathrm{d}t = 0.01\,\Delta^{-1}$.

To stay at the perturbative level for the correlations, the 2-body interaction is taken relatively small, that is $v_0 = 0.05\,\Delta$. In the calculation of the transition probabilities, see Eq. (4.11), the δ_Γ function ensuring energy conservation is approximated by a fixed window

$$\delta_\Gamma(x) = \begin{cases} 1/\Gamma & \text{for} \quad |x| < \Gamma/2 \\ 0 & \text{for} \quad |x| \geq \Gamma/2 \end{cases} \quad . \tag{4.19}$$

As we will see, the results actually presented here depend very little on Γ. We have checked their stability for $10^{-5}\Delta \leq \Gamma \leq 0.1\Delta$. In most of the results, have chosen the value $\Gamma = 0.02$ for reasons that will be explained in section 4.3.2.

The number of particles varies from $\Omega = 4$ to 10 in the comparison between the exact solution and the STDHF. Due to an exponentially increasing computing time for the exact propagation, the cases from $\Omega = 12$ to 20 have been explored in the STDHF scheme only. The number of samples in the STDHF ensemble is always $\mathcal{N}_{\mathrm{ens}} = 100$. We have also checked larger ensembles and found practically the same results.

We have tested various values of the mixing parameter γ, from 0 to 0.6. In the following results, it is set to 0.3 since such a value creates enough disorder at $t = 0$, that is the needed transitions for STDHF to operate (see discussion in Sec. 4.2.5). The excitation energy E^* is defined as the difference between the ground state energy E_{GS} and the energy after the initial boost:

$$E^* = E(0^+) - E_{\mathrm{GS}} \quad . \tag{4.20}$$

Figure 4.2 shows the excitation energy E^* attained as a function of λ in the case of 10 particles, a band width $\sigma = 0.2\ \Delta$ and an interaction strength $v_0 = 0.05\ \Delta$. Three cases are considered $\hat{D}$ only ($\gamma = 0$), $\gamma = 0.3$ and W only. For $\hat{W}$ only, the range of accessible excitation energy is limited to $\approx 2\ \Delta$ which strongly reduces the range of accessible E^*. For the two other cases the energy grows monotonously up to a maximum where it turns to monotonous decrease. The upper limit of E^* reflects the fact that the model Hamiltonian is bound not only from below, as it should be for a

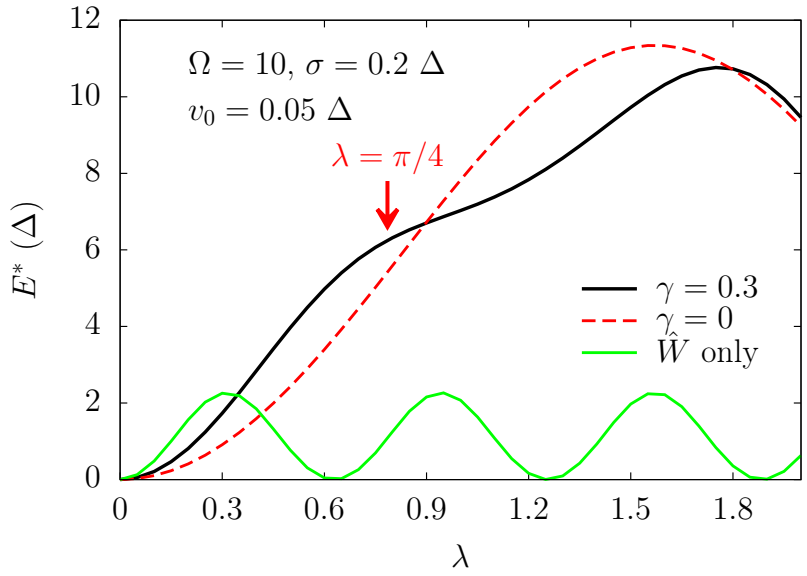

Figure 4.2: Accessible excitation energy E^* (in Δ units) as a function of λ for the initial excitation (4.15) Full black line: with $\gamma = 0.3$. Dashed red line: with $\hat{D}$ only ($\gamma = 0$). Full green line: with $\hat{W}$ only, $\gamma = 0$ and $\hat{D}$ is set to zero. The other STBM parameters are indicated.

non-relativistic Hamiltonian, but also from above. The relevant range of the STBM stays in the region of λ safely below the turning point (which is at $\lambda = \pi/2$ for $\gamma = 0$). In practice, we use $0.6 \leq \lambda \leq 0.8$ close to $\pi/4$ which corresponds to a state with the particles having half weight in the upper band and half weight in the lower band. This value for λ is safely in the regime of increasing E^*. The cases $\gamma = 0$ and $\gamma = 0.3$ provide moderate differences in E^* and does not affect the general trend of the curve. This corroborates the above statement that the overall interaction strength is little affected by virtue of scanning interactions in terms of a unitary transformation.

4.3 Results

4.3.1 A first test case

We start with the analysis of a typical test case from the perspective of the difference of s.p. density matrices, the entropy, and the expectation value of the dipole. The time evolution of these observables is displayed in fig. 4.3. In the upper panel, we compare the density matrix ρ obtained in TDHF and that in STDHF with respect to the exact density matrix $\rho_{\rm ex}$ in terms of norm of the difference δ_ρ, defined in Eq. (4.17), of TDHF or STDHF with respect to the exact solution. STDHF provides a much smaller deviation δ_ρ than TDHF. This indicates that STDHF is indeed able to incorporate a great deal of the dynamical correlations. Both deviations are composed from a global trend plus oscillations. The trend approaches a rather large stable deviation δ_ρ for TDHF and seems to indicate (slow) convergence to small deviation for STDHF.

These oscillations are also observed in the time evolution of the exact entropy per

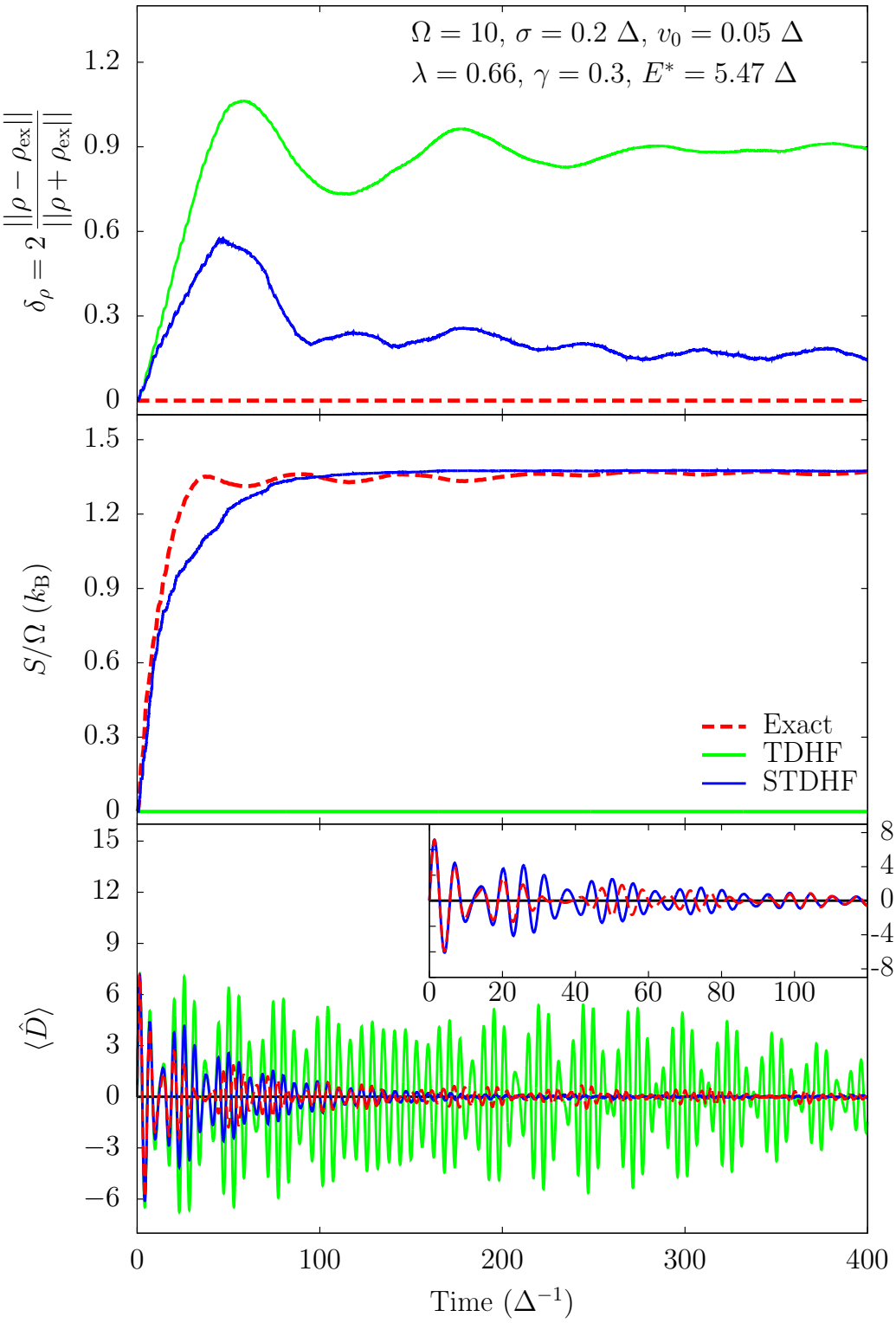

Figure 4.3: Comparison of TDHF, STDHF and exact solution with respect to three observables, as a function of time, with the STBM parameters as indicated. Bottom : expectation value of the dipole operator $\hat{D}$, see Eq. (4.15b); middle : entropy per particle S/Ω, see Eq. (4.16); top : difference of one-body density.

particle, see middle panel of Fig. 4.3. The entropy from STDHF entropy reproduces the exact entropy in the average trend and in the asymptotic value rather well, see also Fig 4.10 and the related discussion. The main discrepancies lie in the lack of oscillations. Indeed, the instantaneous (Markovian) approximation when evaluating the stochastic jumps in STDHF erases at once all coherence and memory effects. Similar features are seen in semi-classical VUU models where the collision term is also treated in Markovian approximation. The oscillating entropy for the exact solution shows that the STBM still carries a substantial amount of memory effects which can only be coped with using a frequency (or time) dependent kernel for the jump probability [104]. The TDHF result (light green line) differs dramatically from STDHF. It maintains zero entropy throughout and never relaxes to anything like a thermalized state. It cannot reproduce at all the long-time behavior of system as soon as dissipation becomes relevant.

It is also interesting to note that the maximum value of entropy $S/N = 2\log 2 \simeq 1.38$ corresponds to an equidistribution of $N = 10$ particles over all $2\Omega = 20$ states with occupation probability $w_\alpha = \rho_{\alpha\alpha} = 1/2$. To that extent, the agreement at the maximum is trivial. However, the STDHF results follow the exact curve also down to lower values and agree as long as the STDHF jumps have their grip. This is the non-trivial result indicating that STDHF catches the basic statistical properties of the system.

The lower panel of Fig. 4.3 shows the evolution of dipole momentum for the three solution schemes. This confirms what we had seen already from the two other observables. TDHF shows long standing oscillations and reverberations and thus stays far off the exact solution. STDHF, on the other hand, constitutes a remarkable improvement, in particular over the first 120 Δ^{-1} (see insert). STDHF is thus providing a reliable description of dissipation. A slight difference comes up at later times. The exact solution shows some reverberations which are absent in STDHF. These reverberations are related to the oscillations in entropy and thus an effect of quantum coherence deliberately suppressed in STDHF. But this is a small effect and the generally good agreement prevails.

This first example shows strengths and weaknesses of STDHF. It is a therefore a great improvement as compared to TDHF in that it properly catches the dissipative aspects of many-dynamics and produces in due time the correct asymptotic state (thermal equilibrium). However, STDHF implies a Markovian approximation (that is, instantaneous jumps) and is unable to incorporate memory effects. It then depends on the system and how important memory effects are in the dynamical regime. The example of fig. 4.3 also shows that S contains most of the information on the other observables: when the entropy increases, the dipole is damped and the difference between the entropies is highly correlated to the difference between the density matrices δ_ρ. Most of the time we confine the further examples to the entropy only.

4.3.2 Check of numerical parameters and conservation laws

So far we just asserted that the numerical parameters used are the suitable ones. Here we justify a little more on this. First we check that the choice of τ does not change drastically the results. Figure 4.4 confirms the stability of the results with respect to τ which is varied from 0.01 to 1 Δ^-1. The main issue was to fulfill the perturbative

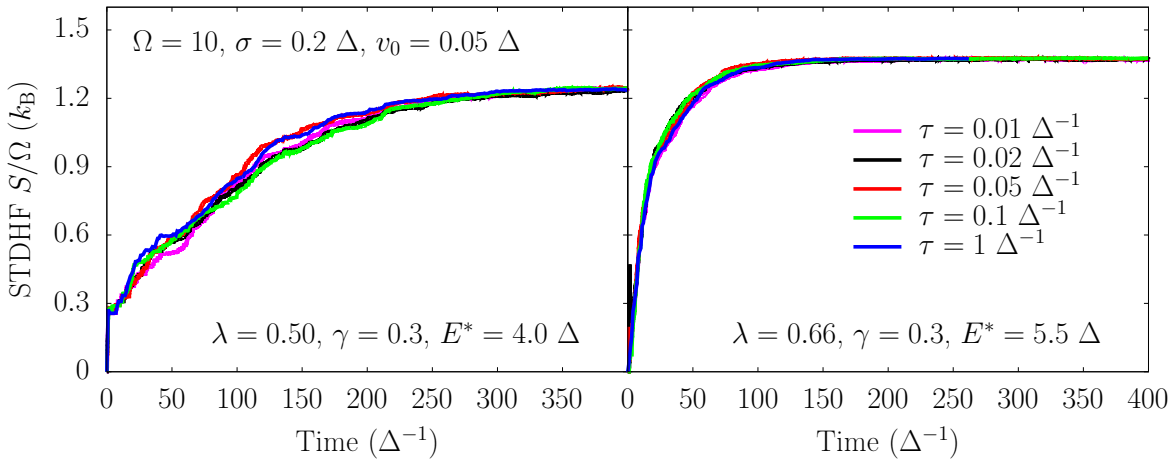

Figure 4.4: Effect of τ on the time evolution of the entropy per particle S/Ω for two different excitation energies $E^* = 4.0\Delta$ and 5.5Δ.

regime criterium

$$\mathcal{P}\tau = \sum_{\kappa_1,\kappa_2,\kappa_3,\kappa_4>0} \mathcal{P}_{\kappa_1\bar{\kappa}_2\bar{\kappa}_3\kappa_4} \quad \tau \leq 1 \tag{4.21}$$

first introduced in Eq. (2.73). It has been sometimes violated for large τ. In this case, the calculation just stops. This has been the case for $\tau = 1\ \Delta^{-1}$ for the presented excitation energy $E^* = 5.5\ \Delta$. As we are testing many cases and energies, we take the safe value of $\tau = 0.05\ \Delta^{-1}$ that almost ensures that we will never violate the perturbative condition (4.21).

As recalled in Eq. (4.19), the delta function that appears in the transition probability of STDHF possesses a finite width Γ because of the discrete spectrum and the finite collision time. A perfect continuous system and a perfect delta function would ensure an exact energy conservation in STDHF. In our case, we need a good compromise between a Γ which is small enough to have a reasonable energy conservation and as large as possible to get the maximum number of transitions for a wide range of excitation energies. Another problem arises: as the delta function is normalized by Γ there is a factor $1/\Gamma$ in the probability of transition and again the perturbative criterium (4.21) can be violated and the calculation can stop. In figure 4.5, we show the evolution of entropy and energy for various Γ, the other STBM parameters being the standard ones. We see that for Γ below $10^{-3}\Delta$, the entropy is not converged and the perturbative regime is not guaranteed. There is still a wide range of possible Γ to pick depending on whether one wants a better energy conservation or a more robust calculation that will work for many energies. A good compromise is achieved with $\Gamma = 2 \times 10^{-2}\Delta$. More generally, if one obtains too irregular a curve when using STDHF, the first thing to try is to enlarge Γ.

A last thing to check is the conservation of $\langle \hat{M} \rangle$ defined in Eq. (4.18). It is enforced by the Hamiltonians themselves in TDHF and exact propagation. In STDHF, it is expected to be *statistically* conserved if we have enough trajectories and the if initial transitions do not lead to diverging trajectories. In figure 4.6 we plot $\langle \hat{M} \rangle$ as a function of time for the three schemes: TDHF, exact and STDHF schemes. It confirms

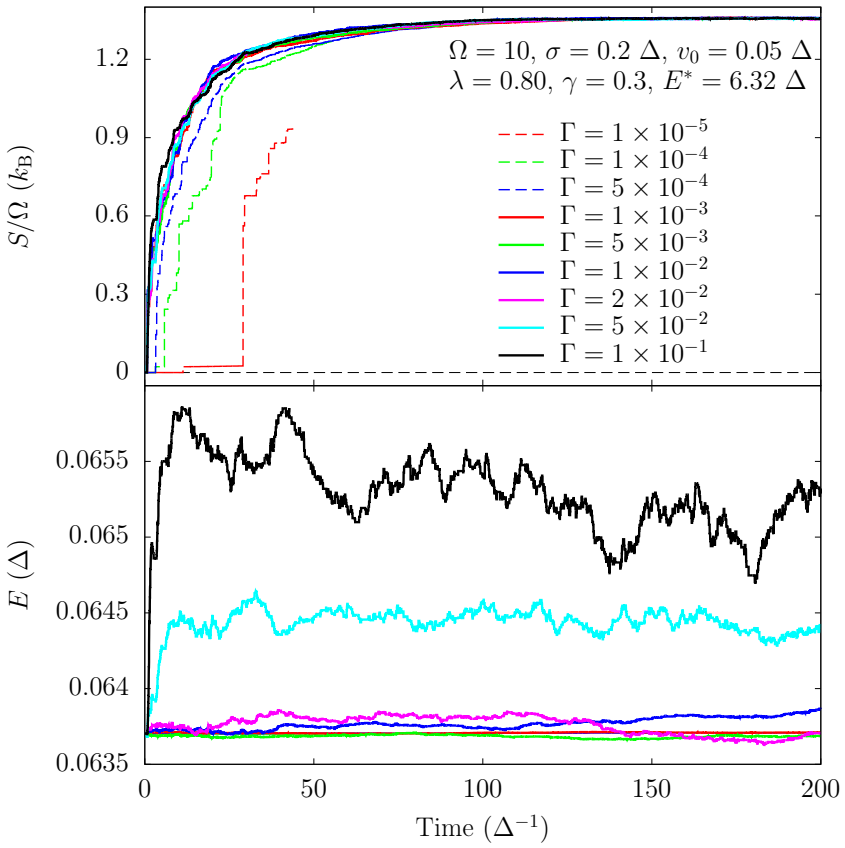

Figure 4.5: Time evolution of entropy per particle S/Ω and energy E for various widths Γ (in units of Δ) of the delta function that appear in Eq. (4.11).

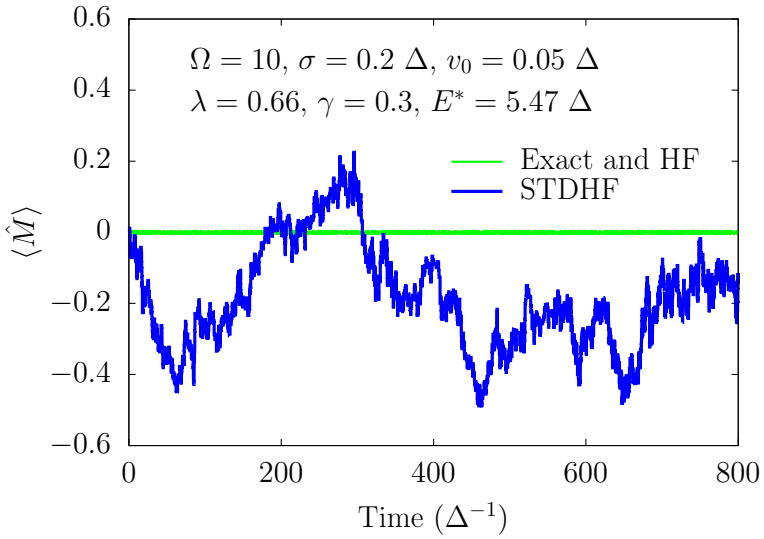

Figure 4.6: $\langle \hat{M} \rangle$ defined in Eq. (4.18) as a function of time for STDHF (thick curve), TDHF and exact (thin curve) solutions.

that TDHF and the exact solution indeed perfectly conserve $\langle \hat{M} \rangle$ and for STDHF, it fluctuates around 0 with an amplitude smaller than 0.5 in a system with $\Omega = 10$ i.e. m_α varies between $-9/5$ to $9/5$.

4.3.3 Varying the excitation energy

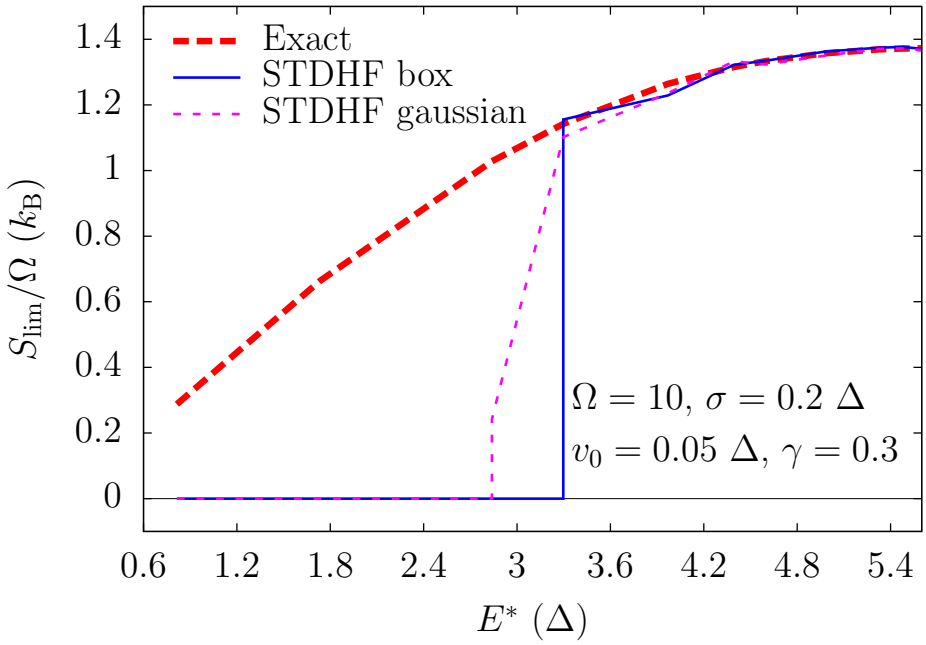

Figure 4.7: Asymptotic entropy per particle $S_{\rm lim}/\Omega$ for the exact solution (thick curves) and for STDHF (thin curves), as a function of the excitation energy E^* obtained by scan of initialization strength λ, see Eq. (4.15), and the other parameters of the model as indicated. For STDHF, two δ_Γ have been used: the box definition of Eq. 4.19 (thin full curve) or a Gaussian of width Γ (thin dashed curve).

Dissipation is usually weak in the regime of low excitations and acquires importance only for sufficiently large excitation energy [105]. Stochastic evaluation of dynamical correlations as done in STDHF is designed for high excitation energies where the phase space for jumps is (hopefully) dense enough. It is thus of interest to check the performance with varying excitation energy E^*. Figure 4.7 shows the asymptotic one-body entropy $S_{\rm lim} = \lim_{t\to\infty} S(t)$ as a function of E^* (in the branch of increasing excitation energy, see discussion of fig. 4.2). Here $S_{\rm lim}$ actually stands for value of $S(t)$ at $t = 800\ \Delta^{-1}$.

The exact solution shows a smooth and monotonous increase. STDHF behaves much different in that it shows a threshold behavior. It remains inactive for $E^* < 3.3\ \Delta$ and suddenly switches to reproduce the exact value once the stochastic jumps get their grip. The result confirms that STDHF is an approach for sufficiently high excitation energy. On the same graph we also show the results obtained when using a Gaussian of width Γ instead of the box function for the delta function. Apart from giving a smoother transition near the threshold it delivers the same limit of the entropy.

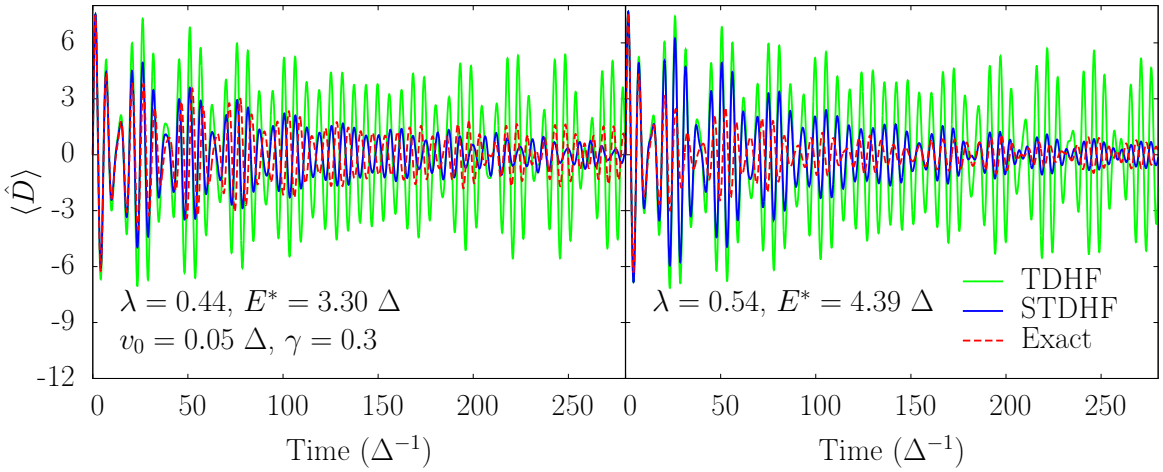

Figure 4.8: Dipole moments for TDHF, STDHF and exact calculations as a function of time for two excitation energies $E^* = 3.30\ \Delta$ and $E^* = 4.39\ \Delta$. The other STBM parameters are indicated and are the same as in figures 4.7 and 4.3.

It is also worth looking at dipole moments for other energies than $E^* = 5.47\ \Delta$ tested in figure 4.3. Figure 4.8 displays the dipole moments with respect to time for $E^* = 3.30\ \Delta$ and $E^* = 4.39\ \Delta$. Since the excitation energies are lower than that in Fig. 4.3, the damping is weaker here. Again STDHF gives a result much closer to the exact one than TDHF and the damping is qualitatively well reproduced.

The effect of the mixing parameter γ has not been discussed yet. It becomes clearer while looking at figure 4.9. This figure shows $S_{\rm lim}$ for exact and STDHF calculations as a function of E^* for various γ. We first observe that the exact limit of the entropy is almost independent from the mixing parameter γ and thus from the way we excite the system. Taking $\gamma = 0$ gives only one point (see blue square) where the asymptotic entropy for STDHF is non zero. Here we see the effect of γ on the range of entropy computable with STDHF scheme: it turns on the interaction between all the particles and brings more disorder to the system, thus allowing more transitions and increases the range of validity of STDHF. So $\gamma \neq 0$ is compulsory but its effect on $S_{\rm lim}$ for STDHF is not trivial nor predictible. For example, $\gamma = 0.2$ and $\gamma = 0.3$ seem to work better than $\gamma = 0.4$.

4.3.4 Impact of band width

We now explore the effect of band width σ. We have studied four values : $\sigma = 0.05$, 0.2, 0.5 and 0.8 Δ. The other model parameters are kept fixed at $\Omega = 10$, $\lambda = 0.8$ and $\gamma = 0.3$. Figure 4.10 compares the time evolution of the entropy between exact solution and STDHF. Decreasing σ reduces the oscillations of the exact entropy and yields generally faster relaxation to equilibrium, i.e. maximum entropy. This is expected because a smaller σ produces a larger density of states. This, in turn, enhances the probability of jumps and thus produces more dissipation. A larger σ spreads the spectrum instead and significantly reduces the phase space accessible to jumps. Only few states remain in communication and then, only few frequencies compete. As a

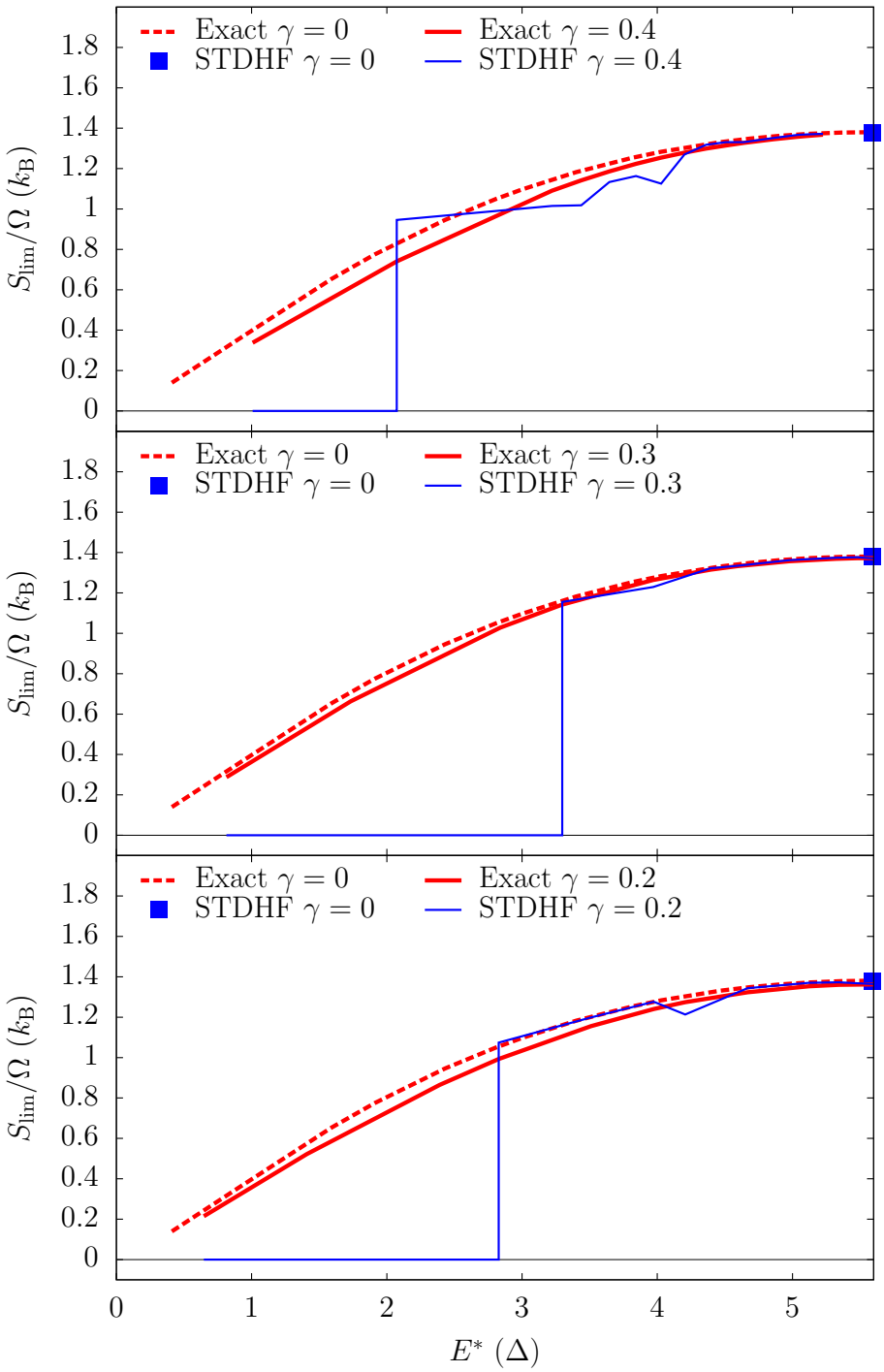

Figure 4.9: Asymptotic entropy per particle $S_{\rm lim}/\Omega$ for the exact solution (thick red curve) and STDHF (thin blue curve) for various values of the mixing parameter: $\gamma = 0$, 0.2 0.3 and 0.4. The unique STDHF point obtained with $\gamma = 0$ is the blue square plotted on the three panels.

consequence, more oscillations are observed before reaching equilibrium.

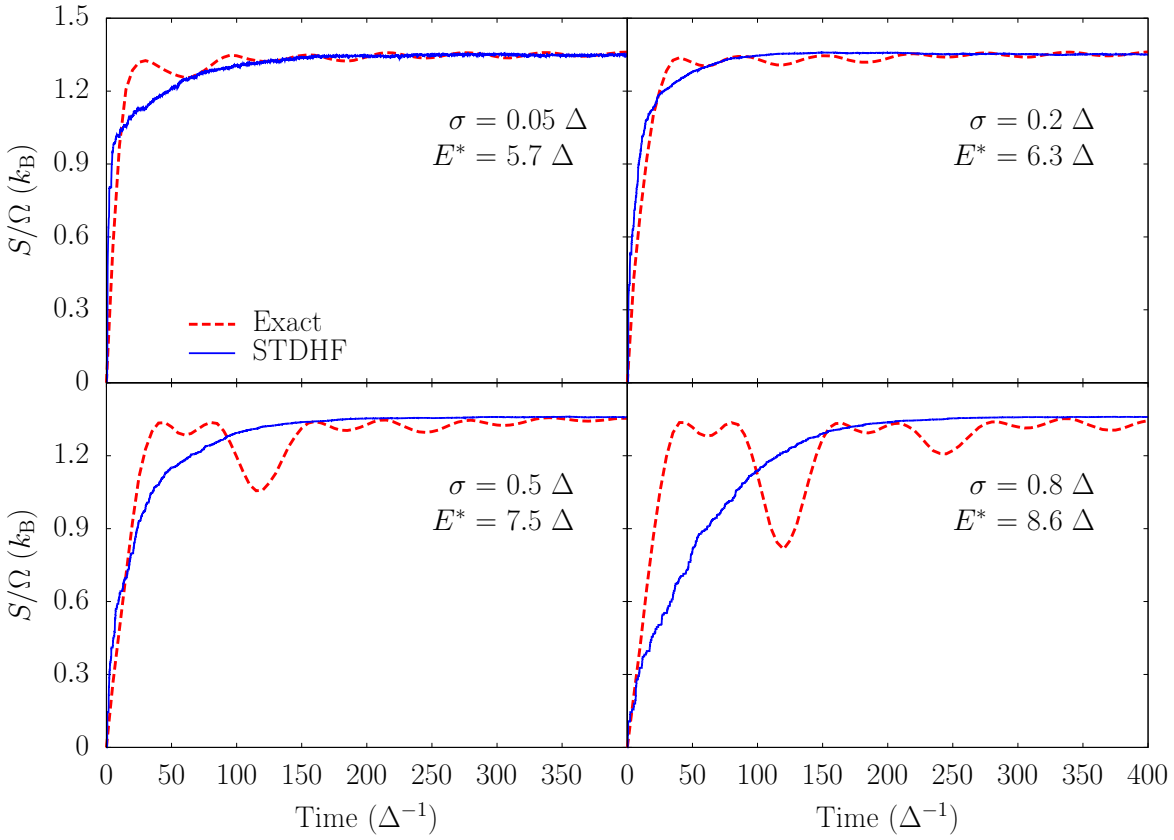

Figure 4.10: Entropy per particle S/Ω as a function of time as obtained from exact solution (dashed lines) and STDHF (full lines). The four panels show results for four different values of band width σ with a corresponding excitation energy E^* as indicated. The other parameters are : $\lambda = 0.8$, $\gamma = 0.3$, $\Omega = 10$ and $v_0 = 0.05\ \Delta$.

STDHF, as expected, is unable to follow the oscillations. But it nicely reproduces the trend to increasing relaxation times with increasing σ. Indeed, for the same reasons as before, increasing σ decreases the probability of $2p2h$ transitions and therefore, provides a slower relaxation time of the STDHF entropy as well. The average predictions are thus still reliable.

4.3.5 Varying the number of particles

Variation of σ as done in the previous section changes the density of states together with energy span for the jumps. We complement that by varying the particle number Ω. Here, we keep the ratio σ/Ω constant (at the value of 0.02). In such a way, the density of states is kept constant. Increasing Ω at constant σ would amount to increase the density of states (as one does when increasing σ at constant Ω). Since the corresponding results (not shown) are very similar to those presented below, we here focus on the impact of increasing the number of particles at constant density of states.

Figure 4.11 shows the time evolution of the entropy for the exact solution (left panel) and for STDHF (right panel). We start at $\Omega = 6$ because STDHF does not become

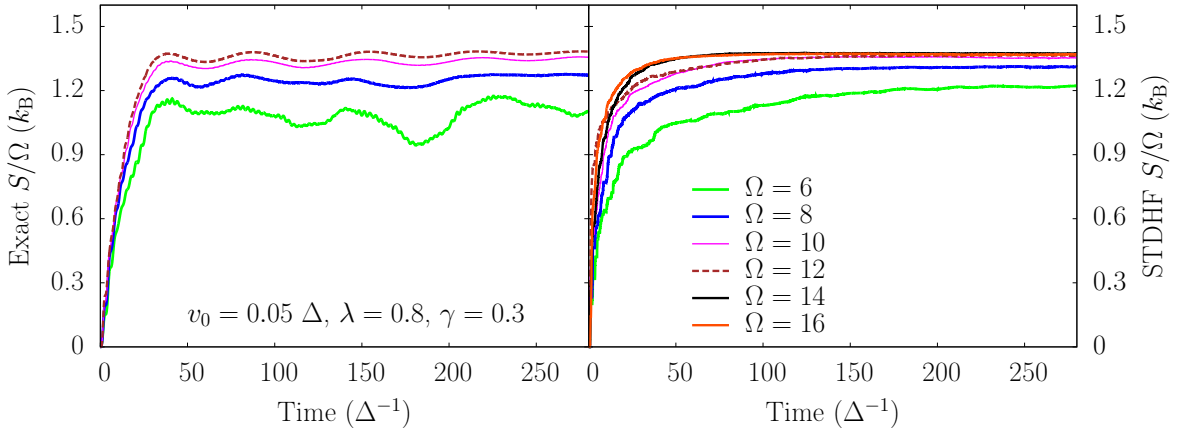

Figure 4.11: Time evolution of the entropy per particle S/Ω for exact solution (left) and STDHF (right) and for different numbers of particles Ω as indicated, while keeping the ratio $\sigma/\Omega = 0.02$. The other model parameters are indicated.

active for smaller Ω. At the upper end, we go up to $\Omega = 12$ for the exact calculation and checked two higher values of Ω for STDHF. The amplitude of oscillations of the exact entropy shrinks with increasing Ω. Because we kept constant the ratio σ/Ω this cannot be related to an increasing density of states but rather to an increasing number of different s.p. energies. Indeed more s.p. energies lead to more disorder, more transitions and a more incoherent behavior of the system. The diagonal assumption of Eq. (2.71) is then more justified. We also see a faster relaxation when increasing Ω, again related to the higher number of possible coupled states. This trend to decreasing relaxation time with increasing Ω is also reproduced by STDHF. We therefore expect that the larger the Ω, the better the agreement between the exact and the STDHF dynamics. We also observe a convergence of the STDHF results at $\Omega \geq 14$.

There is a further interesting feature. The entropy indicates two phases of relaxation. It starts with a fast relaxation at early times and bends over to a different rate at around 20–30 Δ^{-1}. This property is probably also present in the exact solution although masked by the oscillations.

To complement Fig. 4.11, Fig. 4.12 shows the time evolution of δ_ρ, which compares the STDHF and the exact 1-body density matrix in the same conditions as in Fig. 4.11. It confirms that the 1-body density matrix is better reproduced when increasing Ω. At first sight, it seems to stop improving at $\Omega = 10$ but if we compare with figure 4.11 we also see the STDHF entropy for $\Omega = 10$ and $\Omega = 12$ overlap almost perfectly. Therefore we expect δ_ρ to continue to decrease when Ω increases.

4.4 Conclusion

This first study confirms that STDHF is a good scheme to introduce dynamical correlations in a finite quantum system, which allows a direct comparison with the exact solution. Despite the simplicity of the model it has not been possible to go beyond

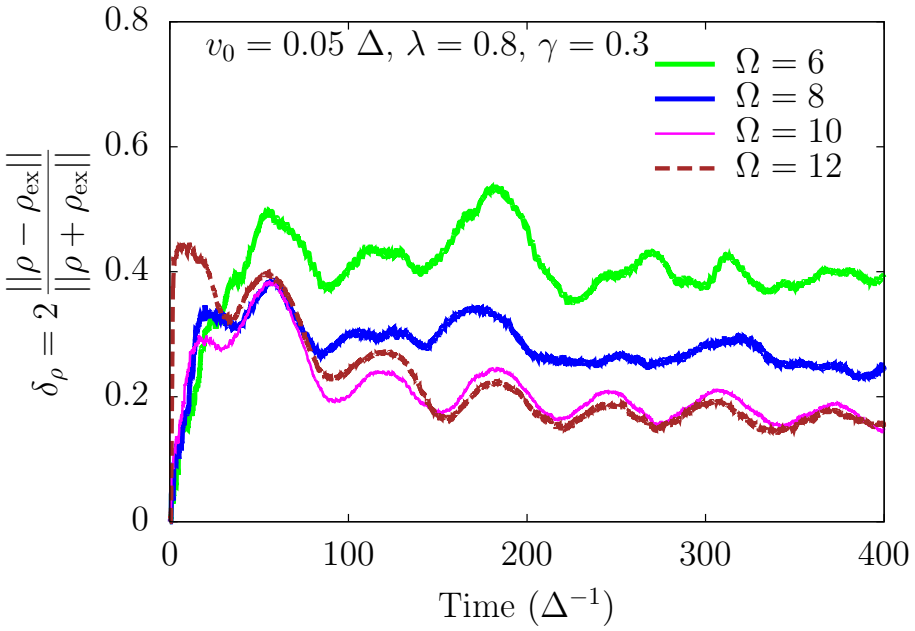

Figure 4.12: Time evolution of δ_ρ, the 1-body density matrix difference where $\rho = \rho_{\rm STDHF}$ and for different numbers of particles Ω as indicated, while keeping the ratio $\sigma/\Omega = 0.02$.

12 particles for the exact calculation. Thus it forced us to stay in a regime where memory effects are still important and the Markovian approximation is questionable. Even in this case STDHF provides results that are undoubtedly better than a mere Hartree-Fock and shows promising trends when approaching the situation it is designed to describe: a large system with a quick loss of coherence. Besides, it shed light on how to tune the numerical parameters for next calculations. This model could serve in the future to test schemes accounting for memory effects and its extension to non half-filled systems could provide more information on the time evolution of the 1-body entropy.

Chapter 5

Comparison between CTDHF, STDHF and ETDHF

Contents

5.1 Introduction

In the previous chapter we have seen that STDHF reproduces qualitatively well the dissipative effects and their consequences on the 1-body density matrix. However, STDHF suffers from many limitations. For example, this theory needs too large a number of trajectories to allow reasonable statistics at low energies when the probability of transitions is too small to be correctly sampled. The STDHF algorithm is also

numerically heavy and does not enable calculations in realistic 3D systems. We have developed Collisional TDHF to tackle these issues. The goal of this chapter is to establish whether it is possible to retrieve the results of STDHF even with the common mean-field assumption of CTDHF. We thus compare CTDHF with STDHF in a 1D system where the calculations are tractable. Since STDHF is expected to perform less well for low energies, ETDHF has also been used as a reference in this regime. As a side study it is then possible to examine the limits of ETDHF for high energies.

A first short publication has been submitted recently[1] and a longer one is currently in preparation. In this chapter we first present the studied model, then the results obtained when varying the physical parameters are discussed. Once the validity of our scheme is established we finally focus on numerical details and stability issues.

5.2 System under study

5.2.1 1D model

For the following calculations we consider a 1D model which Hamiltonian reads

$$h(x,t) = -\frac{\Delta}{2m} + u_{\text{ext}}(x) + \lambda\Big(\varrho(x,t)\Big)^{\sigma} \tag{5.1}$$

where u_{ext} is a Wood-Saxon potential:

$$u_{\text{ext}}(x) = \frac{u_0}{1 + e^{\frac{(x-x_0)}{a}}} \quad . \tag{5.2}$$

This potential is used as a jellium representing the ionic background. The last term of Eq. (5.1) plays the role of a density functional of the simplest form. The chosen values of the parameters are $u_0 = -5$ Ry, $x_0 = 15$ a$_0$, $a = 2$ a$_0$ for what we call in the following "potential 1". The parameters of the self-consistent term will always be $\lambda = 5$ Ry a$_0^2$ and $\sigma = 2$. The system is composed of $N = 9$ spinless physical particles. Figure 5.1 shows the potential and the ground state density for this set of parameters. More realistic calculation in a 3D model could be run in CTDHF or ETDHF. However comparing CTDHF and ETDHF to STDHF is our main purpose here and because of the high computational cost of STDHF, we are then forced to use 1D model.

Starting from the ground state of the mean field Hamiltonian, we apply a instantaneous $1p1h$ excitation at time $t = 0^+$ (see Fig. 5.2). This excitation is done by switching the occupation numbers $0 \leftrightarrow 1$. Other $npnh$ excitations will be explored in Sec. 5.3.5.

5.2.2 Collision term

A collision or residual potential has to be defined to perform the various calculations. The ansatz we used is here $v_{\text{res}}(x - x') = v(x - x') = v_0\delta(x - x')$ as in the electron attachment case (see Sec. 3.2.2). However, this potential appears to be strictly zero

[1] L. Lacombe, P.-G. Reinhard, P. M. Dinh, E. Suraud, "A collisional extension of time-dependent Hartree-Fock", submitted to J. Phys. B (2016).

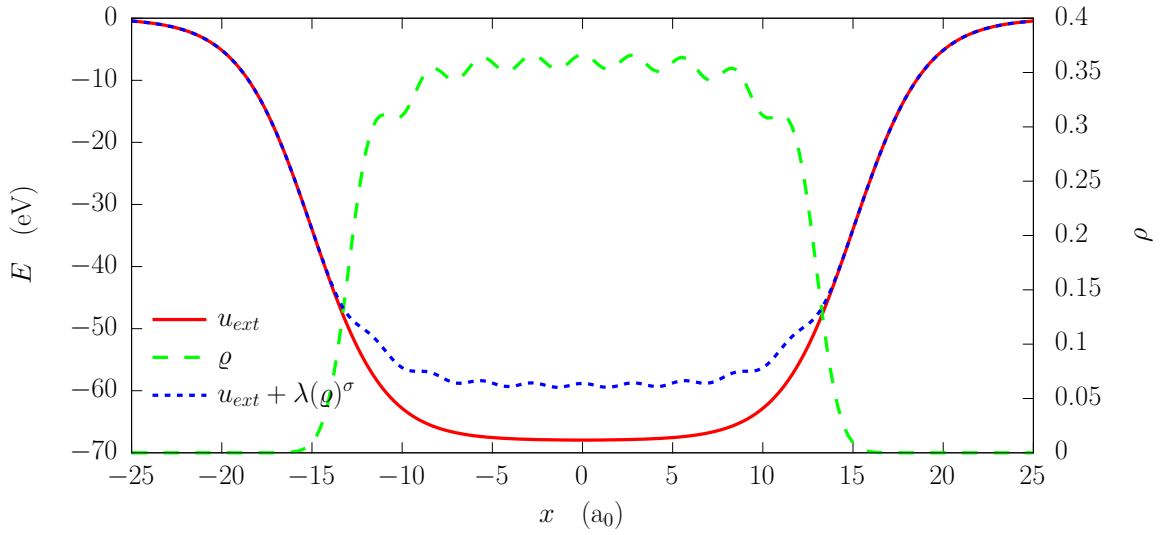

Figure 5.1: External potential coined "1" (red and left vertical scale), ground state density (green dashes and right vertical scale) and full potential (blue dots) plotted against x in the 1D model.

on spinless particles because of the antisymmetrization: there is no possibility for two spinless fermions to be at the same position x. Considering implicit spin in the collision term is one way to circumvent this issue. Technically this is done by assuming $\langle jk|\tilde{v}|lm\rangle = \langle jk|v|lm\rangle \neq 0$ in Eq. (2.51) which is equivalent to cancel the possibility of exchange. Computing this matrix element then simply yields

$$\langle jk|v|lm\rangle = v_0 \int dx \varphi_j(x)\varphi_k(x)\varphi_l^*(x)\varphi_m^*(x) \quad . \tag{5.3}$$

In our calculations, we use $v_0 = 1.345$ Ry $= 18.29$ eV.

5.2.3 Numerical parameters and error bars

Our schemes contain many numerical parameters that should not change significantly the physical results of our calculations as long as we stay in the right range of values. In Fig. 5.5, 5.6 and 5.15 the variations due to numerical parameters are represented by shaded areas of the same color as the corresponding curve. These numerical error bars shall not be misinterpreted: no physical behaviour such as quantum uncertainties are represented this way. Indeed physical variations are represented by standard error bars like for example in figure 5.2. Generally the shaded areas are created by taking the lowest value and the highest value of an observable while exploring different sets of parameters (see Chapter refchap:theory for the definition of the various parameters). We have tested for STDHF:

- the number of trajectories $\mathcal{N} = 100$, 200 and 300,
- the time interval between two jumps $\tau = 0.5$, 1, 2 fs;

for CTDHF:

- $\tau = 0.1$, 0.2, 0.5 and 1 Ry^{-1},
- $\Gamma_{\mathcal{E}} = 1.4$, 4.1, 8.2 and 12.2 Ry;

and for ETDHF

- $\tau = 0.1$, 0.2, 0.5 and 1 Ry^{-1},
- $\Gamma = 0.68$, 1.4, 2.7 Ry.

We also changed the number of single particle (s.p.) wave functions N_{wfs}. Except when the number of wave functions is too restricted (for example $N_{\mathrm{wfs}} = 18$) and the majority of $2p2h$ transitions become inaccessible, there is no noticeable change in the results. Γ is supposed to be of the order of half the energy difference between two s.p. energy levels or lower. We have found that the numerical error bars are always very small for ETDHF, dominated by $\Gamma_{\mathcal{E}}$ for CTDHF, and by $\mathcal{N}$ in STDHF.

5.2.4 Numerical details

The size of the numerical box is 50 a_0 with a grid of 256 points. The time-propagation of the system is done using the time splitting algorithm involving a Fast Fourier Transform (FFT). Reflecting boundary conditions are used and ensured by a harmonic potential at the limit of the box. This potential is fitted such as its maximum value is not higher than $k_{\mathrm{max}}^2/2$, i.e. the maximum energy accessible in the limit of the FFT. This is done to avoid spurious effects when reflecting a wave function.

5.3 Physical results

5.3.1 First exploration

During a time evolution after some initial excitation, one expects correlations to lead the system to a thermalized state for the reduced 1-body density matrix. A thermalized state for an infinite systems of fermions follows a Fermi-Dirac distribution:

$$f(\varepsilon) = \frac{1}{(1 + e^{(\varepsilon - \varepsilon_{\mathrm{F}})/\mathrm{T}})} \quad . \tag{5.4}$$

In figure 5.2 we compare the limit of the occupation numbers of the density matrix with respect to the s.p. energies at 120 fs in ETDHF (top), STDHF (middle) and CTDHF (bottom). The initial $1p1h$ excitation at $t = 0$ fs is represented by the gray shaded areas. We display here two initial excitations, one providing an excitation energy $E^* = 18.1$ eV (left column) and another providing $E^* = 29.8$ eV (right column).

The different methods lead to the expected Fermi-Dirac distribution up to quantum fluctuations. The fit of the final occupation number distribution with a Fermi-Dirac distribution delivers the values of ε_{F} and T indicated on the figure. Because of the sampling involved in the scheme, CTDHF explores a bigger phase space and generally yields comparable or higher temperature than the two other schemes.

Let us comment on the quantum fluctuations mentioned above. As $[h(t), \rho(t)]$ is non-zero we face a choice: either we diagonalize the mean field Hamiltonian and the

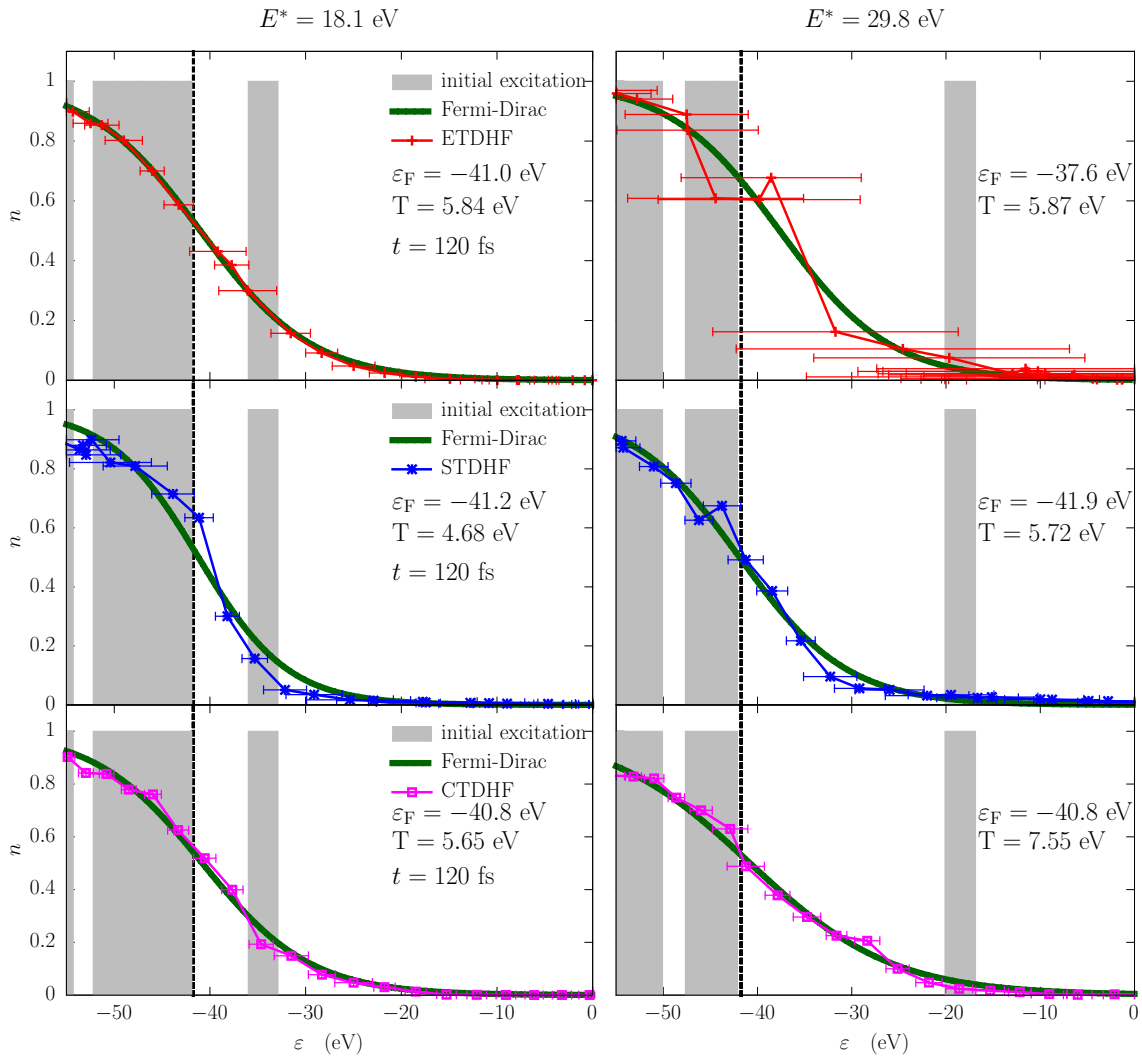

Figure 5.2: Comparison between ETDHF, STDHF and CTDHF for the occupation number distribution at the end of the calculation ($t = 120$ fs).

occupation numbers exhibit an error bar, or we diagonalize the density matrix and $\Delta h \neq 0$. We opted for the second solution and thus placed the error bars on the s.p. energies ε_i. Both error bars of CTDHF and STDHF schemes seem to have a stable width while increasing excitation energies. On the contrary, the error bars of ETDHF expand significantly if one considers high energy excitations. It is not an unexpected behavior as we supposed in our derivation of ETDHF that the mean field Hamiltonian and the density matrix to have the same eigenbasis. This approximation is reasonable when dealing with low energies or if the initial excitation is close to a real excited state of the mean field, which is not *a priori* predictible. Henceforth, the error bars here give us an insight of what we can call "low energies" and at which point the approximation of having the same eigenbasis for h and ρ in ETDHF fails.

Before going further, some details have to be discussed concerning the occupation numbers in STDHF. The STDHF state is composed of many individual trajectories of pure density matrices. There are two ways to define the mean field Hamiltonian from those trajectories: the Hamiltonian can be defined on the mean $\rho = \overline{\rho^{(\alpha)}}$, i.e. $\bar{h} = h[\overline{\rho^{(\alpha)}}]$ or computed on each $\rho^{(\alpha)}$ and averaged afterwards $\bar{h} = \overline{h[\rho^{(\alpha)}]}$. In CTDHF, we only have access to the mean ρ. Thus to be consistent in our definition of $\bar{h}$ we used the first option.

Note also that in all cases presented in this chapter, the CTDHF calculation is twice as long as a simple mean field propagation while a STDHF calculation is more than a hundred times the mean field one. Therefore, whereas Fig. 5.2 provides a first signature that CTDHF is able to allow the system to reach thermalization, numerically speaking CTDHF is much more superior than STDHF. ETDHF provides almost the same calculation time than a pure mean-field propagation but is not always reliable to obtain a thermalized state at the limit.

5.3.2 Stability of a Fermi-Dirac distribution of occupation numbers

As the CTDHF scheme accepts as an input partial occupation numbers, we can test the time evolution of a state initially described by a Fermi-Dirac distribution. The initial occupation numbers follow the rule of Eq. (5.4) with $\varepsilon_{\mathrm{F}} = 41.07727$ eV, T = 4.896 eV. As demonstrated in Fig. 5.3 which displays snapshots of the occupation numbers at different times, the CTDHF and ETDHF calculations conserve fairly well the Fermi-Dirac distribution: it is indeed a fixed point of collision integral $K[\rho]$ defined in Eq. (2.51). There are some numerical fluctuations around this equilibrium. The quantum fluctuations stay equal to zero in the case of ETDHF, and acceptably small in CTDHF.

5.3.3 Short time evolution of occupation numbers

Let us come back to a $1p1h$ initial excitation. To have more insight of the dynamics after this kind of excitation, we also look at a few snapshots of the occupation numbers in CTDHF and STDHF at different times, see Fig. 5.4.

We observe the excitation progressively decaying and the holes disappearing to lead to a smoother distribution of partial occupation numbers. Both schemes have the same

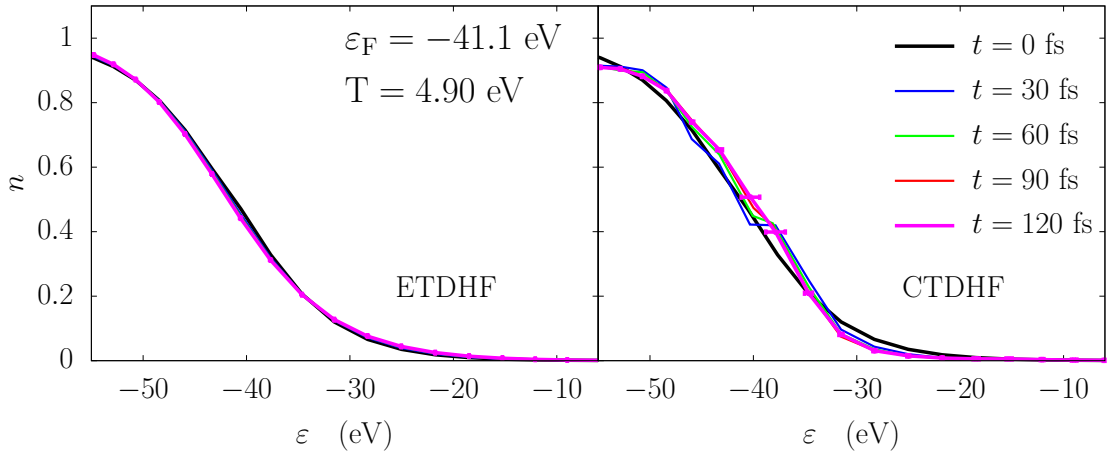

Figure 5.3: Time evolution of occupation numbers starting from a thermal state in ETDHF (left), and CTDHF (right). Quantum error bars are displayed in both cases at final time $t = 120$ fs but are not visible in ETDHF calculation.

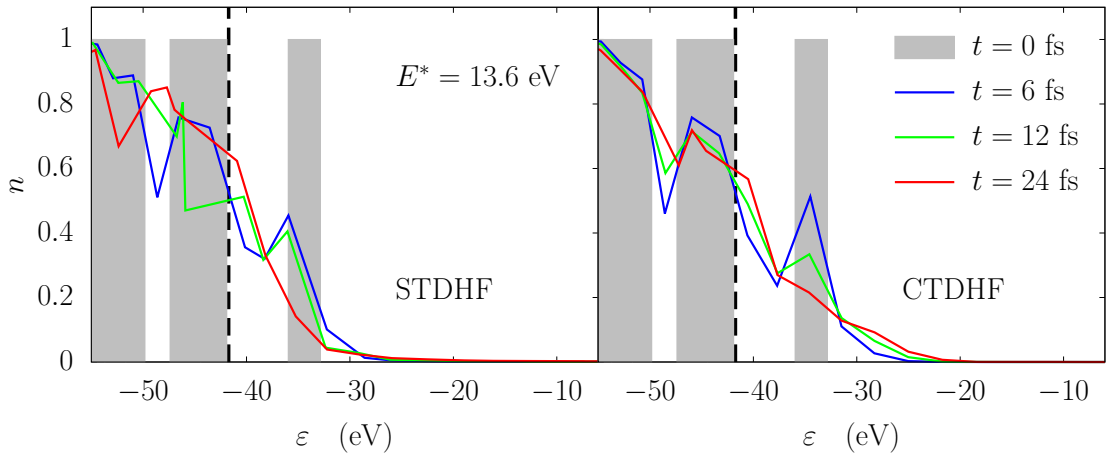

Figure 5.4: Short time evolution of the occupation numbers in STDHF (left) and CTDHF (right), after an initial $1p1h$ excitation delivering an excitation energy $E^* = 13.6$ eV. For the sake of clarity, no error bar is displayed.

kind of evolution although STDHF seems to be a little more erratic. The relaxation to a "thermal" state also seems to be very quick. To estimate more precisely the relaxation time and to describe in a more compact way the evolution of occupation numbers, we now turn to the fermionic entropy defined in Eq. (4.16).

5.3.4 Effect of the excitation energies

We now plot in figure 5.5 the time evolution of the entropy, calculated in STDHF, CTDHF and ETDHF for four excitation energies $E^* = 10.5$ eV, 18.1 eV, 20.7 eV and 29.8 eV, two of them being the same as in Fig. 5.2.

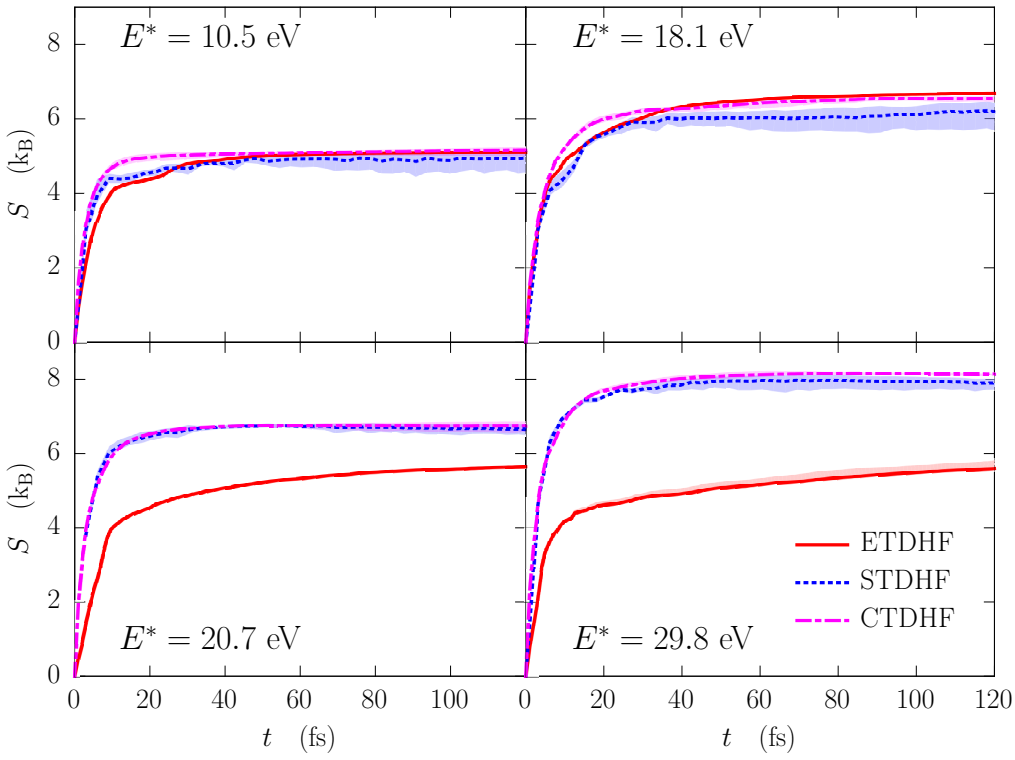

Figure 5.5: Time evolution of the ETDHF (full red curve), STDHF (short blue dashes) and CTDHF (long pink dashes) entropy for four excitation energies E^* as indicated after an initial $1p1h$ excitation.

For $E^* = 18.1$ eV the difference of temperature between STDHF and CTDHF deduced from Fig. 5.2 is visible on the entropy of STDHF which is lower than both CTDHF and ETDHF. For $E^* = 29.8$ eV we have already discussed that ETDHF was not appropriate and this is confirmed by the entropy of ETDHF which stays lower than the other two. We can easily guess the behavior of the occupation numbers for the other two energies. Obviously, a good agreement on occupation numbers corresponds to a good agreement on the entropy. The agreement of the density matrices themselves is not garanteed as seen in Sec. 4.3.1 though they are expected not to be far from each other. STDHF and CTDHF not only have the same limit, but the curves also overlap

almost perfectly. the ETDHF calculation produces the same results at low energy but differs a lot at high energy.

A more systematic study has been done and we plot the asymptotic quantity $S^2_{\rm lim}$ with respect to the excitation energy for the three different schemes in figure 5.6. In an

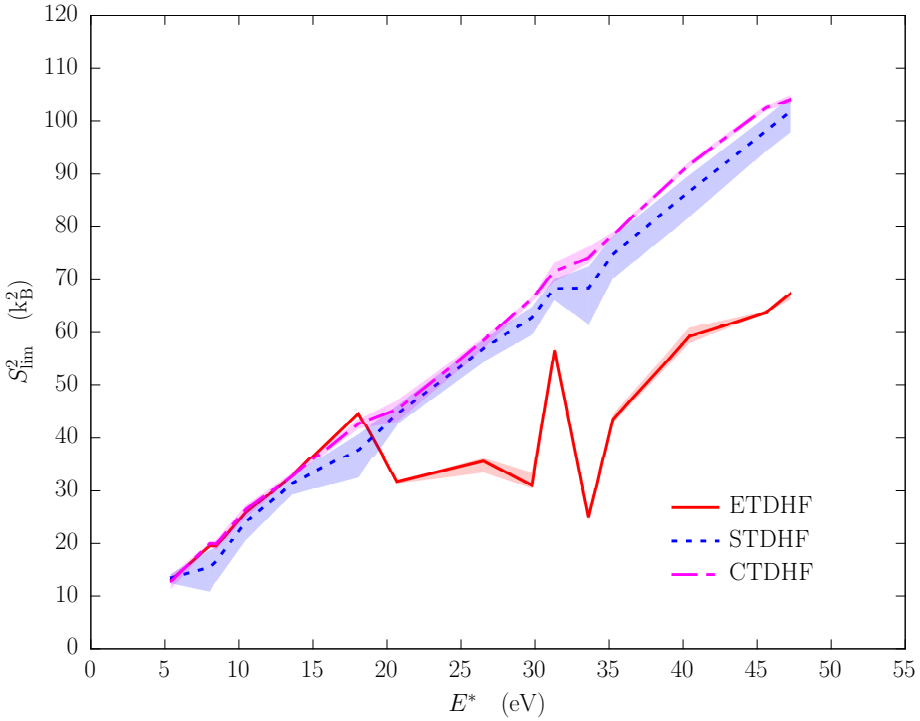

Figure 5.6: Asymptotic value of the square of entropy, $S^2_{\rm lim}$, plotted with respect to the excitation energy for ETDHF, STDHF and CTDHF.

infinite gas of fermions, the equilibrium value $S^2_{\rm equi} \approx S^2_{\rm lim}$ is proportional to excitation energy. In the model considered here, there is a priori no particular reason for this relation to still hold. However it seems to be the case at least for STDHF or CTDHF. Consistently with what has been observed before, for the potential used here, ETDHF fails at energies higher than ~ 18 eV and the equivalence between STDHF and CTDHF is confirmed.

For the sake of completeness, we have also tested two other potentials: one with a less dense spectrum than the first potential, the other one with a denser spectrum. The different spectra are presented in figure 5.7. We remind that "potential 1" stands for the potential of the previous calculations. The other two potentials have the following parameters:

	u_0	x_0	a	box size	$\Delta\varepsilon$	number of s.p. states
potential 1	-5 Ry	15 a_0	2 a_0	50 a_0	≈ 2 eV	23
potential 2	-4 Ry	25 a_0	10 a_0	80 a_0	≈ 1 eV	31
potential 3	-10 Ry	8 a_0	1 a_0	50 a_0	≈ 5 eV	17

Here $\Delta\varepsilon$ is the average energy difference between two successive states.

We look at $S^2_{\rm lim}$ versus E^* for potential 2 and 3 in Fig. 5.8. In the case of a dense spectrum (potential 2), all the numerical schemes agree on the same limit for

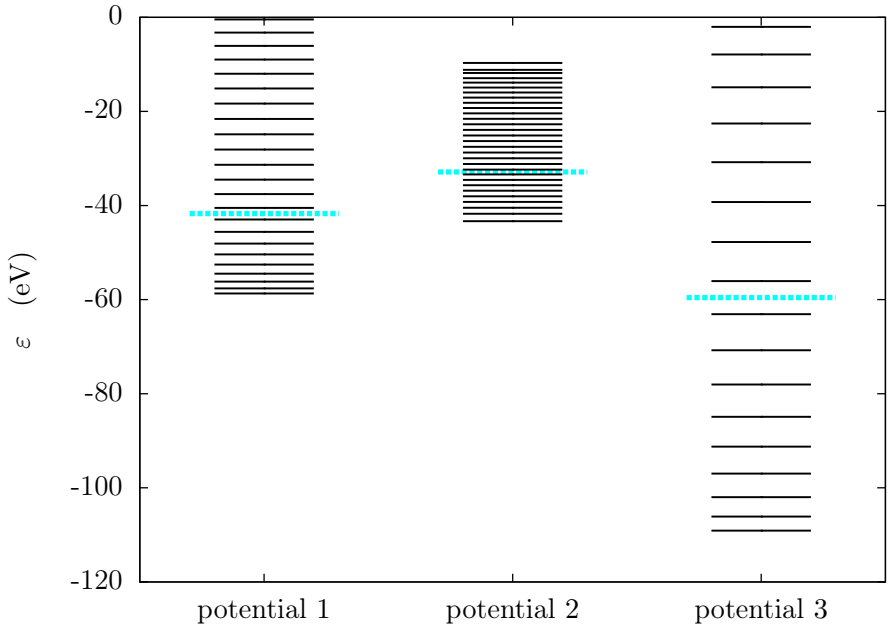

Figure 5.7: Single particle energy levels for the three tested potentials. The blue dotted lines represent the Fermi level of the system. In each case, it corresponds to 9 physical particles.

the entropy. Instead, the results obtained for potential 3 are more intriguing: at low excitation energy, CTDHF gives different results from both STDHF and CTDHF and at high excitation energy, the STDHF asymptotic entropy stays significantly lower than those computed with CTDHF and ETDHF. We have here two behaviors which need to be investigated to clarify which scheme we should trust in this case. To this end, we plot in Fig. 5.9 for the two energies marked by a dashed vertical lines in Fig. 5.8 the time evolution of the entropy for the three schemes, the probability of transition for a sample of four typical STDHF trajectories and the final occupation numbers for both ETDHF and CTDHF and the quantum error bars for ETDHF.

For the lowest energy, i.e. $E^* = 31.6$ eV, both STDHF and ETDHF entropies stop abruptly their increase. When looking at transition probabilities in the STDHF case, we observe that strictly no transition occurs after 10 fs. This illustrates a problem that can occur in STDHF and has already been encountered in Chapter 4: sometimes, the statistics collapses and the entropy cannot reach the expected asymptotic value. Concurrently, ETDHF also exhibits the signature of a failure of the scheme, characterized by the error bars and the irregular occupation numbers while CTDHF displays a relatively smooth distribution.

For the higher energy $E^* = 82.1$ eV, the behavior of the entropy is closer to what would be expected. STDHF and CTDHF agree during the short time evolution of the entropy but STDHF undergoes a spurious decrease after 40 fs. This, again, seems somehow related to the statistics of STHDF that can be compared to a case where STDHF and CTDHF have the same behavior. In Fig. 5.10, we also plot the time evolution of the entropy and the probability of transition for a few trajectories. We observe that, with a constant entropy, the trajectories continue to jump.

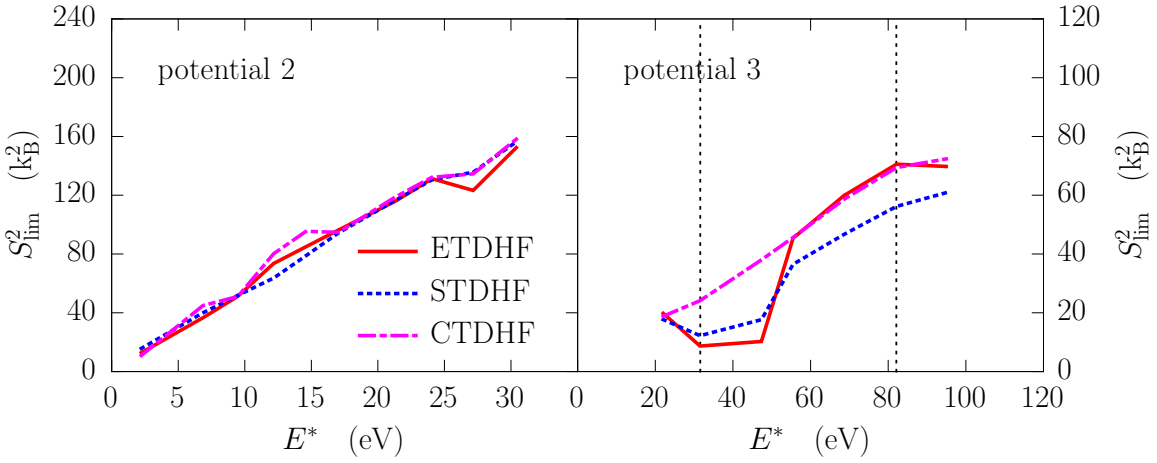

Figure 5.8: Same as Fig. 5.6 but for potential 2 and 3 as indicated. Vertical black dashed line point up the energies studied in Fig. 5.9.

If we now turn to ETDHF, we note that ETDHF entropy increases, as usual, a bit slower than the other two, but still reaches the same limit than CTDHF. The asymptotic occupation numbers exhibit a reassuring Fermi-Dirac shape while having moderate quantum fluctuations. The agreement between CTDHF and ETDHF in the asymptotic state is reproduced in the occupation numbers. All things considered, CTDHF seems to be the only scheme giving a robust and expected behavior in the third potential. Identifying exactly what can cause STDHF to decrease when the transitions stop is still in progress.

5.3.5 Effect of initial excitations

So far we only considered a $1p1h$ excitation. Here $2p2h$ and $3p3h$ initial excitations have been tested. In Fig. 5.11, we look at the occupation numbers at the end of the calculation for a $1p1h$ excitation (left) and a $2p2h$ excitation (right), each excitation delivering about the same $E^* \approx 29.5 - 29.8$ eV. The fit of the final distribution with a Fermi-Dirac distribution gives slightly different values i.e. $\varepsilon_{\rm F} = -40.6$ eV, T = 7.6 eV in a) and $\varepsilon_{\rm F} = -41.1$ eV, T = 8.6 eV in b). This difference can also be observed in the time evolution of the entropy in Fig. 5.12. Here we compare the entropy after a $1p1h$, $2p2h$ and $3p3h$ excitation, once again providing the same E^*. The $1p1h$ excitation, yielding a smaller temperature, also exhibits a smaller asymptotic entropy. The dependence of the type of the excitation is small and seems to be reduced with more complex excitations.

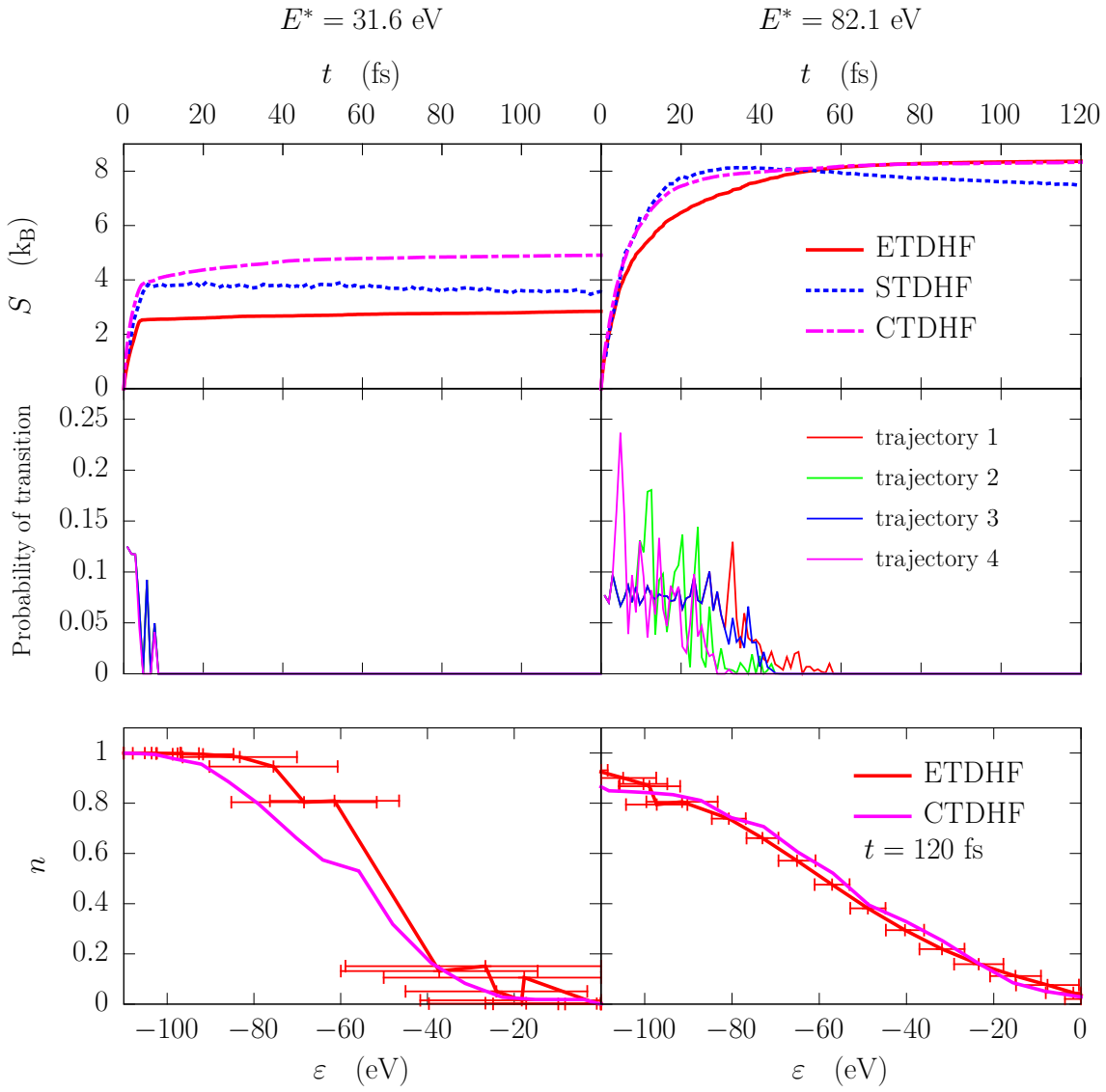

Figure 5.9: Entropy for STDHF, CTDHF and ETDHF (first row), probability to undergo a $2p2h$ transition in STDHF for four trajectories (second row), both plotted as functions of time, and occupation number distribution at final time $t = 120$ fs as a function of the s.p. energy for ETDHF and CTDHF, with quantum error bars on ETDHF (third row). Each column corresponds to an excitation energy in potential 3 (see Fig. 5.8): $E^* = 31.6$ eV (left column), $E^* = 82.1$ eV (right column).

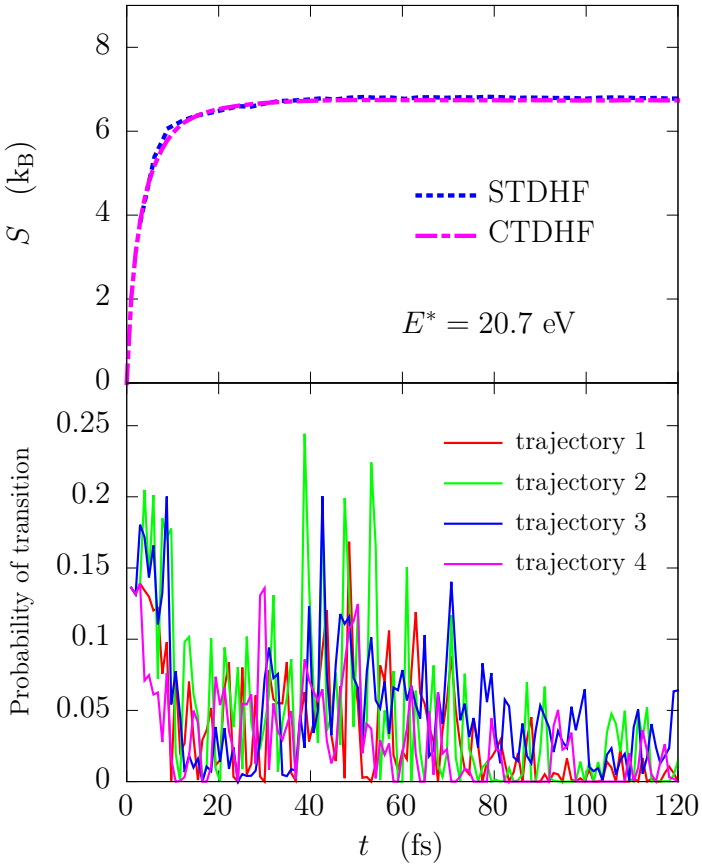

Figure 5.10: Entropy for STDHF and CTDHF (first row) in potential 1 and transition probability in STDHF for four trajectories (second row), all plotted as functions of time.

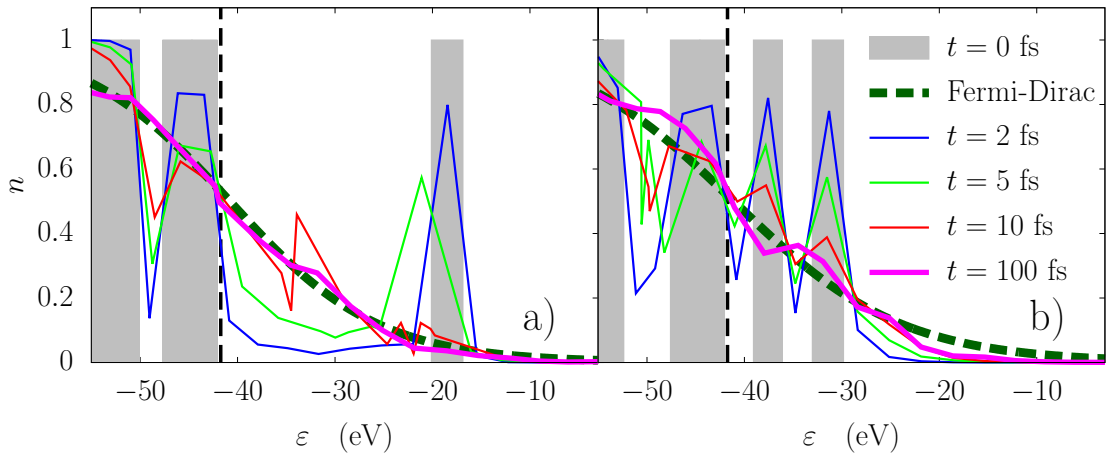

Figure 5.11: Snapshots of the occupation numbers after excitations with about the same energy in the CTDHF scheme at different times as indicated: a) $1p1h$ excitation, $E^* = 29.8$ eV, b) $2p2h$ excitation, $E^* = 29.5$ eV.

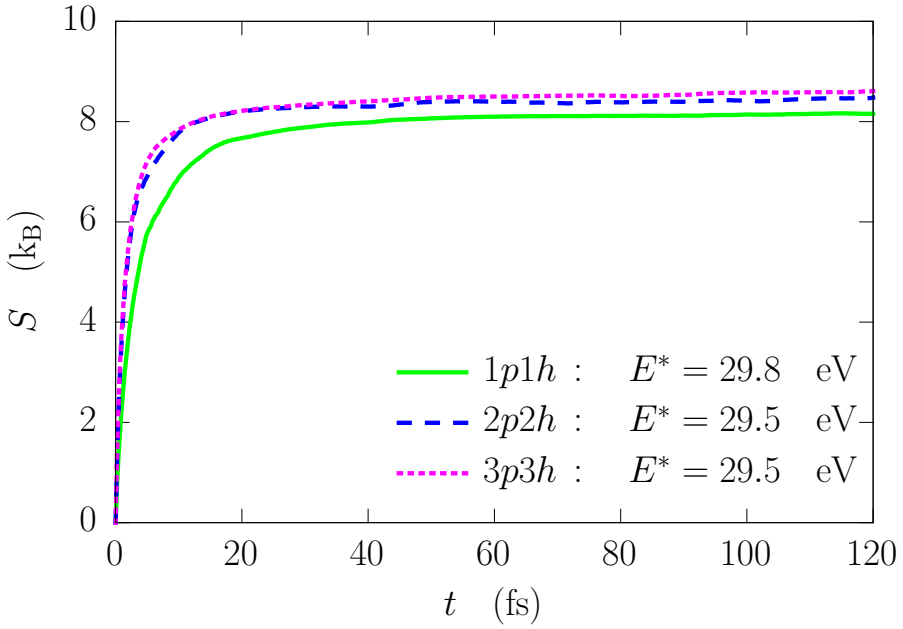

Figure 5.12: Time evolution of the entropy in CTDHF scheme for *npnh* initial excitations delivering about the same excitation energy E^*.

5.4 Numerical discussions

5.4.1 Effect of $\rho_{\rm rem}$

In the previous section, we have demonstrated the performance of CTDHF, either at low and high E^*. We now address in more details numerical technicalities to allow such performances. For example one can check how $\rho_{\rm rem}$ defined in Eq. (7.106) is a crucial ingredient in the implementation of CTDHF. To this end, we define an error the following way:

$$\text{Error} = \text{Tr}\{|\rho_{\rm rem}|\} = \sum_\nu \left| w_\nu - \sum_\alpha n_\nu^{(\alpha)} x^{(\alpha)} \right| \tag{5.5}$$

which is almost a χ^2 as defined in Eq. (2.105) except that we choose the absolute value instead of the square. The absolute value of the matrix $|\rho_{\rm rem}|$ here is a short-hand notation for the absolute value of eigenvalues. This incidentally gives an idea on the amount of particles created during the approximate sampling. In order to preserve artificially the number of particles without $\rho_{\rm rem}$, we renormalize by hand the density matrices after the CTDHF step:

$$\rho = \rho_{\rm non-ren} \left(\frac{\text{Tr}\{\tilde\rho\}}{\text{Tr}\{\rho_{\rm non-ren}\}} \right) \tag{5.6}$$

where $\rho_{\rm non-ren}$ is the density matrix before renormalization and $\tilde\rho$ is the density matrix before the sampling step consistently with notations in Sec. 2.7.4.

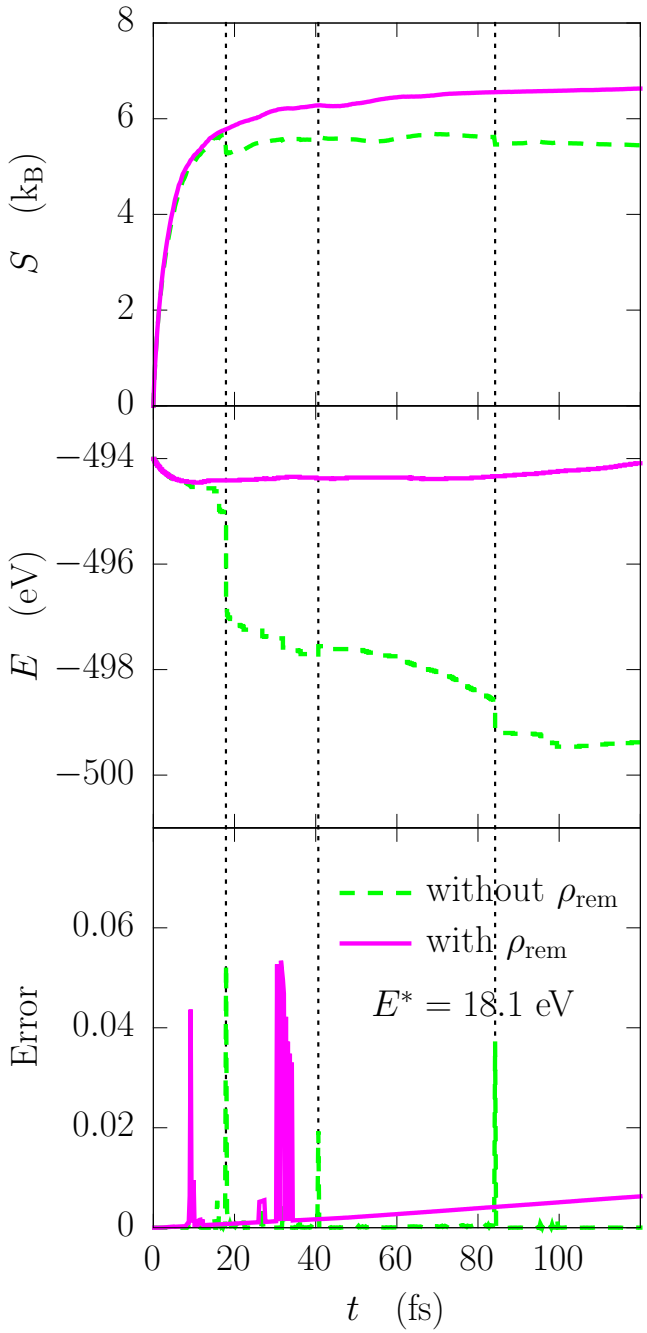

Figure 5.13: Time evolution of the entropy (top), the total energy E (middle), and the error defined in Eq. (5.5), (bottom), calculated in CTDHF with (solid magenta curve) or without (green dashes) ρ_{rem} after an initial $1p1h$ excitation delivering $E^* = 18.1$ eV.

In Fig. 5.13, we show the entropy S, the total energy E and the error on the density matrix after the sampling step described in sec. 2.7.4. Without $\rho_{\rm rem}$, the time evolution of S and E exhibit discontinuities when the sampling is not able to reproduce well the initial density matrix (see vertical dotted lines). The peaks in the error on the density matrix correspond exactly to these discontinuities. Even if the error in the sampled density appears only in a few time steps, they can cause dramatic effects in the energy conservation. With $\rho_{\rm rem}$ instead, the piece which is not sampled is kept, just stored at this time step and added to the density matrix once the dissipative step finished. The continuity of the density matrix and of the various observables are thus ensured, leading to a much more robust scheme. Therefore, in all results discussed previously, the inclusion of $\rho_{\rm rem}$ is performed.

5.4.2 Effect of Γ_ε

We have observed that the entropy and the energy of the system show a slight drift at longer times thus giving a hint on the violation of the energy conservation. This drift is all the more large if E^* is high. This can be actually related to the s.p. energies filter, see Eq. (2.117). The width Γ_ε of the delta function on the *single particle* energies, if too restrictive, hinders transitions that would be accepted if looking at the total mean-field energy and could equilibrate the time evolution numerically speaking.

In figure 5.14 we show the time evolution of the total energy and the entropy for three different Γ_ε, that is 2.72, 5.44 and 10.8 eV after $1p1h$ excitation delivering $E^* = 33.6$ eV while keeping Γ, that is the width of the delta function on the mean-field *total* energy, constant. The effect of the width Γ_ε is clear: when more transitions are

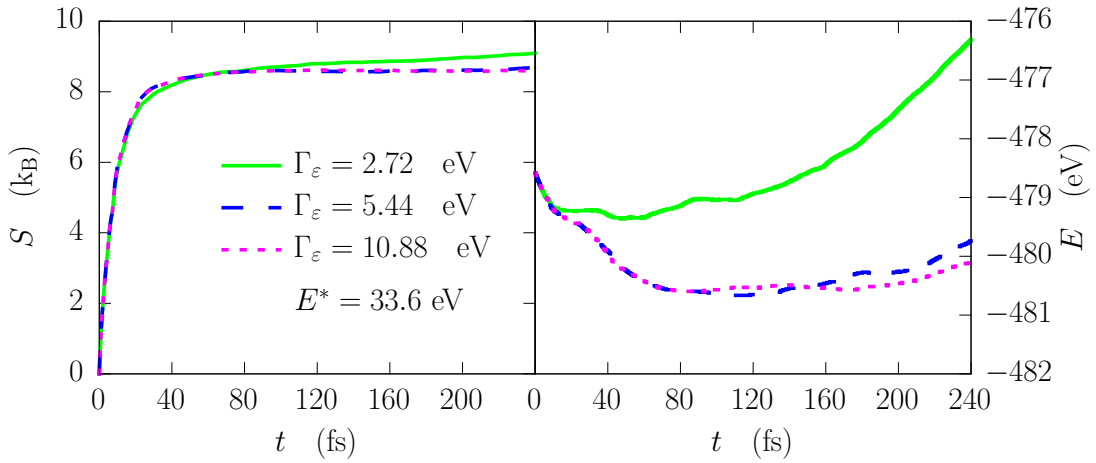

Figure 5.14: Effect of width Γ_ε of the delta function on single particle energies (see Eq. (2.117)) on the time evolution of the entropy and the total energy in CTDHF after an initial $1p1h$ excitation delivering $E^* = 33.6$ eV.

added, the entropy stabilizes and so does the energy. In the best case, the energy is conserved up to 2.4 eV. But in these calculations, we have $\Gamma \approx 1.4$ eV and $\Gamma_\varepsilon \approx 8$ eV so an energy violation of this order of magnitude is not alarming.

5.4.3 Diagonal CTDHF scheme

The CTDHF scheme also offers the possibility to conserve the same basis for each element of the sampling. The density matrix stays diagonal during the dissipative step and we are acting only on these diagonal elements (see Sec. 2.7.4). This diagonal CTDHF is supposed to be closer to ETDHF than "standard" CTDHF. Figure 5.15 compares ETDHF, STDHF, CTDHF and diagonal CTDHF after a $1p1h$ excitation, one giving $E^* = 18.1$ eV (right) and another one giving $E^* = 45.6$ eV (left). It

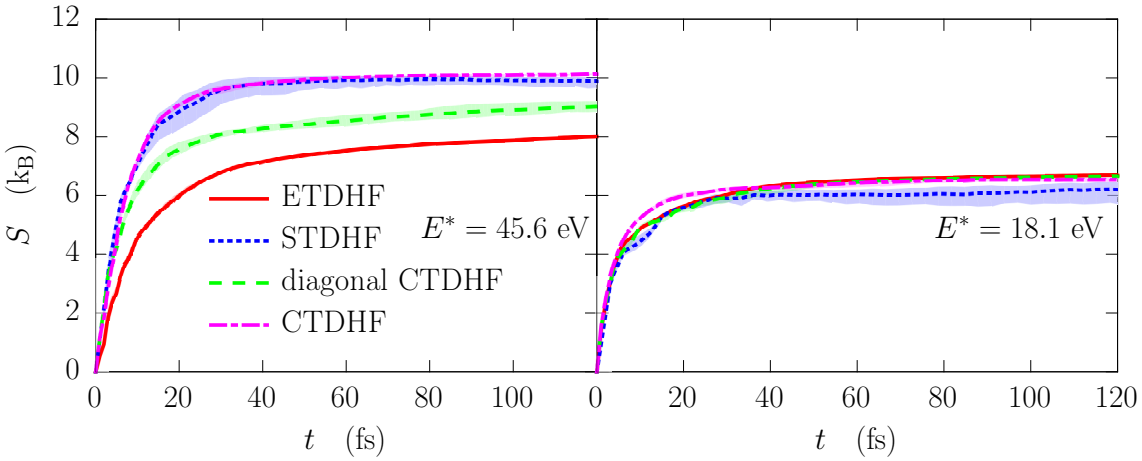

Figure 5.15: Time evolution of the entropy for ETDHF, STDHF, diagonal CTDHF, CTDHF for two initial excitation energies E^* as indicated.

confirms our expectations: At low E^*, all schemes agree with each other. However, at higher E^*, we observe the hierarchy $S_{\text{ETDHF}} < S_{\text{diagonal CTDHF}} < S_{\text{STDHF}} \lesssim S_{\text{CTDHF}}$. This demonstrates the importance of the off-diagonal terms in the CTDHF scheme which indeed contribute more at high energy.

5.5 Conclusion

We have presented a broad study on CTDHF through various observables as the time evolution of the occupation numbers and the entropy. The CTDHF scheme does enable an efficient inclusion of dissipative effects on top of a mean field propagation. This study has to be completed. For instance, one can test what happens if we act on the self-consistent term of Eq. (5.1) by changing its strength or its sign: an attractive self-interaction with no external potential would give a model closer to the nucleus case instead of a molecular one. The intriguing decrease of STDHF has to be studied more in detail even if it has already been related to a problem in the statistics: does the lack of transitions be related to the number of empty states ? In a calculation where STDHF entropy is stable, if we set amplitude of transitions to zero "by hand" would it begin to decrease ? Does this still holds the self-consistent term is set to zero ? Work to address these questions is currently in progress and cannot be at that stage presented in this manuscript.

Apart these open questions, we have also confirmed that CTDHF produces results that are very similar to STDHF but for a much lower numerical cost. This allows a future study in realistic 3D systems where hundreds of STDHF trajectories are not on option. Indeed CTDHF is of the order magnitude of a mere mean field or ETDHF propagation while STDHF is at least a hundred times longer. Because it is basically defined on a mixed density matrix, there is no formal reason to restrict ourselves to a closed system. This encouraging feature allows us to consider ionization scenarios in 3D realistic systems. This is a crucial step in irradiation dynamics where dissipation is known to play a key role for long time emission. However defining correctly our scheme in open systems with absorbing boundaries raises other issues that have not been solved yet. We will discuss in more details these issues in Sec. 6.2.

Chapter 6

Conclusion and perpectives

6.1 Summary

In this thesis, we have presented and studied various quantal approaches for the exploration of dynamical processes in multielectronic systems. The aim of these approaches was to include dynamical effects beyond mean-field by taking into account the 2-body correlation due to electron-electron collisions. This correlation has been added in Markovian approximation on top of Hartree-Fock approach or in the DFT framework. The thermalization of the system is one of the major effect we tried to reproduce.

After an introductory chapter, we have presented in Chapter 2 the formalism of the various schemes and how they allow to include part of the 2-body correlation on top of a mean field theory. Connections between electronic and nuclear systems are strong in that respect. The starting point was Stochastic Time-Dependent Hartree Fock (STDHF). The derivation of Extended TDHF (ETDHF) has also been provided. From STDHF, we have derived a new scheme, namely Collisional TDHF (CTDHF). The latter scheme constitutes in some sense the main achievement of this thesis. The numerical realizations and the limitations of each scheme have also been discussed in detail.

In Chapters 3, 4 and 5, we have applied the approaches discussed in Chapter 2 but in various systems. In Chapter 3, we have first explored a rare reaction channel, that is the probability of an electron to attach on a molecule. Small water clusters have been studied. These calculations are motivated by the understanding of irradiation mechanisms in biological systems as this kind of process is one of those expected to cause DNA strand breaks. To that end, a collision potential has been introduced in a TDDFT calculation in a pertubative manner. We have showed that the probability of attachment exhibits peaks that are consistent with experimental measurements, even with a crude approximation made on the potential of interaction.

In Chapter 4, a schematic model has been derived from the Lipkin-Meshkov-Glick model, which has been widely studied in nuclear physics to describe phase transitions in nuclei. This model has been used here as the benchmark of STDHF as it allows to numerically compute the exact solution. A thorough comparison between STDHF and the exact solution with a small number of physical particles has been performed, by playing with the physical and the numerical parameters entering the model. The

time evolution of 1-body observables agrees well in both schemes, especially what concerns thermal behavior. However coherent oscillations, present in the exact solution, cannot be by nature reproduced by STDHF which treats 2-particle-2-hole jumps in an incoherent way. The overall agreement is nevertheless very satisfactory and thus provides a sound basis for STDHF applied in larger (and consequently less coherent) systems. However, to allow a good description of the dynamics, one is bound to use a large statistics, which can constitute a hindrance of the use of STDHF in larger systems.

To overcome this problem, in Chapter 5, we have tested CTDHF developed in Chapter 2 in a one-dimensional system (and without electronic emission). This system consisted in electrons in a jellium potential with a simplified self-consistent interaction expressed as a functional of the density. The advantage of this 1D model is that STDHF calculations are numerically manageable and therefore allows a direct comparison with CTDHF calculations. The collisional interaction potential used in this case was similar to that introduced in Chapter 3. An initial excitation was produced by a 1-particle-1-hole transition. Playing with this transition has allowed us to explore a large range of excitation energy. In all cases, the system relaxed to a thermalized state described by the famous Fermi-Dirac distribution from which we could extract a temperature. In this proof of concept study, CTDHF compares remarkably well with STDHF.

6.2 Perspectives

Our three approaches have successfully included thermalization in model systems. We however remind that one aim is to provide an efficient description of dissipation in realistic 3D systems to reproduce, for example, PES and PAD in the multiphoton regime, where numerous experimental data already exist, as already mentioned in Chapter 1. To do so, we need to apply our methods in"open" systems, i.e. systems with absorbing boundaries. In this context, STDHF is not only numerically too demanding in 3D calculations but it is also basically not applicable in open systems. Indeed, absorbing boundaries can been seen in a equivalent way by the inclusion of a complex potential. Due to this potential, the time propagator loses its unitary nature. Therefore, during a propagation with absorbing boundaries, the norm and the orthogonality of the single particle wave functions are not conserved. One solution is to work with the so-called natural orbitals which provide an orthonormal set of wave functions but with non-integer occupation number. We have checked that the natural orbitals performs surprisingly very well in highly excited open systems[1]. However, trajectories and transitions in STDHF are only defined if one works with an ensemble pure states, i.e. Slater determinants. Applying STDHF as such in the case of an open system would therefore lead to spurious features like creation of matter.

On the contrary, ETDHF and CTDHF basically work with non-integer occupation numbers. Thus nothing formally prevents them from being applied in such a situation. The transposition of ETDHF in this case is actually straightforward. In CTDHF there are formal issues that still have to be solved. These issues are mostly related to

[1]M. Vincendon, L. Lacombe, P. M. Dinh, P-.G. Reinhard, E. Suraud, "Time-dependent DFT in natural orbitals", in preparation.

the sampling of the mixed density matrix. One has to take into account the energy absorbed at the boundaries concurrently with electronic density. To be consistent with the incoherent approach, one has to expand the pure density matrix as an incoherent sum of pure density matrices. Each of them have lost from 0 to N electrons that went "out" of the numerical box (i.e. had been absorbed by the boundaries). It has the constraint that the sum of the density matrices with their weight should provide the right (non-integer) number of electrons lost at the boundaries. Defining well such a set of density matrices is still under study. Once a well founded solution is found, if any, we can tackle open 3D systems, with or without dissipation. Indeed, if we dispose of an efficient and well founded scheme for the sampling of non-integer occupation numbers, this will allow us to reinterprete and revisit the fact that electronic emission in time-dependent density functional theory is not quantized.

As final words, we give here some formal and deeper questions which remain open and constitute real theoretical challenges. For instance, how to derive formally a good approximation for the collision potential in TDDFT ? How to include memory effects and fluctuations that have been neglected in our scheme and how to deal with memory effects in case of an open system ? Comparing our stochastic and quantal approaches with semiclassical calculations would certainly shed some light in that respect.

Chapter 7

French summary

Contents

7.1 Introduction

Cette thèse présente différentes approches quantiques pour l'exploration de processus dynamiques dans des systèmes multiélectroniques, en particulier après une forte excitation qui peut aboutir à des effets dissipatifs. Les théories de champ moyen sont un outil utile à cet égard. En effet, dans une telle approche, les cloupages individuels sont remplacés par un couplage effectif avec un champ commun (ledit "champ moyen"). Cela permet de calculer l'évolution dynamique d'un système quantique avec un faible coût numérique. Ces théories ont été améliorées dans les dernières décennies avec le développement de la Density Functional Theory (DFT). Comme nous nous intéressons principalement au phénomène non linéaire dépendant du temps, le cadre de cette thèse est sa version dynamique, à savoir Time-Dependent DFT (TDDFT). On peut formellement montrer qu'il existe un champ moyen effectif qui reproduit l'évolution exacte de la densité électronique du système. Aussi, tout observable électronique peut être exprimé comme une fonctionnelle de la densité. Cependant, les fonctionnelles exactes restent inconnues et, dans la pratique, il faut procéder à des approximations.

Une bonne partie des travaux sur ces approximations a été consacrée, dans les deux dernières décennies, à les rendre de plus en plus précises. Néanmoins, ces théories peinent à reproduire complètement la dynamique et la corrélation à deux corps. Et la plupart des améliorations concerne la théorie de la réponse linéaire qui, en principe, n'est fiable que dans les systèmes soumis à une faible perturbation. D'autre part, pour les problèmes non linéaires, les fonctionnelles (quantiques) approximées donnent parfois des résultats qui peuvent s'avérer pires que ceux obtenus avec un calcul semi-classique (i.e. lorsque la dynamique à deux électrons est traitée classiquement).

La thermalisation est un des effets des collisions électron-électron. Les effets de thermalisation ont par exemple été observés dans des expériences sur des agrégats ou des molécules excités par un intense laser femtoseconde. En effet, l'énergie absorbée par l'agrégat peut être, après un moment, répartie entre tous les électrons du système, aboutissant au réchauffement de l'agrégat. La signature de l'émission thermique de l'électron a été observée de façon expérimentale dans les agrégats métalliques et dans le fullerène C_{60}. Ces dernières années, notre groupe a conduit une étude systématique des photoélectrons émis par le C_{60} et observé que les effets dissipatifs sont effectivement sous-estimés dans l'approche champ moyen, en particulier dans le régime multiphoton.

Nous présentons ici le formalisme des différentes méthodes étudiées dans cette thèse, dans la perspective de décrire un tel effet en incluant des termes collisionnels à la théorie du champ moyen. A cet égard, il existe une forte connexion entre les sytèmes électroniques et nucléaires. Nous commençons cette partie par la présentation de la DFT en général puis par la dérivation du champ moyen version Hartree-Fock (HF). En suivant, la dérivation de Extended TDHF (ETDHF) est également fournie. Stochastic Time-Dependent Hartree Fock (STDHF) est ensuite dérivée. A partir de STDHF, nous déduisons une nouvelle méthode, appelée Collisional TDHF (CTDHF). Cette dernière représente d'une certaine façon le résultat principal de cette thèse. L'implémentation numérique de chacune de ces méthodes est aussi examinée en détail. Les acronymes sont écrits en anglais par souci de cohérence avec la littérature.

7.2 Théorie de la Fonctionnelle de la Densité et sa version Dépendante du temps

L'évolution temporelle d'un système est décrite par l'équation de Shrödinger dépendante du temps (TDSE). Pourtant, il est en général impossible de trouver une solution de cette équation pour des systèmes réalistes de plus de quelques particules. La théorie de la fonctionnelle de la densité (DFT) et sa version dépendante du temps (TDDFT) simplifient les calculs en faisant correspondre un système exact de fermions en interaction avec un système de particules fictives sans interactions percevant un potentiel effectif qui ne dépend que de $\varrho(\mathbf{r})$ (ou $\varrho(\mathbf{r},t)$ et la fonction d'onde à N corps à l'instant initial $|\Psi(t=0)\rangle$ pour ce qui est de la TDDFT). Cette transformation est exacte si la fonctionnelle de ϱ est connue [7] ce qui n'est pas le cas. Nous n'entrerons pas ici dans les détails de la dérivation de la DFT ou de la TDDFT qui peuvent être trouvés dans [26, 44, 45, 46, 7, 8] mais fournirons seulement les équations pratiques et une idée des différentes approximations.

Nous considérons d'abord le cas statique par souci de simplicité. Le système d'électrons sans interaction peut être traité directement avec ϱ ou dans le formalisme Kohn-Scham (KS). Dans cette méthode, un ensemble de N orbitales KS sans interaction φ_i remplace les N électrons en interaction avec la même densité électronique totale qui est calculée de la façon suivante :

$$\varrho(\mathbf{r}) = \sum_{i=1}^{N} \left|\varphi_i(\mathbf{r})\right|^2 \quad . \tag{7.1}$$

De cette densité, il est possible de calculer l'énergie en utilisant une fonctionnelle de la forme :

$$E_{\text{total,el}}[\varrho] = E_{\text{kin}}(\{\varphi_i\}' + E_{\text{H}}[\varrho] + E_{\text{xc}}[\varrho] + E_{\text{coupl}} + E_{\text{ext}} \ , \tag{7.2a}$$

$$E_{\text{kin}}\left(\{\varphi_i\}\right) = -\int \mathrm{d}^3\mathbf{r} \sum_{i=1}^{N} \varphi_i^*(\mathbf{r})\ \nabla^2\ \varphi_i(\mathbf{r}) \ , \tag{7.2b}$$

$$E_{\text{H}}[\varrho] = \frac{e^2}{2} \iint \mathrm{d}^3\mathbf{r}\ \mathrm{d}^3\mathbf{r}\,'\ \frac{\varrho(\mathbf{r})\varrho(\mathbf{r}\,')}{|\mathbf{r}-\mathbf{r}\,'|} = \frac{1}{2}\int \mathrm{d}^3\mathbf{r}\ \varrho(\mathbf{r})\ U_{\text{H}}[\varrho] \ , \tag{7.2c}$$

$$E_{\text{ions}} = \int \mathrm{d}^3\mathbf{r} \sum_{i=1}^{N} \varphi_i^*(\mathbf{r})\ \hat{V}_{\text{ions}}\ \varphi_i(\mathbf{r}) \ , \tag{7.2d}$$

$$E_{\text{ext}} = \int \mathrm{d}^3\mathbf{r}\ \varrho(\mathbf{r})\ U_{\text{ext}}(\mathbf{r}) \quad . \tag{7.2e}$$

Ici, les degrés de liberté de spin n'ont pas été écrits pour simplifier les notations. Nous décrivons plus en détail chacun des termes apparaissant dans (7.2a) :

- E_{kin} est l'énergie cinétique des particules sans interaction.
- $E_{\text{H}}[\varrho]$ est le terme de Hartree associé au potentiel de Hartree U_{H}. Ce terme représente la répulsion directe d'une densité de charge.
- E_{ion} est l'énergie venant du couplage avec les ions (noyaux + électrons de coeur) regroupé en un seul terme $\hat{V}_{\text{ion}}$. Une expression explicite de E_{ion} sera donnée dans les Chapitres 3 et 5.

- E_{ext} est le potentiel extérieur (par exemple le champ électrique).
- E_{xc} est le potentiel d'échange-corrélation de la DFT qui contient tout ce qui n'a pas été pris en compte dans les autres termes.

L'approximation locale de la densité (LDA) est une approximation simple est robuste. Elle suppose que le potentiel d'échange-corrélation peut être traité localement dans l'espace :

$$E_{\text{xc}}^{\text{LDA}} = \int e_{\text{xc}}[\varrho(\mathbf{r})]\varrho(\mathbf{r})d\mathbf{r} \quad . \tag{7.3}$$

La LDA souffre néanmoins d'un problème d'auto-interaction. Cela signifie que chaque électron interagit avec sa propre densité participant à la densité totale $\varrho(\mathbf{r})$. Cela aboutit à une queue de décroissance exponentielle du potentiel LDA pour un système chargé au lieu que celle-ci soit proportionnelle à $1/r$. Beaucoup de stratégies ont été inventées pour résoudre ce problème et fournir une correction de l'auto-interaction (SIC). Elles vont des méthodes les plus raffinées (par exemple la méthode 2setSIC [47]) aux plus simples (par exemple ADSIC [48]). Dans le Chapitre 3 nous parlons de ce problème plus en détail sur un exemple. Dans les dernières décennies, plusieurs fonctionnelles plus avancées que la LDA ont été proposées. Comme un gaz d'électron n'est pas uniforme (situation idéale pour la LDA), l'étape suivante a été d'introduire un gradient de la densité électronique dans la fonctionnelle, aboutissant à l'approximation du gradient généralisé (GGA). La fonctionnelle la plus utilisée à ce jour appartient à la classe des fonctionnelles hybrides et s'appelle B3LYP [49, 50]. Les fonctionnelles hybrides sont des combinaisons linéaires d'autres fonctionnelles et contiennent généralement un terme d'échange exact. Dans les travaux présentés ici, nous utilisons majoritairement la LDA à cause de son efficacité numérique et parfois ADSIC (voir Chapitre 3).

En ce qui concerne la DFT dépendante du temps, on peut aussi considérer la LDA locale en temps, que l'on nomme LDA adiabatique (ALDA) et remplacer $\varrho(\mathbf{r})$ par $\varrho(\mathbf{r}, t)$. Dans la suite nous utilisons aussi la notation standard de LDA pour la ALDA.

Une fois obtenue la fonctionnelle de l'énergie, la dérivée fonctionnelle de l'énergie totale par rapport aux fonctions d'onde à une particule nous donne les équations KS :

$$\hat{h}_{\text{KS}}[\varrho]\ |\varphi_i\rangle = \varepsilon_i\ |\varphi_i\rangle\ , \tag{7.4a}$$

$$\hat{h}_{\text{KS}}[\varrho] = -\frac{\nabla^2}{2m} + U_{\text{KS}}[\varrho] + \hat{V}_{\text{ions}} + U_{\text{ext}}\ , \tag{7.4b}$$

$$U_{\text{KS}}[\varrho] = U_{\text{H}}[\varrho] + U_{\text{xc}}[\varrho] \quad . \tag{7.4c}$$

Le potentiel Kohn-Sham local et dépendant de la densité U_{KS} est consitué d'un terme coulombique direct U_{H} et du potentiel d'échange-corrélation, $U_{\text{xc}} = \delta E_{\text{xc}}/\delta\varrho$. Le couplage aux ions et champs externes est trivial. Le problème statique est un problème auto-cohérent vu que le potentiel dépend de $\varrho(\mathbf{r})$.

L'équation KS dépendante du temps s'écrit de même :

$$\mathrm{i}\ \partial_t\varphi_i(\mathbf{r}, t) = \hat{h}_{\text{KS}}[\varrho]\,\varphi_i(\mathbf{r}, t)\ , \tag{7.5}$$

où $\hat{h}_{\text{KS}}$ est généré de la même façon qu'au-dessus à condition de remplacer $\varrho(\mathbf{r})$ par $\varrho(\mathbf{r}, t)$[1]. Cela suppose que la densité électronique s'ajuste instantanément, bien que les effets de mémoire puissent avoir des effets non-négligeables, spécialement dans E_{xc} [53].

[1]Dans cette thèse nous utilisons les unités atomiques $e^2/2 = \hbar = 1$.

7.3 Hartree Fock et terme de collision

Plus simple que la DFT, la célèbre approximation HF fournit une première approximation du hamiltonien exact. Nous dérivons ici le hamiltonien HF pour introduire les notations et la notion d'interaction résiduelle. Nous considérons un hamiltonien non-relativiste pour une système d'électrons en interactions. Ce hamiltonien s'écrit en seconde quantification de la manière suivante :

$$\hat{H} = \int dx\, h^0(x,t)\hat{\Psi}^\dagger(x,t)\hat{\Psi}(x,t) + \frac{1}{2}\int dx dx'\, v(x,x')\hat{\Psi}^\dagger(x,t)\hat{\Psi}^\dagger(x',t)\hat{\Psi}(x',t)\hat{\Psi}(x,t)$$
$$h^0(x,t) = -\Delta_x/2 + u_{\text{ext}}(x,t) \quad . \tag{7.6}$$

Nous utilisons ici la coordonnée généralisée x et des particules sans spin pour simplifier les notations mais ces calculs peuvent être facilement généralisés au cas avec spin. Ce hamiltonien peut s'écrire dans n'importe quelle base de fonctions d'onde à une particule, donnant la forme générale suivante :

$$\hat{H} = \underbrace{\sum_{i,j} h^0_{ij}\hat{a}^\dagger_i\hat{a}_j}_{\hat{h}^0} + \underbrace{\frac{1}{2}\sum_{i,j,k,l} v_{ijkl}\hat{a}^\dagger_i\hat{a}^+_j\hat{a}_l\hat{a}_k}_{\hat{V}} = \sum_{i,j} h^0_{ij}\hat{a}^\dagger_i\hat{a}_j + \frac{1}{4}\sum_{i,j,k,l}\tilde{v}_{ijkl}\hat{a}^\dagger_i\hat{a}^\dagger_j\hat{a}_l\hat{a}_k \tag{7.7}$$

où $\tilde{v}_{ijkl}$ est l'interaction antisymétrisée :

$$\tilde{v}_{ijkl} = v_{ijkl} - v_{ijlk} \quad . \tag{7.8}$$

7.3.1 HF : factorisation

Il y a une façon d'obtenir le hamiltonien HF qui consiste à factoriser directement le terme d'interaction $\hat{V}$:

$$\hat{V} = \frac{1}{2}\sum_{i,j,k,l} v_{ijkl}\hat{a}^\dagger_i\hat{a}^\dagger_j\hat{a}_l\hat{a}_k \quad . \tag{7.9}$$

Le théorème de Wick par rapport à la mer de Fermi permet de réécrire le produit quatre opérateurs de la façon suivante

$$\begin{aligned}\hat{a}^\dagger_i\hat{a}^\dagger_j\hat{a}_l\hat{a}_k =& \langle\hat{a}^\dagger_i\hat{a}_k\rangle\langle\hat{a}^\dagger_j\hat{a}_l\rangle - \langle\hat{a}^\dagger_i\hat{a}_l\rangle\langle\hat{a}^\dagger_j\hat{a}_k\rangle \\ &- \langle\hat{a}^\dagger_i\hat{a}_l\rangle :\hat{a}^\dagger_j\hat{a}_k: \\ &+ \langle\hat{a}^\dagger_i\hat{a}_k\rangle :\hat{a}^\dagger_j\hat{a}_l: \\ &+ \langle\hat{a}^\dagger_j\hat{a}_l\rangle :\hat{a}^\dagger_i\hat{a}_k: \\ &- \langle\hat{a}^\dagger_j\hat{a}_k\rangle :\hat{a}^\dagger_i\hat{a}_l: \\ &+ :\hat{a}^\dagger_i\hat{a}^\dagger_j\hat{a}_l\hat{a}_k: \quad .\end{aligned} \tag{7.10}$$

Le premier terme de l'Eq. (7.10) est un terme constant produisant l'énergie HF de l'interaction. C'est le seul terme qui reste lorsque l'on prend la valeur moyenne de $\hat{V}$ sur le déterminant HF. Tous les autres termes s'annulent à cause des produits normalement ordonnés (: .. :). La valeur moyenne du dernier terme est égale à zéro : c'est ce terme que l'on nommera interaction résiduelle dans la théorie HF. L'approximation

HF consiste à négliger ce terme. Les opérateurs à un corps peuvent être réécrits en utilisant $:\hat{a}_i^\dagger \hat{a}_l := \hat{a}_i^\dagger \hat{a}_l - \langle \hat{a}_i^\dagger \hat{a}_l \rangle$. Nous oublions les termes constants et les seuls éléments qui restent sont les suivants :

$$\begin{aligned} \hat{a}_i^\dagger \hat{a}_j^\dagger \hat{a}_l \hat{a}_k \approx & - \langle \hat{a}_i^\dagger \hat{a}_l \rangle \hat{a}_j^\dagger \hat{a}_k \\ & + \langle \hat{a}_i^\dagger \hat{a}_k \rangle \hat{a}_j^\dagger \hat{a}_l \\ & + \langle \hat{a}_j^\dagger \hat{a}_l \rangle \hat{a}_i^\dagger \hat{a}_k \\ & - \langle \hat{a}_j^\dagger \hat{a}_k \rangle \hat{a}_i^\dagger \hat{a}_l \quad . \end{aligned} \tag{7.11}$$

Cette approximation permet de définir le terme d'interaction HF $\hat{w}$ en utilisant que $\langle \hat{a}_i^\dagger \hat{a}_l \rangle = \delta_{il}$ si i est un état occupé (aussi appelé état trou) et zéro sinon:

$$\hat{w} = \frac{1}{2} \left[- \sum_{\substack{ijk \\ i \in \text{occ}}} v_{ijki} \hat{a}_j^\dagger \hat{a}_k + \sum_{\substack{ijl \\ i \in \text{occ}}} v_{ijil} \hat{a}_j^\dagger \hat{a}_l + \sum_{\substack{ijk \\ j \in \text{occ}}} v_{ijkj} \hat{a}_i^\dagger \hat{a}_k - \sum_{\substack{ijl \\ j \in \text{occ}}} v_{ijjl} \hat{a}_i^\dagger \hat{a}_l \right] \quad . \tag{7.12}$$

En utilisant $v_{ijkl} = v_{jilk}$ cette expression se simplifie en

$$\hat{w} = \sum_{kl} \left(\sum_{j \in \text{occ}} \tilde{v}_{kjlj} \right) \hat{a}_k^\dagger \hat{a}_l \quad . \tag{7.13}$$

Le hamiltonien HF est alors

$$\hat{h} = \hat{h}^0 + \hat{w} \tag{7.14}$$

dont les éléments de matrice sont définis par

$$h_{kl} = h_{kl}^0 + \sum_{j \in \text{occ}} \tilde{v}_{kjlj} \quad . \tag{7.15}$$

Nous rappelons l'expression de l'énergie HF et de la valeur moyenne de $\hat{h}$:

$$E_{\text{HF}} = \langle \Psi_{\text{HF}} | \hat{H} | \Psi_{\text{HF}} \rangle = \sum_{m \in \text{occ}} t_{mm} + \frac{1}{2} \sum_{m,n \in \text{occ}} \tilde{v}_{mnmn} \tag{7.16}$$

$$\langle \Psi_{\text{HF}} | \hat{h} | \Psi_{\text{HF}} \rangle = \sum_{m \in \text{occ}} t_{mm} + \sum_{m,n \in \text{occ}} \tilde{v}_{mnmn} \tag{7.17}$$

7.3.2 Interaction résiduelle

L'interaction résiduelle est définie comme le terme négligé dans l'Eq. (7.10):

$$\hat{V}_{\text{res}} = \frac{1}{2} \sum_{i,j,k,l} v_{ijkl} :\hat{a}_i^\dagger \hat{a}_j^\dagger \hat{a}_l \hat{a}_k: \quad . \tag{7.18}$$

Par définition, la valeur moyenne de ce terme est zéro. Appliqué à un déterminant dans cette base, ce terme est différent seulement si l, k sont des états trous (i.e. occupés) et i, j sont des états particules (i.e. inoccupés). Dans toute autre situation, il existe un opérateur création ou annihilation qui annule le déterminant et l'ordre normal l'applique en premier à celui-ci. L'interaction résiduelle ne génère donc que des excitations 2-particules-2-trous ($2p2h$).

7.4 Dérivation basique de la hiérarchie BBGKY

Au-delà de cette approximation de champ moyen, les particules développent des corrélations à N corps qui doivent être prises en compte sous peine de perdre certains effets physiques. La théorie de la matrice densité réduite est un formalisme qui permet d'avoir un accès direct aux observables à l'interprétation physique des approximations. Les équations d'évolution des matrices densités forment une hiérarchie d'équations appelée hiérarchie BBGKY sur la base de son pendant de physique statistique classique developpée par Born, Bogoliubov, Green, Kirkwood et Yvon [54, 55, 56, 57]. Par référence au formalisme des fonctions de Green, on peut aussi s'y référer en tant que hiérarchie de Martin-Schwinger pour les matrices densités. Cette hiérarchie est parfaitement équivalente à la TDSE mais permet une meilleure compréhension des niveaux possibles d'approximation et de troncation. Nous donnons ici comme exemple une dérivation des deux premiers termes de la hiérarchie. Les équations d'évolution des opérateurs de création et d'annihilation dans la représentation d'Heisenberg sont les suivants

$$\Big(\mathrm{i}\partial_t - h^0(x,t)\Big)\hat{\Psi}(x,t) = \int d\bar{x}\, v(x,\bar{x})\hat{\Psi}^\dagger(\bar{x},t)\hat{\Psi}(\bar{x},t)\hat{\Psi}(x,t) \tag{7.19}$$

$$\Big(-\mathrm{i}\partial_t - h^0(x,t)\Big)\hat{\Psi}^\dagger(x,t) = \hat{\Psi}^\dagger(x,t)\int d\bar{x}\, v(x,\bar{x})\hat{\Psi}^\dagger(\bar{x},t)\hat{\Psi}(\bar{x},t) \quad . \tag{7.20}$$

Les matrices densités réduites sont définies de la manière suivante

$$\rho^{(n)}(x_1\dots x_n; x_{1'}\dots x_{n'}; t) = \langle\hat{\Psi}^\dagger(x_{1'},t)\dots\hat{\Psi}^\dagger(x_{n'},t)\hat{\Psi}(x_n,t)\dots\hat{\Psi}(x_1,t)\rangle \quad . \tag{7.21}$$

Dans la suite, la matrice densité à 1 corps est simplement notée ρ et sa diagonale $\varrho(x,t) = \rho(x;x;t)$. La variable temporelle ne sera pas notée la plupart du temps pour alléger l'écriture. L'équation d'évolution de ρ est évidente :

$$\begin{aligned}\mathrm{i}\partial_t\rho(x_1;x_{1'}) &= \Big(h^0(x_1) - h^0(x_{1'})\Big)\rho(x_1;x_{1'}) \\ &+ \int dx_2\Big(v(x_1,x_2) - v(x_{1'},x_{2'})\Big)\rho^{(2)}(x_1,x_2;x_{1'},x_{2'}) \quad .\end{aligned} \tag{7.22}$$

L'équation de $\rho^{(2)}$ donne plus d'informations sur les étapes de calcul dans un cas général

$$\begin{aligned}\mathrm{i}\partial_t\rho^{(2)}(x_1,x_2;x_{2'},x_{1'}) &= \Big(h^0(x_1) - h^0(x_{1'}) + h^0(x_2) - h^0(x_{2'})\Big)\rho^{(2)}(x_1,x_2;x_{1'},x_{2'}) \\ &+ \int dx_3\Big(v(x_2,x_3) - v(x_{2'},x_3)\Big)\rho^{(3)}(x_1,x_2,x_3;x_{1'},x_{2'},x_3) \\ &+ \int dx_3\Big(v(x_1,x_3)\langle\hat{\Psi}^\dagger(x_{1'},t)\hat{\Psi}^\dagger(x_{2'},t)\hat{\Psi}(x_2,t)\hat{\Psi}^\dagger(x_3,t)\hat{\Psi}(x_3,t)\hat{\Psi}(x_1,t)\rangle \\ &\quad - v(x_{1'},x_3)\langle\hat{\Psi}^\dagger(x_{1'},t)\hat{\Psi}^\dagger(x_3,t)\hat{\Psi}(x_3,t)\hat{\Psi}^\dagger(x_{2'},t)\hat{\Psi}(x_2,t)\hat{\Psi}(x_1,t)\rangle\Big)\end{aligned} \tag{7.23}$$

Quelques commutations sont nécessaires dans le dernier terme pour écrire l'ensemble en fonction de la matrice densité à 3 corps :

$$\begin{aligned}&\mathrm{i}\partial_t\rho^{(2)}(x_1,x_2;x_{2'},x_{1'}) = \\ &\quad\Big(h^0(x_1) - h^0(x_{1'}) + h^0(x_2) - h^0(x_{2'}) + v(x_1,x_2) - v(x_{1'},x_{2'})\Big)\rho^{(2)}(x_1,x_2;x_{1'},x_{2'}) \\ &\quad + \int dx_3\Big(v(x_2,x_3) - v(x_{2'},x_3) + v(x_1,x_3) - v(x_{1'},x_3)\Big)\rho^{(3)}(x_1,x_2,x_3;x_{1'},x_{2'},x_{3'})\end{aligned} \tag{7.24}$$

Ici nous n'avons dérivé que les deux premières équations de la hiérarchie mais la procédure est aisément généralisable pour obtenir les équations pour $\rho^{(n)}$.

7.5 Troncation de la hiérarchie BBGKY

7.5.1 Développement en clusters

La forme générale de ces équations est la suivante :

$$\Big(\mathrm{i}\partial_t - k(x_1..x_n) + k(x_{1'}..x_{n'})\Big)\rho^{(n)}(x_1..x_n; x_{1'}..x_{n'}) = \sum_{j=1}^{n}\int dx_{n+1}\Big(v(x_j, x_{n+1}) - v(x_{j'}, x_{n+1})\Big)\rho^{(n+1)}(x_1..x_n, x_{n+1}; x_{1'}..x_{n'}, x_{n+1}) \tag{7.25}$$

où

$$k(x_1..x_n; t) = \sum_{i=1}^{n} h^0(x_i; t) + \frac{1}{2}\sum_{i\neq j}^{n} v(x_i, x_j) \quad . \tag{7.26}$$

La variable temporelle est invisible dans l'Eq. (7.25). Dans la suite nous remplacerons i par x_i. Les deux premières équations de cette hiérarchie sont écrites à nouveau explicitement :

$$\Big(\mathrm{i}\partial_t - h^0(1) + h^0(1')\Big)\rho(1;1') = \int d2\Big(v(1,2) - v(1',2)\Big)\rho^{(2)}(1,2;1',2)\ , \tag{7.27}$$

$$\Big(\mathrm{i}\partial_t - h^0(1) + h^0(1') - h^0(2) + h^0(2') - v(1,2) + v(1',2')\Big)\rho^{(2)}(1,2;1',2') = \int d3\Big(v(1,3) - v(1',3) + v(2,3) - v(2',3)\Big)\rho^{(3)}(1,2,3;1',2',3) \quad . \tag{7.28}$$

La hiérarchie BBGKY est impossible à résoudre en l'état. Elle doit être tronquée par exemple au niveau $n-1$ et la matrice densité à n corps doit être approximée par un produit de matrices à p corps antisymétrisé, avec $p < n$. Une façon de tronquer a été proposée par Shun-Jin et Cassing [16]. On commence avec un développement en clusters des différentes matrices densités réduites. Par exemple la matrice densité à 2 corps s'écrit

$$\rho^{(2)}(1,2;1',2') = \rho(1;1')\rho(2;2') - \rho(1;2')\rho(2;1') + c^{(2)}(1,2;1',2') \quad . \tag{7.29}$$

L'avantage de cette expression est de pouvoir séparer différents niveaux de corrélation. Pour la matrice densité à 2 corps dans l'Eq. (7.29), $c^{(2)}$ correspond au terme de corrélation à deux particules une fois le champ moyen soustrait. D'une manière plus générale, la matrice densité à n corps peut être écrite d'une manière compacte de la façon suivante :

$$\rho^{(n)} = AS\{\sum_{p=1}^{n-1}\rho^{(n-p)}\rho^{(p)}\} + c^{(n)} \quad , \tag{7.30}$$

où S symétrise par rapport au couple d'indices (i, i') et A antisymétrise les indices i' avec le signe correspondant. Une autre règle est que chaque terme ne doit apparaître

qu'une seule fois. Par exemple, on obtient :

$$\begin{aligned} AS\{\rho\rho^{(2)}\} &= A\left\{\rho(1;1')\rho^{(2)}(2,3;2',3') + \rho(2;2')\rho^{(2)}(1,3;1',3') + \rho(3;3')\rho^{(2)}(1,2;1',2')\right\} \\ &= \rho(1;1')\rho^{(2)}(2,3;2',3') - \rho(1;2')\rho^{(2)}(2,3;1',3') - \rho(1;3')\rho^{(2)}(2,3;2',1') \\ &+ \rho(2;2')\rho^{(2)}(1,3;1',3') - \rho(2;1')\rho^{(2)}(1,3;2',3') - \rho(2;3')\rho^{(2)}(1,3;1',2') \\ &+ \rho(3;3')\rho^{(2)}(1,2;1',2') + \rho(3;1')\rho^{(2)}(1,2;3',2') + \rho(3;2')\rho^{(2)}(1,2;1',3') \quad . \end{aligned} \tag{7.31}$$

Ce qui est une expression assez longue pour un seul terme.

Nous introduisons des notations plus compactes ici : les indices en exposant correspondent au nombre de particules du terme, les indices inférieurs permettent de savoir quelles coordonnées sont couplées entre elles. Ces derniers ne sont pas directement reliés aux x_i de l'opérateur et nous pouvons par exemple écrire

$$c^{(2)}(1,2;1',2') = c_{12}(1,2;1',2') = c_{23}(1,2;1',2') \quad . \tag{7.32}$$

Le nombre d'indices fournissant le nombre de particules, les exposants sont abandonnés quand les indices inférieurs sont utilisés. Nous passerons d'une notation à l'autre et n'écrirons pas les coordonnées quand il n'y pas d'ambiguïté, ce qui mènera parfois à identifier abusivement une matrice à ses éléments. La notation $\mathrm{Tr}_2(F_{12})$ correspond à $\int d2\Big(F(1,2;1',2')_{2=2'}\Big)$ pour une fonction F donnée. Des opérateurs de permutation P_{ij} sont utilisés et définis de la façon suivante :

$$P_{ij}|ij\rangle = |ji\rangle \tag{7.33}$$

$$\text{or } P_{12}(1,2;1',2') = \delta(1-2')\delta(2-1') \quad . \tag{7.34}$$

Par exemple, nous avons :

$$\begin{aligned} (P_{12}\rho_1\rho_2)(1,2;1',2') &= \rho(2,1')\rho(1,2') \ , \\ (\rho_1\rho_2 P_{12})(1,2;1',2') &= \rho(1,2')\rho(2,1') = (P_{12}\rho_1\rho_2)(1,2;1',2') \quad . \end{aligned} \tag{7.35}$$

On en déduit que P_{12} commute avec $\rho_1\rho_2$ et $AS\{\rho\rho\} = \rho_1\rho_2(1-P_{12})$. Par exemple, si $\rho^{(2)}$ est remplacé par $AS\{\rho\rho\} = \rho_1\rho_2(1-P_{12}) + c_{12}$ dans l'Eq. (7.27), on obtient

$$\mathrm{i}\partial_t\rho_1 - [h_1,\rho_1] = \mathrm{Tr}_2[v_{12},c_{12}] \tag{7.36}$$

où

$$h_1\rho_1 = h_1^0\rho_1 + \mathrm{Tr}_2\{v_{12}\rho_2\}\rho_1 - \mathrm{Tr}_2\{v_{12}\rho_2\rho_1 P_{12}\} \tag{7.37}$$

ce qui est tout simplement le hamiltonien HF.

7.5.2 Dérivation de l'équation de Boltzmann-Langevin

L'idée derrière la dérivation de l'équation de Boltzmann-Langevin à partir de la hiérarchie BBGKY est la suivante : d'abord, la hiérarchie est tronquée à l'équation à 2 corps ($c^{(3)} = 0$), puis la solution formelle de l'équation d'évolution de la matrice densité à 2 est insérée dans l'équation d'évolution de la matrice à 1 corps. Pour faire cette troncation, on peut supposer que

$$\rho^{(3)} \approx AS\{\rho^{(2)}\rho\} \tag{7.38}$$

puisque $c^{(3)}$ a été négligé. On obtient exactement le terme explicitement écrit dans l'Eq. (7.31). On peut développer $\rho^{(3)}$ en n"utilisant que $\rho^{(2)} = AS\{\rho\rho\} + c^{(2)}$. On obtient alors

$$\begin{aligned}\rho^{(3)} &\approx AS\{\rho\rho\rho + \rho c^{(2)}\} \\ &= \rho_1 c_{23}(1 - P_{12} - P_{13}) + \rho_2 c_{13}(1 - P_{21} - P_{23}) + \rho_3 c_{12}(1 - P_{31} - P_{32}) \\ &+ \rho_1\rho_2\rho_3(1 - P_{12})(1 - P_{12} - P_{23}) \quad .\end{aligned} \tag{7.39}$$

Donc seule l'équation d'évolution pour $c^{(2)}$ est nécessaire. Tout d'abord, nous avons besoin de l'équation d'évolution du terme $AS\{\rho\rho\}$:

$$\begin{aligned}\mathrm{i}\partial_t \rho_1\rho_1(1 - P_{12}) = [h_1^0, \rho_1]\rho_2(1 - P_{12}) + [h_2^0, \rho_2]\rho_1(1 - P_{12}) \\ + \mathrm{Tr}_3[v_{13}, \rho_{13}]\rho_2(1 - P_{12}) + \mathrm{Tr}_3[v_{23}, \rho_{23}]\rho_1(1 - P_{12}) \quad .\end{aligned} \tag{7.40}$$

On peut voir que cela génère tous les termes non-liés. Une exemple de terme non-lié est $v(2,3)\rho^{(2)}(2,3;2',3')\rho(1;1')$ où v_{12} ne couple pas les deux matrices densités. Une généralisation de ce résultat a été donnée dans [16], mais ici seule la preuve pour les deux premières équations est nécessaire. Nous en déduisons que l'évolution de $c^{(2)}$ ne prend en compte que les termes liés. Après des calculs longs mais simples, on obtient

$$\begin{aligned}\mathrm{i}\partial_t c_{12} - [h_1 + h_2, c_{12}] = \\ \frac{1}{2}\Big(\bar{\rho_1}\bar{\rho_2}(1 - P_{12})v_{12}\rho_1\rho_2(1 - P_{12}) - \rho_1\rho_2(1 - P_{12})v_{12}\bar{\rho_1}\bar{\rho_2}(1 - P_{12})\Big) \\ + O(c_{12}v_{12})\end{aligned} \tag{7.41}$$

où $\bar{\rho_1} = 1 - \rho_1$. Presque tous les termes proportionnels à $c_{12}v_{12}$ sont négligés. Pour une démonstration plus complète, voir [18]. Ces résultats peuvent aussi être obtenus dans [58] qui contient aussi des exemples d'application sur des systèmes plus complexes. Le terme de droite est le terme de collision ou terme de Born B_{12} qui aboutit au terme dissipatif dans la théorie ETDHF (voir Sec. 7.5.3). Ce terme dérive entièrement de $AS\{\rho\rho\rho\}$. L'expression explicite de deux des termes de l'Eq. (7.41) est donnée ici comme exemple pour s'assurer que les notations sont claires :

$$\begin{aligned}\rho_1\rho_2 P_{12} v_{12}\rho_2 &= \int d3v(1';3)\rho(1;3)\rho(2;1')\rho(3;2') \ , \\ -\rho_2 v_{12}\rho_1\rho_2 P_{12} &= -\int d3v(1;3)\rho(1;2')\rho(2;3)\rho(3;1') \quad .\end{aligned} \tag{7.42}$$

Nous rappelons au lecteur que $v(i;j) \leftrightarrow v(i,j;i',j')\delta(i - i')\delta(j - j')$ de sorte que la partie à droite du signe égal est cohérente avec un opérateur à 2 corps. Il faut souligner que ce terme n'est pas dérivé en remplaçant $\rho^{(3)}$ directement par $AS\{\rho\rho\rho\}$ mais aussi en prenant en compte tous les termes non-liés de l'Eq. (7.40) et quelques termes de $\rho_3 c_{12}(1 - P_{13} - P_{23})$ qui permettent de transformer $h_1^0 + h_2^0$ en $h_1 + h_2$. Il est possible de donner la solution formelle de l'Eq. (7.41) qui est

$$c_{12}(t) = -\mathrm{i}\int_{t_0}^{t} ds U_{12}(t,s)B_{12}(s)U_{12}(s,t) + \delta c_{12}(t) \tag{7.43}$$

où $U_{12} = U_1 U_2$ avec $U_i = \mathcal{T}\exp\Big(-i\int_{t_0}^{t} h_i(s)ds\Big)$ et $\mathcal{T}$ l'operateur d'ordre temporel. Le second terme $\delta c_{12}(t) = U_{12}(t,t_0)c_{12}(t_0)U_{12}(t_0,t)$ est la propagation en champ moyen de la corrélation initiale. Maintenant nous pouvons insérer c_{12} dans l'Eq. (7.36):

$$\mathrm{i}\partial_t \rho = [h,\rho] + K[\rho] + \delta K(t)\ , \tag{7.44}$$

$$K[\rho] = -\mathrm{i}\int_{t_0}^{t} ds\, \mathrm{Tr}_2[v_{12}, U_{12}(t,s)B_{12}(s)U_{12}(s,t)]\ , \tag{7.45}$$

$$\delta K(t) = \mathrm{Tr}_2[v_{12}, \delta c_{12}(t)] \quad . \tag{7.46}$$

Dans cette équation $K[\rho]$ est interprété en tant que terme de collision et $\delta K(t)$ comme une force aléatoire, voir [22] pour plus de détails.

Nous écrivons à nouveau explicitement l'intégrale de collision :

$$\begin{aligned} K[\rho] = \frac{\mathrm{i}}{2}\int_{t_0}^{t} ds\, \mathrm{Tr}_2 \Big\{ &\Big[v, U(t,s)AS\{\rho\rho\}vAS\{\bar\rho\bar\rho\}U^\dagger(t,s)\Big] \\ &- \Big[v, U(t,s)AS\{\bar\rho\bar\rho\}vAS\{\rho\rho\}U^\dagger(t,s)\Big]\Big\} \quad . \end{aligned} \tag{7.47}$$

Ici nous avons retiré les indices (12). Quand l'équilibre thermique par rapport au hamiltonien de champ moyen est atteint, le terme c_{12} s'annule. Donc $\mathrm{Tr}_2[v_{12}, c_{12}]$ dans l'Eq. (7.36) s'annule de même et seul le champ moyen dirige l'évolution de ρ. On peut s'attendre à ce qu'une distribution de Fermi-Dirac reste stable au cours du temps. La relation entre la force aléatoire et le terme de collision a été étudiée en détail dans [23].

7.5.3 TDHF étendu (ETDHF)

TDHF étendu a été introduit comme façon d'inclure la dissipation due à la collision entre hadrons dans les noyaux [14]. Au départ, cela a été déduit d'une approche plus semi-classique basée sur les équations VUU. Ce qui est présenté par la suite se réduit à la version "historique" de ETDHF à la limite markovienne. (voir Eq. 7.62).

Pour obtenir ETDHF, le terme de force stochastique δK est mis à zéro. Cela revient à considérer qu'il n'y a aucune corrélation initiale dans notre système. L'Eq. (7.44) s'écrit alors :

$$\mathrm{i}\partial_t \rho = [h,\rho] + K[\rho] \quad . \tag{7.48}$$

Cela aboutit à la version de ETDHF avec un terme de collision non markovien. En effet, le terme de collision (7.47) contient une intégrale sur tous les états passés du système. Nous introduisons la base naturelle instantanée, c'est-à-dire la base qui diagonalise la matrice densité à un corps $\rho(t)$:

$$\rho(t) = \sum_i |i(t)\rangle\, n_i(t)\, \langle i(t)| \tag{7.49}$$

En définissant

$$\langle kj|\tilde v|lm\rangle_s = \langle kj|v|lm\rangle_s - \langle kj|v|ml\rangle_s \tag{7.50}$$

on peut écrire les éléments de matrice de l'intégrale de collision (7.47) dans la base :

$$\begin{aligned} \langle j|K|i\rangle = \frac{\mathrm{i}}{2}\int_{t_0}^{t} ds \sum_{klm} \Big[&\langle jk|\tilde v|lm\rangle_t \langle lm|\tilde v|ik\rangle_s \Big(n_l n_m(1-n_i)(1-n_k) - n_i n_k(1-n_l)(1-n_m)\Big)_s \\ &+ \langle jk|\tilde v|lm\rangle_s \langle lm|\tilde v|ik\rangle_t \Big(n_l n_m(1-n_j)(1-n_k) - n_j n_k(1-n_l)(1-n_m)\Big)_s\Big] \quad . \end{aligned} \tag{7.51}$$

où l'indice inférieur indique que nous avons utilisé la base naturelle au temps s [2]

Il faut souligner que le propagateur U dans l'intégrale de collision K dans l'Eq. (7.47) correspond à la propagation champ moyen de la matrice densité et non à la propagation totale prenant en compte K. De ce fait, les termes au temps s doivent être considérés avec attention. En fait, nous avons $|lm\rangle_t = U(t,s)|lm\rangle_s$ où $|lm\rangle_s$ et réellement la base naturelle au temps s, alors que $|lm\rangle_t$ *ne* l'est *pas*, vu que la propagation champ moyen n'est pas égale à la vraie. De plus amples détails sur l'implémentation numérique de cette équation sont donnés par exemple dans [59].

7.5.4 Approximation markovienne

Le propagateur champ moyen

$$U_i(t,s) = \mathcal{T} \exp\Big(-\mathrm{i} \int_s^t h_i(t')dt' \Big) \tag{7.52}$$

est un terme compliqué parce que le hamiltonien champ moyen dépend de $\rho(t)$ et t, et du fait de l'intégration sur le temps. On suppose que les termes de la forme $\langle jk|\tilde{v}|lm\rangle_t\langle lm|\tilde{v}|ik\rangle_s$ s'annulent pour s loin de t. De ce fait, nous pouvons remplacer sur l'intervalle de temps $[s,t]$:

$$h(t') \approx h(t) \text{ pour } t' \text{ dans } [s,t] \,, \tag{7.53}$$
$$\rho(t') \approx \rho(t) \text{ pour } t' \text{ dans } [s,t] \,. \tag{7.54}$$

Le propagateur à 2 corps en champ moyen devient :

$$U = e^{-\mathrm{i}(t-s)(h_1(t)+h_2(t))} \tag{7.55}$$

On considère maintenant la base propre instantanée du hamiltonien champ moyen, c'est-à-dire la base telle que :

$$h(t)|i\rangle = \varepsilon_i|i\rangle \tag{7.56}$$

à un temps t donné. Dans cette base, le propagateur est diagonal :

$$U_{ijkl} = \delta_{ik}\delta_{jl}e^{-\mathrm{i}(t-s)(\varepsilon_i+\varepsilon_j)} \quad . \tag{7.57}$$

On continue de supposer que l'intégrale de collision a une très courte mémoire. On peut alors étendre la limite d'intégration t_0 à $-\infty$ sans changer le résultat. On fait aussi l'approximation suivante :

$$\int_{-\infty}^{t} ds\, e^{-\mathrm{i}(t-s)(\varepsilon_i+\varepsilon_j-\varepsilon_k-\varepsilon_l)} \approx \pi\delta(\varepsilon_i+\varepsilon_j-\varepsilon_k-\varepsilon_l) \quad . \tag{7.58}$$

Ici, la partie principale a été négligée vu qu'elle ne génère que des éléments hors-diagonaux. Ces éléments s'ajoutent au champ moyen mais nous supposons que le champ moyen prévaut dans l'évolution non dissipative. De manière plus formelle, cela peut être écrit à l'aide du liouvillien du champ moyen $\mathcal{L}_0$:

$$\int_{-\infty}^{t} ds\, e^{-\mathrm{i}(t-s)\mathcal{L}_0} = \pi\delta(\mathcal{L}_0) \tag{7.59}$$

[2] La relation de fermeture $\mathbb{I} = \frac{1}{2}\sum_{lm} |lm\rangle\langle lm| + |ml\rangle\langle ml|$ est utilisée pour faire apparaître $\tilde{v}$.

où $\mathcal{L}_0$ vérifie $\mathcal{L}_0 A_{12} = [h_1+h_2, A_{12}]$. Donc dans l'approximation markovienne, l'intégrale de collision est

$$K = \mathrm{i}\frac{\pi}{2}\,\mathrm{Tr}_2\{[v, \delta(\mathcal{L}_0)AS\{\rho\rho\}vAS\{\bar{\rho}\bar{\rho}\}] - [v, \delta(\mathcal{L}_0)AS\{\bar{\rho}\bar{\rho}\}vAS\{\rho\rho\}]\} \quad . \tag{7.60}$$

On considère maintenant de nouveau l'intégrale de collision de ETDHF de l'Eq. (7.51). En plus de l'approximation markovienne, on suppose qu'il existe une base dans laquelle ρ est diagonal, et h proche de la diagonale, c'est-à-dire

$$\Delta h = \sqrt{\mathrm{Tr}\{h\rho\}^2 - \mathrm{Tr}\{h^2\rho\}} \tag{7.61}$$

est suffisamment petit pour être négligé. Si on ne prend en compte que les éléments diagonaux :

$$\begin{aligned}\langle i|K|i\rangle = \mathrm{i}\pi \sum_{klm} &|\langle ik|\tilde{v}|lm\rangle|^2 \delta(\varepsilon_k + \varepsilon_i - \varepsilon_l - \varepsilon_m) \\ &\times \Big(n_l n_m (1-n_i)(1-n_k) - n_i n_k (1-n_l)(1-n_m)\Big) \quad .\end{aligned} \tag{7.62}$$

Ce terme est en fait le seul terme sur la diagonale à droite du signe égal de l'Eq. (7.48). Il agit directement sur les nombres d'occupation de la matrice densité. On s'attend à ce que l'hypothèse d'un petit Δh soit remplie dans le cas de faibles excitations. Dans la suite, ETDHF fera toujours référence à cette version markovienne réduite à ses éléments diagonaux.

7.6 Stochastique TDHF

Nous nous tournons maintenant vers le coeur de cette thèse basée sur les travaux précurseurs de [23]. Stochastique TDHF (STDHF) est une théorie qui approche la propagation exacte d'un état quantique par un ensembe de déterminants de Slater dont les matrices densités sont propagées en temps selon une théorie de champ moyen et ajoutées de manière incohérente. Cette méthode a été présentée et étudiée dans [24, 23, 61, 62]. La plupart des démonstrations seront faites dans cette partie.

7.6.1 Ensemble de trajectoires

Nous supposons que notre matrice densité à t' est à N corps et de la forme

$$\mathcal{D}(t') = \sum_\alpha x^{(\alpha)}(t') D^{(\alpha)}(t') \quad . \tag{7.63}$$

Ici $D^{(\alpha)}(t') = |\Phi^{(\alpha)}(t')\rangle\langle\Phi^{(\alpha)}(t')|$, $|\Phi^{(\alpha)}(t')\rangle$ étant un déterminant de Slater, et α l'indice pour l'ensemble des matrices densités qui sont additionnées de manière incohérente pour former $\mathcal{D}(t')$. Nous considérons maintenant l'évolution sur l'intervalle de temps $[t', t]$ et definissons $\tau = t - t'$. Pour ce faire, seulement une matrice densité non corrélée $D^{(\alpha)}$ sera considérée au départ. Sans perte de généralité, le temps initial est défini comme $t' = 0$. Chaque $D^{(\gamma)}$ est propagé selon son propre champ moyen, et ceci forme ce que nous appelons une "trajectoire".

7.6.2 Propagation d'une trajectoire

Nous considérons d'abord une seule trajectoire, d'indice α, et partant de l'état $|\Phi^{(\alpha)}(0)\rangle$. Le champ moyen correspondant à n'importe quel temps s est noté $h(s)$ et peut être complété par une interaction résiduelle $V(s)$ pour obtenir le hamiltonien exact $H(s) = h(s) + V(s)$. Les opérateurs d'évolution temporelle sont les suivants :

$$\begin{aligned} U(\tau,\epsilon) &= \mathcal{T} e^{-\mathrm{i}\int_\epsilon^\tau H(s)ds} \\ U_0(\tau,\epsilon) &= \mathcal{T} e^{-\mathrm{i}\int_\epsilon^\tau h(s)ds} \end{aligned} \tag{7.64}$$

avec $\tau > \epsilon$. De la même façon que pour la représentation interaction, on peut obtenir :

$$\mathrm{i}\partial_\epsilon\Big(U(\tau,\epsilon)U_0(\epsilon,\tau)\Big) = -U(\tau,\epsilon)U_0(\epsilon,\tau)\widetilde{V}(\epsilon) \tag{7.65}$$

où

$$\widetilde{V}(\epsilon) = U_0(\tau,\epsilon)V(\epsilon)U_0(\epsilon,\tau) \quad . \tag{7.66}$$

L'expression formelle du produit $U(\tau,\epsilon)U_0(\epsilon,\tau)$ est :

$$U(\tau,\epsilon)U_0(\epsilon,\tau) = \mathcal{T} e^{-\mathrm{i}\int_\epsilon^\tau \widetilde{V}(s)ds} \tag{7.67}$$

A présent, faisons tendre $\epsilon \to 0$. L'opérateur $\Omega_+ = U(\tau,0)U_0(0,\tau)$ permet de passer de l'évolution exacte $|\Psi^{(\alpha)}(\tau)\rangle$ à l'état propagé en champ moyen $|\Phi^{(\alpha)}(\tau)\rangle$ à partir de l'état initial $|\Phi^{(\alpha)}(0)\rangle$:

$$|\Psi^{(\alpha)}(\tau)\rangle = \Omega_+|\Phi^{(\alpha)}(\tau)\rangle \quad . \tag{7.68}$$

Il peut être approximé jusqu'au second ordre en $\widetilde{V}$ comme :

$$|\Psi^{(\alpha)}(\tau)\rangle \approx |\Phi^{(\alpha)}(\tau)\rangle - \mathrm{i}\int \widetilde{V}|\Phi^{(\alpha)}(\tau)\rangle - \frac{1}{2}\mathcal{T}\Big\{\int \widetilde{V}\int \widetilde{V}\Big\}|\Phi^{(\alpha)}(\tau)\rangle \tag{7.69}$$

où $\int \widetilde{V} = \int_0^\tau \widetilde{V}(s)ds$. La matrice densité à N corps dépendant du temps $\mathcal{D}^{(\alpha)}(\tau)$ se lit :

$$\begin{aligned} \mathcal{D}^{(\alpha)}(\tau) &= |\Phi^{(\alpha)}(\tau)\rangle\langle\Phi^{(\alpha)}(\tau)| + \Big(-\mathrm{i}\int \widetilde{V}|\Phi^{(\alpha)}(\tau)\rangle\langle\Phi^{(\alpha)}(\tau)| + \mathrm{h.c.}\Big) \\ &+ \int \widetilde{V}|\Phi^{(\alpha)}(\tau)\rangle\langle\Phi^{(\alpha)}(\tau)|\int \widetilde{V} - \Big(\frac{1}{2}\mathcal{T}\Big\{\int \widetilde{V}\int \widetilde{V}\Big\}|\Phi^{(\alpha)}(\tau)\rangle\langle\Phi^{(\alpha)}(\tau)| + \mathrm{h.c.}\Big) \end{aligned} \tag{7.70}$$

Considérons à présent une base orthonormale instantanée au temps τ, dénotée par $|\kappa\rangle = |\Phi^{(\alpha)}_\kappa(\tau)\rangle$. Nous écrivons $|0\rangle = |\Phi^{(\alpha)}(\tau)\rangle$ afin de simplifier la notation. En conservant seulement les termes diagonaux, la matrice densité à N corps se simplifie de la manière suivante

$$\begin{aligned} \mathcal{D}^{(\alpha)}(\tau) \approx |0\rangle\langle 0| + \sum_\kappa |\kappa\rangle\langle\kappa|\int \widetilde{V}|0\rangle\langle 0|\int \widetilde{V}|\kappa\rangle\langle\kappa| \\ - \frac{1}{2}|0\rangle\langle 0|\mathcal{T}\Big\{\int \widetilde{V}\int \widetilde{V}\Big\}|0\rangle\langle 0| - \frac{1}{2}|0\rangle\langle 0|\bar{\mathcal{T}}\Big\{\int \widetilde{V}\int \widetilde{V}\Big\}|0\rangle\langle 0| \end{aligned} \tag{7.71}$$

où $\bar{\mathcal{T}}$ est l'opérateur d'ordre temporel inversé. Il est possible de se débarrasser des deux opérateurs d'ordre $\mathcal{T}\Big\{\int \widetilde{V}\int \widetilde{V}\Big\} + \bar{\mathcal{T}}\Big\{\int \widetilde{V}\int \widetilde{V}\Big\} = 2\int \widetilde{V}\int \widetilde{V}$. Comme h et V dépendent

a priori du déterminant Slater initial, nous utilisons par la suite un superscript $H = h^{(\alpha)} + V^{(\alpha)}$. Enfin, nous obtenons

$$\mathcal{D}^{(\alpha)}(\tau) \approx |0\rangle\langle 0|\Big(1 - \sum_{\kappa\neq 0}\Big|\langle\kappa|\int \widetilde{V}^{(\alpha)}|0\rangle\Big|^2\Big) + \sum_{\kappa\neq 0}|0\rangle\Big|\langle\kappa|\int \widetilde{V}^{(\alpha)}|0\rangle\Big|^2\langle 0| \quad . \tag{7.72}$$

L'élément de la matrice de transition $\Big|\langle\kappa|\int \widetilde{V}^{(\alpha)}|0\rangle\Big|^2$ peut être approximé par une règle d'or de Fermi :

$$\begin{aligned}\Big|\langle\kappa|\int \widetilde{V}^{(\alpha)}|0\rangle\Big|^2 &= \Big|\langle\Phi^{(\alpha)}_\kappa(\tau)|\int \widetilde{V}^{(\alpha)}|\Phi^{(\alpha)}(\tau)\rangle\Big|^2 \\ &\approx 2\pi\Big|\langle\Phi^{(\alpha)}_\kappa(0)|V^{(\alpha)}(0)|\Phi^{(\alpha)}(0)\rangle\Big|^2\delta(E^{(\alpha)}_\kappa - E^{(\alpha)})\tau = P^{(\alpha)}_\kappa\tau = P_{\alpha\to\kappa[\alpha]}\tau\end{aligned} \tag{7.73}$$

où $E^{(\alpha)}_\kappa$ et $E^{(\alpha)}$ sont les énergies HF de $|\Phi^{(\alpha)}_\kappa(\tau)\rangle$ et $|\Phi^{(\alpha)}(\tau)\rangle$ respectivement.

Comme l'interaction résidueile $V^{(\alpha)}$ est de nature $2p2h$, les seuls termes pris en considération dans la transition sont les excitations $2p2h$ du ket $|\Phi^{(\alpha)}\rangle$. κ est l'index pour ce type d'excitation, c'est-à-dire $\kappa \equiv pp'hh'$. Pour être plus précis, nous avons

$$V^{(\alpha)}|\Phi^{(\alpha)}\rangle = \sum_{pp'hh'} V_{mnji}\underbrace{a^\dagger_p a^\dagger_{p'}a_{h'}a_h|\Phi^{(\alpha)}\rangle}_{|\Phi^{(\alpha)}_\kappa(\tau)\rangle} \tag{7.74}$$

où p, p' sont des états de particules et h, h' sont des états de trous en qui concerne $|\Phi^{(\alpha)}\rangle$. En termes de matrices densités, cela donne :

$$V^{(\alpha)}D^{(\alpha)} = \sum_{\kappa[\alpha]\neq\alpha} D^{(\kappa[\alpha])}V^{(\alpha)}D^{(\alpha)} \tag{7.75}$$

où nous avons utilisé les notations $|0\rangle\langle 0| = D^{(\alpha)}(\tau)$ et $|\kappa\rangle\langle\kappa| = D^{(\kappa[\alpha])}(\tau)$. L'index $\kappa[\alpha] \neq \alpha$ signifie qu'il n'y a pas de terme diagonal. L'équation finale pour la matrice densité est

$$\mathcal{D}^{(\alpha)}(\tau) \approx D^{(\alpha)}(\tau) + \sum_{\kappa[\alpha]\neq\alpha}[D^{(\kappa[\alpha])}(\tau) - D^{(\alpha)}(\tau)]P_{\alpha\to\kappa[\alpha]}\tau \quad . \tag{7.76}$$

Cela donne l'évolution de la matrice exacte sous la forme d'une équation maîtresse avec un terme de gain et de perte par rapport à l'état initial $|\Phi^{(\alpha)}\rangle$.

7.6.3 Equation générale de mouvement pour STDHF

Chaque trajectoire α génère son propre ensemble de $2p2h$ matrices densités $D^{(\alpha)}_\kappa$ et la matrice densité à N corps totale correspondante, à l'instant τ, est la suivante :

$$\begin{aligned}\mathcal{D}(\tau) &= \sum_\alpha x^{(\alpha)}(0)\mathcal{D}^{(\alpha)}(\tau) \\ &\approx \sum_\gamma x^{(\gamma)}(\tau)D^{(\gamma)}(\tau) \quad .\end{aligned} \tag{7.77}$$

Cette équation doit être lue avec précaution: la première ligne est une somme de matrices densités corrélées à N corps, tandis que la seconde ligne contient uniquement

des matrices décorrelées, additionnées de façon incohérente à l'instant τ. Dans la Sec. 7.6.2, nous appliquons la méthode de $t = 0$ à $t = \tau$. Il est possible de refaire la même étape m fois. Le temps peut être discrétisé selon ces étapes et nous écrivons $t_m = m\tau$. En utilisant l'Eq. (7.76), nous réécrivons $\mathcal{D}(t_m)$ sous la forme

$$\begin{aligned}\mathcal{D}(t_m) &= \sum_\alpha x^{(\alpha)}(t_{m-1})\mathcal{D}^{(\alpha)}(t_m) \\ &\approx \sum_\alpha x^{(\alpha)}(t_{m-1})\Big(D^{(\alpha)}(t_m) + \sum_{\kappa\neq\alpha}[D^{(\kappa[\alpha])}(t_m) - D^{(\alpha)}(t_m)]P_{\alpha\to\kappa[\alpha]}\tau\Big) \quad (7.78)\\ &\approx \sum_\gamma x^{(\gamma)}(t_{m-1})D^{(\gamma)}(t_m) + \sum_{\substack{\gamma,\beta\\ \gamma\neq\beta}}(x^{(\beta)}(t_{m-1})P_{\beta\to\gamma} - x^{(\gamma)}(t_{m-1})P_{\gamma\to\beta})D^{(\gamma)}(t_m)\tau \quad (7.79)\end{aligned}$$

où γ est un index général rassemblant à la fois α et $\kappa[\alpha]$. De l'Eq. (7.73) nous avons $P_{\beta\to\gamma} = P_{\gamma\to\beta}$ mais nous gardons la forme la plus générale à ce stade. Nous définissons à présent la dérivée temporelle grossière de n'importe quelle fonction f sous la forme :

$$\partial_t f \approx \frac{f(t_m) - f(t_{m-1})}{\tau} \quad . \tag{7.80}$$

Cette définition utilisée avec $\mathcal{D}(t_{m-1}) \approx \sum_\gamma x^{(\gamma)}(t_{m-1})D^{(\gamma)}(t_{m-1})$, nous permet d'écrire l'équation de mouvement pour $\mathcal{D}$:

$$\mathrm{i}\partial_t\mathcal{D} = \sum_\gamma x^{(\gamma)}[h^{(\gamma)}, D^{(\gamma)}] + \mathrm{i}\sum_{\substack{\gamma,\beta\\ \gamma\neq\beta}}(x^{(\beta)}P_{\beta\to\gamma} - x^{(\gamma)}P_{\gamma\to\beta})D^{(\gamma)} \tag{7.81}$$

Le second terme peut être interprété comme :

$$\partial_t x^{(\gamma)} = \sum_{\substack{\beta\\ \gamma\neq\beta}}(x^{(\beta)}P_{\beta\to\gamma} - x^{(\gamma)}P_{\gamma\to\beta}) \quad . \tag{7.82}$$

A partir de l'Eq. (7.78) nous pouvons donc écrire l'Eq. (7.81) de la façon suivante :

$$\mathrm{i}\partial_t\mathcal{D} = \sum_\gamma x^{(\gamma)}[h^{(\gamma)}, D^{(\gamma)}] + \mathrm{i}\sum_{\substack{\gamma,\beta\\ \gamma\neq\beta}} x^{(\beta)}P_{\beta\to\gamma}(D^{(\gamma)} - D^{(\beta)}) \quad . \tag{7.83}$$

Dans ce qui suit, nous devons introduire l'opérateur de projection à 1 corps e dont la définition dans une base de fonctions d'ondes à une particule arbitraire est

$$\mathrm{Tr}\{eO\} = \sum_{ij}\mathrm{Tr}\{a_j^\dagger a_i O\}a_i^\dagger a_j \tag{7.84}$$

où O est un opérateur à N corps. On remarque que ceci est une notation abusive, étant donné que $\mathrm{Tr}\{eO\}$ n'est pas un nombre mais un opérateur à N corps. Les matrices densités à 1 corps sont alors faciles à obtenir :

$$\begin{aligned}\rho &= \mathrm{Tr}\{e\mathcal{D}\}\ , \\ \rho^{(\gamma)} &= \mathrm{Tr}\{eD^{(\gamma)}\} \quad .\end{aligned} \tag{7.85}$$

Il faut aussi noter que $\rho^{(\gamma)}$ est la matrice densité d'un état pur (avec 0 et 1 comme nombres d'occupation) tandis que ρ est une matrice densité à état mixte (avec des

nombres d'occupation partiels). Pour tout opérateur à 1 corps, e a donc pour propriété

$$\mathrm{Tr}\{e[T,\mathcal{D}]\} = [T,\rho] \tag{7.86}$$

et conserve la liberté de faire des permutations circulaires dans la trace. Nous définissons $\bar{h}$ comme le champ moyen correspondant à $\rho = \mathrm{Tr}\{e\mathcal{D}\}$ et $\bar{V}$ si bien que $H = \bar{h} + \bar{V} = h^{(\gamma)} + V^{(\gamma)}$.

Dérivons à présent l'équation de mouvement de la matrice densité à 1 corps. D'abord, nous utilisons

$$[h^{(\gamma)}, D^{(\gamma)}] = [\bar{h}, D^{(\gamma)}] + [\bar{V}, D^{(\gamma)}] - [V^{(\gamma)}, D^{(\gamma)}] \tag{7.87}$$

pour faire apparaître $\bar{h}$ comme premier terme de l'Eq. (7.83) puis nous projetons cette équation en utilisant $\mathrm{Tr}\{e...\}$. Il est à noter que le dernier terme de (7.87) disparaît alors :

$$\begin{aligned} V^{(\gamma)}D^{(\gamma)} &= \sum_{\kappa[\gamma]\neq\gamma} D^{(\kappa[\gamma])}V^{(\gamma)}D^{(\gamma)} \\ \mathrm{Tr}\{eD^{(\kappa[\gamma])}V^{(\gamma)}D^{(\gamma)}\}_{ji} &= \underbrace{\langle\Phi^{(\gamma)}|a_i^\dagger a_j|\Phi_\kappa^{(\gamma)}\rangle}_{0}\langle\Phi_\kappa^{(\gamma)}|V^{(\gamma)}|\Phi^{(\gamma)}\rangle = 0 \quad . \end{aligned} \tag{7.88}$$

Au total, cela donne

$$\mathrm{i}\partial_t\rho = [\bar{h},\rho] + K + \delta K \tag{7.89}$$

$$K = \mathrm{i}\sum_{\substack{\gamma,\beta \\ \gamma\neq\beta}} x^{(\beta)} P_{\beta\to\gamma}(\rho^{(\gamma)} - \rho^{(\beta)}) \tag{7.90}$$

$$\delta K = \sum_\gamma x^{(\gamma)}\,\mathrm{Tr}\{[e,\bar{V}]D^{(\gamma)}\} \quad . \tag{7.91}$$

On peut montrer [23] que l'intégrale de collision K et la force stochastique δK sont dans une certaine mesure équivalentes à celles trouvées dans l'Eq. (7.44) dans l'approximation markovienne.

7.6.4 STDHF en pratique

La mise en œuvre numérique de STDHF est simple dès lors que la dérivation a été faite. À chaque τ, cet état génère autant de matrices densité $D^{(\kappa[\gamma])}$ que permettent les transitions $2p2h$ d'après l'Eq. (7.73). Cet ensemble est cependant trop grand pour être traité numériquement. L'idée de STDHF est de remplacer l'ensemble des trajectoires pondérées par $P_{\beta\to\gamma}\tau$ par un nombre fixe $\mathcal{N}$ de trajectoires choisies de façon stochastique avec la probabilité $P_{\beta\to\gamma}\tau$ définie dans l'Eq. (7.73). La matrice densité correspondante $\mathcal{D}$ est ainsi

$$\mathcal{D} = \frac{1}{\mathcal{N}}\sum_{\gamma=1}^{\mathcal{N}} D^{(\gamma)}(t) \tag{7.92}$$

où la même matrice $D^{(\gamma)}$ peut apparaître plusieurs fois dans la somme. Notons ce nombre par $\mathcal{N}^{(\gamma)}$. Nous avons :

$$\frac{\mathcal{N}^{(\gamma)}}{\mathcal{N}} \xrightarrow[\mathcal{N}\to\infty]{} x^{(\gamma)} \quad . \tag{7.93}$$

$\mathcal{N}$ est de l'ordre de quelques centaines dans nos calculs pour permettre suffisamment de statistique. Comme chaque trajectoire doit être propagée en utilisant son propre champ moyen, le calcul est encore lourd numériquement. Etant donné que dans un système fini le spectre d'énergie est discret, la fonction delta de $P_{\beta\to\gamma}$ est remplacée par une fonction porte avec une largeur finie Γ, comme :

$$\delta_\Gamma(x) = \begin{cases} \dfrac{1}{2\Gamma} & \text{if } |x| \leq \Gamma \\ \\ 0 & \text{otherwise} \end{cases} \quad . \tag{7.94}$$

Nous avons observé que, par souci d'efficacité numérique, nous avions besoin d'effectuer une pré-sélection des états de transition avec une autre fonction delta de largeur $\Gamma_\varepsilon > \Gamma$. Nous prenons généralement $\Gamma_\varepsilon \approx 5\Gamma$. Cette pré-sélection se fait parmi les énergies à une particule, c'est-à-dire pour l'état $D^{(\alpha)}$ qui passe à un état $D^{(\kappa[\alpha])}$. Plus précisément, la condition de pré-sélection se lit :

$$|\varepsilon_p + \varepsilon_{p'} - \varepsilon_h - \varepsilon_{h'}| \leq \Gamma_\varepsilon \quad . \tag{7.95}$$

Tout ce processus est esquissé dans la Fig. 7.1 où les trajectoires sont représentées en violet et, à chaque τ, un saut instantané se produit (en rouge), choisissant une transition $D^{(\kappa[\gamma])}$ (rouge plein) parmi toutes les transitions possibles (rouge pointillé) avec une certaine probabilité. Il y a également un certain degré de liberté dans la

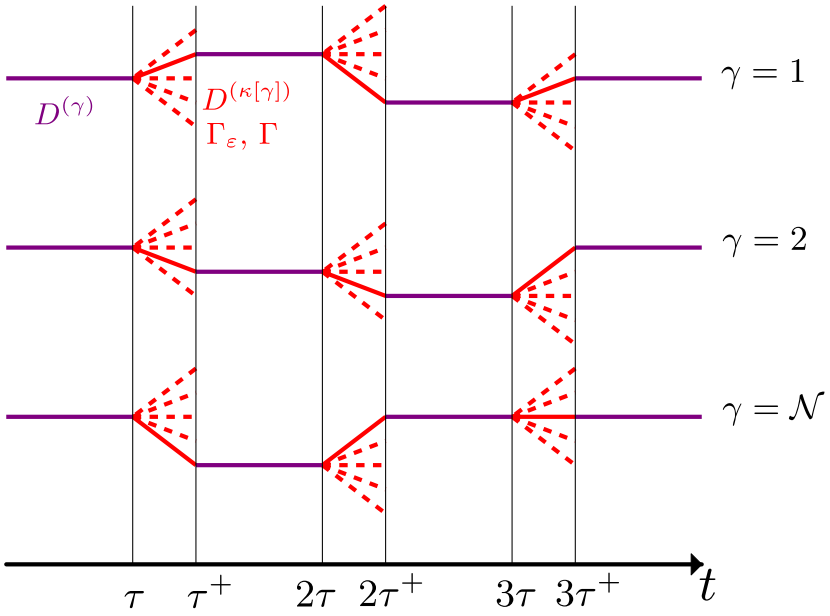

Figure 7.1: Vue schématique de la propagation temporelle de l'ensemble Stochastic TDHF. Voir le texte pour plus de détails.

transition elle-même. En effet, toutes les transformations unitaires qui conservent les sous-espaces des états occupés (espace h) et vides (espace p) dans une trajectoire laissent $D^{(\gamma)}$ inchangé, mais cela change les transitions $2p2h$ possibles. Avant chaque transition, nous choisissons les fonctions d'onde à une particule $|\varphi_\nu^{(\gamma)}\rangle$ qui diagonalisent le champ moyen hamiltonien $h^{(\gamma)}$ dans les espaces h et p séparément. Le but de ce

processus est de réduire l'incertitude sur les énergies à une particule et sur l'énergie totale $E_\kappa^{(\alpha)}$ de la transition $2p2h$.

7.6.5 Limitations de STDHF

Le régime de STDHF présenté ici présente des difficultés pour faire face aux excitations de basse énergie (voir Chapitre 4). En effet, lorsque l'énergie d'excitation est faible, la probabilité de transition diminue et le nombre de trajectoires doit être augmenté en conséquence pour capturer la bonne dynamique. La différence entre le hamiltonien de champ moyen de chacune des trajectoires devient beaucoup plus petit. D'un point de vue numérique, le coût de la propagation de centaines de trajectoires même dans une approche champ moyen peut devenir prohibitif. Ceci a motivé le choix d'utiliser seulement un unique champ moyen $\bar{h}$ pour la propagation. A partir de l'Eq. (7.89), nous déduisons que ceci est équivalent à un calcul ETDHF markovien (où les fluctuations sont négligeables) sans l'hypothèse de basse énergie qui supposait qu'il y a une base commune à $\bar{h}$ et ρ. Par conséquent, comme nous avons gardé seulement l'intégrale collisionnelle, nous appelons cette méthode TDHF collisionnelle.

7.7 CTDHF

Comme expliqué précédemment, le hamiltonien de champ moyen de chaque trajectoire est remplacé dans le régime CTDHF par le champ moyen commun $\bar{h}$, ce qui revient à négliger le terme $[\bar{V}, D^{(\gamma)}]$ dans l'Eq. (7.87). Aussi, la foce stochastique δK n'apparaît pas et nous obtenons seulement

$$i\partial_t \rho = [\bar{h}, \rho] + K \tag{7.96}$$

comme équation de mouvement pour ρ. Avec les Eqs. (7.90) et (7.96) il est à noter que CTDHF ne nécessite pas vraiment les trajectoires de $D^{(\gamma)}$ pour être propagé. Il nécessite seulement la matrice densité d'"état mixte" $\rho(t)$ et l'ensemble des matrices de densité d'état pur $\rho^{(\gamma)}$ pour faire des transitions à chaque τ. Cet ensemble est reconstruit d'une façon approximative qui sera expliquée plus en détail par la suite. Dans CTDHF les transitions possibles ne sont pas échantillonnées comme dans STDHF, mais ajoutées avec leur poids $P_{\beta\to\gamma}$. Le système est alors plus robuste pour les faibles probabilités de transitions. Dans STDHF, l'essentiel du temps de calcul est utilisé pour propager l'ensemble des trajectoires. Dans CTDHF, il n'y a qu'une seule trajectoire et nous avons un temps de calcul qui peut être deux ordres de grandeur plus petit que celui dans STDHF.

7.7.1 Représentation des états mixtes

Le régime CTDHF traite de l'état d'un système à N particules par deux représentations équivalentes : une matrice densité ρ (mixte) à 1 corps et un ensemble $\mathcal{E}$ d'états de Slater purs,

$$\rho = \sum_{\nu=1}^{\Omega} |\varphi_\nu\rangle w_\nu \langle\varphi_\nu| \;\longleftrightarrow\; \mathcal{E} = \{|\Phi^{(\alpha)}\rangle, x^{(\alpha)}, \alpha = 1, ..., \mathcal{N}\} = \{D^{(\alpha)}, x^{(\alpha)}\} \tag{7.97}$$

où les $x^{(\alpha)}$ sont les poids auxquels l'état de Slater $|\Phi^{(\alpha)}\rangle$ contribue. Ce dernier s'écrit en utilisant les nombres d'occupation

$$|\Phi^{(\alpha)}\rangle = |n_1^{(\alpha)}, n_2^{(\alpha)}, ..., n_\Omega^{(\alpha)}\rangle \ , \ n_\nu^{(\alpha)} \in \{0,1\} \ , \ \sum_\nu n_\nu^{(\alpha)} = N \ , \tag{7.98}$$

où N est le nombre total de particules physiques et Ω le nombre total de fonctions d'onde à une particule considérées. Tous les $|\Phi^{(\alpha)}\rangle$ sont formés sur la même base d'états à une particule $\mathcal{B} = \{|\varphi_\nu\rangle, \nu = 1, ..., \Omega\}$ qui est aussi la base qui construit ρ. Un $|\Phi^{(\alpha)}\rangle$ (ou la matrice densité D^α correspondante) est ainsi uniquement caractérisé par les vecteurs $\mathbf{n}^{(\alpha)}$ et l'ensemble par la matrice $A \equiv n_\nu^{(\alpha)}$ de taille $\Omega \times \mathcal{N}$ où $\mathbf{n}^{(\alpha)}$ représente les colonnes. Nous écrirons parfois

$$\{\mathcal{B}, A\} = \{|\Phi^{(\alpha)}\rangle\} = \{D^{(\alpha)}\} \quad . \tag{7.99}$$

De la même façon, nous pouvons définir le vecteur $X \equiv x^{(\alpha)}$ de taille $\mathcal{N}$. L'ensemble défini dans (7.97) peut alors s'écrire

$$\mathcal{E} = \{\mathcal{B}, A, X\} = \{|\Phi^{(\alpha)}\rangle, X\} = \{D^{(\alpha)}, X\} \quad . \tag{7.100}$$

La façon de lire $\{\mathcal{B}, A, X\}$ est représentée à la Fig. 7.2. Chaque $|\Phi^{(\alpha)}\rangle$ correspond à

$$\begin{array}{c} \\ n_1 \\ n_2 \\ n_3 \\ n_4 \\ \vdots \\ n_{\Omega-1} \\ n_\Omega \\ \end{array}
\begin{array}{c} \begin{array}{cccc} A & & & \end{array} \\ \begin{pmatrix} 0 & 1 & ... & 0 \\ 1 & 0 & ... & 0 \\ 0 & 0 & ... & 0 \\ 1 & 0 & ... & 1 \\ \vdots & \vdots & ... & \vdots \\ 0 & 1 & ... & 1 \\ 1 & 1 & ... & 1 \end{pmatrix} \\ |\Phi^{(1)}\rangle |\Phi^{(2)}\rangle \quad |\Phi^{(\mathcal{N})}\rangle \end{array}
\begin{array}{c} \mathcal{B} \\ |\varphi_1\rangle \\ |\varphi_2\rangle \\ |\varphi_3\rangle \\ |\varphi_4\rangle \\ \vdots \\ |\varphi_{\Omega-1}\rangle \\ |\varphi_\Omega\rangle \end{array}
\times
\begin{array}{c} X \\ \begin{pmatrix} x^{(1)} \\ x^{(2)} \\ x^{(3)} \\ \vdots \\ \vdots \\ x^{(\mathcal{N})} \end{pmatrix} \end{array}
=
\begin{array}{c} \\ \\ \\ \\ \\ \\ \\ \\ \end{array}
\begin{pmatrix} w_1 \\ w_2 \\ w_3 \\ w_4 \\ \vdots \\ w_{\Omega-1} \\ w_\Omega \end{pmatrix}$$

Figure 7.2: L'ensemble $\mathcal{E}$ est représenté par le triplet $\{\mathcal{B}, A, X\}$. Le produit matriciel de A par X donne les termes diagonaux de ρ qui doivent être lus dans la base naturelle $\mathcal{B}$.

une matrice densité à 1 corps $\rho^{(\alpha)}$:

$$|\Phi^{(\alpha)}\rangle \ \longleftrightarrow \ \rho^{(\alpha)} = \sum_{\nu=1}^{\Omega} |\varphi_\nu\rangle n_\nu^{(\alpha)} \langle\varphi_\nu| \ . \tag{7.101}$$

Et la connexion de $\mathcal{E}$ à ρ est réalisée en utilisant

$$\rho = \sum_{\alpha=1}^{\mathcal{N}} x^{(\alpha)} \rho^{(\alpha)} = \sum_{\nu=1}^{\Omega} |\varphi_\nu\rangle \underbrace{\sum_{\alpha=1}^{\mathcal{N}} x^\alpha n_\nu^{(\alpha)}}_{=w_\nu} \langle\varphi_\nu| \ . \tag{7.102}$$

La variété des états de Slater(7.98) avec distribution arbitraire de $n_\nu^{(\alpha)}$ est importante. En fait, nous restreignons l'ensemble $\mathcal{E}$ aux $|\Phi^{(\alpha)}\rangle$ qui restent proches de l'énergie de ρ. Ceci sera détaillé au Sec. 7.7.3 dans le cadre du régime de progression.

7.7.2 D'un état mixte à une somme d'états purs

Le passage de $\mathcal{E}$ à ρ est simple, comme vu à partir de l'Eq. (7.102). La transformation inverse

$$w_\nu \longrightarrow x^{(\alpha)} \tag{7.103}$$

est ambiguë et possède seulement des solutions approximatives. Nous determinons le vecteur X par une méthode des moindres carrés

$$\chi^2 = ||W - AX||^2 + \eta||X||^2 = \sum_\nu \left(w_\nu - \sum_\alpha n_\nu^{(\alpha)} x^{(\alpha)} \right)^2 + \eta \sum_\alpha \left(x^{(\alpha)} \right)^2 = \text{minimal} \ , \tag{7.104}$$

où $W \equiv w_\nu$ et η est un paramètre numérique positif proche de zéro. La minimisation est réalisée avec la contrainte $1 \geq x^{(\alpha)} \geq 0$. Le second terme pondéré par η permet de privilégier la solution avec les coefficients $x^{(\alpha)}$ distribués les plus uniformément. Trouver X correspond à résoudre ce problème des moindres carrés non négatifs (NNLS).

Une option pour trouver $X(\lambda_n)$ consiste à minimiser l'expression suivante :

$$\chi^2(\eta_n) = ||W - AX||^2 + \eta_n||X||^2 \tag{7.105}$$

et à utiliser $X(\eta_n)$ comme point de départ pour trouver $X(\eta_{n+1})$ avec $\eta_n \to 0$. Cependant, ce serait numériquement trop exigeant. Par conséquent, cette solution a été évitée.

Au lieu de cela, pendant les étapes de descente du gradient pour résoudre le problème NNLS, η est rapidement réduit. Même si cela n'assure pas que X soit un minimum de χ^2, X reste un minimum de $||W - AX||^2$ et nous pouvons nous attendre à ce que X soit proche de la solution optimale. Cependant, cette solution peut parfois générer un ρ_{sampled} trop différent du ρ d'origine, pour produire des discontinuités dans des observables tels que l'énergie. Pour résoudre ce problème, nous avons introduit la matrice densité restante ρ_{rem} définie comme suit :

$$\rho_{\text{rem}} = \rho - \rho_{\text{sampled}} = \sum_\nu (w_\nu - \sum_\alpha n_\nu^{(\alpha)} x^{(\alpha)}) |\varphi_\nu\rangle\langle\varphi_\nu| \quad . \tag{7.106}$$

Nous supposerons toujours $\rho = \rho_{\text{sampled}}$ dans ce qui suit et utiliserons uniquement ρ. En pratique, toutes les transformations de CTDHF se feront sur ρ_{sampled}, et ρ_{rem} est additionné seulement à la fin de l'étape CTDHF pour préserver la continuité de ρ. L'effet de ρ_{rem} est illustré à la Fig. 7.3 sur un exemple typique qui a été présenté et discuté plus longuement au Chapitre 4.

7.7.3 D'un pas dissipatif à l'autre

La propagation possède deux échelles de temps: à un pas de temps plus grossier τ pour évaluer les sauts à 2 corps et un pas de temps plus fin $\delta t (< \tau)$ pour la propagation TDHF. Nous considérons ici la procédure CTDHF de $t_{m-1} = (m-1)\tau$ à $t_m = m\tau$.

Propagation en champ moyen

On commence à t_{m-1} avec un état donné $\rho(t_{m-1})$ et l'ensemble $\mathcal{E}(t_{m-1})$ correspondant à l'Eq. (7.97). On propage les fonctions d'onde à un corps par un calcul TDHF

$$\varphi_\nu(t_{m-1}) \ \longrightarrow \ \widetilde{\varphi_\nu} = U\varphi_\nu(t_{m-1}) \ . \tag{7.107}$$

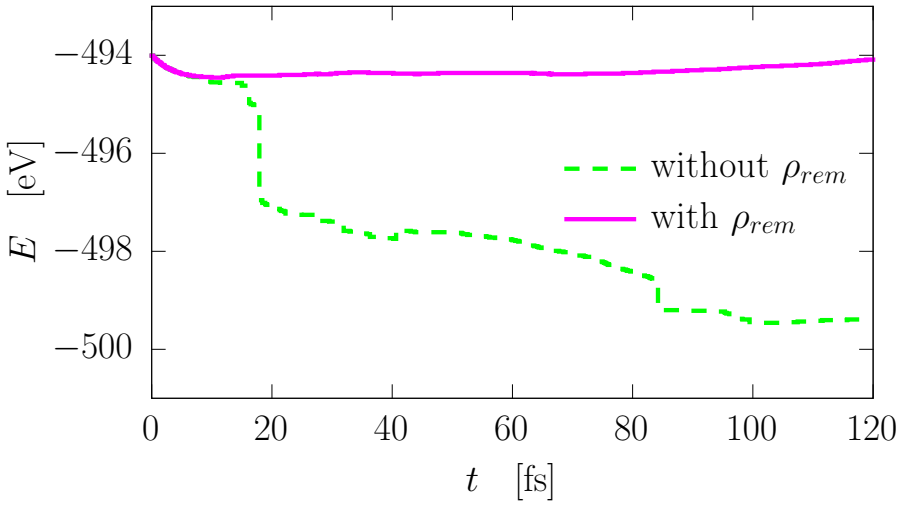

Figure 7.3: Exemple de discontinuités dans l'énergie totale E dans l'évolution temporelle d'un système (presenté dans le Chapitre 5) propagé en CTDHF avec ρ_{rem} (lignes magenta pleines) et sans (pointillés verts).

où $U = U(t_m, t_{m-1})$. Cela définit la base $\widetilde{\mathcal{B}}$ à partir de $\mathcal{B}(t_{m-1})$. On a aussi besoin de la matrice A qui est constante vu que les nombres d'occupation $n_\nu^{(\alpha)}$ restent les mêmes durant l'évolution temporelle. Ces nombres d'occupation sont maintenant lus dans la base propagées $\widetilde{\varphi_\nu}$. C'est équivalent de propager l'ensemble suivant :

$$\{|\Phi^{(\alpha)}(t_{m-1})\rangle\} \to \{|\widetilde{\Phi}^{(\alpha)}\rangle\} \ , \ |\widetilde{\Phi}^{(\alpha)}\rangle = U|\Phi^{(\alpha)}(t_{m-1})\rangle \ . \tag{7.108}$$

L'état mixte propagé est :

$$\widetilde{\rho} = \sum_{\nu=1}^{\Omega} |\widetilde{\varphi}_\nu\rangle w_\nu \langle\widetilde{\varphi}_\nu| \tag{7.109}$$

avec les mêmes nombres d'occupation $w_\nu = w_\nu(t_{m-1})$. Il faut remarquer que $\widetilde{\varphi}_\nu$, $\widetilde{\Phi}^{(\alpha)}$, et $\widetilde{\rho}$ sont des éléments temporaires d'un calcul préliminaire. Les véritables quantités finales à t_m sont déterminées après le pas dissipatif.

Sélection d'un ensemble ayant la bonne énergie

Les états $|\widetilde{\Phi}^{(\alpha)}\rangle$ ont pu diverger en une large distribution d'énergies différentes $\widetilde{E}^{(\alpha)}$ durant la propagation. Nous voulons à nouveau réduire l'ensemble des états échantillonnés à une bande d'énergie plus fine. Nous avons d'abord besoin d'étendre l'ensemble pour produire suffisamment de choix d'états dans une bande d'énergie plus étroite autour de l'énergie totale $E[\rho]$. Dans ce but nous partons des états $|\widetilde{\Phi}^{(\alpha)}\rangle$ et pour chacun d'entre eux considérons les états $2p2h$ correspondants $|\widetilde{\Phi}_\kappa^{(\alpha)}\rangle$ avec $\kappa \equiv pp'hh'$. Cela génère un super ensemble temporaire

$$\{\widetilde{\mathcal{B}}, \tilde{A}^{(\mathrm{S})}\} = \left\{|\widetilde{\Phi}_\kappa^{(\alpha)}\rangle\right\} \ , \ |\widetilde{\Phi}_\kappa^{(\alpha)}\rangle \equiv c_{p'}^\dagger c_p^\dagger c_h c_{h'} |\widetilde{\Phi}^{(\alpha)}\rangle \tag{7.110}$$

où $\kappa = 0$ correspond à l'état $0p0h$ d'origine. Les opérateurs création-annihilation correspondent à la base $\widetilde{\mathcal{B}}$. De ce grand ensemble, nous prélevons $\mathcal{N}$ états $|\widetilde{\Phi}^{(\gamma)}\rangle$ parmi ceux vérifiant

$$\delta E^{(\gamma)} = E[\widetilde{\rho}^{(\gamma)}] - E[\widetilde{\rho}] \leq \Gamma_{\mathcal{E}} \quad , \tag{7.111}$$

où $\Gamma_{\mathcal{E}}$ est un paramètre numérique pris suffisamment petit, et définit la bande d'énergie autorisée de l'ensemble (noté par l'indice $\mathcal{E}$). Le choix de $|\widetilde{\Phi}^{(\gamma)}\rangle$ à garder dans la nouvelle matrice $\widetilde{A}$ n'est pas évident. Nous avons essayé deux techniques :

(i) Nous gardons seulement les $\mathcal{N}$ premiers états avec l'énergie la plus proche de celle d'origine. Cette procédure assure une bonne conservation de l'énergie des états considérés. Ainsi l'ensemble $\widetilde{A}$ n'est construit que sur la base d'un critère énergétique. χ^2 et X ne sont calculés qu'une seule fois à la fin. A cause du critère de positivité, après le calcul de χ^2, voir Eq. (7.105), il s'avère que ce choix aboutit à des valeurs nulles dans le vecteur X pour la majorité des éléments. Cela veut dire que nous travaillons en fait avec beaucoup d'excitations qui n'interviennent pas du tout dans le calcul de ρ. La plus grande partie de l'ensemble est alors inutile.

(ii) On passe en revue les transitions $2p2h$ et on rejette immédiatement celles qui sont trop loin en énergie. Pour celles restant, on regarde $\min_\alpha\ x^{(\alpha)}$. Lorsque le α_0 correspondant à ce minimum est trouvé, on remplace la colonne $[\mathbf{n}^{(\alpha_0)}]$ dans A et on calcule χ^2 à nouveau (voir Fig. 7.4). Si χ^2 diminue alors l'excitation $2p2h$ est acceptée. Le temps de calcul est quelque peu augmenté par rapport à la précédente méthode mais $\mathcal{N}$ peut être pris plus petit et la stabilité numérique est améliorée.

Une fois $\widetilde{A} = \{|\widetilde{\Phi}^{(\gamma)}\rangle\}$ obtenu, les poids correspondants $\widetilde{x}^{(\gamma)}$ sont calculés par ingénierie inverse par rapport à $\widetilde{\rho}$ comme souligné dans la Sec. 7.7.2. L'ensemble $\widetilde{\mathcal{E}} = \{|\widetilde{\Phi}^{(\gamma)}\rangle, \widetilde{x}^{(\gamma)}\}$ ainsi produit devient le point de départ du pas dissipatif suivant. Dans la figure 7.5, cet ensemble de $\widetilde{\rho}^{(\gamma)}$ correspond à la première séparation en branches en violet.

Étape dissipative

Partant de $|\widetilde{\Phi}^{(\gamma)}\rangle$ et de sa matrice densité à un corps $\widetilde{\rho}^{(\gamma)}$, tous les états $2p2h$ correspondants $|\widetilde{\Phi}^{(\gamma)}_\kappa\rangle$ (ou les matrices densités $\widetilde{D}^{(\kappa[\gamma])}$) sont construits en basculant deux $\widetilde{n}^{(\gamma)}_\nu = 0 \nearrow 1$ et deux autres $\widetilde{n}^{(\gamma)}_\nu = 1 \searrow 0$. Nous rappelons que $|\widetilde{\Phi}^{(\gamma)}\rangle$ est un état pur représenté par les nombres d'occupation $\widetilde{n}^{(\gamma)}_\nu$ qui sont soit 0, soit 1. Les transitions $2p2h$ correspondantes ont maintenant un sens physique et ne doivent pas être confondues avec les précédentes utilisées pour échantillonner ρ. On ne se concentre ici que sur un γ spécifique. A ce stade nous n'avons pas encore modifié la fonction d'onde à un corps $\widetilde{\varphi}^{(\gamma)}_\nu$ qui sont strictement les originales $\widetilde{\varphi}_\nu$ au pas de temps considéré.

Il y a maintenant 2 options : soit nous gardons $\widetilde{\varphi}_\nu$ ou nous diagonalisons le hamiltonien champ moyen $h^{(\gamma)}$ dans l'espace des particules et des trous comme nous le faisons en STDHF, ce qui fournit une nouvelle base $\widetilde{\varphi}^{(\gamma)}_\nu$. La première option est appelée "diagonal CTDHF" car elle agit seulement sur la partie diagonale de la matrice densité et la deuxième option est simple appelée "CTDHF". Sans perte de généralités on peut considérer la seconde option qui éventuellement se réduit à diagonal CTDHF (bien que fournissant des taux de transition différents) en remplaçant $\widetilde{\varphi}^{(\gamma)}_\nu$ par $\widetilde{\varphi}_\nu$.

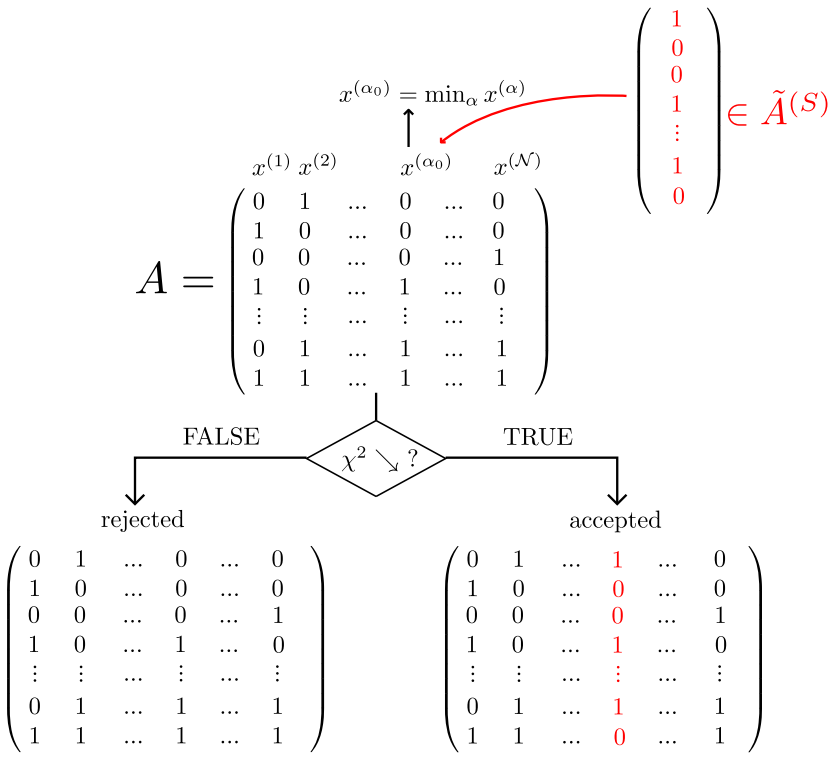

Figure 7.4: Représentation schématique du choix des états $|\Phi^{(\alpha)}\rangle$ pour créer $\tilde{A}$ à partir de A et $\tilde{A}^{(S)}$. Cela est répété autant de fois qu'il y a d'états dans $\tilde{A}^{(S)}$.

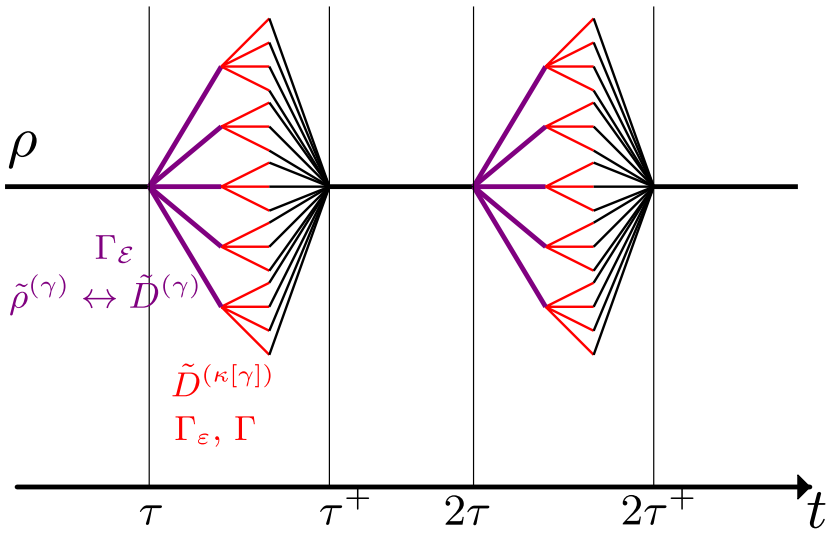

Figure 7.5: Vue schématique de l'évolution temporelle de la méthode du collisionnel TDHF. Voir le texte pour les détails

Pour notre état $|\widetilde{\Phi}^{(\gamma)}\rangle$ en particulier on évalue les taux de transition $P^{(\gamma)}_{pp'hh'} \equiv P^{(\gamma)}_{\kappa}$ definis dans l'Eq. (7.73) et le complémentaire $P^{(\gamma)}_0 = 1 - \sum_\kappa P^{(\gamma)}_\kappa$. La fonction delta qui apparaît dans le taux de transition $P^{(\gamma)}_\kappa$ est remplacée par une sélection en énergie des transitions séparée en deux étapes comme en STDHF (voir Sec. 7.6.4). Une fois l'ensemble des états accessibles $|\widetilde{\Phi}^{(\gamma)}_\kappa\rangle$, on calcule $\rho^{(\gamma)}$:

$$\rho^{(\gamma)} = P^{(\gamma)}_0 \sum_\nu \widetilde{n}^{(\gamma)}_\nu |\widetilde{\varphi}^{(\gamma)}_\nu\rangle\langle\widetilde{\varphi}^{(\gamma)}_\nu| + \sum_\kappa P^{(\gamma)}_\kappa \sum_\nu \widetilde{n}^{(\gamma)}_{\nu,\kappa} |\widetilde{\varphi}^{(\gamma)}_\nu\rangle\langle\widetilde{\varphi}^{(\gamma)}_\nu| \tag{7.112}$$

où $\widetilde{n}^{(\gamma)}_{\nu,\kappa} = \begin{cases} 1 & \text{if } \nu = p \text{ or } \nu = p' \\ 0 & \text{if } \nu = h \text{ or } \nu = h' \\ \widetilde{n}^{(\gamma)}_\nu & \text{otherwise} \end{cases}$.

Cette étape est représentée dans la Fig. 7.5 par l'embrachement rouge partant d'une ligne violette qui représente un γ particulier. Une fois ceci fait pour chaque γ, on ajoute de manière incohérente les différents $\rho^{(\gamma)}$ comme dans l'Eq. (7.102) pour obtenir le $\rho(t_m)$ final avec dissipation:

$$\rho = \sum_{\gamma=1}^{\mathcal{N}} \widetilde{x}^{(\gamma)} \rho^{(\gamma)} = \sum_{\nu=1}^{\Omega} |\varphi_\nu(t_m)\rangle w_\nu(t_m) \langle\varphi_\nu(t_m)| \,. \tag{7.113}$$

A droite du signe égal, $\mathcal{B}(t_m) = \{|\varphi_\nu(t_m)\rangle\}$ est obtenue par diagonalisation du nouveau ρ. Avant de continuer, on doit définir la nouvelle matrice A des nombres d'occupation à utiliser comme point de départ pour notre ensemble au pas suivant. La solution la plus simple est de recycler l'ensemble de nombres d'occupation $\widetilde{A} = \widetilde{n}^{(\gamma)}_\nu$ et de les combiner avec $\mathcal{B}(t_n)$. On peut finalement commencer un nouveau cycle et propager jusqu'au prochain pas dissipatif.

7.8 Conclusion

Dans cette partie, les bases des théories utilisées dans cette thèse ont été dérivées. Les trois approches présentées ici (CTDHF, STDHF, ETDHF) sont réductibles à une équation de Boltzmann (ou de Boltzmann-Langevin pour STDHF) avec des approximations différentes STDHF et ETDHF ont déjà été étudiées dans le passé dans différents travaux [62, 61, 59]. CTDHF est une nouvelle méthode à mi-chemin entre STDHF et ETDHF. On s'attend que CTDHF s'accord avec les résultats de STDHF (les fluctuations en moins) à de hautes énergies d'excitations et d'avoir le même comportement que ETDHF à basse énergie.

Bibliography

[1] T. Fennel, K.-H. Meiwes-Broer, J. Tiggesbäumker, P.-G. Reinhard, P. M. Dinh, and E. Suraud, "Laser-driven nonlinear cluster dynamics," Reviews of Modern Physics, vol. 82, pp. 1793–1842, June 2010.

[2] H. D. Meyer, U. Manthe, and L. S. Cederbaum, "The multi-configurational time-dependent Hartree approach," Chemical Physics Letters, vol. 165, pp. 73–78, Jan. 1990.

[3] H.-D. Meyer, F. Gatti, and G. A. Worth, eds., Multidimensional Quantum Dynamics. Weinheim, Germany: Wiley-VCH Verlag GmbH & Co. KGaA, Apr. 2009.

[4] P. Hohenberg and W. Kohn, "Inhomogeneous Electron Gas," Physical Review, vol. 136, pp. B864–B871, Nov. 1964.

[5] E. H. Lieb, "Density functionals for coulomb systems," International Journal of Quantum Chemistry, vol. 24, pp. 243–277, Sept. 1983.

[6] M. Levy, "Universal variational functionals of electron densities, first-order density matrices, and natural spin-orbitals and solution of the v-representability problem," Proceedings of the National Academy of Sciences, vol. 76, pp. 6062–6065, Dec. 1979.

[7] E. Runge and E. K. U. Gross, "Density-Functional Theory for Time-Dependent Systems," Physical Review Letters, vol. 52, pp. 997–1000, Mar. 1984.

[8] M. A. L. Marques, N. T. Maitra, F. M. S. Nogueira, E. K. U. Gross, and A. Rubio, eds., Fundamentals of time-dependent density functional theory. No. 837 in Lecture notes in physics, Heidelberg: Springer, 2012. OCLC: 785830422.

[9] E. A. Uehling and G. E. Uhlenbeck, "Transport Phenomena in Einstein-Bose and Fermi-Dirac Gases. I," Physical Review, vol. 43, pp. 552–561, Apr. 1933.

[10] U. Saalmann, C. Siedschlag, and J. M. Rost, "Mechanisms of cluster ionization in strong laser pulses," Journal of Physics B: Atomic, Molecular and Optical Physics, vol. 39, no. 4, p. R39, 2006.

[11] C.-Y. Wong and H. H. K. Tang, "Dynamics of nuclear fluid. V. Extended time-dependent Hartree-Fock approximation illuminates the approach to thermal equilibrium," Physical Review C, vol. 20, pp. 1419–1452, Oct. 1979.

[12] C.-Y. Wong and H. H. K. Tang, "Extended Time-Dependent Hartree-Fock Approximation with Particle Collisions," Physical Review Letters, vol. 40, pp. 1070–1073, Apr. 1978.

[13] H. Orland and R. Schaeffer, "Two-body collisions and time dependent Hartree-Fock theory," Zeitschrift für Physik A Atoms and Nuclei, vol. 290, no. 2, pp. 191–204, 1979.

[14] K. Goeke, P. G. Reinhard, H. Araki, J. Ehlers, K. Hepp, R. Kippenhahn, H. A. Weidenmüller, and J. Zittartz, eds., Time-Dependent Hartree-Fock and Beyond, vol. 171 of Lecture Notes in Physics. Berlin, Heidelberg: Springer Berlin Heidelberg, 1982.

[15] H. Reinhardt, P. G. Reinhard, and K. Goeke, "Non-markovian treatment of collective motion in extended time-dependent mean-field theories," Physics Letters B, vol. 151, pp. 177–180, Feb. 1985.

[16] S. J. Wang and W. Cassing, "Explicit treatment of N-body correlations within a density-matrix formalism," Annals of Physics, vol. 159, no. 2, pp. 328–350, 1985.

[17] W. Cassing, K. Niita, and S. J. Wang, "Dynamical aspects of intermediate-energy nucleus-nucleus collisions," Zeitschrift für Physik A Atomic Nuclei, vol. 331, pp. 439–449, Dec. 1988.

[18] W. Cassing and U. Mosel, "Many-body theory of high-energy heavy-ion reactions," Progress in Particle and Nuclear Physics, vol. 25, pp. 235–323, Jan. 1990.

[19] R. F. Snider, "Quantum-Mechanical Modified Boltzmann Equation for Degenerate Internal States," The Journal of Chemical Physics, vol. 32, pp. 1051–1060, Apr. 1960.

[20] W. Botermans and R. Malfliet, "Two-body collisions and mean-field theory: The Brueckner-Boltzmann equation," Physics Letters B, vol. 171, no. 1, pp. 22–27, 1986.

[21] A. S. Umar, M. R. Strayer, and P. G. Reinhard, "Resolution of the fusion window anomaly in heavy-ion collisions," Physical Review Letters, vol. 56, pp. 2793–2796, June 1986.

[22] P.-G. Reinhard and E. Suraud, "Stochastic TDHF and the Boltzman-Langevin equation," Annals of Physics, vol. 216, no. 1, pp. 98–121, 1992.

[23] P.-G. Reinhard, E. Suraud, and S. Ayik, "The Boltzmann-Langevin equation derived from the real-time path formalism," Annals of Physics, vol. 213, pp. 204–229, Jan. 1992.

[24] Y. Abe, S. Ayik, P.-G. Reinhard, and E. Suraud, "On stochastic approaches of nuclear dynamics," Physics reports, vol. 275, no. 2, pp. 49–196, 1996.

[25] D. Lacroix and S. Ayik, "Stochastic quantum dynamics beyond mean field," The European Physical Journal A, vol. 50, June 2014.

[26] W. Kohn and L. J. Sham, "Self-Consistent Equations Including Exchange and Correlation Effects," Physical Review, vol. 140, pp. A1133–A1138, Nov. 1965.

[27] M. Petersilka, U. J. Gossmann, and E. K. U. Gross, "Excitation Energies from Time-Dependent Density-Functional Theory," Physical Review Letters, vol. 76, pp. 1212–1215, Feb. 1996.

[28] P. Wopperer, P. M. Dinh, P. G. Reinhard, and E. Suraud, "Electrons as probes of dynamics in molecules and clusters: A contribution from Time Dependent Density Functional Theory," Physics Reports, vol. 562, pp. 1–68, Feb. 2015.

[29] D. C. Langreth and J. P. Perdew, "Theory of nonuniform electronic systems. I. Analysis of the gradient approximation and a generalization that works," Physical Review B, vol. 21, pp. 5469–5493, June 1980.

[30] J. P. Perdew and W. Yue, "Accurate and simple density functional for the electronic exchange energy: Generalized gradient approximation," Physical Review B, vol. 33, pp. 8800–8802, June 1986.

[31] A. Pribram-Jones, D. A. Gross, and K. Burke, "DFT: A Theory Full of Holes?," Annual Review of Physical Chemistry, vol. 66, no. 1, pp. 283–304, 2015.

[32] A. J. Cohen, P. Mori-Sánchez, and W. Yang, "Challenges for Density Functional Theory," Chemical Reviews, vol. 112, pp. 289–320, Jan. 2012.

[33] D. G. Lappas and R. v. Leeuwen, "Electron correlation effects in the double ionization of He," Journal of Physics B: Atomic, Molecular and Optical Physics, vol. 31, no. 6, p. L249, 1998.

[34] D. Bauer, "Two-dimensional, two-electron model atom in a laser pulse: Exact treatment, single-active-electron analysis, time-dependent density-functional theory, classical calculations, and nonsequential ionization," Physical Review A, vol. 56, pp. 3028–3039, Oct. 1997.

[35] C.-Z. Gao, P. Wopperer, P. M. Dinh, E. Suraud, and P.-G. Reinhard, "On the dynamics of photo-electrons in C 60," Journal of Physics B: Atomic, Molecular and Optical Physics, vol. 48, no. 10, p. 105102, 2015.

[36] Y. Huismans, E. Cormier, C. Cauchy, P.-A. Hervieux, G. Gademann, A. Gijsbertsen, O. Ghafur, P. Johnsson, P. Logman, T. Barillot, C. Bordas, F. Lépine, and M. J. J. Vrakking, "Macro-atom versus many-electron effects in ultrafast ionization of c_{60}," Physical Review A, vol. 88, p. 013201, July 2013.

[37] E. E. B. Campbell, K. Hansen, K. Hoffmann, G. Korn, M. Tchaplyguine, M. Wittmann, and I. V. Hertel, "From Above Threshold Ionization to Statistical Electron Emission: The Laser Pulse-Duration Dependence of C_{60} Photoelectron Spectra," Physical Review Letters, vol. 84, pp. 2128–2131, Mar. 2000.

[38] K. Pernal, O. Gritsenko, and E. J. Baerends, "Time-dependent density-matrix-functional theory," Physical Review A, vol. 75, p. 012506, Jan. 2007.

[39] K. Pernal and K. J. H. Giesbertz, "Reduced Density Matrix Functional Theory (RDMFT) and Linear Response Time-Dependent RDMFT (TD-RDMFT)," in Density-Functional Methods for Excited States (N. Ferré, M. Filatov, and M. Huix-Rotllant, eds.), no. 368 in Topics in Current Chemistry, pp. 125–183, Springer International Publishing, 2015. DOI: 10.1007/128_2015_624.

[40] H. Appel and E. K. U. Gross, "Time-dependent natural orbitals and occupation numbers," EPL (Europhysics Letters), vol. 92, no. 2, p. 23001, 2010.

[41] A. K. Rajam, I. Raczkowska, and N. T. Maitra, "Semiclassical Electron Correlation in Density-Matrix Time Propagation," Physical Review Letters, vol. 105, p. 113002, Sept. 2010.

[42] P. Elliott and N. T. Maitra, "Density-matrix propagation driven by semiclassical correlation," International Journal of Quantum Chemistry, vol. 116, pp. 772–783, May 2016.

[43] A. Akbari, M. J. Hashemi, A. Rubio, R. M. Nieminen, and R. van Leeuwen, "Challenges in truncating the hierarchy of time-dependent reduced density matrices equations," Physical Review B, vol. 85, no. 23, p. 235121, 2012.

[44] M. Ruggenthaler and R. v. Leeuwen, "Global fixed-point proof of time-dependent density-functional theory," EPL (Europhysics Letters), vol. 95, no. 1, p. 13001, 2011.

[45] M. Ruggenthaler, K. J. H. Giesbertz, M. Penz, and R. van Leeuwen, "Density-potential mappings in quantum dynamics," Physical Review A, vol. 85, p. 052504, May 2012.

[46] R. M. Dreizler and E. K. U. Gross, Density Functional Theory. Berlin, Heidelberg: Springer Berlin Heidelberg, 1990.

[47] J. Messud, P. M. Dinh, P.-G. Reinhard, and E. Suraud, "Time-Dependent Density-Functional Theory with a Self-Interaction Correction," Physical Review Letters, vol. 101, no. 9, p. 096404, 2008.

[48] C. Legrand, E. Suraud, and P. G. Reinhard, "Comparison of self-interaction-corrections for metal clusters," Journal of Physics B: Atomic, Molecular and Optical Physics, vol. 35, no. 4, p. 1115, 2002.

[49] A. D. Becke, "Density-functional thermochemistry. III. The role of exact exchange," The Journal of Chemical Physics, vol. 98, pp. 5648–5652, Apr. 1993.

[50] C. Lee, W. Yang, and R. G. Parr, "Development of the Colle-Salvetti correlation-energy formula into a functional of the electron density," Physical Review B, vol. 37, pp. 785–789, Jan. 1988.

[51] P.-G. Reinhard and E. Suraud, Introduction to Cluster Dynamics. John Wiley & Sons, July 2008.

[52] M. A. L. Marques, ed., Time-dependent density functional theory. No. 706 in Lecture notes in physics, Berlin: Springer, 2006. OCLC: ocm71008305.

[53] N. T. Maitra, "Memory: History , Initial-State Dependence , and Double-Excitations," in Fundamentals of Time-Dependent Density Functional Theory (M. A. L. Marques, N. T. Maitra, F. M. S. Nogueira, E. K. U. Gross, and A. Rubio, eds.), no. 837 in Lecture Notes in Physics, pp. 167–184, Springer Berlin Heidelberg, 2012. DOI: 10.1007/978-3-642-23518-4_8.

[54] N. N. Bogoliubov, The dynamical theory in statistical physics. Delhi: Hindustan Pub. Corp., 1965. OCLC: 2294879.

[55] M. Born and H. S. Green, "A General Kinetic Theory of Liquids. IV. Quantum Mechanics of Fluids," Proceedings of the Royal Society of London A: Mathematical, Physical and Engineering Sciences, vol. 191, pp. 168–181, Nov. 1947.

[56] J. G. Kirkwood, "The Statistical Mechanical Theory of Transport Processes I. General Theory," The Journal of Chemical Physics, vol. 14, pp. 180–201, Mar. 1946.

[57] J. Yvon, "Une méthode d'étude des corrélations dans les fluides quantiques en équilibre," Nuclear Physics, vol. 4, pp. 1–20, Aug. 1957.

[58] D. Lacroix, "Quantum nuclear many-body dynamics and related aspects," hdr thesis, 2011.

[59] D. Lacroix, P. Chomaz, and S. Ayik, "On the simulation of extended TDHF theory," Nuclear Physics A, vol. 651, no. 4, pp. 369–378, 1999.

[60] N. T. Maitra, K. Burke, and C. Woodward, "Memory in Time-Dependent Density Functional Theory," Physical Review Letters, vol. 89, p. 023002, June 2002.

[61] E. Suraud and P.-G. Reinhard, "Non-equilibrium quantum dynamics with collisional correlations," New Journal of Physics, vol. 16, p. 063066, June 2014.

[62] N. Slama, P. G. Reinhard, and E. Suraud, "On the inclusion of collisional correlations in quantum dynamics," Annals of Physics, vol. 355, pp. 182–203, Apr. 2015.

[63] V. Franc, V. Hlaváč, and M. Navara, "Sequential Coordinate-Wise Algorithm for the Non-negative Least Squares Problem," pp. 407–414, Springer Berlin Heidelberg, Sept. 2005.

[64] L. Sanche, "Low-Energy Electron Interaction with DNA: Bond Dissociation and Formation of Transient Anions, Radicals, and Radical Anions," in Radical and Radical Ion Reactivity in Nucleic Acid Chemistry (r. M. Greenberg, ed.), pp. 239–293, John Wiley & Sons, Inc., 2009.

[65] B. Boudaïffa, P. Cloutier, D. Hunting, M. A. Huels, and L. Sanche, "Resonant Formation of DNA Strand Breaks by Low-Energy (3 to 20 eV) Electrons," Science, vol. 287, pp. 1658–1660, Mar. 2000.

[66] Y. Zheng and L. Sanche, "Gold Nanoparticles Enhance DNA Damage Induced by Anti-cancer Drugs and Radiation," Radiation Research, vol. 172, pp. 114–119, July 2009.

[67] J. D. Gorfinkiel, L. A. Morgan, and J. Tennyson, "Electron impact dissociative excitation of water within the adiabatic nuclei approximation," Journal of Physics B: Atomic, Molecular and Optical Physics, vol. 35, p. 543, Feb. 2002.

[68] J. Tennyson, "Electron–molecule collision calculations using the -matrix method," Physics Reports, vol. 491, no. 2–3, pp. 29–76, 2010.

[69] M. Smyth and J. Kohanoff, "Excess Electron Localization in Solvated DNA Bases," Physical Review Letters, vol. 106, no. 23, p. 238108, 2011.

[70] N. Douguet, S. Fonseca dos Santos, M. Raoult, O. Dulieu, A. E. Orel, and V. Kokoouline, "Theory of radiative electron attachment to molecules: Benchmark study of CN-," Physical Review A, vol. 88, Nov. 2013.

[71] S. Bhowmick, R. B, M. K. Mishra, and M. Sarma, "Investigation of dissociative electron attachment to 2'-deoxycytidine-3'-monophosphate using DFT method and time dependent wave packet approach," The Journal of Chemical Physics, vol. 137, p. 064310, Aug. 2012.

[72] L. Lacombe, P. M. Dinh, P.-G. Reinhard, E. Suraud, and L. Sanche, "Rare reaction channels in real-time time-dependent density functional theory: the test case of electron attachment," The European Physical Journal D, vol. 69, pp. 1–8, Aug. 2015.

[73] F. Calvayrac, P. G. Reinhard, E. Suraud, and C. A. Ullrich, "Nonlinear electron dynamics in metal clusters," Physics Reports, vol. 337, pp. 493–578, Oct. 2000.

[74] S. Goedecker, M. Teter, and J. Hutter, "Separable dual-space Gaussian pseudopotentials," Physical Review B, vol. 54, no. 3, p. 1703, 1996.

[75] V. Blum, G. Lauritsch, J. A. Maruhn, and P. G. Reinhard, "Comparison of coordinate-space techniques in nuclear mean-field calculations," Journal of Computational Physics, vol. 100, pp. 364–376, June 1992.

[76] M. D. Feit, J. A. Fleck, and A. Steiger, "Solution of the Schrödinger equation by a spectral method," Journal of Computational Physics, vol. 47, pp. 412–433, Sept. 1982.

[77] J. W. Eastwood and D. R. K. Brownrigg, "Remarks on the solution of poisson's equation for isolated systems," Journal of Computational Physics, vol. 32, no. 1, pp. 24–38, 1979.

[78] J. Maruhn, P.-G. Reinhard, P. Stevenson, and A. Umar, "The TDHF code Sky3d," Computer Physics Communications, vol. 185, pp. 2195–2216, July 2014.

[79] E. K. U. Gross, J. F. Dobson, and M. Petersilka, "Density functional theory of time-dependent phenomena," in Density Functional Theory II (P. R. F. Nalewajski, ed.), no. 181 in Topics in Current Chemistry, pp. 81–172, Springer Berlin Heidelberg, 1996. DOI: 10.1007/BFb0016643.

[80] J. P. Perdew and Y. Wang, "Accurate and simple analytic representation of the electron-gas correlation energy," Physical Review B, vol. 45, no. 23, pp. 13244–13249, 1992.

[81] P.-G. Reinhard, P. D. Stevenson, D. Almehed, J. A. Maruhn, and M. R. Strayer, "Role of boundary conditions in dynamic studies of nuclear giant resonances and collisions," Physical Review E, vol. 73, Mar. 2006.

[82] Y. Itikawa and N. Mason, "Cross Sections for Electron Collisions with Water Molecules," Journal of Physical and Chemical Reference Data, vol. 34, no. 1, p. 1, 2005.

[83] J. P. Perdew and A. Zunger, "Self-interaction correction to density-functional approximations for many-electron systems," Physical Review B, vol. 23, pp. 5048–5079, May 1981.

[84] A. Pohl, P.-G. Reinhard, and E. Suraud, "Towards single-particle spectroscopy of small metal clusters," Physical review letters, vol. 84, no. 22, p. 5090, 2000.

[85] A. Pohl, P.-G. Reinhard, and E. Suraud, "Angular distribution of electrons emitted from Na clusters," Physical Review A, vol. 70, p. 023202, Aug. 2004.

[86] U. De Giovannini, D. Varsano, M. A. L. Marques, H. Appel, E. K. U. Gross, and A. Rubio, "Ab initio angle- and energy-resolved photoelectron spectroscopy with time-dependent density-functional theory," Physical Review A, vol. 85, no. 6, p. 062515, 2012.

[87] E. Fermi and E. Amaldi, "Le orbite oos degli elementi," Accad. Ital. Rome, vol. 6, p. 117, 1934.

[88] P. Klüpfel, P. M. Dinh, P.-G. Reinhard, and E. Suraud, "Koopmans' condition in self-interaction-corrected density-functional theory," Physical Review A, vol. 88, Nov. 2013.

[89] C. E. Melton, "Cross Sections and Interpretation of Dissociative Attachment Reactions Producing OH-, O-, and H- in H_2O," The Journal of Chemical Physics, vol. 57, pp. 4218–4225, Nov. 1972.

[90] P. Rawat, V. S. Prabhudesai, G. Aravind, M. A. Rahman, and E. Krishnakumar, "Absolute cross sections for dissociative electron attachment to H2o and D2o," Journal of Physics B: Atomic, Molecular and Optical Physics, vol. 40, p. 4625, Dec. 2007.

[91] J. Fedor, P. Cicman, B. Coupier, S. Feil, M. Winkler, K. Głuch, J. Husarik, D. Jaksch, B. Farizon, N. J. Mason, P Scheier, and T. D. Märk, "Fragmentation of transient water anions following low-energy electron capture by H2o/D2o," Journal of Physics B: Atomic, Molecular and Optical Physics, vol. 39, no. 18, p. 3935, 2006.

[92] R. N. Compton and L. G. Christophorou, "Negative-Ion Formation in H2o and D2o," Physical Review, vol. 154, pp. 110–116, Feb. 1967.

[93] N. G. Adams, V. Poterya, and L. M. Babcock, "Electron molecular ion recombination: Product excitation and fragmentation," Mass Spectrometry Reviews, vol. 25, pp. 798–828, Sept. 2006.

[94] L. Vejby-Christensen, L. H. Andersen, O. Heber, D. Kella, H. B. Pedersen, H. T. Schmidt, and D. Zajfman, "Complete Branching Ratios for the Dissociative Recombination of H2o+, H3o+, and CH3+," The Astrophysical Journal, vol. 483, no. 1, p. 531, 1997.

[95] A. Neau, A. A. Khalili, S. Rosén, A. L. Padellec, A. M. Derkatch, W. Shi, L. Vikor, M. Larsson, J. Semaniak, R. Thomas, M. B. Någård, K. Andersson, H. Danared, and M. a. Ugglas, "Dissociative recombination of D3o+ and H3o+: Absolute cross sections and branching ratios," The Journal of Chemical Physics, vol. 113, pp. 1762–1770, Aug. 2000.

[96] H. J. Lipkin, N. Meshkov, and A. J. Glick, "Validity of many-body approximation methods for a solvable model: (I). Exact solutions and perturbation theory," Nuclear Physics, vol. 62, no. 2, pp. 188–198, 1965.

[97] N. Meshkov, A. J. Glick, and H. J. Lipkin, "Validity of many-body approximation methods for a solvable model: (II). Linearization procedures," Nuclear Physics, vol. 62, no. 2, pp. 199–210, 1965.

[98] A. J. Glick, H. J. Lipkin, and N. Meshkov, "Validity of many-body approximation methods for a solvable model: (III). Diagram summations," Nuclear Physics, vol. 62, no. 2, pp. 211–224, 1965.

[99] G. Holzwarth, "Four approaches to the function of inertia in a solvable model," Nuclear Physics A, vol. 207, pp. 545–564, June 1973.

[100] P.-G. Reinhard, A. S. Umar, K. T. R. Davies, M. R. Strayer, and S.-J. Lee, "Dissipation and forces in time-dependent Hartree-Fock calculations," Physical Review C, vol. 37, pp. 1026–1035, Mar. 1988.

[101] D. Agassi, H. J. Lipkin, and N. Meshkov, "Validity of many-body approximation methods for a solvable model: (IV). The deformed Hartree-Fock solution," Nuclear Physics, vol. 86, pp. 321–331, Oct. 1966.

[102] P. Ring and P. Shuck, The Nuclear Many-Body Problem. Springer, 1980.

[103] J. Crank and P. Nicolson, "A practical method for numerical evaluation of solutions of partial differential equations of the heat-conduction type," Mathematical Proceedings of the Cambridge Philosophical Society, vol. 43, pp. 50–67, Jan. 1947.

[104] C. Greiner, K. Wagner, and P.-G. Reinhard, "Memory effects in relativistic heavy ion collisions," Physical Review C, vol. 49, pp. 1693–1701, Mar. 1994.

[105] L. P. Kadanoff and G. Baym, Quantum statistical mechanics: Green's function methods in equilibrium and nonequilibrium problems. W.A. Benjamin, 1962.

This thesis presents various quantal approaches for the exploration of dynamical processes in multielectronic systems, especially after an intense excitation which can possibly lead to dissipative effects. Mean field theories constitute useful tools in that respect. Despite the existence of numerous works during the past two decades, they have strong difficulties to capture full 2-body correlations. Thermalization is one of these effects that stems from electron-electron collisions. After an introductory chapter, we present in Chapter 2 the formalism of the various schemes studied in this thesis toward the description of such an effect by including collisional terms on top of a mean field theory. These schemes are called Stochastic Time-Dependent Hartree Fock (STDHF), Extended TDHF (ETDHF) and Collisional TDHF (CTDHF). The latter scheme constitutes in some sense the main achievement of this thesis. The numerical realizations of each scheme are also discussed in detail. In Chapters 3, 4 and 5, we apply the approaches discussed in Chapter 2 but in various systems. In Chapter 3, we first explore a rare reaction channel, that is the probability of an electron to attach on small water clusters. Good agreement with experimental data is achieved. In Chapter 4, a model widely used in nuclear physics is exactly solved and quantitatively compared to STDHF. The time evolution of 1-body observables agrees well in both schemes, especially what concerns thermal behavior. However, to allow a good description of the dynamics, one is bound to use a large statistics, which can constitute a hindrance of the use of STDHF in larger systems. To overcome this problem, in Chapter 5, we go for a testing of CTDHF developed in Chapter 2 in a one-dimensional system (and without electronic emission). This system consists in electrons in a jellium potential with a simplified self-consistent interaction expressed as a functional of the density. The advantage of this 1D model is that STDHF calculations are numerically manageable and therefore allows a direct comparison with CTDHF calculations. In this proof of concept study, CTDHF compares remarkably well with STDHF. This thus paves the road toward an efficient description of dissipation in realistic 3D systems by CTDHF.

Cette thèse présente différentes approches quantiques pour l'exploration de processus dynamiques dans des systèmes multiélectroniques, en particulier après une forte excitation qui peut aboutir à des effets dissipatifs. Les théories de champ moyen sont un outil utile à cet égard. Malgré l'existence de nombreux travaux réalisés ces deux dernières décennies, ces théories peinent à reproduire complètement la corrélation à deux corps. La thermalisation est un des effets des collisions électron-électron. Après un chapitre introductif, on présentera dans le chapitre 2 le formalisme de plusieurs méthodes étudiées dans cette thèse, ayant pour but la description de ces effets en ajoutant un terme de collision au champ moyen. Ces méthodes sont appelées Stochastic Time-Dependent Hartree Fock (STDHF), Extended TDHF (ETDHF) et Collisional TDHF (CTDHF). Cette dernière méthode représente d'une certaine façon le résultat principal de cette thèse. L'implémentation numérique de chacune de ces méthodes sera aussi examinée en détail. Dans les chapitres 3, 4 et 5, nous appliquerons à différents systèmes les méthodes présentées dans le chapitre 2. Dans le chapitre 3, nous étudions d'abord un canal de réaction rare, ici la probabilité d'un électron de s'attacher à un petit agrégat d'eau. Un bon accord avec les données expérimentales a été observé. Dans le chapitre 4, un modèle fréquemment utilisé en physique nucléaire est résolu exactement et comparé quantitativement à STDHF. L'évolution temporelle des observables à un corps s'accorde entre les deux méthodes, plus particulièrement en ce qui concerne le comportement thermique. Néanmoins, pour permettre une bonne description de la dynamique, il est nécessaire d'avoir une grande statistique, ce qui peut être un frein à l'utilisation de STDHF sur de larges systèmes. Pour surpasser cette difficulté, dans le chapitre 5 nous testons CTDHF, qui a été introduit dans le chapitre 2, sur un modèle à une dimension (et sans émission électronique). Le modèle se compose d'électrons dans un potentiel de type jellium avec une interaction auto-cohérente sous la forme d'une fonctionnelle de la densité. L'avantage de ce modèle à une dimension est que les calculs STDHF sont possibles numériquement, ce qui permet une comparaison directe aux calculs CTDHF. Dans cette étude de validité du concept, CTDHF s'accorde remarquablement bien avec STDHF. Cela pose les jalons pour une description efficace de la dissipation dans des systèmes réalistes en trois dimensions par CTDHF.